Università degli Studi della Tuscia di Viterbo

Dipartimento di Scienze Ecologiche e Biologiche

Corso di Dottorato di Ricerca in

Ecologia e gestione sostenibile delle risorse ambientali - **XXXV ciclo**

AN INTEGRATED STUDY OF ECOLOGICAL, GENOMIC, AND METABOLIC FACTORS IN RADIORESISTANCE OF BLACK FUNGI

Settore scientifico-disciplinare

(**s.s.d. BIO/03**)

Tesi di dottorato di:

Dott. Lorenzo Aureli

Coordinatore del corso

Prof. Claudio Carere

Tutore

Prof.ssa Laura Selbmann

Co-tutore

Prof. Silvano Onofri

Prof. Dag Ahren

Dott. Claudia Coleine

Dott. Claudia Pacelli

A.A. 2022/23 (A.Y. 2022/23)

Summary

Abstract

The high levels of ionizing radiation experienced in extraterrestrial environments and in a few places on Earth make the study of the limits and adaptation of life to it a key concern in the fields of astrobiology, bioprotection and bioremediation. Notably, some microorganisms can survive doses of ionizing radiation that are fatal to most known life-forms, becoming potential models for studying the factors that contribute to withstanding hazardous radiation environments. Among them, meristematic black fungi, constituting a polyphyletic and extremophilic guild that displays the ability to thrive in a wide range of extreme environments, is a very promising group. Previous studies have already demonstrated the extraordinary capacity of one of them in particular, *Cryomyces antarcticus* MNA-CCFEE515, to tolerate high levels of various forms of ionizing radiation. However, several fundamental questions still need to be answered regarding the overall radioresistance limits of the whole group and the evolutionary and genetic factors underlying this trait. From this perspective, the present study comprehensively defined, for the first time, the radioresistance limits of this group and pointed out the potential adaptive and genomic factors that are responsible for this capacity. To reach this goal, we first further tested the ability of the black fungus *C. antarcticus* MNA-CCFEE515 to tolerate highly damaging accelerated helium and iron ions, which represent part of the spectrum of the cosmic rays pervading the environment beyond Earth. Successively, the survival limits of the broadest set of black fungi ever tested before were defined, and we demonstrated, for the first time, through a machine learning approach how differences in radioresistance among strains may be the consequence of the adaptation to various environmental factors occurring in their natural habitats. Finally, through a comparative genomic analysis among the strains, we showed that radioresistance is driven by a range of different cellular mechanisms that could be correlated to evolutionary and ecological factors. Altogether, the findings of this study showed radioresistance as a factor strictly associated with the extremotolerance capacity of microorganisms, providing novel insights into the ability of life to survive in extreme conditions on Earth and beyond. Additionally, these results may serve as a foundation for future investigations into the molecular mechanisms that underlie the radioresistance of eukaryotic organisms.

Chapter 1

Introduction

1.1 Space and terrestrial radiation environments

Ionizing radiation (IR) represents one of the major damaging factors for life in extraterrestrial and some terrestrial environments. There are two main types of IR, referred to as particle and electromagnetic radiation. One of the most damaging types of particle radiation is represented by Cosmic rays (CRs). CRs are fully ionized atomic nuclei whose electrons have been removed due to their acceleration at speeds close to that of light, thereby resulting in high-energy charged particles. Depending on their origin, CRs detected in our solar system are classified into two main categories: Galactic Cosmic Rays (GCRs) and Solar Energetic Particles (SEPs) (O'Sullivan, 2007) (Fig. 1).

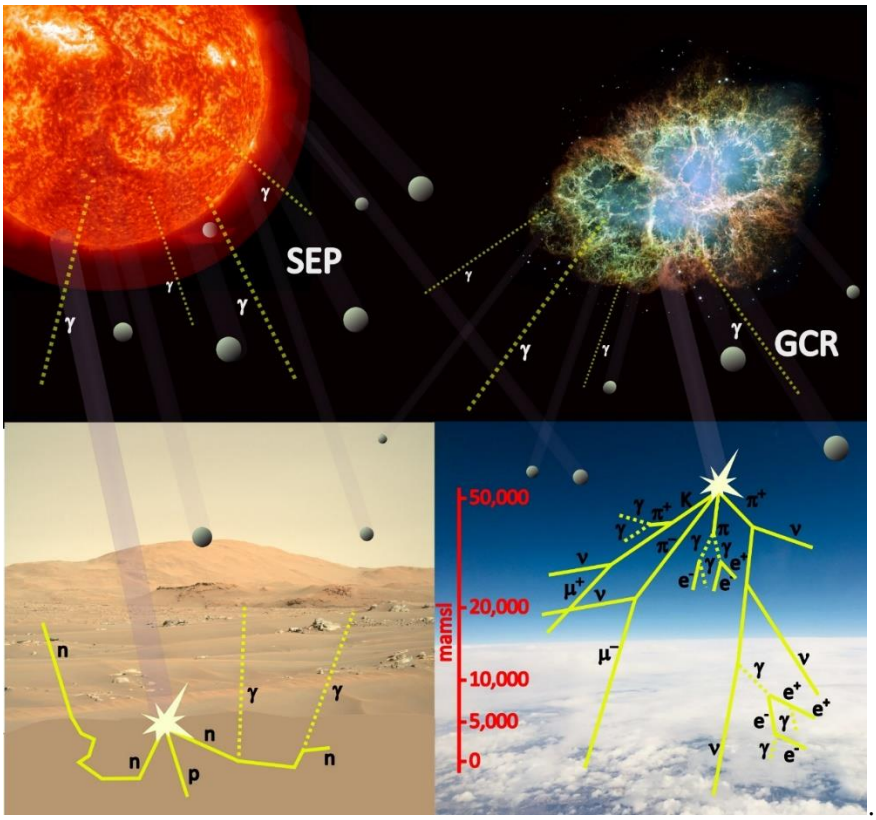

Figure 1.1. Space sources of the main IR types. On the top panel: sources of Solar Energetic Particles (SEPs) and Galactic Cosmic Rays (GCRs). On the panel below: gamma radiation from secondary cosmic rays on Mars (left) and in the terrestrial atmosphere (right). γ: gamma radiation; π: pions; ν: neutrinos; μ: muons; K: kaons; n: neutrons; p: protons.

GCRs originated from various events, such as the shocks of supernova remnants, occurring outside the heliosphere. They consist of nuclei from all natural elements, although these occur in different abundances. Indeed, 87% of GCRs are represented by accelerated protons, 12% by accelerated helium nuclei (called α-particles) and the remaining part of heavier nuclei, called High Atomic Number Energy (HZE) (Simpson, 1983). Instead, SEPs originate from the sun, specifically from coronal mass ejections (CMEs) and solar flares occurring on its surface (Bronarska et al., 2018). The distinct origin of GCRs and SEPs entails different temporal and spatial distributions and energies in the heliosphere, which mainly depends on Sun activity. Indeed, due to their positive charge, CRs can be modulated by magnetic fields, such as the one created by the magnetic clouds carried by the solar wind flowing outward from the Sun (Rahmanifard et al., 2020). Consequently, when GCRs with energies lower than 1 GeV reach the heliosphere, i.e. the space pervaded by the charged solar wind, they can be deflected (Parker, 1965). Instead, GCRs with energies higher than 1 GeV can overcome this effect and penetrate the heliosphere, despite losing their energies while propagating through the solar wind. For this reason, the heliosphere represents the first shield against GCRs in our solar system. However, this shield largely depends on the 11 years of solar activity, during which changes in solar activity are reflected in variations in magnetic field strength inside the heliosphere and, finally, in the spectrum of GCRs that can penetrate it. Indeed, a decrease in the low-energy GCRs from 30 to 50% is observed during solar maximum, during which strong solar wind flow from the Sun (Turner et al., 2008; Ross and Chaplin, 2019). On the other hand, SEPs originate from the Sun during transient events occurring at solar maximum and propagate radially throughout the heliosphere (Anastasiadis et al., 2019). Due to the short duration of the solar events from which they derive, their fluxes can markedly vary over time (Hu et al., 2022). Therefore, in contrast to low-energy GCRs, the fluxes of SEPs are in general directly proportional to solar activity. Together, the origin and the modulation of GCRs and SEPs make the fluxes of CRs in our solar system highly variable. In the view of space missions and astrobiology, the spatial and temporal variability in the CRs spectrum observed in interplanetary space could be of primary importance, significantly affecting the different levels of IR to which any biological system could be exposed beyond Earth.

Additionally, due to their charge, CRs can be deflected by the magnetic fields produced by planets as well. Furthermore, in some planetary bodies, a significant shield from CRs is represented by a dense atmosphere. This is the case of Earth, whose surface is protected from CRs by the terrestrial magnetic field and atmosphere, which prevent their direct contribution to the radiation environment on the surface of the planet (Singh et al., 2011). Instead, the current Mars is characterized by a rarefied atmosphere and scattered and transient localized magnetic fields (Langlais et al., 2004; Johnson et al., 2020; Banfield et al., 2020). Consequently, the surface of the planet is constantly exposed to a major part of the CRs spectrum pervading the Solar system, thus contributing significantly to its radiation environment (Hassler et al., 2014). Additionally, once passed into the atmosphere, the highly penetrating CRs can cross the shallowest layers of Martian regolith and rocks, even reaching depths up to a few meters, depending on their energy (Dartnell et al., 2007; Röstel et al., 2020; Chen et al., 2022). Therefore, from an astrobiological point of view, the presence of high levels of CRs could

make the radiation environment on the Martian surface and in its shallowest subsurface one of the main hazards for both putative Martian and terrestrial forms of life.

Unlike cosmic rays, electromagnetic radiation consists of highly energized photons having wavelengths lower than 124 nm, that can penetrate through matter and cause ionization of atoms by knocking out electrons. The most energetic form of this radiation is represented by gamma rays, which show wavelengths lower than 0.1 nm. The sources and the levels of gamma radiation can significantly vary depending on the environment where they are detected. In our solar system, a gamma ray background mainly depends on the activity of the stars in the galaxy, the remnants of supernova explosions and the interaction between the cosmic rays and the interstellar gas (Orlando et al., 2007; Aharonian, 2013; Jóhannesson et al., 2018). Furthermore, the levels of this background can considerably vary depending on the activity of the Sun (Ackermann et al., 2014; Linden et al., 2018; Bartoli et al., 2019). Due to their high levels, gamma rays represent, along with CRs, the main IR contributing to the space radiation environment in our solar system (Chancellor, 2014).

On the surface of celestial bodies endowed with an atmosphere, such as Earth and Mars, gamma rays can originate from the collision of cosmic rays with the atoms of the atmosphere. Indeed, when cosmic rays hit nuclei in the atmosphere, they generate a series of short-lived particles known as secondary cosmic rays. In turn, these particles can decay and propagate through the atmosphere interacting with other nuclei, thus generating a cascade of events known as cosmic ray showers. The decay of these particles, such as pions, is responsible for the emission of gamma radiation over the atmosphere (MacKinnon et al., 2020) (Fig. 1). However, the Martian atmosphere is too rarefied to shield most of the CRs hitting it. Therefore, when they reach the surface of the planet, they collide with the nuclei of the atoms in the regolith and rocks, triggering showers of secondary particles and gamma rays that can propagate in all directions through the subsurface environment and backscatter to the surface (Da Pieve et al., 2021; Mitrofanov et al., 2022). For this reason, similarly to CRs, gamma rays significantly contribute to the radiation environment on the surface and shallowest subsurface of Mars and must be considered in an astrobiological optic. Consequently, along with CRs, gamma rays make the interplanetary space and the surface of various celestial bodies environments highly pervaded by IR, thereby representing a considerable limiting factor for the survival of any organisms beyond Earth (Dartnell 2011). This makes the investigation of the impact of IR on biological systems a pivotal subject in the quest for life beyond Earth and the field of radioprotection research with regard to manned space missions (Dartnell, 2011; Sihver and Mortazavi, 2021).

On the other hand, there are various sources of gamma radiation on Earth. These are represented by naturally occurring radioactive isotopes (such as ^{40}K, ^{14}C and those in ^{232}Th and ^{238}U series), human-made sources (such as nuclear power plants,) radioactive waste, and remains of nuclear accidents ((Ichimiya et al., 1998; Hu et al., 2010; Walencik-Łata, 2022). This extends the research on the resistance of life to IR to the field of bioprotection and bioremediation of radioactive sites, which involves the use of microorganisms to degrade, immobilize, or transform radioactive contaminants in soil or water (Vandana et al., 2021).

1.2 Cellular responses to ionizing radiation

The investigation of the resistance of life to the radiation environments experienced beyond Earth and in some terrestrial localities requires an understanding of the protective mechanisms used by the cells to cope with the lethal effects of IR. Indeed, the characterization of gene sets, metabolic pathways, and compounds involved in the cellular response to IR can provide valuable insights into defining the limits of radioresistance in life and unveil their underlying adaptive mechanisms. Additionally, this knowledge can be utilized for biotechnological purposes by utilizing radioresistant microorganisms in the context of bioprotection and bioremediation in radioactive environments (Tkavc et al., 2018; Liu et al., 2022.). In this regard, organisms from all three domains of life have been described to express a plethora of these mechanisms, suggesting as these may have evolved independently during the evolutionary history of life. Although part of these mechanisms varies among the different taxa, they all aim to counteract the destructive effects of the chemical species produced by IR in the cells (Fig. 2) (Krisko et al., 2013).

Indeed, when IR pass through matter, it transfers energy to atoms near its path, inducing the separation of electrons from nuclei and the ionization of these. In the case of accelerated charged particles (i.e. CRs), several ionization events occur along their path through the matter, which are directly correlated with the Linear Energy Transfer (LET) of the crossing particle (Moeller et al., 2017). In turn, the LET of an accelerated ion increases with its charge. For this reason, heavy charged particles (HZE), such as iron ions, transfer higher amounts of energy per unit path length, inducing massive, clustered ionization events near their trajectories (Timoshenko and Gordeev, 2021). This phenomenon explains why HZE exposure results in higher damage than exposure to accelerated protons and α-particles. Similarly, gamma rays interacting with the atoms can cause electrons to be ejected from the nuclei through two distinct processes defined as photoionization and Compton scattering (Desouky et al., 2015; Qiao et al., 2021).

In both cases, when the crossed substrate is a biological system, the ionization events affect biological molecules and structures, leading to alterations to their chemical and structural properties (Reisz et al., 2014). Specifically, IR can cause damage to biomolecules in the cell through both direct and indirect effects (Alizadeh et al., 2015). Direct effects occur when ionizing radiation interacts directly with the target biomolecule, causing physical and chemical changes in them. Instead, indirect effects occur when ionizing radiation interacts with water molecules in the cell, producing reactive species such as hydroxyl radicals ($^{\bullet}OH$, $O_2^{\bullet}$, $^{\bullet}H$ and e_{aq}^-) and other molecular species (H_2, O_2, H_2O_2) through radiolysis (Riley, 1994). These highly reactive compounds containing oxygen are collectively called reactive oxygen species (ROS). Due to their unpaired electrons, the radicals can interact with and induce oxidative damage in a wide range of biomolecules leading to their structural and functional alteration (Pruchniak et al., 2016; Halliwell et al., 2021).

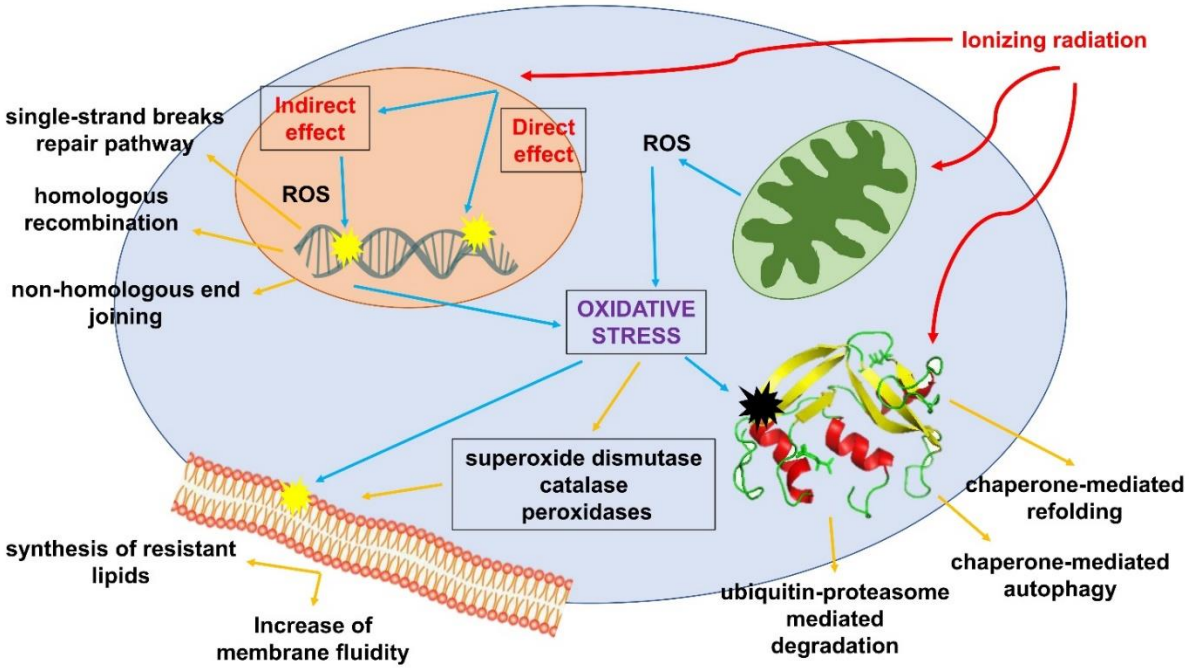

Figure 1.2. Common responses of eukaryotic cells to IR-induced oxidative damage to DNA, proteins and membrane lipids.

Therefore, all organisms have evolved defense mechanisms to counteract the oxidative stress induced by these highly reactive species on biomolecules. These mechanisms have been deeply studied in microorganisms, both prokaryotic and eukaryotic, which represent valuable tools for understanding the cellular responses to IR due to their simplicity and ease of handling (Daly, 2012; Shuryak, 2019). Among these, a plethora of studies performed on radiosensitive and radioresistant microorganisms across different taxa have shown the existence of both IR defense mechanisms ubiquitous in most species and mechanisms unique to certain radioresistant microorganisms (Jung et al., 2017). Furthermore, these findings suggest that the cellular response to IR is the result of the combined action of multiple systems of protection (Krisko and Radman, 2013).

Among the ubiquitous mechanisms of response to IR, those involved in the repair of DNA damage have been the first to be described and represent the most characterized. The most critical lesions of DNA are single- and double-strand breaks (SSB and DSB, respectively) (Shikazono et al., 2009). In eukaryotic cells, there are three main mechanisms of repair of SSB and DSB, that are the SSB repair pathway for SSB and homologous recombination (HR) and the non-homologous end joining (NHEJ) for DSB (Davis et al., 2013; Jasin and Rothstein, 2013; Mei et al., 2020). Similar mechanisms have been described in prokaryotic cells, although they are mediated by different molecular apparatus (Badrinarayanan et al., 2015; Amare et al., 2021).

Along with DNA, proteins represent another target of reactive species produced after IR exposure. The oxidation process can affect both the backbone of proteins and the residue side-chains, mainly methionine and cysteine residues (Davies, 2005). In turn, this can cause

protein misfolding, protein fragmentation or protein aggregation, making them interfere with their normal cellular processes. In bacteria, response to oxidative damage can involve the repair of protein in the cytoplasmatic and periplasmatic compartment by oxidoreductases (e.g. sulfoxide reductases) or the activation of degradation pathways such as the Clp protease system, the Lon protease system, and the FtsH protease system to eliminate damaged or misfolded proteins (Langklotz et al., 2012; Ezraty et al., 2017; He et al., 2018, Illigmann et al., 2021). Similarly, eukaryotic microbial cells can respond to oxidative damage through protein degradation by ubiquitin-proteasome systems and chaperone-mediated autophagy pathways or through protein repair by oxidoreductases or chaperone-mediated refolding (Moskovitz et al., 1997; Young et al., 2004; Yang et al., 2019; Work et al., 2020).

Additionally, the ROS generated can react with lipids, resulting in changes in membrane fluidity, disruption of membrane structure, and alterations of its permeability. The responses of prokaryotic and eukaryotic cells to lipid damage induced by IR are complex and multifaceted, involving both enzymatic (superoxide dismutase, catalase, and peroxidases) and structural adaptations (Lee et al., 2001; Spitz and Hauer-Jensen, 2014). These latter include the synthesis of specific lipids more resistant to oxidative damage, and modifications of the fatty acid composition of membranes to maintain their fluidity and integrity in the presence of oxidative stress (Ghorbal et al., 2022).

Along with the mechanisms in all microbial cells, most of the radioresistant microorganisms express a series of compounds that have been implicated in their ability to cope with IR. Among these compounds, several pigments have been demonstrated to play a key role in the radioresistance of both prokaryotic and eukaryotic cells. One such pigment is carotenoids, which are a class of orange to red pigments found ubiquitously in many extremophilic microorganisms (Maoka, 2020). Carotenoids have been shown to play a protective role against oxidative stress and ionizing radiation by scavenging reactive oxygen species and absorbing ionizing radiation (Reis-Mansur et al., 2019; Yan, 2021; Lin and Xu, 2022). Furthermore, some bacterial species, such as the radioresistant *Deinococcus radiodurans*, produce a red-pigmented molecule called deinoxanthin, which has been shown to protect against ionizing radiation by acting as an antioxidant and by absorbing ionizing radiation (Farci et al., 2016). Another ubiquitous pigment that has been related to radioresistance is melanin, a dark pigment found in some bacterial species and fungi (Cordero and Casadevall, 2017; Pavan et al., 2020). Melanin has been shown to protect cells from ionizing radiation by absorbing and dissipating the energy of ionizing radiation and by scavenging free radicals produced by ionizing radiation (Dadachova et al., 2007; Dadachova et al., 2008; Casadevall et al., 2017).

Finally, radioresistance has been associated with the presence of low molecular-weight Mn^{2+} complexes antioxidants at high concentrations inside the cells, which have been found to be effective as protectants against ionizing radiation-induced damage in both bacterial and eukaryotic cells (Sharma et al., 2017). In particular, these complexes can be involved in scavenging ROS, maintaining the redox balance within cells and protecting proteins against oxidative damage (Daly et al., 2010; Peana et al., 2016).

Noticeably, most of the mechanisms of defense against IR described in microorganisms are associated with responses to other environmental stressors (Ujaoney et al., 2017; Liu et al., 2021). Indeed, various physicochemical factors, such as desiccation, low and high temperature, saline stress, and toxic compounds can induce cell damage through oxidative stress, thereby requiring the activation of the same molecular responses observed after exposure to IR (França et al., 2007; Chattopadhyay et al., 2011; Amiraux et al., 2017; Mejía-Barajas et al., 2017). Hence, the presence of specific defense pathways and compounds in microorganisms can be involved not only in their radioresistance, but also in their capability to withstand various detrimental factors. While no study has yet been conducted to explore this perspective, the potential association between radioresistance and resistance to other environmental factors may offer valuable insights into the ecological and adaptive mechanisms underlying radioresistance in certain microorganisms.

1.3 Microbial life adaptation to ionizing radiation

Resistance to IR can vary markedly. Microorganisms capable to cope with chronic or acute doses of IR lethal for the vast majority of other organisms (i.e. radioresistant microorganisms) have been described in Archaea, Bacteria and Eukarya (Confalonieri and Sommer, 2011; Shuryak, 2019). Noticeably, these microorganisms can tolerate doses of IR significantly higher than those to which they are exposed in their natural environments, opening up questions on the evolutionary significance of such extraordinary ability. In this regard, there are various hypotheses concerning the origin of the impressive radioresistance observed in some microorganisms, such as the adaptation to periods of IR exposure during their evolutionary history or its arising as a by-product of the adaptation to other environmental stressors (Hessen, 2008; Shuryak, 2019). Additionally, radioresistant microorganisms are known to possess the capability to tolerate a variety of adverse conditions, thereby enabling them to survive in poly-extreme environments (Zu et al., 2020; Kochhar et al., 2022). Hence, the investigation of the evolutionary and genetic bases of radioresistance may be strictly related with the understanding of the general adaptation of life to extreme environments.

Regardless of its evolutionary origin, the ability of radioresistant microorganisms to withstand high doses of IR depends on the existence of various physiological and structural characteristics that are described in different taxa, thereby suggesting as they appeared independently numerous times during evolution (Pavlopoulou et al., 2016; Jung et al., 2017). From an astrobiological perspective, the existence of microorganisms capable of surviving and even flourishing in highly radioactive environments can change the perception of IR as a critical limiting factor for the persistence of life in any place, thereby changing the vision of the possible role of radioactivity in planetary habitability. Additionally, the ability of these microorganisms to produce protective primary and secondary metabolic compounds entails their biotechnological potential for space mission radioprotection and bioremediation (Vasileiou and Summerer, 2020; Berliner et al. 2021).

Previous studies have defined the resistance limits of a wide variety of microorganisms to IR both in terms of survival through D10 (the IR dose required to reduce a microbial population

by 90%) values and in terms of metabolic response to IR exposure (Dighton et al., 2008; Castillo and Smith, 2017). Among radioresistant microorganisms, *Deinococcus radiodurans* and *Rubrobacter radiotolerans*, the most radioresistant known bacteria, exhibit D10 values up to 12 and 11 kGy, respectively (Cox et al., 2005; Daly, 2009; Sukhi et al., 2009). Of these, strains of *D. radiodurans* have represented a model for the study of the molecular mechanisms mediating the resistance to IR (Daly, 2009). Noticeably, along with their radioresistance, these microorganisms exhibited the ability to endure a number of other hazardous conditions, including exposure to real space conditions on board the International Space Station (Dartnell et al., 2010; Ott at al., 2020). Previous research showed the extraordinary radioresistance of *D. radiodurans* to be mediated by the combination of active mechanisms of DNA repair and the antioxidant capacity of the cell due to ROS scavenging complexes, proteases and S-layer specific proteins (Daly et al., 2010; Farci et al., 2018; Ott et al., 2019; Narasimha and Basu, 2021). Similar defense mechanisms have been described in *R. radiotolerance* strains, showing again as they are involved in the resistance to various damaging factors (Sghaier et al., 2008; Terato et al., 2011).

Within eukaryotes, fungi exhibit the highest radioresistance. Among these, the basidiomycete *Ustilago maydis* shows a D10 of 6 kGy, whereas *Filobasidium* strains can reach a value of 7 kGy (Holliday, 2004; Singh et al., 2013). Finally, the strains of *Cryptococcus neoformans*, a melanized basidiomycete widely used as a model for studies on radiation resistance, show D10 values up to 2 kGy (Shuryak et al., 2015; Jung et al., 2016). Additionally, some fungal species (e.g. *C. neoformans*, *Cladosporium sphaerospermum*, *Cladosporium cladosporioides*, *Exophiala dermatitis*) have been observed to thrive in highly radioactive environments such as sites of nuclear accidents or nuclear waste repositories (Zhdanova et al., 2000: Zhdanova et al., 2004; Jung et al., 2016).

Previous experiments on species colonizing radioactive environments have described not only their tolerance to high levels of IR, but also the tendency to grow towards sources of IR, a phenomenon referred to as positive radiotropism (Zhdanova et al., 2001; Tugaj et al., 2003). In turn, this attraction to IR may be linked to the radiotrophisms, that is the ability to utilize IR as an energy source for growth and metabolism (Vázquez Sánchez, 2014). Again, these findings suggest a critical review of the classical concept of IR as a limiting factor for the survival and persistence of life as we know it, also requiring further investigation of the possible ecological role of IR in these microorganisms.

1.4 Black fungi as a model for radioresistance studies

Meristematic black fungi (thereafter black fungi) represent a polyphyletic group of extremophilic/extreme-tolerant fungi that share a number of physiological and morphological traits, such as meristematic growth (isodiametric cellular expansion), deeply melanized and thick cell wall, and yeast-like polar budding (Fig. 3) (Sterflinger, 2006). Although all exhibit the same features, black fungi belong to two main separate lineages, represented by the class *Eurotiomycetes*, mainly represented by the order *Chaetothyriales*, and the class *Dothideomycetes*, mainly represented by the order *Capnodiales* (Fig. 3). From an evolutionary

perspective, the physiological and morphological traits described in all members of the two lineages may represent the convergent adaptation to a range of extremely harmful physicochemical factors, such as low and high temperatures, lack of water, osmotic stress, exposure to toxic compounds, and IR (Wollenzien et al. 1995; Selbmann et al. 2005; Malo and Dadachova, 2019). In this regard, black fungi have been described to survive and flourish in a vast range of different stressing environments, including the harshest localities on our planet (Coleine et al., 2022). These include external natural and anthropized environments, such as hyperarid hot and cold deserts (e.g. Antarctic deserts), saltpans, exposed natural rocks, photocatalytic and solar panel surfaces, and the surface of monuments (Gorbushina et al., 1993; Gunde-Cimerman et al., 1998; Gunde-Cimerman et al., 2000; Ruibal et al., 2005; Plemenitaš and Gunde-Cimerman, 2005; Sterflinger et al., 2012; Isola et al., 2016; Ruibal et al., 2018; Martin-Sanchez et al., 2018; Isola et al., 2022; De Leo et al., 2022).

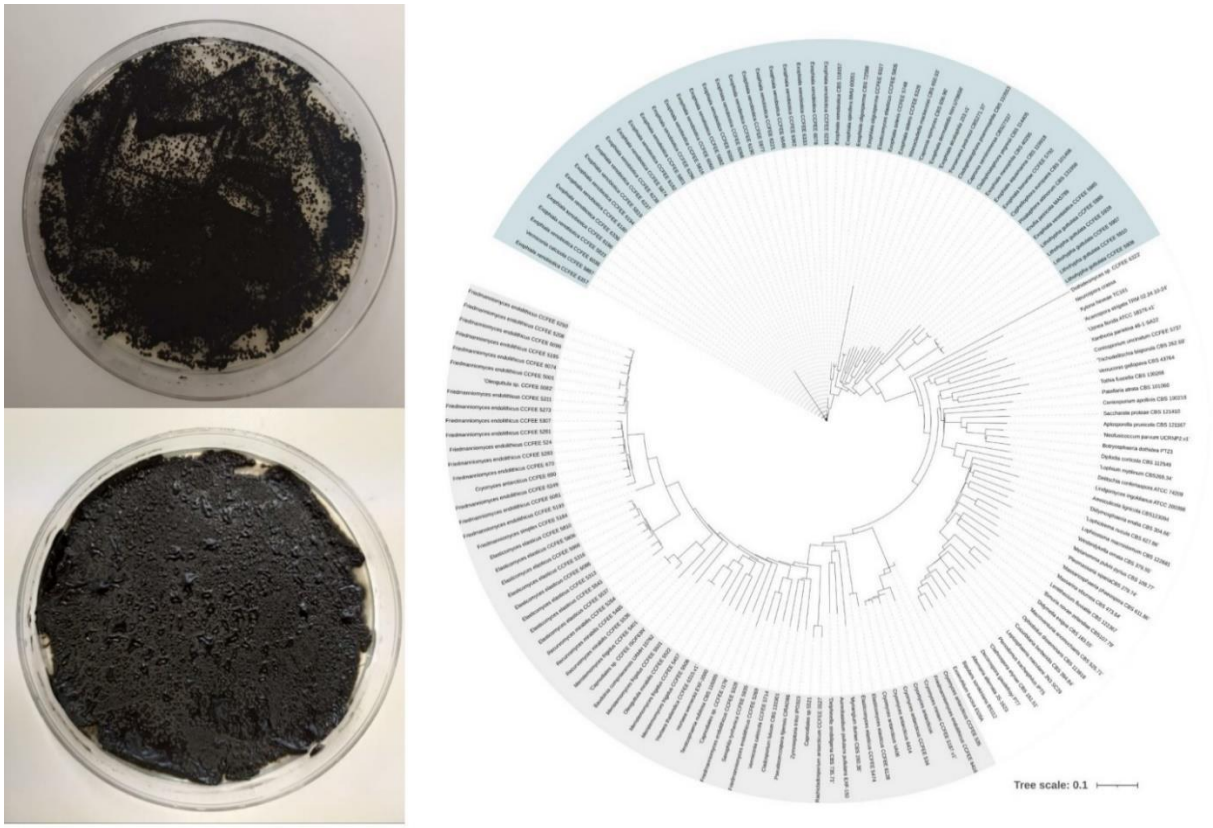

Figure 1.3. *Dothideomycetes* and *Eurotiomycetes* classes in black fungi. On the left: *Cryomyces antarcticus* MNA-CCFEE515 (on the top) and *Exophiala xenobiotica* CCFEE5810 (on the bottom) as representative members of *Dothideomycetes* and *Eurotiomycetes*, respectively. On the right: phylogenetic tree displaying the *Dothideomycetes* and *Eurotiomycetes* lineages.

They often grow in cryptoendolithic communities inside of rock porosities in most of these habitats, where they find a buffered environment and are sheltered from external hostile conditions (Selbmann et al., 2005; Coleine et al., 2021). Additionally, these fungi exhibit the extraordinary capacity to colonize anthropized close and polluted environments, such as hydrocarbon-contaminated sites, dishwashers, sauna facilities, and hospital environments

(Listemann and Freiesleben, 1996; Matos et al., 2002; Zalar et al., 2011; Isola et al., 2013; Prenafeta-Boldú et al., 2022).

Besides, members of the *Eurotiomycetes* and *Dothideomycetes* classes show a propensity to colonize distinct hostile environments, suggesting their ability to tolerate different ranges of hazardous factors (Selbmann et al., 2005; Gorbushina et al. 2018; Isola et al., 2021; Tesei, 2022; Coleine et al., 2022). *Eurotiomycetes* species are predominantly observed in human-influenced environments in temperate areas, like contaminated and polluted habitats. Conversely, *Dothideomycetes* species are predominantly detected in the most extreme natural places on Earth, such as the cold deserts of the Dry Valleys region in Antarctica, the Atacama Desert, and hot deserts. This varying tendency of individuals from the two classes to inhabit diverse environments and display different ecologies may be attributed to their distinct evolutionary histories. Indeed, phylogenetic and fossil analyses showed that the two lineages present a different evolutionary history correlated with distinct climate scenarios, thereby explaining their adaptation to various habitats (Gueidan et al., 2008, Gueidan et al., 2011). Hence, due to their capacity to survive under a broad spectrum of extreme circumstances, *Eurotiomycetes* and *Dothideomycetes* classes have been identified as some of the most extremotolerant eukaryotes on Earth.

Noticeably, a few strains of *Dothideomycetes*, namely *Cryomyces antarcticus* MNA-CCFEE515 and *Cryomyces minteri* MNA-CCFEE5187, showed the ability to endure even simulated Martian and real space conditions at the low Earth orbit on board the International Space Station, including microgravity, vacuum and IR (Onofri et al., 2012; Onofri et al., 2015; Onofri et al., 2018; Onofri et al., 2019). These findings indicate black fungi as potential models for the investigation of the outer resistance limits of life in extreme environments, such as extraterrestrial environments, and the understanding of the genetic and metabolic traits underlying these limits (Selbmann et al., 2015).

Among the extreme environmental parameters tolerated by black fungi, IR represents one of the most damaging factors encountered both in extraterrestrial and some terrestrial environments. Previous studies showed overall extraordinary radioresistance of black fungi, although they have been performed only on representative members of *Eurotiomycetes* and *Dothideomycetes* (Selbmann et al., 2011; Pacelli et al., 2018; Shuryak et al., 2019a; Aureli et al., 2020, Pacelli et al., 2020; Schultzhaus et al., 2020; Malo et al., 2021). Within *Dothideomycetes*, most of the studies concerning IR exposure have been performed on the strain *C. antarcticus* MNA-CCFEE515 (Selbmann et al., 2018). The ability of the fungus to withstand various types of radiation has been evaluated in terms of its growth ability, DNA and plasmatic membrane integrity, metabolic activity, and ultrastructural damage. When subjected to desiccated conditions, the fungus was able to tolerate α-particles (energy 150 MeV/n, LET 2.2 keV/μm) up to 1kGy, as well as high doses of gamma radiation (^{60}Co) up to 55 kGy (Pacelli et al., 2017a, 2017b). In metabolically active conditions, the fungus also displayed resistance to acute irradiation from densely and sparsely rays, deuterons (LET 40-43 keV/μm) up to 1.5 KGy and X-rays (up to 0.3 KGy), respectively (Pacelli et al., 2017c). Additionally, the fungus was capable of resisting chronic exposure to X-rays (Pacelli et al., 2018). Similarly, the strain *Friedmanniomyces endolithicus* MNA-CCFEE 5208 displayed the ability to maintain

metabolic activity after gamma rays exposure up to a dose of 0.4 kGy (Pacelli et al., 2018). Within the *Eurotiomycetes* class, *Exophiala* strains have demonstrated the capability to tolerate and respond metabolically to chronic and acute doses of gamma radiation that surpass the resistance limits of many microorganisms (Shuryak et al., 2019; Schultzhaus et al., 2020; Malo et al. 2021). However, it is important to note that their resistance levels are lower compared to the *Dothideomycetes* strains that have been tested thus far.

Altogether, these findings suggest that black fungi may be among the most radioresistant microorganisms on Earth. In this optic, studying the overall radioresistance limits of different species belonging to *Eurotiomycetes* and *Dothideomycetes*, as well as examining the ecological and physiological factors that contribute to their exceptional resistance, could potentially play a significant role in advancing knowledge in the fields of astrobiology, radioprotection and bioremediation. However, while the radioresistance of a few representative members of black fungi has been defined, the responses to IR of the major part of black fungi are still unknown to date, leaving a gap in knowledge of the overall resistance limits of the group. Similarly, only limited information concerning the possible ecological, genomic, and metabolic determinants of such extraordinary radioresistance is available to date.

1.5 Aims of the thesis and chapters description

The exceptional tolerance to different types of IR exhibited by a few strains of black fungi makes them ideal candidates for exploring the resistance limits of life in radioactive environments and the factors that may contribute to these. However, the investigation into how *Eurotiomycetes* and *Dothideomycetes* respond to IR has only focused on a small number of strains, leaving several knowledge gaps regarding the general radioresistance of the group and its drivers. Indeed, the possible differences in resistance limits occurring among different species and different strains within the group are only vaguely known to date, and any speculation on the evolutionary and genomic drivers of radioresistance in black fungi remains puzzling. In this regard, because most of the black fungi have been described in non-radioactive environments, the adaptive and ecological significance of their remarkable resistance to IR remains unknown. Similarly, how potential evolutionary drivers may have shaped the genome characteristic of black fungi towards radioresistance has been never investigated thus far. Moreover, comprehensive knowledge of the metabolic and molecular determinants of the radioresistance of black fungi is still missing. To fill this knowledge gap, this study aims to define, for the first time, the resistance limits of a vast range of strains of *Eurotiomycetes* and *Dothideomycetes* classes to different types of IR and to disentangle the genomic, lipidomic and metabolomic determinants that underlie the various radioresistance levels observed in these fungi.

The investigation is presented in the following chapters of the thesis.

In Chapter 2, entitled “Iron Ion Particle Radiation Resistance of Dried Colonies of *Cryomyces antarcticus* Embedded in Martian Regolith Analogues”, the responses of the *Dothideomycetes* strain *C. antarcticus* MNA-CCFEE515 to accelerated iron ions in dry conditions are investigated. Although their low fluxes compared with other CRs, the high

charge (26+) makes these particles one of the most damaging components of the radiation environments beyond Earth, giving them a critical astrobiological importance. Specifically, the responses of fungal colonies to the exposure to accelerated iron ions were assessed in terms of cell survival, DNA and membrane damage and metabolic activity. Besides, the possible role of three distinct types of Martian regolith in affecting the responses of exposed fungal colonies on the surface of the planet was investigated.

Similarly, Chapter 3 ("The Responses of the Black Fungus *Cryomyces antarcticus* to High Doses of Accelerated Helium Ions Radiation within Martian Regolith Simulants and their Relevance for Mars") focuses on the responses of *C. antarcticus* MNA-CCFEE515 to α-particles exposure in dry conditions. Unlike accelerated iron ions, α-particles (i.e. accelerated helium ions) display a lower LET, which entails lower biological effectiveness and a higher penetration power in the matter. Furthermore, the high fluxes recorded for these particles (12% of the CR spectrum) make them another critical component of the radiation environment experienced beyond Earth. Again, the ability of rehydrated colonies of the fungus to endure α-particle exposure was assessed in terms of cell survival, DNA and membrane damage and metabolic activity. Additionally, the study investigated how the presence of three different types of Martian regolith may influence the responses of desiccated fungal colonies to this type of CRs.

Once demonstrated the capacity of *C. antarcticus* MNA-CCFEE515 to survive the exposure to part of the CR spectrum encountered beyond Earth, the research aimed to define the overall radioresistance limits of black fungi through the study of the broadest set of strains of black fungi ever tested before (Chapter 4, "Geography and environmental pressure are predictive of class-specific radioresistance in black fungi"). To reach this goal, the survival limits of 101 strains from *Eurotiomycetes* and *Dothideomycetes* species to exposure to gamma radiation were assessed. The strains were isolated from extreme (mainly Antarctica) and mild regions, to examine black fungi exhibiting different evolutionary histories and adapted to distinct environmental conditions. Additionally, the study focused, for the first time, on the understanding of the taxonomical and ecological factors associated with the radioresistance of these microorganisms, providing valuable insights into the investigation of the adaptation of life in extreme environments.

Once defined the ecological bases of the radioresistance in black fungi, the present research focused on the genomic determinants of this, as described in Chapter 5, entitled "Multiple genomic factors underlie the radioresistance of black fungi and its connection to other phenotypic traits". The chapter shows our preliminary results of a genomic comparative study on 95 strains of black fungi exhibiting different resistance to IR and ecologies was assessed through different statistical and analytical approaches. In addition to providing information on the possible genomic bases of the radioresistance, the study gives new insights into how selective pressure experienced in the extreme environments where black fungi thrive can shape genomic features that result in varying degrees of radioresistance.

References

Ackermann, M., Ajello, M., Albert, A., Allafort, A., Baldini, L., Barbiellini, G., ... & Yang, Z. (2014). High-energy gamma-ray emission from solar flares: Summary of Fermi large area telescope detections and analysis of two M-class flares. The Astrophysical Journal, 787(1), 15.

Aharonian, F. A. (2013). Gamma rays from supernova remnants. Astroparticle Physics, 43, 71-80.

Alizadeh, E., Orlando, T. M., & Sanche, L. (2015). Biomolecular damage induced by ionizing radiation: the direct and indirect effects of low-energy electrons on DNA. Annual review of physical chemistry, 66, 379-398.

Amare, B., Mo, A., Khan, N., Sowa, D. J., Warner, M. M., Tetenych, A., & Andres, S. N. (2021). LigD: a structural guide to the multi-tool of bacterial non-homologous end joining. Frontiers in Molecular Biosciences, 8, 787709.

Amiraux, R., Belt, S. T., Vaultier, F., Galindo, V., Gosselin, M., Bonin, P., & Rontani, J. F. (2017). Monitoring photo-oxidative and salinity-induced bacterial stress in the Canadian Arctic using specific lipid tracers. Marine Chemistry, 194, 89-99.

Anastasiadis, A., Lario, D., Papaioannou, A., Kouloumvakos, A., & Vourlidas, A. (2019). Solar energetic particles in the inner heliosphere: status and open questions. Philosophical Transactions of the Royal Society A, 377(2148), 20180100.

Badrinarayanan, A., Le, T. B., & Laub, M. T. (2015). Rapid pairing and resegregation of distant homologous loci enables double-strand break repair in bacteria. Journal of Cell Biology, 210(3), 385-400.

Banfield, D., Spiga, A., Newman, C., Forget, F., Lemmon, M., Lorenz, R., ... & Banerdt, W. B. (2020). The atmosphere of Mars as observed by InSight. Nature Geoscience, 13(3), 190-198.

Bartoli, B., Bernardini, P., Bi, X. J., Cao, Z., Catalanotti, S., Chen, S. Z., ... & ARGO-YBJ Collaboration. (2019). Search for gamma-ray emission from the Sun during solar minimum with the ARGO-YBJ experiment. The Astrophysical Journal, 872(2), 143.

Ben Ghorbal, S., Werhani, R., & Abdelwaheb, C. (2022). Effects of certain physical stresses on the composition of the membrane of bacteria implicated in food and environmental contamination. International Journal of Environmental Health Research, 1-11.

Berliner, A. J., Hilzinger, J. M., Abel, A. J., McNulty, M. J., Makrygiorgos, G., Averesch, N. J., ... & Arkin, A. P. (2021). Towards a biomanufactory on Mars. Frontiers in Astronomy and Space Sciences, 8, 711550.

Bronarska, K., Wheatland, M. S., Gopalswamy, N., & Michalek, G. (2018). Very narrow coronal mass ejections producing solar energetic particles. Astronomy & Astrophysics, 619, A34.

Bütikofer, R. (2018). Cosmic ray particle transport in the Earth's magnetosphere. Solar Particle Radiation Storms Forecasting and Analysis: The HESPERIA HORIZON 2020 Project and Beyond, 79-94.

Casadevall, A., Cordero, R. J., Bryan, R., Nosanchuk, J., & Dadachova, E. (2017). Melanin, radiation, and energy transduction in fungi. Microbiology spectrum, 5(2), 5-2.

Castillo, H., & Smith, G. B. (2017). Below-background ionizing radiation as an environmental cue for bacteria. Frontiers in Microbiology, 8, 177.

Chancellor, J. C., Scott, G. B., & Sutton, J. P. (2014). Space radiation: the number one risk to astronaut health beyond low earth orbit. Life, 4(3), 491-510.

Chattopadhyay, M. K., Raghu, G., Sharma, Y. V. R. K., Biju, A. R., Rajasekharan, M. V., & Shivaji, S. (2011). Increase in oxidative stress at low temperature in an Antarctic bacterium. Current microbiology, 62, 544-546.

Chen, J. L., Yun, S. J., Dong, T. K., Ren, Z. Z., & Zhang, X. P. (2022). Studies of the radiation environment on the Mars surface using the Geant4 toolkit. Nuclear Science and Techniques, 33(1), 11.

Coleine, C., Stajich, J. E., & Selbmann, L. (2022). Fungi are key players in extreme ecosystems. Trends in Ecology & Evolution.

Coleine, C., Stajich, J. E., de Los Ríos, A., & Selbmann, L. (2021). Beyond the extremes: Rocks as ultimate refuge for fungi in drylands. Mycologia, 113(1), 108-133.

Confalonieri, F., & Sommer, S. (2011). Bacterial and archaeal resistance to ionizing radiation. In Journal of Physics: Conference Series (Vol. 261, No. 1, p. 012005). IOP Publishing.

Cordero, R. J., & Casadevall, A. (2017). Functions of fungal melanin beyond virulence. Fungal Biology Reviews, 31(2), 99-112.

Da Pieve, F., Gronoff, G., Guo, J., Mertens, C. J., Neary, L., Gu, B., ... & Cleri, F. (2021). Radiation environment and doses on mars at oxia planum and mawrth vallis: Support for exploration at sites with high biosignature preservation potential. Journal of Geophysical Research: Planets, 126(1), e2020JE006488.

Dadachova, E., & Casadevall, A. (2008). Ionizing radiation: how fungi cope, adapt, and exploit with the help of melanin. Current opinion in microbiology, 11(6), 525-531.

Dadachova, E., Bryan, R. A., Huang, X., Moadel, T., Schweitzer, A. D., Aisen, P., ... & Casadevall, A. (2007). Ionizing radiation changes the electronic properties of melanin and enhances the growth of melanized fungi. PloS one, 2(5), e457.

Daly, M. J. (2012). Death by protein damage in irradiated cells. DNA repair, 11(1), 12-21.

Daly, M. J., Gaidamakova, E. K., Matrosova, V. Y., Kiang, J. G., Fukumoto, R., Lee, D. Y., ... & Levine, R. L. (2010). Small-molecule antioxidant proteome-shields in Deinococcus radiodurans. PloS one, 5(9), e12570.

Daly, M. J., Gaidamakova, E. K., Matrosova, V. Y., Kiang, J. G., Fukumoto, R., Lee, D. Y., ... & Levine, R. L. (2010). Small-molecule antioxidant proteome-shields in Deinococcus radiodurans. PloS one, 5(9), e12570.

Dartnell, L. R., Desorgher, L., Ward, J. M., & Coates, A. J. (2007). Martian sub-surface ionising radiation: biosignatures and geology. Biogeosciences, 4(4), 545-558.

Dartnell, L. R., Hunter, S. J., Lovell, K. V., Coates, A. J., & Ward, J. M. (2010). Low-temperature ionizing radiation resistance of Deinococcus radiodurans and Antarctic Dry Valley bacteria. Astrobiology, 10(7), 717-732.

Davis, A. J., & Chen, D. J. (2013). DNA double strand break repair via non-homologous end-joining. Transl cancer res, 2(3), 130-143.

De Leo, F., Marchetta, A., & Urzì, C. (2022). Black fungi on stone-built heritage: current knowledge and future outlook. Applied Sciences, 12(8), 3969.

Desouky, O., Ding, N., & Zhou, G. (2015). Targeted and non-targeted effects of ionizing radiation. Journal of Radiation Research and Applied Sciences, 8(2), 247-254.

Dighton, J., Tugay, T., & Zhdanova, N. (2008). Fungi and ionizing radiation from radionuclides. FEMS microbiology letters, 281(2), 109-120.

Ezraty, B., Gennaris, A., Barras, F., & Collet, J. F. (2017). Oxidative stress, protein damage and repair in bacteria. Nature Reviews Microbiology, 15(7), 385-396.

Farci, D., Slavov, C., & Piano, D. (2018). Coexisting properties of thermostability and ultraviolet radiation resistance in the main S-layer complex of Deinococcus radiodurans. Photochemical & Photobiological Sciences, 17, 81-88.

Farci, D., Slavov, C., Tramontano, E., & Piano, D. (2016). The S-layer protein DR_2577 binds deinoxanthin and under desiccation conditions protects against UV-radiation in Deinococcus radiodurans. Frontiers in microbiology, 7, 155.

França, M. B., Panek, A. D., & Eleutherio, E. C. A. (2007). Oxidative stress and its effects during dehydration. Comparative Biochemistry and Physiology Part A: Molecular & Integrative Physiology, 146(4), 621-631.

Geophysical Research: Planets, 109(E2).

Gorbushina, A. A., Krumbein, W. E., Hamman, C. H., Panina, L. K. S. S., Soukharjevski, S., & Wollenzien, U. (1993). Role of black fungi in color change and biodeterioration of antique marbles. Geomicrobiology Journal, 11(3-4), 205-221.

Gostinčar, C., Stajich, J. E., Kejžar, A., Sinha, S., Nislow, C., Lenassi, M., & Gunde-Cimerman, N. (2021). Seven years at high salinity—experimental evolution of the extremely halotolerant black yeast Hortaea werneckii. Journal of fungi, 7(9), 723.

Gueidan, C., Ruibal, C., De Hoog, G. S., & Schneider, H. (2011). Rock-inhabiting fungi originated during periods of dry climate in the late Devonian and middle Triassic. Fungal biology, 115(10), 987-996.

Gueidan, C., Villaseñor, C. R., De Hoog, G. S., Gorbushina, A. A., Untereiner, W. A., & Lutzoni, F. (2008). A rock-inhabiting ancestor for mutualistic and pathogen-rich fungal lineages. Studies in Mycology, 61(1), 111-119.

Gunde-Cimerman, N., Zalar, P., & Hoog, G. S. (1998). Black yeas-like fungi isolated from hypersaline waters of the Seca saltpans. In 2nd Congress of Slovenian Microbiologists with International Participation, Portoroz (Slovenia), 27-30 Sep 1998.

Gunde-Cimerman, N., Zalar, P., de Hoog, S., & Plemenitaš, A. (2000). Hypersaline waters in salterns–natural ecological niches for halophilic black yeasts. FEMS Microbiology Ecology, 32(3), 235-240.

Halliwell, B., Adhikary, A., Dingfelder, M., & Dizdaroglu, M. (2021). Hydroxyl radical is a significant player in oxidative DNA damage in vivo. Chemical Society Reviews, 50(15), 8355-8360.

Hassler, D. M., Zeitlin, C., Wimmer-Schweingruber, R. F., Ehresmann, B., Rafkin, S., Eigenbrode, J. L., ... & Berger, G. (2014). Mars' surface radiation environment measured with the Mars Science Laboratory's Curiosity rover. science, 343(6169), 1244797.

He, L., Luo, D., Yang, F., Li, C., Zhang, X., Deng, H., & Zhang, J. R. (2018). Multiple domains of bacterial and human Lon proteases define substrate selectivity. Emerging Microbes & Infections, 7(1), 1-18.

Hessen, D. O. (2008). Solar radiation and the evolution of life. Solar radiation and human health, 123-

Hu, J., Airapetian, V. S., Li, G., Zank, G., & Jin, M. (2022). Extreme energetic particle events by superflare-associated CMEs from solar-like stars. Science Advances, 8(12), eabi9743.

Hu, Q. H., Weng, J. Q., & Wang, J. S. (2010). Sources of anthropogenic radionuclides in the environment: a review. Journal of environmental radioactivity, 101(6), 426-437.

Ichimiya, T., Narita, T., & Kitao, K. (1998). Natural background gamma-ray spectrum. List of gamma-rays ordered in energy from natural radionuclides.

Illigmann, A., Thoma, Y., Pan, S., Reinhardt, L., & Brötz-Oesterhelt, H. (2021). Contribution of the Clp protease to bacterial survival and mitochondrial homoeostasis. Microbial Physiology, 31(3), 260-279.

Isola, D., Bartoli, F., Meloni, P., Caneva, G., & Zucconi, L. (2022). Black fungi and stone heritage conservation: Ecological and metabolic assays for evaluating colonization potential and responses to traditional biocides. Applied Sciences, 12(4), 2038.

Isola, D., Scano, A., Orrù, G., Prenafeta-Boldú, F. X., & Zucconi, L. (2021). Hydrocarbon-contaminated sites: Is there something more than Exophiala xenobiotica? New insights into black fungal diversity using the long cold incubation method. Journal of Fungi, 7(10), 817.

Isola, D., Selbmann, L., de Hoog, G. S., Fenice, M., Onofri, S., Prenafeta-Boldú, F. X., & Zucconi, L. (2013). Isolation and screening of black fungi as degraders of volatile aromatic hydrocarbons. Mycopathologia, 175, 369-379.

Isola, D., Zucconi, L., Onofri, S., Caneva, G., De Hoog, G. S., & Selbmann, L. (2016). Extremotolerant rock inhabiting black fungi from Italian monumental sites. Fungal Diversity, 76, 75-96.

Jasin, M., & Rothstein, R. (2013). Repair of strand breaks by homologous recombination. Cold Spring Harbor perspectives in biology, 5(11), a012740.

Jóhannesson, G., Porter, T. A., & Moskalenko, I. V. (2018). The three-dimensional spatial distribution of interstellar gas in the milky way: implications for cosmic rays and high-energy gamma-ray emissions. The Astrophysical Journal, 856(1), 45.

Johnson, C. L., Mittelholz, A., Langlais, B., Russell, C. T., Ansan, V., Banfield, D., ... & Banerdt, W. B. (2020). Crustal and time-varying magnetic fields at the InSight landing site on Mars. Nature Geoscience, 13(3), 199-204.

Jung, K. W., Lim, S., & Bahn, Y. S. (2017). Microbial radiation-resistance mechanisms. Journal of Microbiology, 55, 499-507.

Jung, K. W., Yang, D. H., Kim, M. K., Seo, H. S., Lim, S., & Bahn, Y. S. (2016). Unraveling fungal radiation resistance regulatory networks through the genome-wide transcriptome and genetic analyses of Cryptococcus neoformans. MBio, 7(6), e01483-16.

Krisko, A., & Radman, M. (2013). Biology of extreme radiation resistance: the way of Deinococcus radiodurans. Cold Spring Harbor perspectives in biology, 5(7), a012765.

Kumar, M., Kochhar, N., Kavya, I. K., Shrivastava, S., Ghosh, A., Rawat, V. S., & Sodhi, K. K. (2022). Perspectives on the microorganism of extreme environments and their applications. Current Research in Microbial Sciences, 100134.

Langklotz, S., Baumann, U., & Narberhaus, F. (2012). Structure and function of the bacterial AAA protease FtsH. Biochimica Et Biophysica Acta (BBA)-Molecular Cell Research, 1823(1), 40-48.

Langlais, B., Purucker, M. E., & Mandea, M. (2004). Crustal magnetic field of Mars. Journal of

Lee, J. H., Choi, I. Y., Kil, I. S., Kim, S. Y., Yang, E. S., & Park, J. W. (2001). Protective role of superoxide dismutases against ionizing radiation in yeast. Biochimica et Biophysica Acta (BBA)-General Subjects, 1526(2), 191-198.

Lin, L., & Xu, J. (2022). Production of Fungal Pigments: Molecular Processes and Their Applications. Journal of Fungi, 9(1), 44.

Linden, T., Zhou, B., Beacom, J. F., Peter, A. H., Ng, K. C., & Tang, Q. W. (2018). Evidence for a new component of high-energy solar gamma-ray production. Physical review letters, 121(13), 131103.

Listemann, H., & Freiesleben, H. (1996). Exophiala mesophila spec. nov. Exophiala mesophila spec. nov. Mycoses, 39(1-2), 1-3.

Liu, R., Meng, X., Mo, C., Wei, X., & Ma, A. (2022). Melanin of fungi: From classification to application. World Journal of Microbiology and Biotechnology, 38(12), 228.

Liu, Y., Zhang, C., Wang, Z., Lin, M., Wang, J., & Wu, M. (2021). Pleiotropic roles of late embryogenesis abundant proteins of Deinococcus radiodurans against oxidation and desiccation. Computational and Structural Biotechnology Journal, 19, 3407-3415.

MacKinnon, A., Szpigel, S., Gimenez de Castro, G., & Tuneu, J. (2020). FLUKA simulations of pion decay gamma-radiation from energetic flare ions. Solar Physics, 295(12), 174.

Malo, M. E., & Dadachova, E. (2019). Melanin as an energy transducer and a radioprotector in black fungi. Fungi in extreme environments: ecological role and biotechnological significance, 175-184.

Malo, M. E., Schultzhaus, Z., Frank, C., Romsdahl, J., Wang, Z., & Dadachova, E. (2021). Transcriptomic and genomic changes associated with radioadaptation in Exophiala dermatitidis. Computational and Structural Biotechnology Journal, 19, 196-205.

Maoka, T. (2020). Carotenoids as natural functional pigments. Journal of natural medicines, 74(1), 1-16.

Martin-Sanchez, P. M., Gebhardt, C., Toepel, J., Barry, J., Munzke, N., Günster, J., & Gorbushina, A. A. (2018). Monitoring microbial soiling in photovoltaic systems: A qPCR-based approach. International Biodeterioration & Biodegradation, 129, 13-22.

Matos, T., De Hoog, G. S., De Boer, A. G., De Crom, I., & Haase, G. (2002). High prevalence of the neurotrope Exophiala dermatitidis and related oligotrophic black yeasts in sauna facilities. mycoses, 45(9-10), 373-377.

Mei, C., Lei, L., Tan, L. M., Xu, X. J., He, B. M., Luo, C., ... & Liu, Z. Q. (2020). The role of single strand break repair pathways in cellular responses to camptothecin induced DNA damage. Biomedicine & Pharmacotherapy, 125, 109875.

Mejía-Barajas, J. A., Montoya-Pérez, R., Salgado-Garciglia, R., Aguilera-Aguirre, L., Cortés-Rojo, C., Mejía-Zepeda, R., ... & Saavedra-Molina, A. (2017). Oxidative stress and antioxidant response in a thermotolerant yeast. brazilian journal of microbiology, 48, 326-332.

Mitrofanov, I. G., Litvak, M. L., Sanin, A. B., Anikin, A. A., Mokrousov, M. I., Golovin, D. V., ... & Shvetsov, V. N. (2022). Laboratory demonstration of space gamma-ray spectroscopy experiment with tags of Galactic cosmic rays for testing different types of Martian regolith. Nuclear Instruments and Methods in Physics Research Section A: Accelerators, Spectrometers, Detectors and Associated Equipment, 1028, 166364.

Moeller, R., Raguse, M., Leuko, S., Berger, T., Hellweg, C. E., Fujimori, A., ... & STARLIFE Research Group. (2017). STARLIFE—An international campaign to study the role of galactic cosmic radiation in astrobiological model systems. Astrobiology, 17(2), 101-109.

Moskovitz, J., Berlett, B. S., Poston, J. M., & Stadtman, E. R. (1997). The yeast peptide-methionine sulfoxide reductase functions as an antioxidant in vivo. Proceedings of the National Academy of Sciences, 94(18), 9585-9589.

Murgia, M., Fiamma, M., Barac, A., Deligios, M., Mazzarello, V., Paglietti, B., ... & Al-Ahdal, M. N. (2019). Biodiversity of fungi in hot desert sands. MicrobiologyOpen, 8(1), e00595.

Narasimha, A., & Basu, B. (2021). New insights into the activation of radiation desiccation response regulon in Deinococcus radiodurans. Journal of Biosciences, 46, 1-16.

Onofri, S., de la Torre, R., de Vera, J. P., Ott, S., Zucconi, L., Selbmann, L., ... & Horneck, G. (2012). Survival of rock-colonizing organisms after 1.5 years in outer space. Astrobiology, 12(5), 508-516.

Onofri, S., de Vera, J. P., Zucconi, L., Selbmann, L., Scalzi, G., Venkateswaran, K. J., ... & Horneck, G. (2015). Survival of Antarctic cryptoendolithic fungi in simulated Martian conditions on board the International Space Station. Astrobiology, 15(12), 1052-1059.

Onofri, S., Selbmann, L., Pacelli, C., De Vera, J. P., Horneck, G., Hallsworth, J. E., & Zucconi, L. (2018). Integrity of the DNA and cellular ultrastructure of cryptoendolithic fungi in space or Mars conditions: a 1.5-year study at the International Space Station. Life, 8(2), 23.

Onofri, S., Selbmann, L., Pacelli, C., Zucconi, L., Rabbow, E., & de Vera, J. P. (2019). Survival, DNA, and ultrastructural integrity of a cryptoendolithic Antarctic fungus in Mars and Lunar rock analogs exposed outside the International Space Station. Astrobiology, 19(2), 170-182.

Orlando, E., & Strong, A. W. (2007). Gamma rays from halos around stars and the Sun. In The Multi-Messenger Approach to High-Energy Gamma-Ray Sources (pp. 359-363). Springer Netherlands.

O'sullivan, D. (2007). Exposure to galactic cosmic radiation and solar energetic particles. Radiation protection dosimetry, 125(1-4), 407-411.

Ott, E., Kawaguchi, Y., Özgen, N., Yamagishi, A., Rabbow, E., Rettberg, P., ... & Milojevic, T. (2019). Proteomic and metabolomic profiling of Deinococcus radiodurans recovering after exposure to simulated low earth orbit vacuum conditions. Frontiers in microbiology, 10, 909.

Parker, E. N. (1965). The passage of energetic charged particles through interplanetary space. Planetary and Space Science, 13(1), 9-49.

Pavan, M. E., López, N. I., & Pettinari, M. J. (2020). Melanin biosynthesis in bacteria, regulation and production perspectives. Applied Microbiology and Biotechnology, 104, 1357-1370.

Pavlopoulou, A., Savva, G. D., Louka, M., Bagos, P. G., Vorgias, C. E., Michalopoulos, I., & Georgakilas, A. G. (2016). Unraveling the mechanisms of extreme radioresistance in prokaryotes: lessons from nature. Mutation Research/Reviews in Mutation Research, 767, 92-107.

Peana, M., Medici, S., Pangburn, H. A., Lamkin, T. J., Ostrowska, M., Gumienna-Kontecka, E., & Zoroddu, M. A. (2016). Manganese binding to antioxidant peptides involved in extreme radiation resistance in Deinococcus radiodurans. Journal of inorganic biochemistry, 164, 49-58.

Plemenitaš, A., & Gunde-Cimerman, N. (2005). Cellular responses in the halophilic black yeast Hortaea werneckii to high environmental salinity (pp. 453-470). Springer Netherlands.

Prenafeta-Boldú, F. X., Medina-Armijo, C., & Isola, D. (2022). Black fungi in the built environment—The good, the bad, and the ugly. In Viruses, Bacteria and Fungi in the Built Environment (pp. 65-99). Woodhead Publishing.

Pruchniak, M. P., Araźna, M., & Demkow, U. (2016). Biochemistry of oxidative stress. Advances in Clinical Science, 9-19.

Qiao, C. K., Wei, J. W., & Chen, L. (2021). An overview of the Compton scattering calculation. Crystals, 11(5), 525.

Rahmanifard, F., de Wet, W. C., Schwadron, N. A., Owens, M. J., Jordan, A. P., Wilson, J. K., ... & Townsend, L. W. (2020). Galactic cosmic radiation in the interplanetary space through a modern secular minimum. Space Weather, 18(9), e2019SW002428.

Reis-Mansur, M. C. P., Cardoso-Rurr, J. S., Silva, J. V., de Souza, G. R., Cardoso, V. D. S., Mansoldo, F. R. P., ... & Vermelho, A. B. (2019). Carotenoids from UV-resistant Antarctic Microbacterium sp. LEMMJ01. Scientific reports, 9(1), 1-14.

Reisz, Julie A., et al. "Effects of ionizing radiation on biological molecules—mechanisms of damage and emerging methods of detection." Antioxidants & redox signaling 21.2 (2014): 260-292.

Riley, P. A. (1994). Free radicals in biology: oxidative stress and the effects of ionizing radiation. International journal of radiation biology, 65(1), 27-33.

Ross, E., & Chaplin, W. J. (2019). The behaviour of galactic cosmic-ray intensity during solar activity cycle 24. Solar physics, 294, 1-17.

Röstel, L., Guo, J., Banjac, S., Wimmer-Schweingruber, R. F., & Heber, B. (2020). Subsurface radiation environment of Mars and its implication for shielding protection of future habitats. Journal of Geophysical Research: Planets, 125(3), e2019JE006246.

Ruibal, C., Platas, G., & Bills, G. F. (2005). Isolation and characterization of melanized fungi from limestone formations in Mallorca. Mycological Progress, 4, 23-38.

Ruibal, C., Selbmann, L., Avci, S., Martin-Sanchez, P. M., & Gorbushina, A. A. (2018). Roof-inhabiting cousins of rock-inhabiting fungi: novel melanized microcolonial fungal species from photocatalytically reactive subaerial surfaces. Life, 8(3), 30.

Schultzhaus, Z., Romsdahl, J., Chen, A., Tschirhart, T., Kim, S., Leary, D., & Wang, Z. (2020). The response of the melanized yeast Exophiala dermatitidis to gamma radiation exposure. Environmental microbiology, 22(4), 1310-1326.

Selbmann, L., Pacelli, C., Zucconi, L., Dadachova, E., Moeller, R., de Vera, J. P., & Onofri, S. (2018). Resistance of an Antarctic cryptoendolithic black fungus to radiation gives new insights of astrobiological relevance. Fungal biology, 122(6), 546-554.

Selbmann, L., Zucconi, L., Isola, D., & Onofri, S. (2015). Rock black fungi: excellence in the extremes, from the Antarctic to space. Current Genetics, 61, 335-345.

Sghaier, H., Ghedira, K., Benkahla, A., & Barkallah, I. (2008). Basal DNA repair machinery is subject to positive selection in ionizing-radiation-resistant bacteria. BMC genomics, 9(1), 1-7.

Sharma, A., Gaidamakova, E. K., Grichenko, O., Matrosova, V. Y., Hoeke, V., Klimenkova, P., ... & Daly, M. J. (2017). Across the tree of life, radiation resistance is governed by antioxidant Mn2+, gauged by paramagnetic resonance. Proceedings of the National Academy of Sciences, 114(44), E9253-E9260.

Shikazono, N., Noguchi, M., Fujii, K., Urushibara, A., & Yokoya, A. (2009). The yield, processing, and biological consequences of clustered DNA damage induced by ionizing radiation. Journal of radiation research, 50(1), 27-36.

Shuryak, I. (2019). Review of microbial resistance to chronic ionizing radiation exposure under environmental conditions. Journal of environmental radioactivity, 196, 50-63.

Shuryak, I., Tkavc, R., Matrosova, V. Y., Volpe, R. P., Grichenko, O., Klimenkova, P., ... & Daly, M. J. (2019). Chronic gamma radiation resistance in fungi correlates with resistance to chromium and elevated temperatures, but not with resistance to acute irradiation. Scientific reports, 9(1), 11361.

Sihver, L., & Mortazavi, S. M. J. (2021). Biological protection in deep space missions. Journal of Biomedical Physics & Engineering, 11(6), 663.

Singh, A. K., Siingh, D., & Singh, R. P. (2011). Impact of galactic cosmic rays on Earth's atmosphere and human health. Atmospheric Environment, 45(23), 3806-3818.

Spitz, D. R., & Hauer-Jensen, M. (2014). Ionizing radiation-induced responses: where free radical chemistry meets redox biology and medicine. Antioxidants & redox signaling, 20(9), 1407-1409.

Sterflinger, K. (2006). Black yeasts and meristematic fungi: ecology, diversity and identification. Biodiversity and ecophysiology of yeasts, 501-514.

Sterflinger, K., Tesei, D., & Zakharova, K. (2012). Fungi in hot and cold deserts with particular reference to microcolonial fungi. Fungal ecology, 5(4), 453-462.

Terato, H., Suzuki, K., Nishioka, N., Okamoto, A., Shimazaki-Tokuyama, Y., Inoue, Y., & Saito, T. (2011). Characterization and radio-resistant function of manganese superoxide dismutase of Rubrobacter radiotolerans. Journal of radiation research, 52(6), 735-742.

Timoshenko, G. N., & Gordeev, I. S. (2021). Computation of linear energy transfer of space radiation in biological tissue analog. Planetary and Space Science, 199, 105190.

Tkavc, R., Matrosova, V. Y., Grichenko, O. E., Gostinčar, C., Volpe, R. P., Klimenkova, P., ... & Daly, M. J. (2018). Prospects for fungal bioremediation of acidic radioactive waste sites: characterization and genome sequence of Rhodotorula taiwanensis MD1149. Frontiers in microbiology, 8, 2528.

Tugaj, T. I., Zhdanova, N. N., Redchits, T. I., Zheltonozhskij, V. A., & Sadovnikov, L. V. (2003). Influence of low level ionizing irradiation on spread of positive radiotropism among fungi. Zbyirnik naukovikh prats' Yinstitutu Yadernikh Doslyidzhen', 72-79.

Turner, R. E., Farrier, T. A., Mazur, J. E., Walterscheid, R. L., & Seibold, R. W. (2008). Space weather biological and systems effects for suborbital flights (No. ATR-2009 (5390)-1). Aerospace Corporation.

Ujaoney, A. K., Padwal, M. K., & Basu, B. (2017). Proteome dynamics during post-desiccation recovery reveal convergence of desiccation and gamma radiation stress response pathways in Deinococcus radiodurans. Biochimica et Biophysica Acta (BBA)-Proteins and Proteomics, 1865(9), 1215-1226.

Vandana, U. K., Gulzar, A. B. M., Laskar, I. H., Meitei, L. R., & Mazumder, P. B. (2021). Role of microbes in bioremediation of radioactive waste. Microbial Rejuvenation of Polluted Environment: Volume 1, 329-352.

Vasileiou, T., & Summerer, L. (2020). A biomimetic approach to shielding from ionizing radiation: the case of melanized fungi. PLoS One, 15(4), e0229921.

Vázquez Sánchez, D. A. (2014). Black radiotrophic fungi: adaptation and exploitation of ionizing radiation and potential applications.

Walencik-Łata, A., Szkliniarz, K., Kisiel, J., Polaczek-Grelik, K., Jędrzejczak, K., Kasztelan, M., ... & Fuławka, K. (2022). Characteristics of Natural Background Radiation in the GIG Experimental Mine 'Barbara', Poland. Energies, 15(3), 685.

Wollenzien, U., De Hoog, G. S., Krumbein, W. E., & Urzi, C. (1995). On the isolation of microcolonial fungi occurring on and in marble and other calcareous rocks. Science of the total Environment, 167(1-3), 287-294.

Work, J. J., & Brandman, O. (2020). Adaptability of the ubiquitin-proteasome system to proteolytic and folding stressors. Journal of Cell Biology, 220(3), e201912041.

Yang, Q. (2021). Crucial roles of carotenoids as bacterial endogenous defense system for bacterial radioresistance of Deinococcus radiodurans. bioRxiv, 2021-05.

Yang, Q., Wang, R., & Zhu, L. (2019). Chaperone-mediated autophagy. Autophagy: Biology and Diseases: Basic Science, 435-452.

Young, J. C., Agashe, V. R., Siegers, K., & Hartl, F. U. (2004). Pathways of chaperone-mediated protein folding in the cytosol. Nature reviews Molecular cell biology, 5(10), 781-791.

Zalar, P., Novak, M., de Hoog, G. S., & Gunde-Cimerman, N. (2011). Dishwashers–a man-made ecological niche accommodating human opportunistic fungal pathogens. Fungal biology, 115(10), 997-1007.

Zhdanova, N. N., Tugay, T., Dighton, J., Zheltonozhsky, V., & Mcdermott, P. (2004). Ionizing radiation attracts soil fungi. Mycological research, 108(9), 1089-1096.

Zhdanova, N. N., Zakharchenko, V. A., Vember, V. V., & Nakonechnaya, L. T. (2000). Fungi from Chernobyl: mycobiota of the inner regions of the containment structures of the damaged nuclear reactor. Mycological Research, 104(12), 1421-1426.

Zhdanova, N., Fomina, M., Redchitz, T., & Olsson, S. (2001). Chernobyl effect: growth characteristics of soil fungi Cladosporium cladosporioides [Fresen] de Vries with and without positive radiotropism. Polish Journal of Ecology, 49(4).

Zhu, D., Adebisi, W. A., Ahmad, F., Sethupathy, S., Danso, B., & Sun, J. (2020). Recent development of extremophilic bacteria and their application in biorefinery. Frontiers in Bioengineering and Biotechnology, 483.

Chapter 2

Iron ion particle radiation resistance of dried colonies of *Cryomyces antarcticus* embedded in Martian regolith analogues

Lorenzo Aureli[1], Claudia Pacelli[1,2*], Alessia Cassaro[1], Akira Fujimori[3], Ralf Moeller[4,5], and Silvano Onofri[1]

[1]Department of Ecological and Biological Sciences, University of Tuscia, Largo dell'Università snc, 01100, Viterbo, Italy

[2]Italian Space Agency, Via del Politecnico snc, 00133, Rome, Italy

[3]Molecular and Cellular Radiation Biology Group, Department of Basic Medical Sciences for Radiation Damages, National Institutes for Quantum and Radiological Science and Technology (QST), 263-8555, Chiba, Japan

[4]German Aerospace Center, Institute of Aerospace Medicine, Radiation Biology Department, Aerospace Microbiology, DLR, Linder Höhe, D-51147 Köln, Germany

[5]University of Applied Sciences Bonn-Rhein-Sieg (BRSU), Natural Sciences, von-Liebig-Straße 20, D-53359 Rheinbach, Germany

Published on *Life*, 10(12), 306. https://doi.org/10.3390/life10120306

Abstract

Among the celestial bodies in the Solar System, Mars currently represents the main target for the search for life beyond Earth. However, its surface is constantly exposed to high doses of Cosmic Rays (CRs) that may pose a threat to any biological system. For this reason, the investigations into the limits of resistance of life to space relevant radiation is fundamental to speculate on the chance of finding extraterrestrial organisms on Mars. In the present work, as part of the STARLIFE project, the responses of dried colonies of the black fungus *Cryomyces antarcticus* CCFEE 515 to the exposure to accelerated iron (LET: 200 keV/μm) ions, which mimic part of CRs spectrum, were investigated. Samples were exposed to the iron ions up to 1000 Gy in the presence of Martian regolith analogues. Our results showed an extraordinary resistance of the fungus in terms of survival, recovery of metabolic activity and DNA integrity. These experiments give new insights into the survival probability of possible terrestrial-like life forms on the present or past Martian surface and shallow subsurface environments.

Keywords: Cosmic rays; Accelerated iron ions; Mars; Fungi; Life on Mars

2.1 Introduction

The search for life beyond Earth requires to define the limits of resistance within which it can persist. In this context, one of the main limiting factors for any terrestrial form of life outside the terrestrial magnetic field is represented by the Cosmic Rays (CRs) (Horneck et al., 2010). CRs, which pervade the interstellar and interplanetary space, consist of totally ionized atomic nuclei accelerated at nearly the speed of light inside and outside our solar system (Ferrari and Szuszkiewicz, 2009). These highly energetic ions can penetrate any biological system, causing densely packed ionization events in the molecules along their path by the transferring energy to the crossed medium. For this reason, exposure to Galactic Cosmic Rays (GCRs) can result in dramatic consequences in cellular structures and functions (Belisheva et al., 2012). The average energy transferred from an accelerated ion to the penetrated medium per unit path length is described by the Linear Energy Transfer (LET), and it increases with the square of the ionic charge (Bethe, 1932). Because CRs are totally ionized, High (H) atomic number (Z) Energy (E) particles (HZE) represent the most damaging component of the CRs spectra, although they constitute only 1% of these (Mewaldt, 1994).

The surface of celestial bodies lacking in a dense atmosphere and a global magnetic field are exposed to high doses of CRs. Among them, Mars is currently the main target for the search for extraterrestrial life due to the biocompatible environmental conditions during its early history and the accessibility for explorative missions (Vago et al., 2017). Although there is no location on Earth reproducing exactly the Martian environmental conditions, some places as the ice-free area of the McMurdo Dry Valleys in Antarctica have a combination of physicochemical parameters similar to those described on Mars (Preston and Dartnell, 2014). Here, a few microorganisms evolved strategies to withstand the extreme environmental factors; one of these is the cryptoendolithism, that is the colonization of the small interstices inside porous rocks, where microorganisms can find protection from the external harsh conditions (Friedmann, 1982; Selbmann et al., 2005). It is reasonable to speculate that, if Martian forms of life exist or ever existed, they may have adopted a similar strategy to cope with the extreme environment found on the planet (Friedmann, 1986). In this regard, sandstones and subsurface environment might provide a shield against CRs incident on the Martian surface.

In the frame of the study of the limits of resistance of the terrestrial life to CRs, an international consortium called STARLIFE was established in 2012, with the aim to test the biological responses of several selected extremophilic organisms to irradiations with high energetic ions representative of CRs spectrum (Moeller et al., 2017). Among the microorganisms tested in STARLIFE experiments, the Antarctic cryptoendolithic black fungus *Cryomyces antarcticus*, which lives inside the rocks in the McMurdo Dry Valleys, showed a high tolerance to accelerated He ions (150 MeV/n, LET 2.2 keV/μm) up to 1 kGy and γ-radiation (^{60}Co) up to 55.61 kGy in desiccated conditions (Pacelli et al., 2017a; 2017b). In distinct experiments, the fungus was also able to resist to acute irradiation with deuterons up to 1.5 kGy and X-rays up to 0.3 kGy, in metabolically active conditions (Pacelli et al., 2017c) and to protracted X-ray exposure (Pacelli et al., 2018). Additionally, the microorganism survived 18 months real space exposure and Martian simulated conditions, and therefore space

radiation environment, in the frame of LIFE (Lichens and Fungi Experiment) and BIOMEX (BIOlogy and Mars EXperiment) experiments (Onofri et al., 2012; 2015; 2019).

Here, the responses of dried colonies of *C. antarcticus* to the exposure to HZE particles iron (Z = 26) up to 1 kGy during the second STARLIFE-irradiation campaign, were investigated. Although iron ions only constitute 17.8 x 10-3 % of the totality of the CRs (Mewaldt, 1994), their high LET make them some of the most damaging particles in the CRs spectrum.

The aim of the work is to investigate the effects of the presence of Martian dry regolith analogues to the survival of the fungus *C. antarcticus* after irradiation with accelerated iron ions. The regoliths are Phyllosilicatic Mars Regolith Simulant (P-MRS), which mimics the regolith of phyllosilicate deposits mainly observed on early Mars, and Sulfatic Mars Regolith Simulant (S-MRS), which is an analogue of regolith in present Martian sulphate deposits. The fungal responses were assessed on different levels by i) cultivation test (CFUs count); ii) metabolic activity assessment (MTT assay); iii) membrane damage assessment (PMA assay); iv) DNA damage assessment (single gene PCRs, quantitative qPCR and fingerprinting analysis).

2.2 Materials and Methods

2.2.1. Samples preparation and exposure conditions

The Antarctic cryptoendolithic strain of the black fungus *C. antarcticus* CCFEE 515 was isolated from Antarctic sandstone (Selbmann et al., 2005). Fungal colonies were grown (2000 Colony-Forming Units, CFUs) on Malt Extract Agar (MEA) medium in Petri dishes and incubated at 15 °C for 3 months. The colonies in the Petri dishes were dried under laminar flow in a sterile cabinet for one night, and subsequently detached from the medium for the exposure. Dry colonies were mixed to different materials and put in tubes with a volume of 200 µl (10 colonies per tube). Four sets of samples were thus obtained (Figure S2.1):

i) Only dried colonies, with no materials (here referred as directly exposed cells).

ii) Dried colonies mixed with grinded Antarctic sandstone, that is the Original Substratum (OS) where the fungus naturally occurs.

iii) Dried colonies mixed with Phyllosilicatic Mars Regolith Simulant (P-MRS).

iv) Dried colonies mixed with Sulfatic Mars Regolith Simulant (S-MRS).

The mineralogical composition of the Martian analogues is reported in Table S2.1. All materials were previously dried-sterilized (140 °C for 4 hours). Depending on the position of each colony in the tubes, OS, P-MRS and S-MRS exhibited a shielding thickness ranging from 0 to 1.48 g/cm^2, 1.55 g/cm^2 and 1.53 g/cm^2, respectively. This configuration allowed to simulate the Martian surface and shallow subsurface environment.

Colonies were separately irradiated with different doses of accelerated iron (Fe) ion particle irradiation (with an energy of 500 MeV/n (nucleon), LET in water: 200 keV/µm) at the Heavy Ion Medical Accelerator (HIMAC) at the National Institutes for Quantum and Radiological Science and Technology (QST) in Chiba, Japan.). The applied doses were 50,

250, 500 and 1000 Gy and the dose rate of 12 Gy/min. Controls (non-irradiated samples) were treated identical as the irradiated samples. All tests were performed in triplicate.

2.2.2. Survival assessment

2.2.2.1. Cultivation test

Microorganisms survival after ions exposure was assessed through the count of developed colonies related to the number of CFUs spread on MEA medium in Petri dishes. Three colonies from each sample were rehydrated at 15 °C in 1 mL of physiological solution (NaCl 0.9%) for 72 h; 0.1 mL of suspensions (50,000 cells/mL) were spread on Petri dishes supplemented with MEA in quintuplicate. Samples were incubated at 15 °C for 3 months and formed colonies were counted. Means and standard deviations were calculated for every replicate series. Statistical analyses were performed by one-way analysis of variance (Anova) and pair wise multiple comparison procedure (Box et al., 1978), carried out using the statistical software SigmaStat 2.0 (Jandel). The Pearson correlation factors between the dose exposure and the growth colonies were calculated.

2.2.2.2. Metabolic activity assessment by MTT assay

In order to evaluate cells metabolic activity, the MTT (3-(4,5-dimethylthiazol-2-yl)-2,5-diphenyltetrazolium bromide) assay was performed. . Cell suspensions were put in quadruplicate into 96-well microplates and 100 µL of 0.5 mg/mL MTT salt in Phosphate-Buffered Saline (PBS) were added to each well. Four wells were filled only with MTT solution. After incubation in the dark at room temperature for 48, MTT solution was removed and 100 µL of dimethyl sulfoxide was added to each cell suspension. The absorbance was read at 595 nm, and the average absorbance of wells containing only MTT was subtracted from the others. Mean and standard deviations were determined for each quadruplicate and results were normalized with the laboratory controls.

2.2.2.3. Membrane damage assessment

Quantitative PCR (qPCR) in DNA from samples treated with Propidium MonoAzide (PMA) was performed to assess the membrane integrity in exposed samples. An aliquot of each rehydrated sample was added with 5 µL of a PMA solution (200 µM) and incubated in the dark for 1 h with occasional shaking. Samples were then placed in ice and exposed to a halogen lamp for 10 min. PMA can selectively penetrate cells with damaged membranes and cross-link to DNA under exposure to light, thereby preventing Polymerase Chain Reaction (PCR). DNA extraction and purification were performed on PMA treated and untreated aliquots from each sample. DNAs were quantified and normalized at same concentration (2 ng/mL) using Qubit dsDNA HS Assay Kit (Life Technologies, USA) and qPCR was performed to quantify the number of fungal internal transcribed spacer (ITS) ribosomal DNA fragments (281 bp) present in both PMA-treated and untreated samples, according to the work of Onofri et al., (2012). All tests were performed in triplicate.

2.2.3. DNA integrity assessment

2.2.3.1. DNA extraction, single gene PCR reactions and RAPD analysis

DNA extraction was performed on dried colonies using NucleoSpin® Plant kit (Macherey-Nagel, Düren, Germany) following the protocol optimized for fungi (Selbmann et al., 2014). Quantitation of extracted genomic DNA was performed using Qubit system and all the samples were diluted to the same concentration (2 ng/mL). Three overlapping tracts in the Internal Transcribed Spacer (ITS) regions and the Large SubUnit-coding Sequences (LSU) of the nuclear ribosomal RNA (rRNA) gene complex were amplified. The used primers were ITS4a (ATTTGAGCTGTTGCCGCTTCA), ITS5 (GGAAGTAAAAGTCGTAACAAGG), LR5 (TCCTGAGGGAAACTTC) and LR7 (TACTACCACCAAGATCT). PCR reactions were carried out for each sample in a solution consisting of 12.5 µL of BioMixTM (BioLine Ltd., London), 1 µL of each primer solution (5 pmol/µL) and 0.2 ng of DNA template, in a final volume of 25 µL. MyCycler Thermal Cycler (Bio-Rad Laboratories GmbH, Munich, Germany) equipped with a heated lid was used and amplification conditions are as reported in Selbmann et al., (2011). The whole genome integrity was assessed by Random Amplified Polymorphic DNA (RAPD). PCR reactions were carried out for each sample in a final solution containing 12.5 µL of BioMixTM, 5 pmol of primer $(GGA)_7$ and 0.2 ng of DNA sample, in a final volume of 25 µL. Amplifications were performed according to Selbmann et al., (2011).

2.2.3.2. Quantitative assay of DNA damage by qPCR

Quantitative PCR was carried out to quantify the number of ITS fragments by using LR0R (ACCCGCTGAACTTAAGC) and LR5 primers. The qPCR reactions were performed in triplicate with a solution containing 7.5 µL of qPCR cocktail (iQ SYBER Green Supermix, Biorad, MI, Italy), 1 µL of each primer solution (5 pmol/µL) and 0.1 ng of DNA template in a final volume of 15 µL. The amplifications were carried out by Biorad CFX96 real time PCR detection system.

2.2.3.3. DNA mutation detection

Sequencing of a tract with a length of 1440 bp localized in rRNA gene region was performed to assay the presence of small DNA mutation after irradiation. Sequencing was performed by Macrogen Inc (Spanish branch, Avda. Sur del Aeropuerto, 28, Madrid, Spain) using ITS4 and ITS5 primers. Alignment among obtained sequences from all the samples was carried out by using Molecular Evolutionary Genetics Analysis version 7.0 (MEGA 7). Sequences were also hierarchically clustered using UPGMA method by MEGA 7.

2.3 Results

2.3.1. Survival assessment

2.3.1.1. Cultivation test

The ability of *C. antarcticus* cells to grow after the exposure to accelerated iron ions was investigated by counting the number of colonies formed in MEA medium. As shown in Figure 2.1, samples exposed to ions in absence of any material exhibited a progressive dose-

dependent decrease of growth, with a Pearson correlation coefficient value (r) of -0.90. Significantly, 13% of colonies were able to grow after exposure to a dose of 1000 Gy (Figure 2.1a). Differently, samples exposed to iron ions in the presence of the three distinct materials (i.e. OS, P-MRS, S-MRS) showed different trends with a significant drop of growth colonies, compared to the respective controls, starting from the dose of 50 Gy (Figure 2.1b, c and d). Moreover, a correlation between the colony number and the exposure dose was reported for samples exposed while mixed to P-MRS analogue (r=-0.88). Notably, the growth ability was maintained at the highest dose of 1 kGy in every set, with a percentage of developed colonies of 1.6, 0.13 and 3.5% in the presence of OS, P-MRS and S-MRS, respectively (Figure 2.1b, c and d).

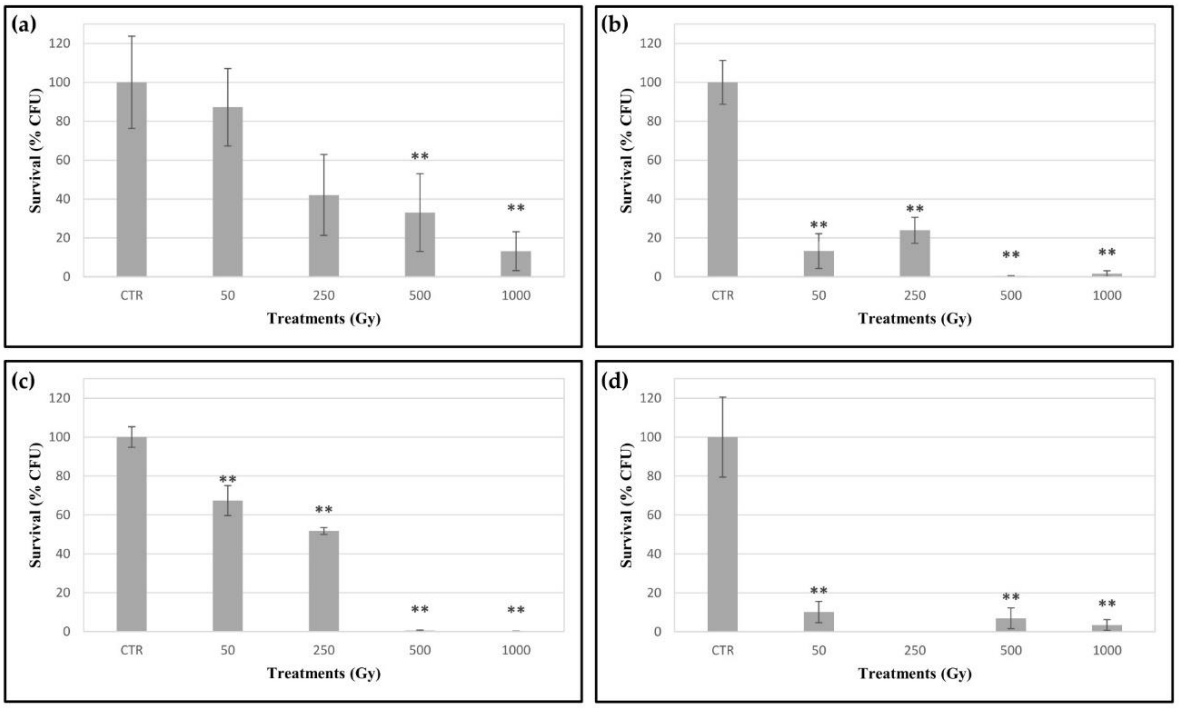

Figure 2.1. Survival of *C. antarcticus* exposed to accelerated Fe ions expressed as CFUs. (a) directly exposed colonies, and colonies mixed with (b) OS substratum, (c) P-MRS analogue, (d) S-MRS analogue. CTR: control. Data were normalized against the control. Significant differences were calculated by Tukey test with *=p <0.05 and **=p <0.001.

2.3.1.2 Metabolic activity assessment by MTT assay

MTT dye, a yellow water-soluble compound, is reduced to purple colored formazan crystals by mitochondrial succinate dehydrogenase in metabolically active cells. The DMSO dissolved formazan can be quantified spectrophotometrically at a wavelength of 595 nm, with the absorbance being linearly correlated with the metabolic activity of the cells in the sample. Here, MTT assay was performed to assess the metabolic activity recovery of *C. antarcticus* cells exposed to accelerated iron ions, after 48 and 72 hours of rehydration. All samples showed a detectable metabolic activity, and samples from each set exhibited slight differences according to the irradiation dose (Figure 2.2). In samples rehydrated for 48 h after exposure in OS, P-MRS and S-MRS, a common trend with an increase in formazan absorbance

corresponding to a dose of 50 Gy, followed by a decrease at the dose of 250 Gy and a new increase at the dose of 500 Gy was observed.

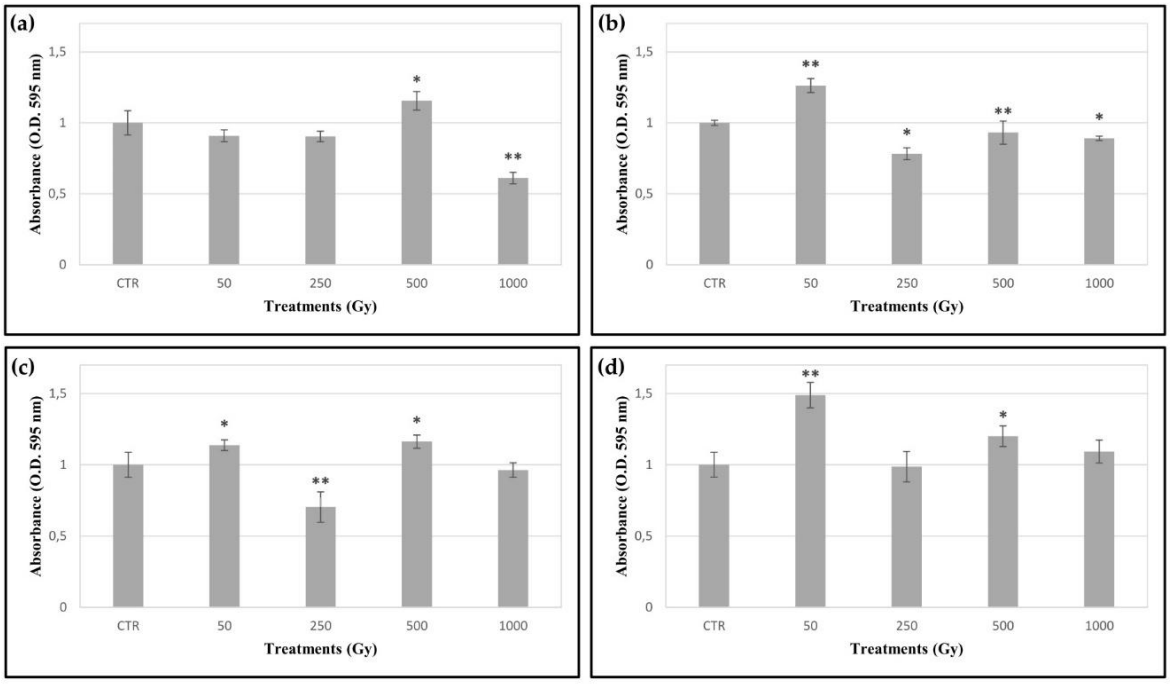

Figure 2.2. Effect of accelerated Fe ions irradiation on metabolic activity recovery of *C. antarcticus*. (a) directly exposed colonies, and colonies mixed with (b) OS substratum, (c) P-MRS analogue, (d) S-MRS analogue. CTR: control. Statistical analyses as reported in Fig. 2.1.

2.3.1.3 Membrane damage assessment

The PMA assay combined with qPCR was used to discriminate compromised membrane to membrane-intact cells. PMA is a compound that can covalently bind to DNA only in cells with a compromised cell membrane, thereby preventing PCR amplification. Figure 2.3 shows the ratio between cells with damaged membranes and cells with intact membranes after the exposure to increasing doses of accelerated iron ions. No significative damaged membranes were detected at the lowest doses in directly exposed cells, even though a sharp drop of cells with intact membrane- at 1 kGy was observed (1% of all cells) (Figure 2.3a). A similar drop at 1 kGy dose was only observed in cells exposed in the presence of P-MRS (4% of intact-membrane cells) (Figure 2.3c). Membrane damage in cells exposed in the presence of OS, P-MRS and S-MRS did not show any apparent correlation with the dose, although a reduction of cells with intact membrane was observed in most of the samples exposed to iron ions. In OS and S-MRS samples, a steep increase in damaged cell-membranes at the dose of 500 and 250 Gy was observed (98.4 and 99.3% cells with damaged cells-membranes, respectively) (Figure 2.3b and 2.3d).

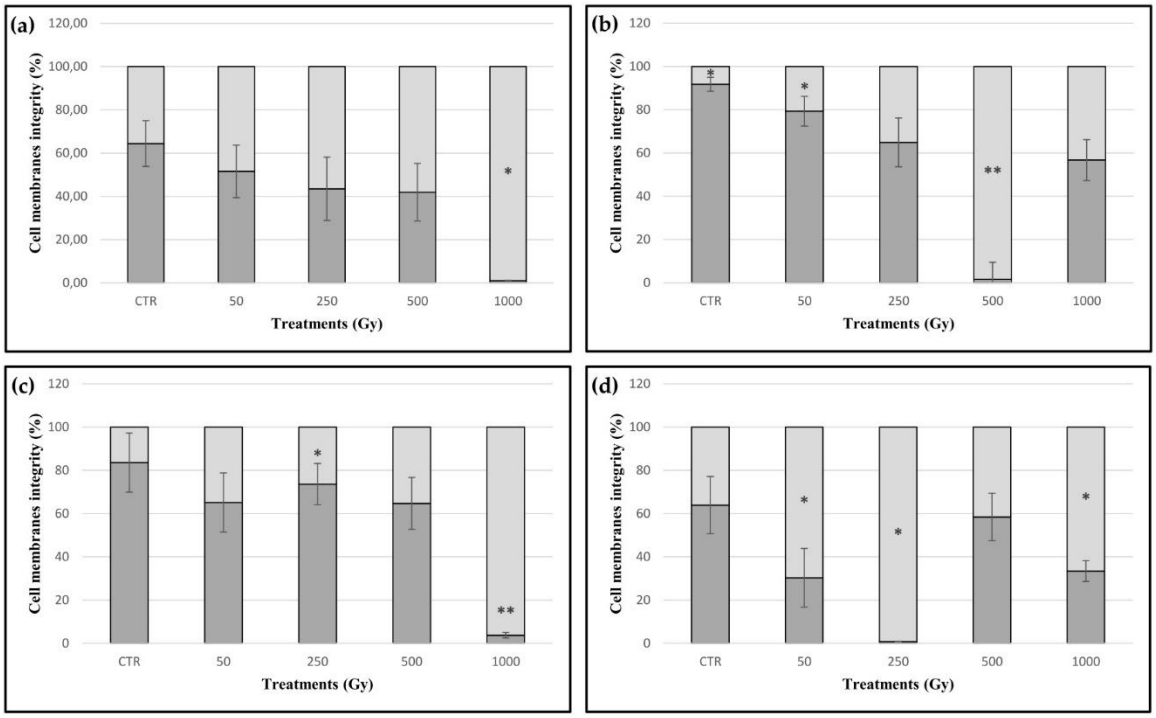

Figure 2.3. Percentage of intact and damaged cell-membranes measured with PMA assay coupled with qPCR of *C. antarcticus* exposed to accelerated Fe ions. (a) directly exposed colonies, and colonies mixed with (b) OS substratum, (c) P-MRS analogue, (d) S-MRS analogue. Light grey bars represent the percentage of cells with damaged cell membranes; dark grey bars represent the percentage of cells with un-damaged cell membranes. CTR: control. Statistical analyses as reported in Fig. 2.1.

2.3.2. DNA integrity assessment

After exposure to accelerated iron ions, structural damage to DNA in *C. antarcticus* cells was assessed in three overlapping tracts in the ITS-LSU region with a length of 700, 1600 and 2000 bp. DNA amplification was observed both in controls and samples exposed to doses up to 1 kGy of iron ions in each set (Figure S2.2, S2.3 and S2.4). The whole genome integrity of the exposed cells was investigated by RAPD assay. No evident change in amplicon profiles was shown by cells exposed up to 1 kGy of iron ions in each sample's set (Figure S2.5). To assess levels of eventual DNA damage in cells of *C. antarcticus*, a quantitative PCR assay was performed in a target sequence of 939 bp in length mapping in the LSU region. Figure 2.4 shows the number of amplicons detected in cells on *C. antarcticus* after the exposure to increasing doses of iron ions, performed directly and in the presence of OS substratum, P-MRS and S-MRS analogues. Significative differences were detected among the controls and the cells exposed to doses from 50 Gy to 1 kGy of accelerated iron ions in the presence of OS, P-MRS and S-MRS (Figure 2.4 b, c and d). Instead, only a 500 Gy dose caused a significative reduction of the number of the amplicons in cells exposed to accelerated iron ions in absence of any material. In order to detect the alteration in DNA sequences after accelerated iron ions exposure, the sequencing of a target tract of 1440 bp in the ITS-LSU region was performed. The results showed that *C. antarcticus* DNA was not affected by any point mutation, maintaining the nucleotide sequence after all the exposure doses.

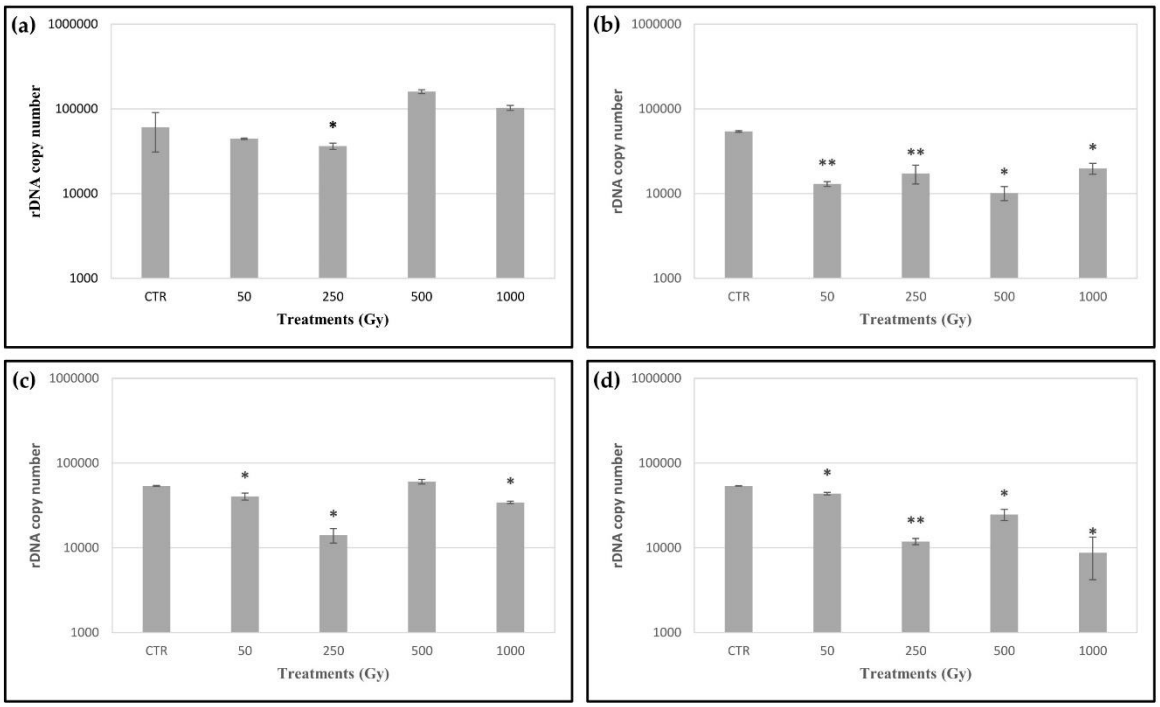

Figure 2.4. rDNA (ITS-LSU region) copy number quantification by qPCR of DNA of *C. antarcticus* colonies exposed to accelerated iron ions. (a) directly exposed colonies, and colonies mixed with (b) OS substratum, (c) P-MRS analogue, (d) S-MRS analogue. CTR: control. Statistical analyses as reported in Fig. 2.1.

2.4 Discussion

Among the celestial bodies in our solar system, Mars represents the main target for the search for extraterrestrial life. However, due to the lack of a global magnetic field and a dense atmosphere (Jakosky et al., 2017; Langlais et al., 2004), the surface of the planet is constantly hit by CRs, high energized ions which pervade the interplanetary medium. The continuous exposure to these energized particles experienced on the surface on Mars may represent one of the most harmful factors for any terrestrial-like form of life. Significantly, different types of CRs diverge in their biological effectiveness according to their energy deposition in the traversed medium, which is defined by the (LET) value (Heinrich et al., 1991). In this regard, a positive correlation exists between the charge of the accelerated ions and the LET. Consequently, despite their low fluxes, HZE particles represent the most damaging component of the CRs spectrum. Additionally, high LET ions can travel shorter distances than lower LET ions in the penetrated matter.

Therefore, although Martian surface is exposed to most of the part of the CRs spectrum, HZE particles can be shielded by the top centimeters of the regolith (Röstel et al., 2020), making the subsurface Martian environment suitable for the colonization by putative extraterrestrial microorganisms. Conversely, any hypothetical microorganisms present on the surface of Mars or in the top few centimeters of Martian regolith would be directly exposed to high doses of

these extremely harmful particles. For this reason, it can be assumed that any hypothetical Martian form of life may have adopted an endolithic strategy or colonized the subsurface environment to survive the extremely harsh conditions reported on the surface of the planet (Friedmann, 1986). However, due to the liquid water availability in transient brines in the uppermost centimeters of regolith (Martin-Torres et al., 2015) and the movement of the soil by wind (Jackson et al., 2015), there may be a chance to find microorganisms on the surface of Mars. For this reason, the understanding if the life can survive and persist in this environment may be of primary importance in the ambit of the search for life on Mars.

In this context, the present study aimed to test the effects of increasing doses (up to 1 kGy) of one of the most abundant CRs HZE, namely accelerated iron ions (Fe^{26+}) (Simpson, 1983), on dried colonies of the extremophilic black fungus *C. antarcticus*. The exposure was performed both directly and while mixed to small amounts of Antarctic sandstones and two Martian regolith analogues in order to reproduce part of the surface and the shallow subsurface environments of Mars. Dried cells were employed to simulate a scenario where hypothetical Martian microorganisms may persist in a metabolically dormant state for extended periods until the transient availability of liquid water. In this scenario, the microorganisms may accumulate high doses of HZE cosmic rays until the reactivation of the cellular metabolism. Therefore, on the point of view of the reactivated cells, the total amount of absorbed dose, and not the dose rate, is the critical factor.

In this experiment, rehydrated cells of *C. antarcticus* showed the ability to grow after the exposure up to 1 kGy of accelerated iron ions in the absence of any materials and while mixed to OS substratum and P-MRS and S-MRS analogues (Figure 2.1). Nevertheless, a clear correlation between the growth ability and the exposure dose is only showed by colonies exposed without materials and in P-MRS. Additionally, cells exposed in absence of materials exhibited higher growth ability after exposition to higher doses than cells mixed with OS, P-MRS and S-MRS. This latter result was similar to those found in a previous works in which dried colonies of *C. antarcticus* were exposed to accelerated helium ions (Pacelli et al., 2020). The maximum shielding depths of grinded OS, P-MRS and S-MRS were of 1.48 g/cm^2, 1.55 g/cm^2 and 1.53 g/cm^2, respectively. Therefore, according to the LET of the accelerated iron ions (200 keV/μm in water), the more harmful effects of the exposure in the presence of the materials cannot be explained by the localization of the cells inside the Bragg peak region along the particle's track. Instead, these results may be explained by the effects of the secondary particles produced by the collisions of the accelerated ions with the atoms in the materials. These secondary particles, such as pions and kaons, decay into neutrinos, muons, gamma rays and beta particles (electrons and positrons) (Dartnell et al., 2007; Mei and Hime, 2006). The propagation of this radiation in the minerals surrounding the cells may both amplify the damaging effects of accelerated ions and affect the cells in a dose-unrelated fashion. In this context, the differences in the colonies growth among the different sets may be due to the distinct properties of OS, P-MRS and S-MRS materials. Alternatively, the production of reactive oxygen species (ROS) from the water absorbing minerals in the OS and the regolith simulants may have differently affected the cells in the distinct sets (Moeller et al., 2010). Compared to our previous results on the growth of *C. antarcticus* cells exposed to accelerated

helium ions (Pacelli et al., 2020), these results showed that the fungus exhibit a lower resistance when directly exposed to the more damaging iron ions (Figure 2.1), accordingly to the different LET values among helium and iron ions. However, differently from the survival reported after accelerated helium ions in the presence of OS, P-MRS and S-MRS materials, no linear survival trend was reported in this experiment. These results are related to the interaction between the accelerated Iron particles and the materials in which *C. antarcticus* colonies were exposed; these interactions (and the related secondary effects) are lower in helium ions.

The metabolic activity of *C. antarcticus* exposed cells was assessed after 48h of rehydration by MTT assay. The MTT assay is a colorimetric test based on the detection of the enzymatic reduction of MTT to MTT-formazan by mitochondrial succinate dehydrogenase. Therefore, two main parameters may influence the formazan production, that are the relative number of viable cells in the sample and the mitochondrial respiration. In this respect, one of the main cellular responses after radiation exposure is represented by mitochondrial biogenesis, which leads to an increase of enzymatic MTT reduction (Rai et al., 2018). An apparently irregular trend was observed in formazan absorbance among the samples in each set. In this case, the absence of a clear trend of dose-dependent alteration of metabolic activity may be explained through the simultaneous and opposite effects of the killed cell ratio and activation of response to irradiation by survived cells in each sample. Therefore, the higher metabolic activity of the damaged cells may result in an increase of the total amount of formazan in every samples, thus compensating for the reduced number of viable cells after the exposure. In this regard, although cells exposed at 250 Gy of accelerated iron ions in the presence of S-MRS analogue did not exhibit growth, they showed a metabolic activity. Such discordance may be explained by the inability of the survived cells to grow after three months incubation, due to the high levels of cellular damages.

All the DNA sequences mapping in the target ITS-LSU region showed the amplification in cells exposed up to the highest doses, regardless of the material present during the exposure (Figure S2.2, S2.3 and S2.4). The good maintenance of the DNA structural integrity at the target region was confirmed by qPCR assay (Figure 2.4). Similarly, a whole genomic analysis of exposed cells showed no significant changes in the RAPD profiles up to a dose of 1 kGy, in every set of samples (Figure S2.5). Similarly, no point mutations were detected in the target sequence (1440 bp) mapping in the ITS-LSU region in all the samples. Overall, these results showed that the main cause of the cell mortality may not be only due to the production of single and double strand breaks in the DNA molecules, but also to damages to other cellular components. Instead, HZE exposure can led to the production of ROS and reactive nitrogen species (RNS) inside the cells (Tseng et al., 2014). In turn, these reactive species can promote the alteration of cellular structures, such as the cell membrane (Wang et al., 2017). In this regard, the PMA assay showed as the relative number of membrane-damaged cells increased in most of exposed samples, albeit not in a dose-related trend, accordingly to the survival trend.

All the reported results showed how dried colonies of the cryptoendolithic black fungus *C. antarcticus* can survive the exposure of a dose up to 1 kGy of HZE particles, albeit exhibiting a significant reduction in colony growth at the highest doses. Through the LET value of the accelerated iron ions (200 keV/μm), it is possible to calculate the number of the particles that

hit every sample at each exposure dose (Alpen et al., 1994). However, depending on the solar modulation and differences in atmospheric depth, CRs fluxes on Martian surface can vary over time (Hassler et al., 2014; Berger et al., 2020). Therefore, an accurate estimation of the time frame required to absorb similar numbers of particles is not possible. Besides, HZE particles reaching the Martian surface have a wide range of energy values, whereas in the present experiment only particles with an energy of 500 MeV/n were employed. Nevertheless, our results give a rough estimate of the resistance of terrestrial life to HZE exposure in a Martian-like scenario. In this context, the volumes of regolith mixed with colonies of *C. antarcticus* used in our experiment would require approximately more than 10 million years to accumulate a dose of 1 kGy of accelerated iron ions on the Martian surface (Table S2.2). Therefore, the ability of dried colonies of *C. antarcticus* to reactivate their metabolism and growth after such dose, maintaining the structural integrity of DNA, shows how a hypothetical *C. antarcticus*-like microorganism may tolerate the surface and shallow subsurface Martian environment for years. However, the differences occurring among the distinct sets of samples show how the responses to CRs exposure strongly may depend on the material surrounding the cells. Because of the reduced depth of the material used in the exposed samples, these differences are not attributable to their shield from the accelerated ions. Instead, the distinct responses of the cells to CRs exposure may be due to other processes, such as the production of secondary radiation and ROS, that may amplify in an irregular trend the effects of this kind of radiation on the cells.

References

Alpen, E. L., Powers-Risius, P., Curtis, S. B., DeGuzman, R., & Fry, R. J. M. (1994). Fluence-based relative biological effectiveness for charged particle carcinogenesis in mouse Harderian gland. *Advances in Space Research*, *14*(10), 573-581.

Belisheva, N. K., Lammer, H., Biernat, H. K., & Vashenuyk, E. V. (2012). The effect of cosmic rays on biological systems–an investigation during GLE events. *Astrophysics and Space Sciences Transactions*, *8*(1), 7-17.

Berger, T., Matthiä, D., Burmeister, S., Zeitlin, C., Rios, R., Stoffle, N., ... & Wimmer-Schweingruber, R. F. (2020). Long term variations of galactic cosmic radiation on board the International Space Station, on the Moon and on the surface of Mars. *Journal of Space Weather and Space Climate*, *10*, 34.

Bethe, H. (1932). Bremsformel für elektronen relativistischer geschwindigkeit. *Zeitschrift für Physik*, *76*(5-6), 293-299.

Box, G. E., Hunter, W. H., & Hunter, S. (1978). *Statistics for experimenters* (Vol. 664). New York: John Wiley and sons.

Dartnell, L. R., Desorgher, L., Ward, J. M., & Coates, A. J. (2007). Martian sub-surface ionising radiation: biosignatures and geology. *Biogeosciences*, *4*(4), 545-558.

Ferrari, F., & Szuszkiewicz, E. (2009). Cosmic rays: a review for astrobiologists. *Astrobiology*, *9*(4), 413-436.

Friedmann, E. I. (1982). Endolithic microorganisms in the Antarctic cold desert. *Science*, *215*(4536), 1045-1053.

Friedmann, E. I. (1986). The Antarctic cold desert and the search for traces of life on Mars. *Advances in Space Research*, *6*(12), 265-268.

Hassler, D. M., Zeitlin, C., Wimmer-Schweingruber, R. F., Ehresmann, B., Rafkin, S., Eigenbrode, J. L., ... & Berger, G. (2014). Mars' surface radiation environment measured with the Mars Science Laboratory's Curiosity rover. *science*, *343*(6169), 1244797.

Heinrich, W., Wiegel, B., & Kraft, G. (1991). *β, Z eff, dE/dx, range and restricted energy loss of heavy ions in the region 1≤E≤1000 MeV/nucleon* (No. GSI--91-30 (PREPR.)). Gesellschaft fuer Schwerionenforschung mbH.

Horneck, G., Klaus, D. M., & Mancinelli, R. L. (2010). Space microbiology. *Microbiology and molecular biology reviews*, *74*(1), 121-156.

Jackson, D. W., Bourke, M. C., & Smyth, T. A. (2015). The dune effect on sand-transporting winds on Mars. *Nature Communications*, *6*(1), 8796.

Jakosky, B. M., Slipski, M., Benna, M., Mahaffy, P., Elrod, M., Yelle, R., ... & Alsaeed, N. (2017). Mars' atmospheric history derived from upper-atmosphere measurements of 38Ar/36Ar. *Science*, *355*(6332), 1408-1410.

Langlais, B., Purucker, M. E., & Mandea, M. (2004). Crustal magnetic field of Mars. *Journal of Geophysical Research: Planets*, *109*(E2).

Martín-Torres, F. J., Zorzano, M. P., Valentín-Serrano, P., Harri, A. M., Genzer, M., Kemppinen, O., ... & Vaniman, D. (2015). Transient liquid water and water activity at Gale crater on Mars. *Nature Geoscience*, *8*(5), 357-361.

Mei, D. M., & Hime, A. (2006). Muon-induced background study for underground laboratories. *Physical Review D*, *73*(5), 053004.

Mewaldt, R. A. (1994). Galactic cosmic ray composition and energy spectra. *Advances in Space Research*, *14*(10), 737-747.

Moeller, R., Raguse, M., Leuko, S., Berger, T., Hellweg, C. E., Fujimori, A., ... & STARLIFE Research Group. (2017). STARLIFE—An international campaign to study the role of galactic cosmic radiation in astrobiological model systems. *Astrobiology*, *17*(2), 101-109.

Moeller, R., Rohde, M., & Reitz, G. (2010). Effects of ionizing radiation on the survival of bacterial spores in artificial martian regolith. *Icarus*, *206*(2), 783-786.

Onofri, S., de la Torre, R., de Vera, J. P., Ott, S., Zucconi, L., Selbmann, L., ... & Horneck, G. (2012). Survival of rock-colonizing organisms after 1.5 years in outer space. *Astrobiology*, *12*(5), 508-516.

Onofri, S., de Vera, J. P., Zucconi, L., Selbmann, L., Scalzi, G., Venkateswaran, K. J., ... & Horneck, G. (2015). Survival of Antarctic cryptoendolithic fungi in simulated Martian conditions on board the International Space Station. *Astrobiology*, *15*(12), 1052-1059.

Onofri, S., Selbmann, L., Pacelli, C., Zucconi, L., Rabbow, E., & de Vera, J. P. (2019). Survival, DNA, and ultrastructural integrity of a cryptoendolithic Antarctic fungus in Mars and Lunar rock analogs exposed outside the International Space Station. *Astrobiology*, *19*(2), 170-182.

Pacelli, C., Bryan, R. A., Onofri, S., Selbmann, L., Shuryak, I., & Dadachova, E. (2017c). Melanin is effective in protecting fast and slow growing fungi from various types of ionizing radiation. *Environmental microbiology*, *19*(4), 1612-1624.

Pacelli, C., Bryan, R. A., Onofri, S., Selbmann, L., Zucconi, L., Shuryak, I., & Dadachova, E. (2018). The effect of protracted X-ray exposure on cell survival and metabolic activity of fast and slow growing fungi capable of melanogenesis. *Environmental microbiology reports*, *10*(3), 255-263.

Pacelli, C., Cassaro, A., Aureli, L., Moeller, R., Fujimori, A., & Onofri, S. (2020). The responses of the black fungus Cryomyces antarcticus to high doses of accelerated helium ions radiation within martian regolith simulants and their relevance for Mars. *Life*, *10*(8), 130.

Pacelli, C., Selbmann, L., Moeller, R., Zucconi, L., Fujimori, A., & Onofri, S. (2017a). Cryptoendolithic Antarctic black fungus Cryomyces antarcticus irradiated with accelerated helium ions: survival and metabolic activity, DNA and ultrastructural damage. *Frontiers in Microbiology*, *8*, 2002.

Pacelli, C., Selbmann, L., Zucconi, L., Raguse, M., Moeller, R., Shuryak, I., & Onofri, S. (2017b). Survival, DNA integrity, and ultrastructural damage in Antarctic cryptoendolithic eukaryotic microorganisms exposed to ionizing radiation. *Astrobiology*, *17*(2), 126-135.

Preston, L. J., & Dartnell, L. R. (2014). Planetary habitability: lessons learned from terrestrial analogues. *International Journal of Astrobiology*, *13*(1), 81-98.

Rai, Y., Pathak, R., Kumari, N., Sah, D. K., Pandey, S., Kalra, N., ... & Bhatt, A. N. (2018). Mitochondrial biogenesis and metabolic hyperactivation limits the application of MTT assay in the estimation of radiation induced growth inhibition. *Scientific reports*, *8*(1), 1-15.

Röstel, L., Guo, J., Banjac, S., Wimmer-Schweingruber, R. F., & Heber, B. (2020). Subsurface radiation environment of Mars and its implication for shielding protection of future habitats. *Journal of Geophysical Research: Planets*, *125*(3), e2019JE006246.

Selbmann, L., De Hoog, G. S., Mazzaglia, A., Friedmann, E. I., & Onofri, S. (2005). Fungi at the edge of life: cryptoendolithic black fungi from Antarctic desert. *Stud Mycol*, *51*(1), 1-32.

Selbmann, L., Isola, D., Egidi, E., Zucconi, L., Gueidan, C., De Hoog, G. S., & Onofri, S. (2014). Mountain tips as reservoirs for new rock-fungal entities: Saxomyces gen. nov. and four new species from the Alps. *Fungal Diversity*, *65*, 167-182.

Selbmann, L., Isola, D., Zucconi, L., & Onofri, S. (2011). Resistance to UV-B induced DNA damage in extreme-tolerant cryptoendolithic Antarctic fungi: detection by PCR assays. *Fungal Biology*, *115*(10), 937-944.

Simpson, J. A. (1983). Elemental and isotopic composition of the galactic cosmic rays. *Annual Review of Nuclear and Particle Science*, *33*(1), 323-382.

Tseng, B. P., Giedzinski, E., Izadi, A., Suarez, T., Lan, M. L., Tran, K. K., ... & Limoli, C. L. (2014). Functional consequences of radiation-induced oxidative stress in cultured neural stem cells and the brain exposed to charged particle irradiation. *Antioxidants & redox signaling*, *20*(9), 1410-1422.

Vago, J. L., Westall, F., Coates, A. J., Jaumann, R., Korablev, O., Ciarletti, V., ... & Carreau, C. (2017). Habitability on early Mars and the search for biosignatures with the ExoMars Rover. *Astrobiology*, *17*(6-7), 471-510.

Wang, T. Y., Libardo, M. D. J., Angeles-Boza, A. M., & Pellois, J. P. (2017). Membrane oxidation in cell delivery and cell killing applications. *ACS chemical biology*, *12*(5), 1170-1182.

Supplementary materials

Table S2.1. Phillosilicate Mars Regolith Simulant (P-MRS) and Sulfatic Mars Regolith Simulant (S-MRS) analogues composition (from Böttger et al., 2012).

P-MRS		S-MRS	
Mineral	**Weight (%)**	**Mineral**	**Weight (%)**
Montmorillonite	45	Gabbro	32
Chamosite	20	Gypsum	30
Quartz	10	Dunite	15
Iron(III)-oxide	5	Hematite	13
Kaolinite	5	Goethite	7
Siderite	5	Quartz	3
Hydromagnesite	5		
Gabbro	3		
Dunite	2		

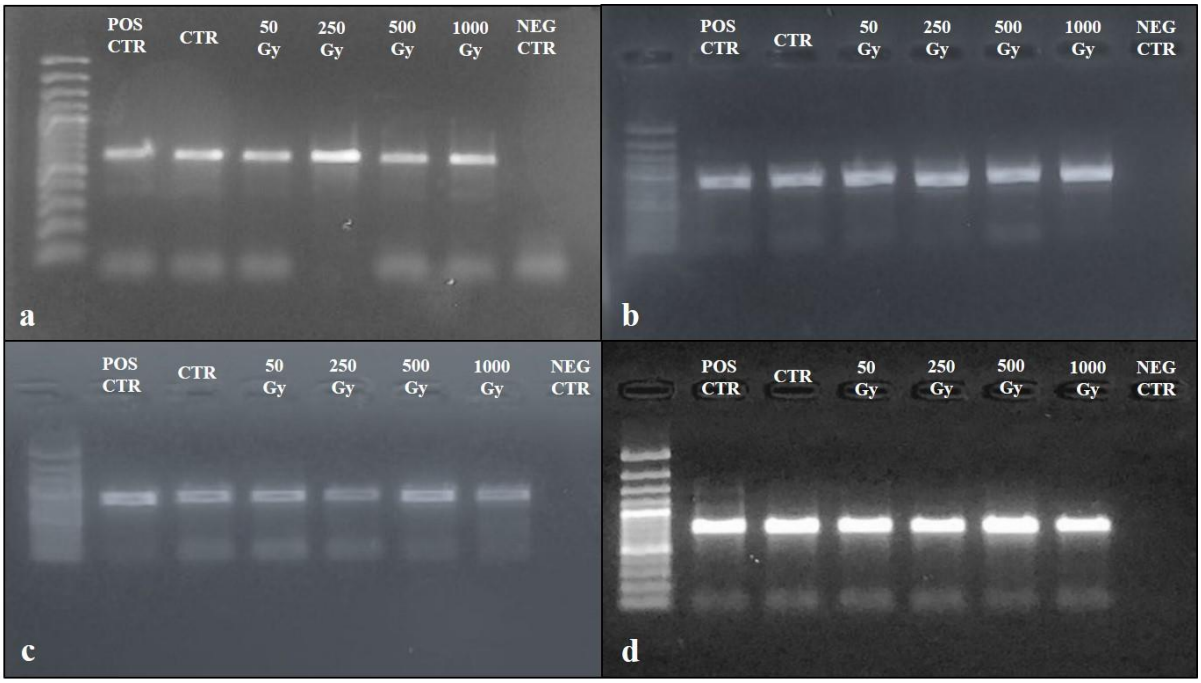

Figure S2.1. PCR amplification of the Internal Transcriber Spacer (ITS) region (600 bp), of samples accelerated Fe ions from each set: (**a**) directly exposed *C. antarcticus* colonies; (**b**) *C. antarcticus* colonies exposed in the (Original Substrate (OS) substratum; (**c**) *C. antarcticus* colonies exposed in the Phillosilicate Mars Regolith Simulant (P-MRS) analogue; (**d**) *C. antarcticus* exposed in the Sulfatic Mars Regolith Simulant (S-MRS) analogue. POS CTR: laboratory control; CTR: Control; NEG CTR: Negative Control.

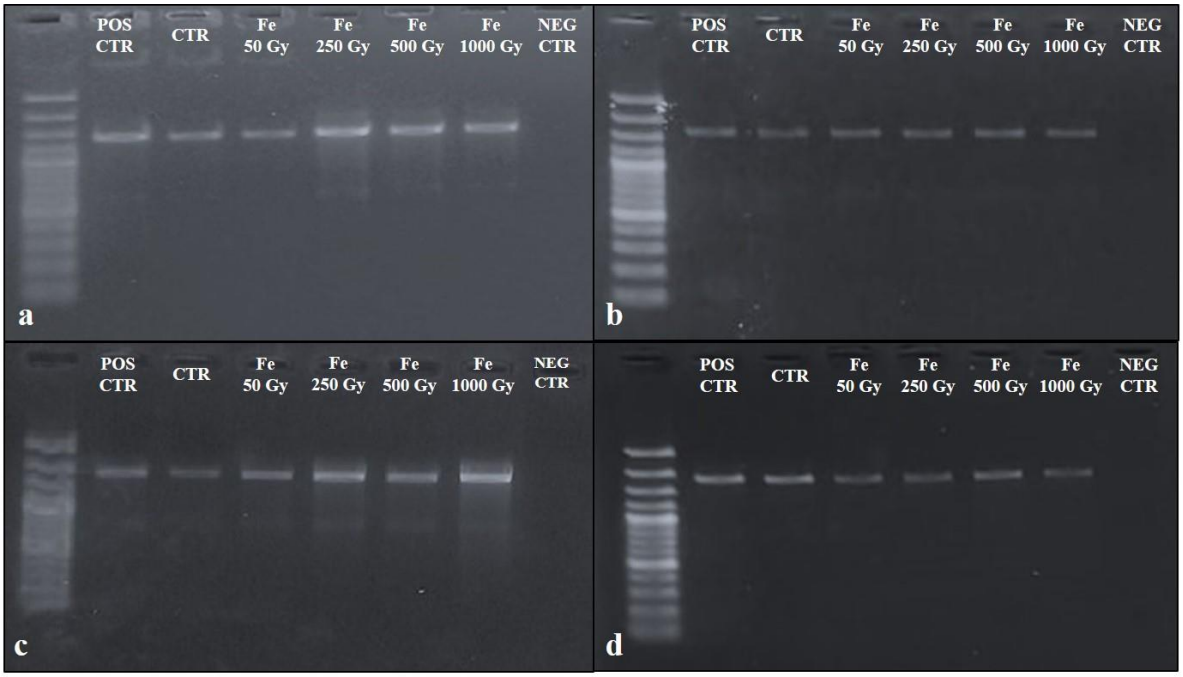

Figure S2.2. PCR amplification of the ITS- Large SubUnit region (LSU) region (1600 bp), of samples exposed to accelerated Fe ions from each set: (**a**) directly exposed *C. antarcticus* colonies; (**b**) *C. antarcticus* colonies exposed in the (Original Substrate (OS) substratum; (**c**) *C. antarcticus* colonies exposed in the Phillosilicate Mars Regolith Simulant (P-MRS) analogue; (**d**) *C. antarcticus* exposed in the Sulfatic Mars Regolith Simulant (S-MRS) analogue. POS CTR: laboratory control; CTR: Control; NEG CTR: Negative Control.

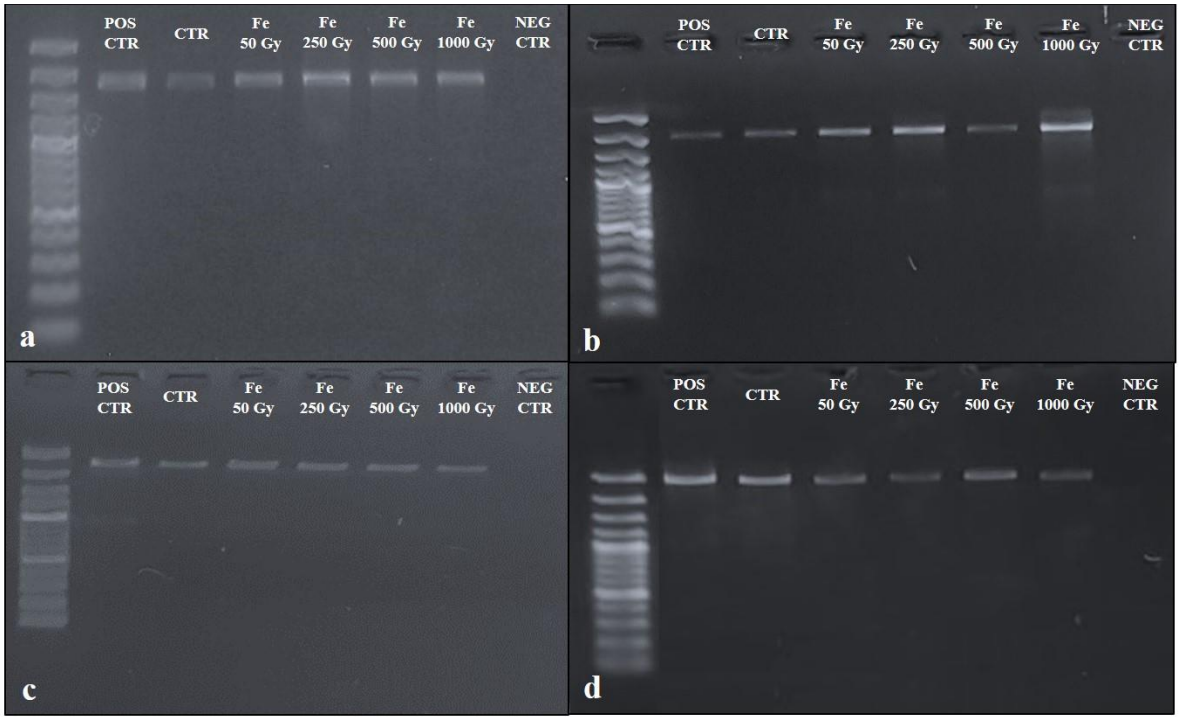

Figure S2.3. PCR amplification of the ITS- Large SubUnit region (LSU) region (2000 bp), of samples exposed to accelerated Fe ions from each set: (**a**) directly exposed *C. antarcticus* colonies; (**b**) *C. antarcticus* colonies exposed in the (Original Substrate (OS) substratum; (**c**) *C. antarcticus* colonies exposed in the Phillosilicate Mars Regolith Simulant (P-MRS) analogue; (**d**) *C. antarcticus* exposed in the Sulfatic Mars Regolith Simulant (S-MRS) analogue. POS CTR: laboratory control; CTR: Control; NEG CTR: Negative Control.

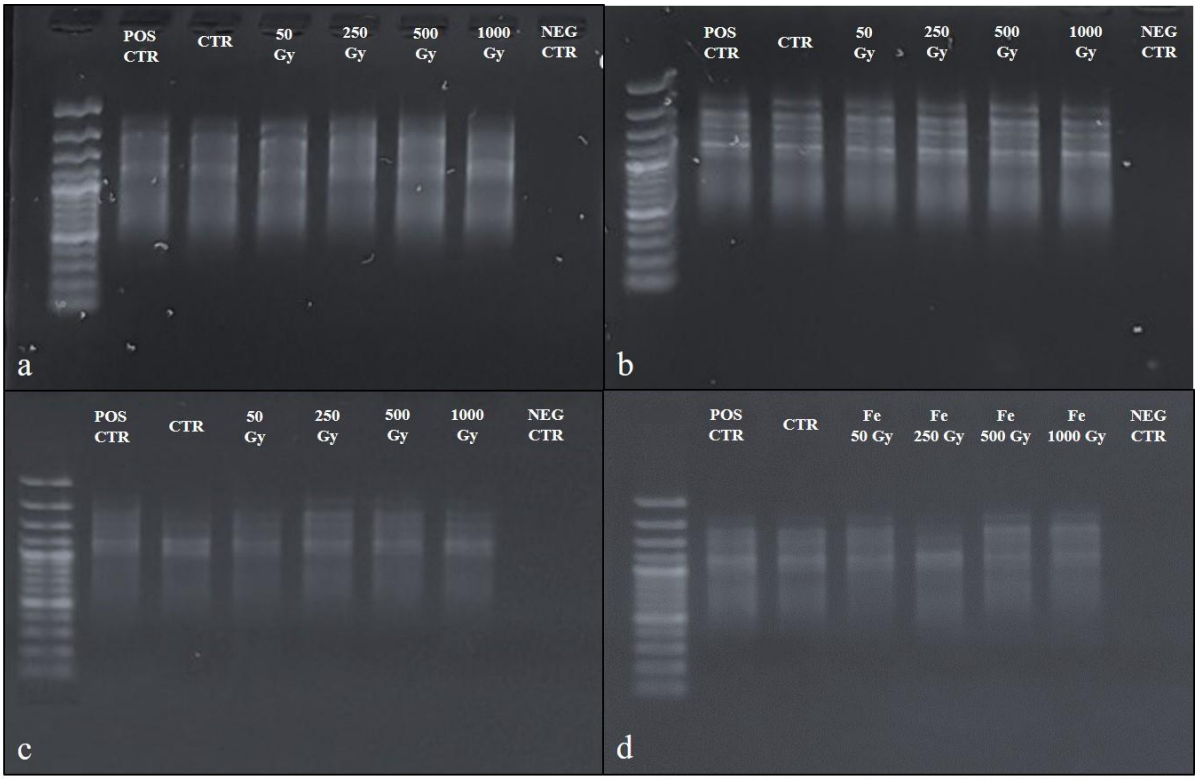

Figure S2.4. Random Amplification of Polymorphic DNA (RAPD) assay in *C. antarcticus* colonies after exposure to accelerated Fe ions from each set: (**a**) directly exposed *C. antarcticus* colonies; (**b**) *C. antarcticus* colonies exposed in the (Original Substrate (OS) substratum; (**c**) *C. antarcticus* colonies exposed in the Phillosilicate Mars Regolith Simulant (P-MRS) analogue; (**d**) *C. antarcticus* exposed in the Sulfatic Mars Regolith Simulant (S-MRS) analogue. POS CTR: laboratory control; CTR: Control; NEG CTR: Negative Control.

Table S2.2. Estimated resistance of dried colonies of *C. antarcticus* to HZE on the Martian surface and shallow subsurface. Based on the survival of *C. antarcticus* colonies after accelerated Fe ions exposure, it is possible to determine the resistance of the fungus to HZE cosmic rays in a hypothetical Martian scenario. The second column shows the estimated number of the accelerated Fe ions that hit each sample (Martian regolith mixed to *C. antarcticus* colonies, 200 ml) in our experiment, calculated according to Alpen et al., 1994. In the third column, an estimation of the years required by the same volume of Martian regolith to absorb the calculated number of HZE ($Z \geq 26$) on Mars. Due to their relative abundances and high LET, accelerated Fe ions can be considered as representative of HZE cosmic rays reaching the Martian surface. The values were estimated by using the fluxes measured by The RAD Curiosity for CRs having atomic numbers ≥ 26, with the atmospheric depth of 21 g/cm^2 and the solar modulation parameter (F) of 577 MV (Ehresmann et al., 2014). The fourth column shows survival of *C. antarcticus* colonies, relative to the respective controls, at every dose of exposure in the distinct materials.

Dose (Gy)	**Fe Ions Fluence (Ions/Sample)**	**Time Exposure on Mars (Earth Years)**	***C. antarcticus* survival (% colonies)**
50	111×10^6	532×10^3	Directly exposed: 87.2; OS: 13.3; P-MRS: 67.3; S-MRS: 10.2
250	552×10^6	$2{,}662 \times 10^3$	Directly exposed: 42.1; OS: 23.9; P-MRS: 51.7; S-MRS: 0
500	$1{,}105 \times 10^6$	$5{,}327 \times 10^3$	Directly exposed: 33.1; OS: 0.3; P-MRS: 0.5; S-MRS: 6.9
1000	$2{,}211 \times 10^6$	$10{,}653 \times 10^3$	Directly exposed: 13.2; OS: 1.6; P-MRS: 0.1; S-MRS: 3.1

Alpen, E. L., Powers-Risius, P., Curtis, S. B., DeGuzman, R., & Fry, R. J. M. (1994). Fluence-based relative biological effectiveness for charged particle carcinogenesis in mouse Harderian gland. Advances in Space Research, 14(10), 573-581.

Böttger, U., de Vera, J. P., Fritz, J., Weber, I., Hübers, H. W., & Schulze-Makuch, D. (2012). Optimizing the detection of carotene in cyanobacteria in a martian regolith analogue with a Raman spectrometer for the ExoMars mission. Planetary and Space Science, 60(1), 356-362.

Ehresmann, B., Zeitlin, C., Hassler, D. M., Wimmer-Schweingruber, R. F., Böhm, E., Böttcher, S., ... & Reitz, G. (2014). Charged particle spectra obtained with the Mars Science Laboratory Radiation Assessment Detector (MSL/RAD) on the surface of Mars. Journal of Geophysical Research: Planets, 119(3), 468-479.

Chapter 3

The Responses of the Black Fungus *Cryomyces antarcticus* to High Doses of Accelerated Helium Ions Radiation within Martian Regolith Simulants and Their Relevance for Mars

Claudia Pacelli[1,2], Alessia Cassaro[2]*, Lorenzo Aureli[2], Ralf Moeller[3,4], Akira Fujimori[5], and Silvano Onofri[2]

[1]Italian Space Agency, Via del Politecnico snc, 00133 Rome, Italy; claudia.pacelli@asi.it

[2]Department of Ecological and Biological Sciences, University of Tuscia, Largo dell'Università snc, 01100 Viterbo, Italy;

[3]German Aerospace Center, Institute of Aerospace Medicine, Radiation Biology Department,

Space Microbiology Research Group, DLR, Linder Höhe, D-51147 Köln, Germany;

[4]Natural Sciences, University of Applied Sciences Bonn-Rhein-Sieg (BRSU), von-Liebig-Straße 20, D-53359 Rheinbach, Germany

[5]Molecular and Cellular Radiation Biology Group, Department of Basic Medical Sciences for Radiation Damages, NIRS/QST, Chiba 263-8555, Japan

Published on *Life*, 10(8), 130. https://doi.org/10.3390/life10080130

Abstract

One of the primary current astrobiological goals is to understand the limits of microbial resistance to extraterrestrial conditions. Much attention is paid to ionizing radiation, since it can prevent the preservation and spread of life outside the Earth. The aim of this research was to study the impact of accelerated He ions (150 MeV/n, up to 1 kGy) as a component of the galactic cosmic rays on the black fungus C. antarcticus when mixed with Antarctic sandstones—the substratum of its natural habitat—and two Martian regolith simulants, which mimics two different evolutionary stages of Mars. The high dose of 1 kGy was used to assess the effect of dose accumulation in dormant cells within minerals, under long-term irradiation estimated on a geological time scale. The data obtained suggests that viable Earth-like microorganisms can be preserved in the dormant state in the near-surface scenario for approximately 322,000 and 110,000 Earth years within Martian regolith that mimic early and present Mars environmental conditions, respectively. In addition, the results of the study indicate the possibility of maintaining traces within regolith, as demonstrated by the identification of melanin pigments through UltraViolet-visible (UV-vis) spectrophotometric approach.

Keywords: Galactic Cosmic Rays (GCRs); Mars environment; black fungi; survival; UV-vis spectroscopy; resistance; melanin

3.1 Introduction

Mars is the prime target for the search of life beyond Earth, primarily because of the environmental conditions that have occurred in the past. Mars has evidence for past liquid water on the surface and an atmosphere that contains the essential elements for life (Di Achille and Hynek 2010; Jakosky et al., 2017); moreover, the cold and dry conditions on the planet provide the opportunity that evidence for putative life may be well preserved. However, the Martian surface is characterized by an ionizing radiation environment significantly greater than that of Earth and therefore represents the major limitations for microbial survival in dormant state on present-day Mars. The thin Martian atmosphere and the absence of an ozone shield offer practically no protection against solar UV. The primary effects of UV radiation are a concern only on the surface of Mars, since the penetration of UV photons is limited to only a few micrometers (Parnell et al., 2007) in the Martian near-subsurface or up to meters under a layer of snow or water (Fornaro et al., 2018).

The ionizing radiation of solar energetic protons (SEP) and galactic cosmic rays (GCR) dominate in the top few meters (Parnell et al., 2007; Fornaro et al., 2018). It has been measured by a Radiation Assessment Detector (RAD) instrument that the GCR dose rate that reached the Martian surface vary between 180–225 μGy/day (Hassler et al., 2014). The GCR spectrum is composed of 85% protons, 14% alpha particles (He ions), and a small fraction of heavy ions (fully ionized atomic nuclei). Ionizing radiation is measured in Gy, which is the total amount of energy deposited by ionizing radiation in a unit mass of the target material; different qualities of radiation can have different biological effectiveness, depending on their Linear Energy Transfer (LET) (Kiefer et al., 1993). With increasing LET, it increases the density of ionization leading to a condensation of radiation effects in cells (Kiefer, 1990; 1993; Hassler et al., 2014). Densely ionizing radiation, such as the heavy ions and helium nuclei, can cause clusters of nearby DNA strand breaks, and so are particularly detrimental to cellular survival. Ionizing radiation can damage cellular components through direct deposition of radiation energy into biomolecules and indirectly by generating reactive oxygen species (ROS) (Kiefer, 1990). While a metabolically active microorganism can repair the damages, the current freezing and water conditions in the Martian near-subsurface imply that any putative form of life could be dormant, so that the total dose accumulated over these periods could be crucial in determining cell survival (Dartnell et al., 2007).

Consequently, ionizing radiation imposes an upper boundary on the amount of time that a microbial organism can remain dormant in the near-subsurface of Mars. While a lot of experiments have been performed under simulated Martian conditions, mainly to study the microbial response to Martian UV, diurnal temperature shifts, and surface pressure (Rettberg et al., 2004; Newcombe et al., 2005; Osman et al., 2008), there has been relatively few investigations on the impact on ionizing radiation for (potential) microbial life on Mars. In natural Earth environments, microorganisms have capabilities to adapt to extreme conditions, including high dose of radiation uncommon on Earth, expanding the limits of habitability of Earth-like life beyond Earth. For example, melanized fungi are able to colonize environments with high radiation levels. A previous study (Zhdanova, 2000) has reported that some fungal

species are able to survive in the area around the Chernobyl reactor, growing towards the radiation source. Black fungi are also able to colonize spacecrafts that are considered high radiation environments (Schuerger et al., 2003; 2006).

The black fungus *C. antarcticus*, which thrives in the extreme environment of ice-free land of McMurdo Dry Valleys in Antarctica (Selbmann et al., 2005), has an unbelievable ability to resist physical extremes beyond its natural environment. Based on this extraordinary resistance, it has been widely used as test-organisms for astrobiological studies in both spaceflight and ground-based simulations. On board the European Space Agency (ESA) exposure facility EXPOSE E (Selbmann et al., 2005; Onofri et al., 2012; 2015), dried colonies of *C. antarcticus* were exposed during 18 months to the extreme parameters encountered in space, including space vacuum, temperature cycles, and different spectral ranges of solar UV radiation, and also a simulated Mars environment in space (solar UV radiation 200–400 nm MJ/m^2, cosmic radiation between 220–238 mGy and temperature cycles between −21.7 to +42.9 °C). Recent studies have also demonstrated its ability to resist a different kind of densely and sparsely ionizing radiation (Onofri et al., 2018; Pacelli et al., 2017a; 2017b; 2018; Selbmann et al., 2018).

Part of this resistance was attributed to the presence of melanin in the cell-walls (Pacelli et al., 2017b), the protection of extra-cellular polymeric substances (Onofri et al., 2007), and probably the production of compatible endocellular cryoprotectants such as glycerol (Brown et al., 1978) and trehalose (Weinstein et al., 2000). Here, in the frame of the STARLIFE irradiation campaign which aims to characterize the response of selected microorganisms to space-relevant radiation (Moeller et al., 2017), we have analyzed the survival of *C. antarcticus* after irradiation with accelerated He ions, which is a component of the galactic cosmic spectrum. The goal was to address the following question: does radiation of accelerated He ions affect the survival of fungal cells within Mars regolith simulants? To answer this question, dried colonies of the fungus were mixed with Antarctic sandstones (the substratum in which they naturally live) and with two Mars regolith simulants, namely Phyllosilicatic Mars Regolith Simulant (P-MRS; early evolutionary stages of Mars) and Sulfatic Mars Regolith Simulant (S-MRS; late evolutionary stages of Mars) (Böttger et al., 2012), and exposed to increasing doses of He ions. The post-exposure viability was assessed by both cultivation and molecular methods in terms of growing ability, DNA and plasmatic membrane integrity, and metabolic activity recovery. Moreover, the stability of melanin pigments, as component of fungal cell-wall, after radiation was checked by UV-vis spectroscopy.

3.2 Materials and Methods

3.2.1 Samples Preparation and Exposure Conditions

The Antarctic cryptoendolithic black fungus Cryomyces antarcticus CCFEE 515 was isolated by R. Ocampo-Friedmann from sandstone collected by H. Vishniac at Linnaeus Terrace (McMurdo Antarctic Dry Valleys, Southern Victoria Land) during the expedition in 1980–1981.

The fungus was isolated in Malt Extract Agar Petri Dishes as reported in [16], and since then it has been stored in the Culture Collection of Fungi From Extreme Environment (CCFEE) of University of Tuscia (Viterbo, Italy) that is a section of the Italian National Antarctic Museum. Firstly, a total of 2000 Colony-Forming Units (CFU) was spread from a 15 °C culture on Malt Extract Agar (MEA) medium (malt extract, powdered 30 g/L; agar 15 g/L; Applichem, GmbH) in Petri dishes, incubated at 15 °C for 3 months.

After growth, the colonies were desiccated under laminar flow in a sterile cabinet for one night. Once dried, colonies were mixed to three distinct materials and standard PCR tubes (200 μL volume) were totally filled with the different mixtures and fungal colonies. The mineral mixtures were previously dried-sterilized at 140 °C for 4 hours.

Three sets of samples were thus investigated: i) colonies mixed with grinded Antarctic sandstone that is the Original Substratum (OS) where the fungus naturally occurs; ii) colonies mixed with P-MRS that mimics the regolith of phyllosilicate deposits mainly occurred on early Mars; iii) colonies mixed with S-MRS that is an analogue of regolith mainly observed in the current Martian sulphate deposits. The mineralogical composition of the Martian analogues is reported in Table S3.1 (from Böttger et al., 2012).

Samples were exposed to increasing doses of accelerated He ions (He^{2+}, 150 MeV/n, LET in water: 2.2 keV/μm) at the Heavy Ion Medical Accelerator in Chiba (HIMAC) facility at the National Institute of Radiological Sciences (NIRS) in Japan. The applied doses were 50, 250, and 1000 Gy and the dose rate was 4.4 Gy/min; all samples were irradiated in a homogenous beam area. Laboratory controls (0 Gy) were kept in the laboratory at room temperature. All tests were performed in triplicate.

3.2.2 Survival Assessment

3.2.2.1 Cultivation Test

Cultivation test was performed to determine the survival of fungal colonies after exposure to increasing doses of accelerated helium ions. Colonies from each set of samples were removed from the respective analogue with a sterile tweezer and rehydrated at 15 °C adding 1 mL of physiological solution (NaCl 0.9%) for 72 h.

The colonies were diluted to a final concentration of 50000 CFU/mL, and 0.1 mL (5000 CFUs) for each sample was spread on MEA Petri dishes in quintuplicate. Samples were incubated at 15 °C for 3 months and the grown colonies were counted. Non-irradiated samples were kept in laboratory under room temperature and used as controls. In addition, dried colonies exposed without minerals to increasing doses of accelerated He ions from previous experiment (Pacelli et al., 2017b) were used as reference and they are referred as un-shielded colonies.

3.2.2.2 Membrane Damage Assessment

Quantitative PCR (qPCR) of DNA from samples treated with Propidium MonoAzide (PMA) was performed to assess the membrane integrity in samples. An aliquot of each rehydrated sample was added with 5 μL of a PMA solution (200 μM) and incubated in the dark for 1 h with constant shaking. Samples were then placed in ice and exposed to a halogen lamp

for 10 min. PMA can selectively penetrate cells with damaged membranes and cross-link to DNA under exposure to light, thereby preventing Polymerase Chain Reaction (PCR). DNA extraction and purification were performed on PMA treated and untreated aliquots from each sample. DNAs were quantified and normalized at the same concentration (2 ng/mL) using the Qubit dsDNA HS Assay Kit (Thermo Fisher Scientific, Massachusetts, USA) and qPCR was performed to quantify the number of fungal internal transcribed spacer (ITS) ribosomal DNA fragments (281 bp) in both PMA-treated and untreated samples, according to (Onofri et al., 2018). All tests were performed in triplicate.

3.2.2.3 Metabolic Activity Assessment by MTT (3-(4,5-dimethylthiazol-2-yl)-2,5-diphenyltetrazolium bromide) Assay

MTT assay was performed as a colorimetric test to evaluate metabolic activity of fungal cells. A total of 100 µL of cell suspensions (3.5 × 105 cells/mL) in Phosphate-Buffered Saline (PBS), containing 0.5 mg/mL MTT salt (Thermo-Fisher scientific) were put into 96-well microplates. After incubation in the dark at room temperature for 48 and 72 h, MTT solution was removed with a multi-channel pipette and 100 µL of DiMethyl SulfOxide was added. The absorbance was read at 595 nm, and the average absorbance of wells containing only MTT was subtracted from the others. Means and standard deviations were calculated, and results were normalized with the laboratory controls.

3.2.2.4 Statistical Analyses

Statistical analyses were performed by one-way analysis of variance (ANOVA) and pair wise multiple comparison procedure (Tukey's test, Parameswaran et al., 1979), carried out using the statistical software SigmaStat 2.0 (Jandel).

3.2.3 DNA Integrity Assessment

3.2.3.1 DNA Extraction, Single Gene PCRs, and Random Amplified Polymorphic DNA Analysis

DNA extraction was performed on dried colonies using the NucleoSpin® Plant kit (Macherey-Nagel, Düren, Germany) following the protocol optimized for fungi (Onofri et al., 2015). Quantitation of extracted genomic DNA was performed using the Qubit system and all the samples were diluted to the same concentration (2 ng/mL). Three overlapping tracts in the Internal Transcribed Spacer (ITS) regions and the Large SubUnit-coding Sequences (LSU) of the nuclear ribosomal RNA (rRNA) gene complex were amplified. The used primers were ITS4a (ATTTGAGCTGTTGCCGCTTCA), ITS5 (GGAAGTAAAAGTCGTAACAAGG), LR5 (TCCTGAGGGAAACTTC) and LR7 TACTACCACCAAGATCT). PCR reactions were carried out for each sample in a solution consisting of 12.5 µL of BioMixTM (BioLine Ltd., London), 1 µL of each primer solution (5 pmol/µl), and 0.2 ng of DNA template, nuclease-free water was added until to reach the final volume of 25 µL. MyCycler Thermal Cycler (Bio-Rad Laboratories GmbH, Munich, Germany) equipped with a heated lid was used and amplification conditions are as reported in Selbmann et al., (2011). Relative band intensities were measured and compared by using Image Lab Software Version 6.1 (Bio-Rad, Hercules, California, USA).

The whole genome integrity was assessed by Random Amplified Polymorphic DNA (RAPD). PCR reactions were carried out for each sample in a final solution containing 12.5 µL of BioMixTM, 5 pmol of primer $(GGA)_7$ and 0.2 ng of DNA sample, in a final volume of 25 µL. Amplifications were performed according to Selbmann et al., (2011).

3.2.3.2 DNA Integrity by Quantitative qPCR Assay

Quantitative PCR was carried out to quantify the number of amplified ITS rDNA region by using LR0R and LR5 primers. The qPCR reactions were performed in triplicate with a solution containing 7.5 µL of qPCR cocktail (iQ SYBER Green Supermix, Biorad, MI, Italy), 1 µL of each primer solution (5 pmol/µL), and 0.1 ng of DNA template in a final volume of 15 µL. The amplifications were carried out by Biorad CFX96 real time PCR detection system.

3.2.4 Fungal Melanin Extraction and Spectrophotometric Analysis

Melanin was extracted from dried colonies of C. antarcticus grown on different substrata, following the protocol optimized for black fungi (Pacelli et al., 2020). After the extraction, purified pigments were dissolved in 500 µL of NaOH 1M and its UV-Visible spectrum was measured in VWR-UV 1600 PC Spectrophotometer by using M.Wave professional 2.0 software (VWR, Radnor, Pennsylvania, USA).

A standard graph for estimation was used and was made using synthetic melanin. NaOH 1M was used as a blank and the instrument was set in a range of 200–800 nm for the analysis. The correlation between absorbance and wavelength was defined. To determine the concentration of extracted melanin, synthetic DHN (1,8-DiHydroxyNaphthalene) melanin (Thermo Fisher Scientific) was prepared in 1M NaOH at concentrations of 500 mg/mL and a standard curve at 650 nm was obtained as reported in (Raman and Ramasamy, 2017).

3.3 Results

3.3.1 Cultivation Test

The survivability of the black fungus *C. antarcticus* after irradiation with accelerated helium ions was determined by counting the numbers of colonies formed on MEA plates, compared to the controls. Colonies survival was plotted as a function of the applied dose of accelerated He ions (Figure 3.1). Obtained data were compared with previous results, where the fungus was irradiated in absence of any substratum (Pacelli et al., 2017b). D_{10} values, the dose lethal for 90% of the initial colonies, were calculated from the survival curves, expressed by LogN values and are reported in Table 3.1.

Overall, survival results showed a common trend that is a fungal growth decrease as the radiation dose increases (Figure 3.1). Figure 3.1 (black line) shows the survival of *C. antarcticus* colonies mixed with OS substratum; appreciable growth ability up to 50 Gy, with a 31% of survivors, and loss of growth at the doses of 250 and 1000 Gy. Samples mixed with the P-MRS analogue showed a dose-dependent growth decrease, although the survival was reported even at the highest dose (6% of survivors at 1000 Gy; Figure 3.1, grey line). For

colonies mixed in S-MRS analogue, the growth ability was maintained up to 250 Gy, with 6.5% of survivors (Figure 3.1, light grey line). No growth was recorded for samples irradiated with 1000 Gy.

Table 3.1. D_{10} values = dose (Gy) of He ions irradiation leading to a 90% inactivation of the initial Coloning Forming Unit (CFU).

Samples	D_{10}
Un-shielded colonies[a]	5000
Colonies mixed with OS	101
Colonies mixed with P-MRS	667
Colonies mixed with S-MRS	227

[a]Reference samples from Pacelli et al., (2017b). OS= Original Substrate; P-MRS= Phyllosilicatic Mars Regolith Simulant; S-MRS= Sulfatic Mars Regolith Simulant.

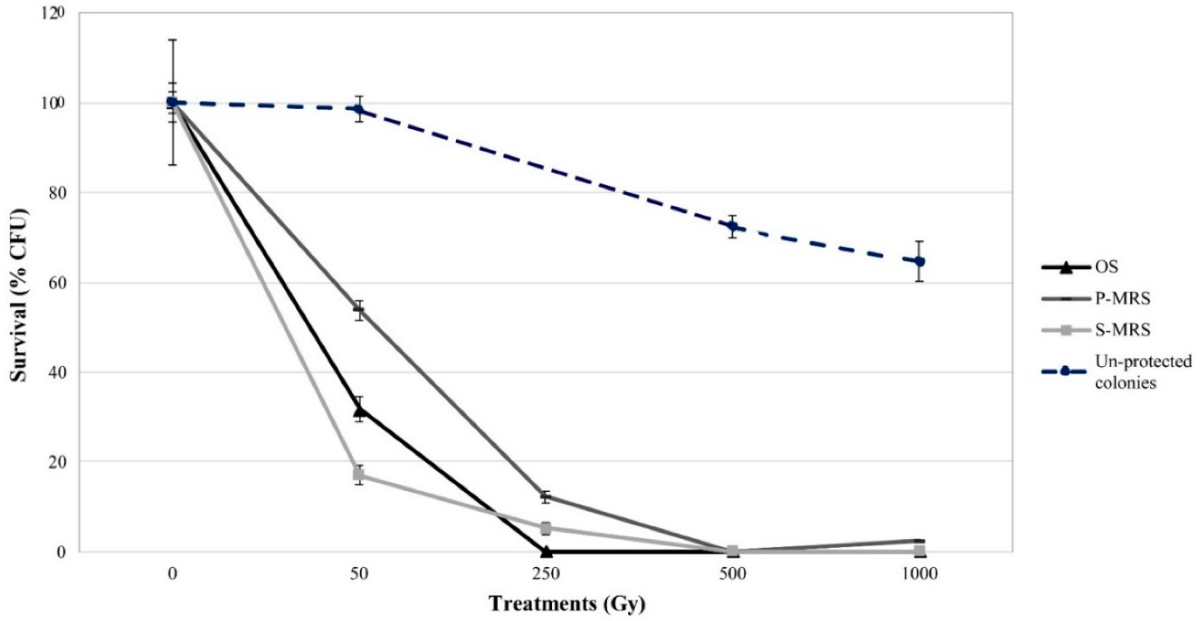

Figure 3.1. Cultivation test performed in colonies exposed to accelerated helium ions in presence of OS (Original Substrate) (black line), P-MRS (Phyllosilicatic Mars Regolith Simulant) analogue (grey line), and S-MRS (Sulfatic Mars Regolith Simulant) analogue (light grey line); compared with irradiated un-shielded colonies (dashed blue line; data from Pacelli et al., 2017b). Significant differences werecalculated by Tukey's test with * $p < 0.05$ and ** $p < 0.001$.

3.3.2 Membrane Damage Assessment

The PMA assay coupled with qPCR was used to discriminate damaged cell-membranes to undamaged cell-membranes. PMA is a compound that can only penetrate cells with compromised cell membranes, binds DNA and prevents amplification. Figure 3.2A showed progressive cell-membranes damage with the increasing of irradiation for colonies mixed with OS substratum (up to35.3% of damaged membranes at 1000 Gy). The doses of 50 Gy and 250

Gy did not show a significant difference compared to the control. *C. antarcticus* colonies mixed with P-MRS analogue (Figure 3.2B) maintained 12.87% of intact cell membranes at the highest dose (1000 Gy), while colonies mixed with S-MRS showed a low percentage of compromised membranes as 13.25 and 7.46% for 50 and 250 Gy, respectively (Figure 3.2C). However, non-statistically significant differences were found among 50 and 250 Gy irradiated samples, compared with the relative control. Around 30% of cells with damaged cell-membranes were recorded for colonies after irradiation at 1000 Gy.

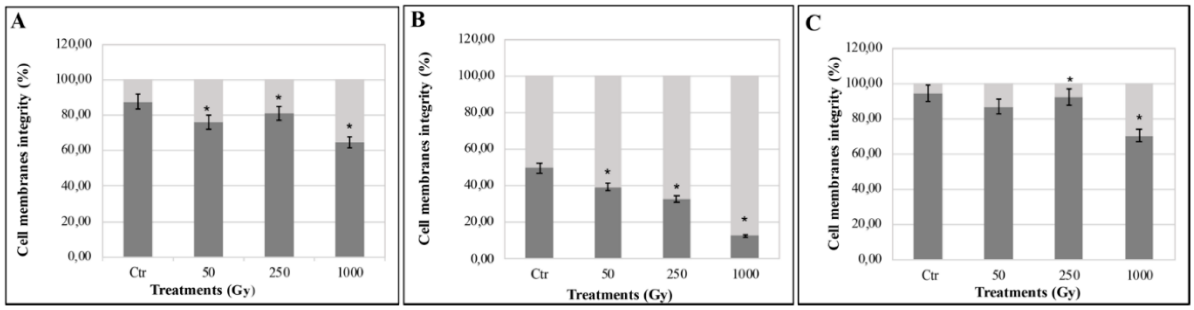

Figure 3.2. Percentage of intact and damaged cell-membranes measured with Propidium Mono Azide (PMA) assay coupled with qPCR of *C. antarcticus* mixed with (A) OS substratum, (B) P-MRS, and (C) S-MRS analogues. Light grey bars represent the percentage of cells with damaged cell membranes; dark grey bars represent the percentage of cells with un-damaged cell membranes. Statistical analyses are as in Figure 3.1.

3.3.3 Metabolic Activity Assessment by MTT Assay

In metabolically active cells, MTT is reduced to a water-insoluble blue formazan by the succinate dehydrogenase, enzyme of the mitochondrial respiratory chain. The reduced product is quantified spectrophotometrically by dissolution in an organic solvent (DMSO), and the measured concentration is directly proportional to the number of metabolically active cells. Here, the MTT assay was performed to investigate to which extent cells are able to re-activate metabolic activity after the irradiation treatments. Figure 3.3 shows the metabolic activity recovery of irradiated cells after 48 h of rehydration. The MTT results of colonies mixed with OS substratum, demonstrated a decrease in *C. antarcticus* metabolic activity, with the increasing of helium ions irradiation doses (Figure 3.3A). Formazan production of colonies mixed with P-MRS analogue (Figure 3.3B) revealed a high quantity at 250 Gy dose and a low formation at 50 and 1000 Gy doses, compared with the control. A similar trend for samples exposed at 250 Gy of accelerated helium ions has been found for samples mixed with S-MRS analogue (Figure 3.3C). However, a good amount of metabolic activity was reported at the highest tested dose of 1000 Gy in all samples, despite the analogues.

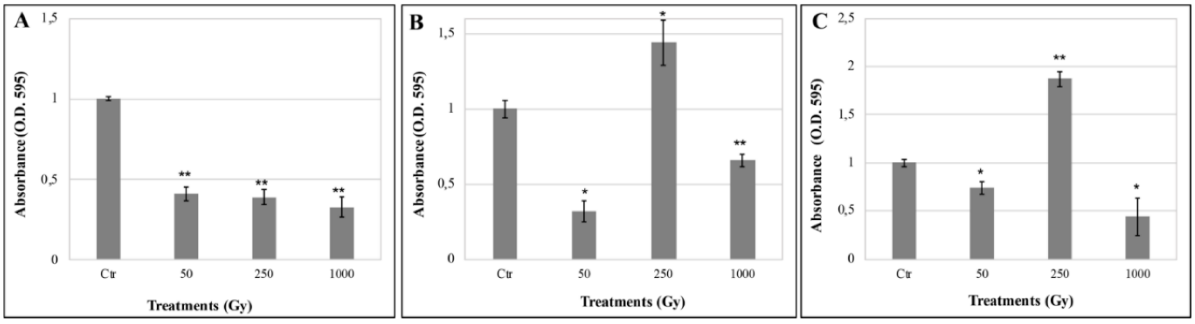

Figure 3.3. Effect of accelerated helium ions irradiation on metabolic activity recovery of *C. antarcticus* mixed with (A) OS substratum, (B) P-MRS, and (C) S-MRS analogues by MTT assay. Statistical analyses are as in Figure 3.1.

3.3.4. DNA Integrity Assessment

The amplified DNA fragments were obtained from amplification of ITS-LSU regions of 700, 1600, and 2000 bp, respectively. Figure 3.4A–C reported electrophoresis gels from amplification obtained from ITS5-ITS4a, ITS5-LR5, and ITS5-LR7 primers. Results showed no evident differences in DNA amplification among controls and irradiated samples of each sets. The whole genome was investigated by RAPD assay, based on PCR amplifications of genomic DNA, utilizing a short unspecific primer that is able to bind to different points in the genome and to reproduce a specific band pattern for the tested organism. The RAPD profiles were preserved in all the conditions tested (Figure S3.2). Any disappearance of high molecular weight band, that is expected in case of extensive DNA damage (Atienzar et al., 2000), was reported in the irradiated samples, indicating a good integrity of the whole DNA.

DNA damage analysis was performed by quantitative amplification of a gene, spanning the ribosomal LSU, of 939 bp length. Figure 3.4A–C showed the number of amplified DNA fragments after irradiation with increasing doses of accelerated helium ions mixed with the OS substratum, P-MRS, and S-MRS analogues, respectively. The results revealed a reduced DNA amplification while increasing the radiation doses for all tested samples. In overall, around 19,000 DNA copies were amplified on average and the amplification never goes less than 100 copies. Summarizing, all the gene amplifications worked out and the number of amplified DNA copies was never under the amplification limit.

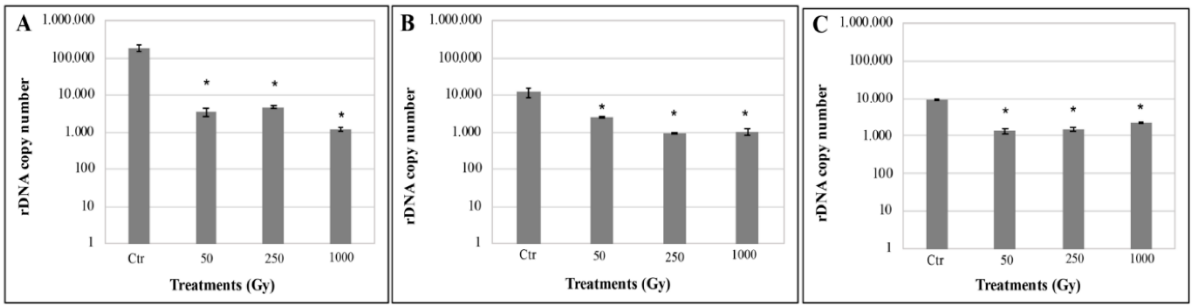

Figure 3.4. rDNA (Internal Transcriber Spacer (ITS)-Large SubUnit region (LSU)) copy number quantification by qPCR of DNA of *C. antarcticus* colonies mixed with (A) OS substratum, (B) P-MRS, and (C) S-MRS analogues exposed to accelerated helium ions. Statistical analyses are as in Figure 3.1.

3.3.5. Melanin Investigation by Spectrophotometric Analyses

Spectrophotometric analyses were performed on fungal melanin extracted from *C. antarcticus* colonies mixed with OS substratum and P-MRS and S-MRS analogues, after exposure to accelerated helium ions. The wavelength of maximum absorbance was scanned at a range of 200 to 800 nm. The UV-visible absorbance spectrum of the purified pigments showed a strong absorbance in the UV region. The strong absorption in the UV region with a progressive decrease at high wavelengths is due to the presence of complex conjugated structures in the melanin molecule (Bell and Wheeler, 1986). Figure 3.5 shows the melanin spectra obtained from colonies mixed with OS substratum (Figure 3.5A), P-MRS (Figure 3.5B) and S-MRS (Figure 3.5C) analogues, exposed to 50 (black lines), 250 (grey lines), and 1000 Gy (light grey lines), compared with the controls (blue lines).

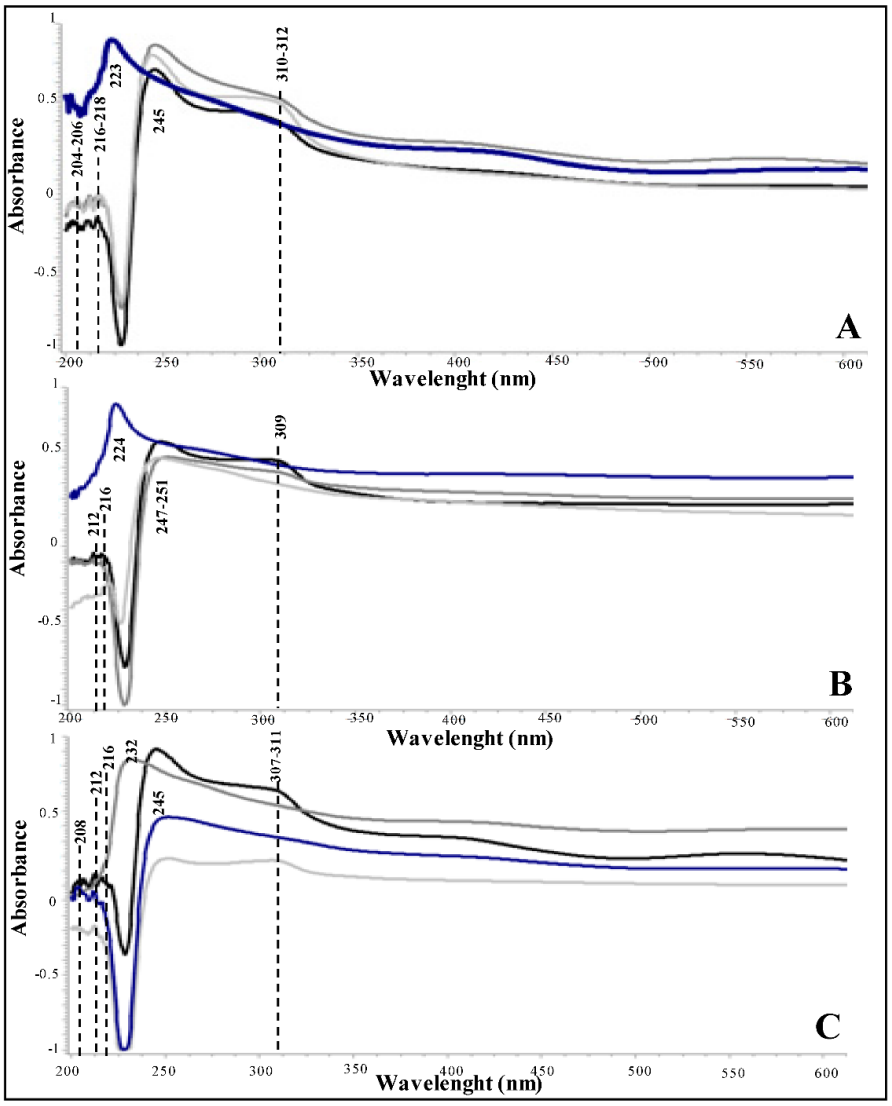

Figure 3.5. UV-Vis spectra of melanin pigment extracted from *C. antarcticus* colonies mixed with (A) OS substratum exposed to simulated space conditions and (B) P-MRS, and (C) S-MRS analogues and exposed to accelerated helium ions at the doses of 50 Gy (black line), 250 Gy (grey line), 1000 Gy (light grey line), and the respective control (blue line).

Changes in melanin absorbance has been reported in the irradiated samples, with an absorption peak around 245–251 nm; compared with relative controls, which shown an absorption peak at 223–224 nm, the typical wavelength of absorbance of *C. antarcticus* melanin pigments (Pacelli et al., 2020). In addition, a bulge at ~310–312 nm was revealed only in exposed samples of OS set, in 50 Gy irradiated samples of P-MRS set, and 50 and 250 Gy irradiated samples of S-MRS sets, probably due to the presence of minerals during the UV-vis detection process. In fact, it could be representative of the goethite, which in general shows an UV absorbance near 330 nm, attributable to an Fe^{3+}–O charge transfer (Cloutis et al., 2008; Öztekin et al., 2008).

In the initial part of the spectrum, which corresponds to lower wavelengths, the additional near 216–218 nm could be associated with the presence of montmorillonite, the main component (45%wt) of the P-MRS analogue (Cloutis et al., 2008; Öztekin et al., 2008), as further confirmation of the presence of mineral grains in the sample during the detection.

The concentration of extracted melanin was estimated by comparing the absorbance value at 650 nm of each melanin sample with the A650 standard curve of synthetic DHN melanin (Fig. S3.3), and concentration values (mg/mL) were reported for all OS, P-MRS, and S-MRS samples in Table S3.2.

3.4 Discussion

The surface of Mars, unshielded by a thick atmosphere or by a global magnetic field, is exposed to high levels of cosmic radiation. This radiation environment is deleterious to the survival of dormant cells or spores and to the persistence of molecular biomarkers in the subsurface. The effects of ionizing radiation on Earth life is of high astrobiological interest. Among radiation, the direct effects of UV are a concern only on the surface of Mars, and the penetration of UV photons is limited to only a few micrometers (Parnell et al., 2007; . Johnson et al., 2011); while ionizing radiation has to be considered also for the subsurface. Indeed, Martian atmosphere is continuously traversed by GCR, which mainly consist of accelerated protons (about 87%) and helium ions (about 12%) (Simpson, 1983). These particles are the main radiation component both of the Martian radiative environments, either of the deep space. Primary GCR particles with energies that exceed the atmosphere cut-off, which has an average shielding depth of 23 g/cm^2, hit the Martian surface. Here, due to the relative abundances of the particles and their different penetrating depths, accelerated protons and helium ions (Ehresmann et al., 2014) dominate the radiation environment. Ions incident on the Martian surface can penetrate the top meters of regolith until attenuated (Newcombe et al., 2005). Therefore, the shielding by the regolith against GCR may play a critical role in fostering the persistence of hypothetical forms of life in the subsurface environment of Mars. However, a decrease in the absorbed dose due to GCR particles is only observed from a few centimeters beneath the surface, without significant variations within the near-surface layer (Röstel et al., 2020). Therefore, this phenomenon makes GCR particles a critical hazard not only for any putative form of life colonizing the first few centimeters of Martian regolith, but also for the future space missions around the lunar orbit and towards Martian cruise.

In this context, the present experiment reproduced part of the radiation environment predicted in the loose dry regolith making up the shallowest layer of Martian surface, in order to assess its suitability to survival of terrestrial-like forms of life. To this purpose, we have exposed dry colonies of the cryptoendolithic black fungus C. antarcticus to increasing doses of accelerated He ions (up to 1 kGy), while mixed with Antarctic sandstones and two Martian regolith analogues. Indeed, accelerated He ions, together with protons, contribute to the major part of the absorbed dose induced by GCR in the surface and the shallow subsurface environments of Mars (Matthiä et al., 2017; Röstel et al., 2020). A study of the effect of elevated radiation doses, which significantly exceed the radiation on the surface of Mars (i.e., 76 mGy/yr) (Hassler et al., 2014) as in the case of this experiment, is necessary for the extrapolation of biological effects on the geological time scale. Furthermore, in addition to ionizing radiation, the uppermost layer of the Martian subsurface is characterized by conditions of hyperaridity and extreme temperature variations. However, the presence of salts (namely perchlorates, sulphates, chlorides carbonates and nitrates (Smith et al., 2014), may let to a periodical formation of transient brines by deliquescence in the uppermost centimeters of the subsurface, thus making available limited amounts of liquid water in a latitude-dependent fashion (Martín-Torres et al., 2015). Although no strong evidence of liquid water in an adequate amount to support terrestrial-like forms of life exists, the seasonality of the availability of shallow brines (Jones, 2018) would imply that any putative extant life in the near-surface environment is dormant (i.e., metabolically inactive) for long periods of time, thereby accumulating GCR doses over seasonal periods, until being reactivated by the presence of liquid water. Alternatively, the dormant state may expand over geological periods, until the cellular reactivation by global or local changes in the environmental parameters. Therefore, the total dose accumulated over these periods will be crucial in determining cell survival, and not the rate at which it is absorbed.

In our experiment, irradiation with up to 0.5 kGy of He ions, did not eradicate populations of *C. antarcticus* and did not induce high damage to either DNA or cell membranes.

The fungus survives doses up to 250, 1000, and 250 Gy when mixed with OS substratum and PMRS and S-MRS analogues, respectively (Figure 3.1). These values are lower when compared with the same fungus exposed to the same He ions radiation without the minerals, where 70% of survivors were reported at the dose of 1000 Gy (Pacelli et al., 2017b, reported as reference in Figure 3.1, dashed line). This is more evident when looking at the D_{10} values (Table 3.1). The observation that fungi mixed with Antarctic sandstones and Martian regolith simulants were significantly more sensitive, with D_{10} values of 10, 667, and 227 Gy, respectively, than un-shielded fungal colonies (D_{10} = 5000 Gy, extrapolated data from Pacelli et al., 2017b) to He ions radiation was quite surprising. This means that in the presence of Martian regolith simulants, instead of having protection, the number of secondary generated radiation, reduce the possibility for dormant fungal cells to persist in Martian subsurface environment of 10 times (Table 3.1). It can be suggested that fungal cells mixed with artificial Martian regolith, a complex mixture of various water-absorbing minerals (e.g., montmorillonite, kaolinite, hematite, anhydrite) were additionally affected by the generation

of ROS such as peroxide, superoxide, or hydroxyl radicals in the Martian regolith simulants (Dianov et al., 2001; Bibring et al., 2005; Moeller et al., 2010; Saganti and Cucinotta, 2014). In our experiment, accelerated He ions radiation allows a re-activation of metabolic activity that was, however, not dose-dependent in *C. antarcticus*, as irradiation at 250 Gy led to an increase in metabolic activity in colonies mixed with P-MRS and S-MRS analogues (Figure 3.3). This would be explained by the fact that, depending on the extent of cellular damage, the ionizing radiation can either kill the cell or activate a response. In the latter case, one of the main cellular responses after radiation exposure is represented by mitochondrial biogenesis. The MTT assay for evaluating the metabolic activity is the MTT assay used to measure the mitochondrial activity, therefore an enhanced production of mitochondria as response to radiation exposure may lead to an increase of the general metabolic activity (Moeller et al., 2010). Accordingly, the increase of metabolic activity reported for cells mixed with PMRS and S-MRS analogues (Figure 3.3B and 3.3C, respectively) can be attributed to an activated response of colonies to repair the radiation-caused damages after re-hydration.

Accelerated He ion radiation caused a certain amount of damage to cell membranes, with a decrease of membrane-intact cells by ~36%, 87%, and 30% at the dose of 1000 Gy in cells mixed with Antarctic sandstones, P-MRS, and S-MRS analogues, respectively (Figure 3.2).

DNA damage was not detectable at all *C. antarcticus* extracted DNA through single gene amplifications that were successful even at highest dose and longest gene sequences tested (Figure S3.1); accordingly, the fingerprinting profiles were perfectly maintained (Figure S3.2). We quantify the number of amplifiable DNA copies, and therefore, the presumably intact DNA molecules through qPCR; it resulted in few DNA degradation (likely caused by the formation of double strand breaks, DSBs) as shown by the reduced amplification efficiencies of DNA from irradiated cells in qPCR reactions (Figure 3.4). Nevertheless, an average of 1000 amplified DNA copies were reported even at 1 kGy exposure and even in samples where no survival was reported.

To put our results in the context of the possible survival of dormant Earth-like cells on Mars, we calculated the time necessary to inactivate 90% of fungal cells (see Supplementary material, Table S3.3). In the present experiment, we only considered the effects of accelerated He ions, which make up 12% of GCR spectrum (Matthiä et al., 2017). The fluxes of He ions on the Martian surface were measured by the Radiation Assessment Detector (RAD) on the Mars Science Laboratory's Curiosity rover over two distinct periods (Ehresmann et al., 2014; Matthiä et al., 2017); the GCR fluxes on Martian surface depends on the thickness of the atmosphere and the modulation by heliosphere, both of which vary periodically (Usoskin et al., 2005; Saganti and Cucinotta, 2014; Berger et al., 2020), and are not composed exclusively of α particles (similar to He ions), they also includes gamma rays and a large proportion of protons, as well as some heavier nuclei. However, a simplified model may be proposed which gives an approximation of the time that would be required by each fungal cell to be hit by as many particles (He ions) as used in the present experiment. He ions used in our experiment had energy of 150 MeV/nuc. Ions with energies lower than this value are more damaging, but less penetrating with very low fluxes. Therefore, in our estimation we considered only particles

measured on Martian surface with energies above 135 MeV/nuc (Matthiä et al., 2017), and we calculated the estimated number of particles that hit the surface of each fungal cell depending on the exposure doses and the average size of fungal cells (around 35 μm). Despite the approximations of our simplified model, our results show as the time necessary to inactivate 90% of fungal cells in a hypothetical Martian surface and near-surface scenario may markedly vary depending on not only the depth in the regoliths at which cells are exposed, but also on the type of the mineral of the regoliths. We estimated that a dormant cell of *C. antarcticus* may be preserved in the surface of Mars for about 322,000 and 110,000 years within P-MRS and S-MRS analogues, respectively (see Table S2.2). Our calculations do not take into account the possibility that in some areas on Mars, temperatures above 0 °C and formation of liquid water are possible (Jones et al., 2011; Jones and Shallow, 2018). In such a case, active cells may be able to repair damages and to reproduct, then they can go in a dormant state until the next period of favorable environmental conditions (i.e., liquid water, warmer temperature) (Westall et al., 2013). Considering this, we can assume an even longer preservation of putative Earth-like life on Mars.

The resistance of *C. antarcticus* to UV radiation doses uncommon for any habitat on Earth was suggested to be partially due to the presence of melanin pigments in the cell-wall (Selbmann et al., 2015), therefore we investigated the preservation of fungal melanin pigments through spectrophotometric approach. Results showed that irradiation with accelerated helium ions may alter the melanin structure. In Figure 3.5A, B and C is reported a shift of the typical melanin absorbance peak near 245–251 nm, with respect to *C. antarcticus* melanin pigment (Pacelli et al., 2020). The additional peaks in the spectra (Figure 3.5A–C) revealed the presence of mineral grains during the detection. Overall, despite the presence of minerals, the detection of melanic pigments is always obtained. Due to their detection properties, it is possible to conclude that melanin pigments have high stability even in highly radiative environments and may have a double role in astrobiological research; their high radiation resistance has significant implications for the radioresistance of hypothetical life form on Mars and for the identification of potential biomarkers in the search for life beyond Earth. This greater radiation resistance has important implications for the estimation of potential survival times of microorganisms near the Martian surface and for the planetary protection issue.

3.5. Conclusions

In conclusion, the present study demonstrated the ability of the terrestrial black fungus *C. antarcticus*, to survive to accelerated He ions exposure in dehydrated form, when mixed with two Martian regolith simulants. Moreover, its biomolecules such as DNA and melanin are stable and detectable with our approaches. These results could have deep implications for future space missions, demonstrating the chance of long-term preservation of terrestrial-like microorganisms and their biomolecules on Mars.

References

Alekhova, T. A., Aleksandrova, A. A., Novozhilova, T. Y., Lysak, L. V., Zagustina, N. A., & Bezborodov, A. M. (2005). Monitoring of microbial degraders in manned space stations. *Applied Biochemistry and Microbiology*, *41*, 382-389.

Atienzar, F., Evenden, A., Jha, A., Savva, D., & Depledge, M. (2000). Optimized RAPD analysis generates high-quality genomic DNA profiles at high annealing temperature. *Biotechniques*, *28*(1), 52-54.

Bell, A. A., & Wheeler, M. H. (1986). Biosynthesis and functions of fungal melanins. *Annual review of phytopathology*, *24*(1), 411-451.

Berger, T., Matthiä, D., Burmeister, S., Zeitlin, C., Rios, R., Stoffle, N., ... & Wimmer-Schweingruber, R. F. (2020). Long term variations of galactic cosmic radiation on board the International Space Station, on the Moon and on the surface of Mars. *Journal of Space Weather and Space Climate*, *10*, 34.

Bibring, J. P., Langevin, Y., Gendrin, A., Gondet, B., Poulet, F., Berthé, M., ... & Omega Team. (2005). Mars surface diversity as revealed by the OMEGA/Mars Express observations. *Science*, *307*(5715), 1576-1581.

Böttger, U., de Vera, J. P., Fritz, J., Weber, I., Hübers, H. W., & Schulze-Makuch, D. (2012). Optimizing the detection of carotene in cyanobacteria in a martian regolith analogue with a Raman spectrometer for the ExoMars mission. *Planetary and Space Science*, *60*(1), 356-362.

Brown, A. D. (1978). Compatible solutes and extreme water stress in eukaryotic micro-organisms. *Advances in microbial physiology*, *17*, 181-242.

Cloutis, E. A., McCormack, K. A., Bell III, J. F., Hendrix, A. R., Bailey, D. T., Craig, M. A., ... & Riner, M. A. (2008). Ultraviolet spectral reflectance properties of common planetary minerals. *Icarus*, *197*(1), 321-347.

Dartnell, L. R., Desorgher, L., Ward, J. M., & Coates, A. J. (2008). Modelling the surface and subsurface martian radiation environment: implications for astrobiology. *International Journal of Astrobiology*, 7(1), 64-64.

Di Achille, G., & Hynek, B. M. (2010). Ancient ocean on Mars supported by global distribution of deltas and valleys. *Nature Geoscience*, 3(7), 459-463.

Dianov, G. L., O'Neill, P., & Goodhead, D. T. (2001). Securing genome stability by orchestrating DNA repair: removal of radiation-induced clustered lesions in DNA. *Bioessays*, *23*(8), 745-749.

Ehresmann, B., Zeitlin, C., Hassler, D. M., Wimmer-Schweingruber, R. F., Böhm, E., Böttcher, S., ... & Reitz, G. (2014). Charged particle spectra obtained with the Mars Science Laboratory

Radiation Assessment Detector (MSL/RAD) on the surface of Mars. *Journal of Geophysical Research: Planets*, *119*(3), 468-479.

Fornaro, T., Steele, A., & Brucato, J. R. (2018). Catalytic/protective properties of martian minerals and implications for possible origin of life on Mars. *Life*, 8(4), 56.

Hassler, D. M., Zeitlin, C., Wimmer-Schweingruber, R. F., Ehresmann, B., Rafkin, S., Eigenbrode, J. L., ... & Berger, G. (2014). Mars' surface radiation environment measured with the Mars Science Laboratory's Curiosity rover. *Science*, 343(6169), 1244797.

Jakosky, B. M., Slipski, M., Benna, M., Mahaffy, P., Elrod, M., Yelle, R., ... & Alsaeed, N. (2017). Mars' atmospheric history derived from upper-atmosphere measurements of $^{38}Ar/^{36}Ar$. *Science*, 355(6332), 1408-1410.

Johnson, A. P., Pratt, L. M., Vishnivetskaya, T., Pfiffner, S., Bryan, R. A., Dadachova, E., ... & Onstott, T. C. (2011). Extended survival of several organisms and amino acids under simulated martian surface conditions. *Icarus*, *211*(2), 1162-1178.

Jones, E. G. (2018). Shallow transient liquid water environments on present-day mars, and their implications for life. *Acta Astronautica*, *146*, 144-150.

Jones, E. G., Lineweaver, C. H., & Clarke, J. D. (2011). An extensive phase space for the potential martian biosphere. *Astrobiology*, *11*(10), 1017-1033.

Kiefer, J. (1990), Radiation Effects on Subcellular Systems. In Biological Radiation Effects: (pp. 121–136). Springer Germany.

Kiefer, J. (1993). Theoretical Analysis of Heavy Ion Action on Cells: Model-Free Approaches, Consequences for Radiation Protections. In Biological Effects and Physics of Solar and Galactic Cosmic Radiation: Part A (pp. 283-290). Springer US.

Martín-Torres, F. J., Zorzano, M. P., Valentín-Serrano, P., Harri, A. M., Genzer, M., Kemppinen, O., ... & Vaniman, D. (2015). Transient liquid water and water activity at Gale crater on Mars. *Nature Geoscience*, *8*(5), 357-361.

Matthiä, D., Hassler, D. M., de Wet, W., Ehresmann, B., Firan, A., Flores-McLaughlin, J., ... & Zeitlin, C. (2017). The radiation environment on the surface of Mars-Summary of model calculations and comparison to RAD data. *Life sciences in space research*, *14*, 18-28.

Moeller, R., Raguse, M., Leuko, S., Berger, T., Hellweg, C. E., Fujimori, A., ... & STARLIFE Research Group. (2017). STARLIFE—An international campaign to study the role of galactic cosmic radiation in astrobiological model systems. *Astrobiology*, *17*(2), 101-109.

Moeller, R., Rohde, M., & Reitz, G. (2010). Effects of ionizing radiation on the survival of bacterial spores in artificial martian regolith. *Icarus*, *206*(2), 783-786.

Newcombe, D. A., Schuerger, A. C., Benardini, J. N., Dickinson, D., Tanner, R., & Venkateswaran, K. (2005). Survival of spacecraft-associated microorganisms under simulated martian UV irradiation. *Applied and Environmental Microbiology*, *71*(12), 8147-8156.

Onofri, S., de la Torre, R., de Vera, J. P., Ott, S., Zucconi, L., Selbmann, L., ... & Horneck, G. (2012). Survival of rock-colonizing organisms after 1.5 years in outer space. *Astrobiology*, *12*(5), 508-516.

Onofri, S., de Vera, J. P., Zucconi, L., Selbmann, L., Scalzi, G., Venkateswaran, K. J., ... & Horneck, G. (2015). Survival of Antarctic cryptoendolithic fungi in simulated Martian conditions on board the International Space Station. *Astrobiology*, *15*(12), 1052-1059.

Onofri, S., Selbmann, L., De Hoog, G. S., Grube, M., Barreca, D., Ruisi, S., & Zucconi, L. (2007). Evolution and adaptation of fungi at boundaries of life. *Advances in Space Research*, *40*(11), 1657-1664.

Onofri, S., Selbmann, L., Pacelli, C., De Vera, J. P., Horneck, G., Hallsworth, J. E., & Zucconi, L. (2018). Integrity of the DNA and cellular ultrastructure of cryptoendolithic fungi in space or Mars conditions: a 1.5-year study at the International Space Station. *Life*, *8*(2), 23.

Osman, S., Peeters, Z., La Duc, M. T., Mancinelli, R., Ehrenfreund, P., & Venkateswaran, K. (2008). Effect of shadowing on survival of bacteria under conditions simulating the Martian atmosphere and UV radiation. *Applied and Environmental Microbiology*, *74*(4), 959-970.

Öztekin, L., Nicole, M., Badre, D. (2008). Genetic Changes. NIH Public Access. *Bone*, *23*, 1–7.

Pacelli, C., Bryan, R. A., Onofri, S., Selbmann, L., Zucconi, L., Shuryak, I., & Dadachova, E. (2018). The effect of protracted X-ray exposure on cell survival and metabolic activity of fast and slow growing fungi capable of melanogenesis. *Environmental microbiology reports*, *10*(3), 255-263.

Pacelli, C., Cassaro, A., Maturilli, A., Timperio, A. M., Gevi, F., Cavalazzi, B., ... & Onofri, S. (2020). Multidisciplinary characterization of melanin pigments from the black fungus Cryomyces antarcticus. *Applied Microbiology and Biotechnology*, *104*, 6385-6395.

Pacelli, C., Selbmann, L., Moeller, R., Zucconi, L., Fujimori, A., & Onofri, S. (2017b). Cryptoendolithic Antarctic black fungus Cryomyces antarcticus irradiated with accelerated helium ions: survival and metabolic activity, DNA and ultrastructural damage. *Frontiers in Microbiology*, *8*, 2002.

Pacelli, C., Selbmann, L., Zucconi, L., Raguse, M., Moeller, R., Shuryak, I., & Onofri, S. (2017a). Survival, DNA integrity, and ultrastructural damage in Antarctic cryptoendolithic eukaryotic microorganisms exposed to ionizing radiation. *Astrobiology*, *17*(2), 126-135.

Parameswaran, R. (1979). Statistics for experimenters: an introduction to design, data analysis, and model building. *JMR, Journal of Marketing Research (pre-1986)*, *16*(000002), 291.

Parnell, J., Cullen, D., Sims, M. R., Bowden, S., Cockell, C. S., Court, R., ... & Vago, J. (2007). Searching for life on Mars: selection of molecular targets for ESA's Aurora ExoMars mission. *Astrobiology*, 7(4), 578-604.

Raman, N. M., & Ramasamy, S. (2017). Genetic validation and spectroscopic detailing of DHN-melanin extracted from an environmental fungus. *Biochemistry and biophysics reports*, *12*, 98-107.

Rettberg, P., Rabbow, E., Panitz, C., & Horneck, G. (2004). Biological space experiments for the simulation of Martian conditions: UV radiation and Martian soil analogues. *Advances in Space Research*, *33*(8), 1294-1301.

Röstel, L., Guo, J., Banjac, S., Wimmer-Schweingruber, R. F., & Heber, B. (2020). Subsurface radiation environment of Mars and its implication for shielding protection of future habitats. *Journal of Geophysical Research: Planets*, *125*(3), e2019JE006246.

Saganti, P. B., Cucinotta, F. A., Wilson, J. W., Simonsen, L. C., & Zeitlin, C. (2004). Radiation climate map for analyzing risks to astronauts on the Mars surface from galactic cosmic rays. *2001 Mars Odyssey*, 143-156.

Schuerger, A. C., Mancinelli, R. L., Kern, R. G., Rothschild, L. J., & McKay, C. P. (2003). Survival of endospores of Bacillus subtilis on spacecraft surfaces under simulated martian environments:: implications for the forward contamination of Mars. *Icarus*, *165*(2), 253-276.

Schuerger, A. C., Richards, J. T., Newcombe, D. A., & Venkateswaran, K. (2006). Rapid inactivation of seven Bacillus spp. under simulated Mars UV irradiation. *Icarus*, *181*(1), 52-62.

Selbmann, L., De Hoog, G. S., Mazzaglia, A., Friedmann, E. I., & Onofri, S. (2005). Fungi at the edge of life: cryptoendolithic black fungi from Antarctic desert. *Stud Mycol*, *51*(1), 1-32.

Selbmann, L., Isola, D., Zucconi, L., & Onofri, S. (2011). Resistance to UV-B induced DNA damage in extreme-tolerant cryptoendolithic Antarctic fungi: detection by PCR assays. *Fungal Biology*, *115*(10), 937-944.

Selbmann, L., Pacelli, C., Zucconi, L., Dadachova, E., Moeller, R., de Vera, J. P., & Onofri, S. (2018). Resistance of an Antarctic cryptoendolithic black fungus to radiation gives new insights of astrobiological relevance. *Fungal biology*, *122*(6), 546-554.

Selbmann, L., Zucconi, L., Isola, D., & Onofri, S. (2015). Rock black fungi: excellence in the extremes, from the Antarctic to space. *Current Genetics*, *61*, 335-345.

Sherman, D. M., & Vergo, N. (1988). Optimal spectrum, site occupancy, and oxidation state of Mn in montmorillonite. *American Mineralogist*, *73*(1-2), 140-144.

Simpson, J. A. (1983). Elemental and isotopic composition of the galactic cosmic rays. *Annual Review of Nuclear and Particle Science*, *33*(1), 323-382.

Smith, M. L., Claire, M. W., Catling, D. C., & Zahnle, K. J. (2014). The formation of sulfate, nitrate and perchlorate salts in the martian atmosphere. *Icarus*, *231*, 51-64.

Usoskin, I. G., Alanko-Huotari, K., Kovaltsov, G. A., & Mursula, K. (2005). Heliospheric modulation of cosmic rays: Monthly reconstruction for 1951–2004. *Journal of Geophysical Research: Space Physics*, *110*(A12).

Weinstein, R. N., Montiel, P. O., & Johnstone, K. (2000). Influence of growth temperature on lipid and soluble carbohydrate synthesis by fungi isolated from fellfield soil in the maritime Antarctic. *Mycologia*, *92*(2), 222-229.

Westall, F., Loizeau, D., Foucher, F., Bost, N., Betrand, M., Vago, J., & Kminek, G. (2013). Habitability on Mars from a microbial point of view. *Astrobiology*, *13*(9), 887-897.

Zhdanova, N. N., Zakharchenko, V. A., Vember, V. V., & Nakonechnaya, L. T. (2000). Fungi from Chernobyl: mycobiota of the inner regions of the containment structures of the damaged nuclear reactor. *Mycological Research*, *104*(12), 1421-1426.

Supplementary material

Table S3.1. Phillosilicate Mars Regolith Simulant (P-MRS) and Sulfatic Mars Regolith Simulant (S-MRS) analogues composition (from Böttger et al., 2012).

P-MRS		S-MRS	
Mineral	**Weight (%)**	**Mineral**	**Weight (%)**
Montmorillonite	45	Gabbro	32
Chamosite	20	Gypsum	30
Quartz	10	Dunite	15
Iron(III)-oxide	5	Hematite	13
Kaolinite	5	Goethite	7
Siderite	5	Quartz	3
Hydromagnesite	5		
Gabbro	3		
Dunite	2		

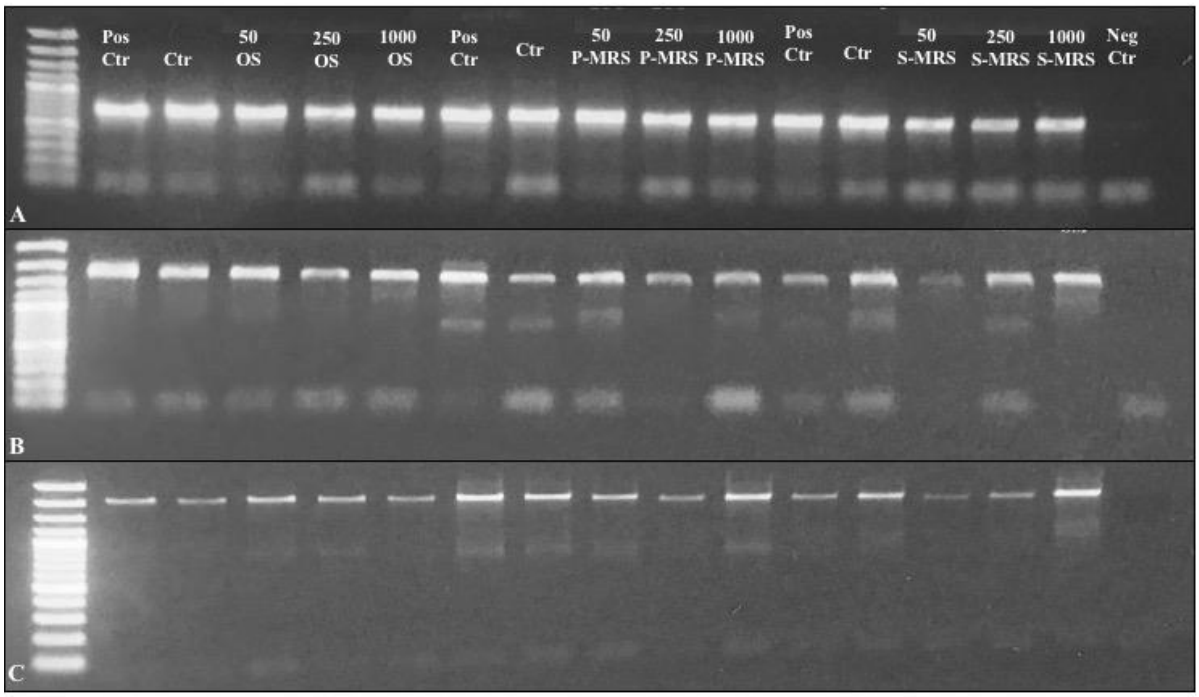

Figure S3.1. PCR amplification of the (A) Internal Transcriber Spacer (ITS) region (600 bp), (B) ITS-Large SubUnit region (LSU) region (1600 bp) and (C) ITS-LSU region (2000 bp) of samples of each set (Original Substrate (OS) substratum, Phillosilicate Mars Regolith Simulant (P-MRS) and Sulfatic Mars Regolith Simulant (S-MRS) analogues). Pos Ctr: laboratory control; Ctr: Control; Neg Ctr: Negative Control.

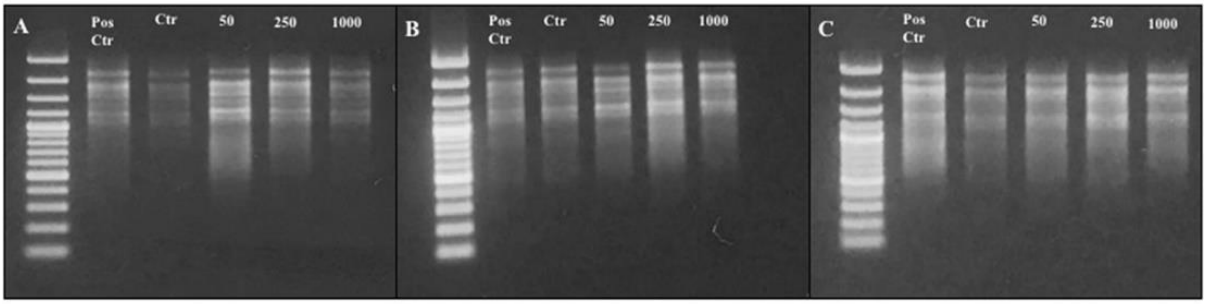

Figure S3.2. Random Amplification of Polymorphic DNA (RAPD) assay from *C. antarcticus* colonies extracted DNA, after exposure to accelerated helium ions irradiation. OS: Original substrate; P-MRS: Phyllosilicate Mars Regolith Simulant; and S-MRS: Sulfatic Mars Regolith Simulant.

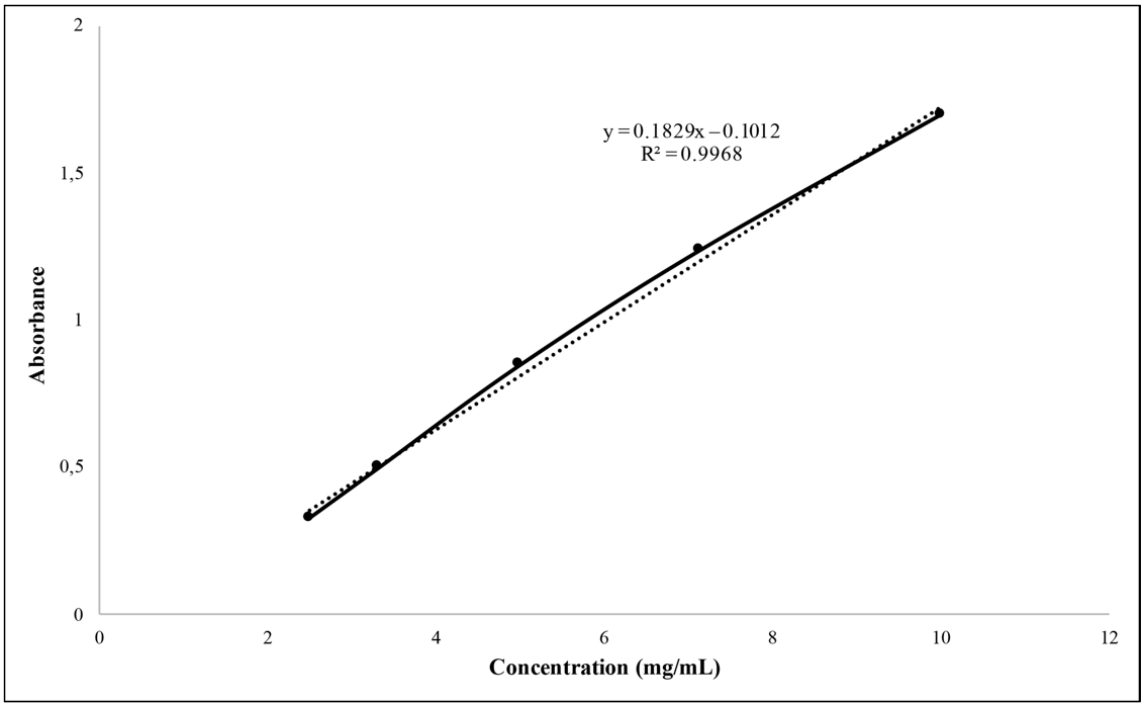

Figure S3.3. Correlation between synthetic 1,8-dihydroxynaphthalene (DHN)-melanin at five concentrations and absorbance at 650 nm used as standard curve for melanin quantification according to Raman and Ramasamy (2017).

Table S3.2. Concentration (in mg/mL) of extracted melanin from *C. antarcticus* colonies of exposed to accelerated He ions.

Samples	Concentration (mg/mL)
OS Control	2.53
OS 50 Gy	1.08
OS 250 Gy	1.59
OS 1000 Gy	1.30
P-MRS Control	1.92
P-MRS 50 Gy	2.52
P-MRS 250 Gy	1.88
P-MRS 1000 Gy	5.47
S-MRS Control	1.35
S-MRS 50 Gy	1.16
S-MRS 250 Gy	5.11
S-MRS 1000 Gy	1.33

OS= Original Substrate; P-MRS= Phyllosilicatic Mars Regolith Simulant; S-MRS= Sulfatic Mars Regolith Simulant.

Calculation for Predictions of *C. antarcticus* Survival Period on the Surface of Mars

Based on survival results, we calculated the hypothetical survival time of cells of *C. antarcticus* on Mars considering the type of radiation and the doses applied in our experiment (Table S3). The second column shows the estimated number of particles that hit the surface of each fungal cells depending on the exposure doses in the experiment (Alpen et al., 1994) and on the size of *C. antarcticus* cells (around 35 μm). The third column gives an approximation of the time required by each fungal cell to be hit by the corresponding number of particles on the Martian surface or near-surface environment. The values were calculated from the data reported by (Ehresmann et al., 2014), measured in the presence of an average atmosphere thickness of 23 g/cm^2 and a solar modulation parameter of 550 MV. Only He isotopes (^{3}He and ^{4}He) with energies above 135 ± 15 MeV were considered. The fourth column shows the estimated Earth years required to inactivate 90% of fungal cells (D_{10}) within the three different substrata on Martian surface and shallow subsurface environment, considering only accelerated He nuclei as component of GCR.

Table S3.3. Predictions of *C. antarcticus* survival period on the surface of Mars.

Dose (Gray)	He Ions Fluence (Ions/Cell)	Time Exposure on Mars (Earth Years)	Estimated Survival* Time on Mars (Earth Years)
50 Gy	4970	24,236	OS = 48,835
250 Gy	24,815	121,010	P-MRS = 322,493
1000 Gy	99,260	484,041	S-MRS = 109,748

*Survival is intended as D_{10} values.

Böttger et al., 2012. Planetary and Space Science, 60(1), 356-362.
Raman and Ramasamy, 2017. Biochemistry and biophysics reports, 12, 98-107.
Alpen et al., 1994. Advances in Space Research, 14(10), 573-581
Ehresmann et al., 2014. Journal of Geophysical Research: Planets, 119(3), 468-479

Chapter 4

Geography and environmental pressure are predictive of class-specific radioresistance in black fungi

Lorenzo Aureli[1,2], Claudia Coleine[1,*], Manuel Delgado-Baquerizo[3,4], Dag Ahren[2,5], Alessia Cemmi[6], Ilaria Di Sarcina[6], Silvano Onofri[1], Laura Selbmann[1,7]

[1]Department of Ecological and Biological Sciences, University of Tuscia, Viterbo, Italy

[2]Department of Biology, Lund University, Lund, Sweden

[3]Unidad Asociada CSIC-UPO (BioFun). Universidad Pablo de Olavide, Sevilla, 41013, Spain.

[4]Laboratorio de Biodiversidad y Funcionamiento Ecosistémico. Instituto de Recursos Naturales y Agrobiología de Sevilla (IRNAS), CSIC, Sevilla, Spain.

[5]National Bioinformatics Infrastructure Sweden (NBIS), Department of Biology, Lund University, Lund, Sweden

[6]Fusion and Technology for Nuclear Safety and Security Department, Italian National Agency for New Technologies, Energy and Sustainable Economic Development (ENEA FSN-FISS-SNI), Rome, Italy

[7]Italian Antarctic National Museum (MNA), Mycological Section, Genoa, Italy.

Submitted to *Environmental microbiology*; unrevised preprint available at https://doi.org/10.1101/2023.02.08.527471

Originality statement

Although previous studies showed the extraordinary ability of a few strains of black fungi to survive ionizing radiation, the overall radioresistance of this group of organisms has not been defined yet. Moreover, how and why radioresistance shifts across environmental gradients remain virtually unknown. Here, we collected black fungi from locations across the globe and found that biogeography shapes the responses of black fungi to environmental stress with UV light being significantly correlated with radiotolerance. Our study provides a clear picture of the boundaries of life for black fungi under ionizing radiation; further, we demonstrate, for the first time, that this ability in such microorganisms, not only is related to the taxonomy, but also may be a consequence of their adaptation to various factors encountered in the environment where they live.

Abstract

Black fungi are among the most resistant organisms to ionizing radiation on Earth. However, our current knowledge is based on studies on a few isolates, while the overall radioresistance limits across this microbial group and the relationship with local environmental conditions remain largely undetermined. To address this knowledge gap, we assessed the survival of 101 strains of black fungi isolated across a worldwide spatial distribution to gamma radiation doses up to 100 kGy. We found that intra and inter-specific taxonomy, UV radiation and precipitation levels primarily influence the radioresistance in black fungi. Altogether, this study provides insights into the adaptive mechanisms of black fungi to extreme environments and highlights the role of local adaptation in shaping the survival capabilities of these extreme-tolerant organisms.

Keywords: Ionizing radiation, black fungi, survival, extremophiles, astrobiology, environmental pressure

4.1 Introduction

Radiation is one of the most dangerous hazards for life, among which gamma rays (i.e. high energy photons having wavelengths less than 0.1 nm) represent a serious challenge for the survival and integrity of any life-forms (Dartnell, 2011). They may induce dramatic damage in biomolecules and cellular structures by direct ionization or by causing radiolysis of water and, consequently, oxidative stress (Azzam et al., 2012). On Earth, there are three principal sources of gamma rays: (i) the natural radioactive nuclides, mainly ^{40}K and the radionuclides from the ^{232}Th and ^{238}U series (Ichimiya et al., 1998; Walencik-Łata, 2022); (ii) the cosmic rays colliding with the nuclei in the atmosphere (Share et al., 2001; Wissmann et al. 2005); and (iii) human activities as in radioactive wastes, nuclear test and nuclear accident sites (Yamamoto et al., 2008; Hu et al., 2010). Albeit radioactive environments are limited only to restricted sites on our planet (Khan et al., 2020; Mousseau et al., 2020), ionizing radiation is one of the major damaging factors encountered beyond Earth (Evans et al., 2003; Dartnell et al., 2007; Roth et al., 2021); indeed, high gamma rays backgrounds are ubiquitous in interplanetary space and on the surface of most of the planetary bodies.

Among terrestrial life-forms, a small number of microorganisms have been reported to survive gamma radiation levels significantly higher than the background in the environments where they live (Gabani et al., 2013; Kwang-Woo Jung et al., 2017; Coleine et al. 2022; Coleine & Delgado-Baquerizo, 2022). Black meristematic fungi (thereafter black fungi) form an ascomycetous polyphyletic group spanning two classes (*Dothideomycetes* and *Eurotiomycetes*, mainly represented by the orders *Capnodiales* and *Chaetothyriales*, respectively) (Selbmann et al., 2020). Despite being phylogenetically distant, they share morphological characteristics as a convergent adaptation to the extreme conditions where they live (Selbmann et al., 2005; Eisenman et al., 2012; Tesei, 2022). These fungi are among the most extreme-tolerant organisms on our planet, encompassing a stunning ability to survive and even flourish under prohibitive conditions, including radiation (Gorbushina et al. 2018; Selbmann et al., 2018; Coleine et al., 2022). Indeed, it has been recently reported an extraordinary resistance of these fungi to both acute and chronic exposure to a plethora of terrestrial and space-relevant radiation (e.g. UV-B, X-rays, gamma rays, and cosmic rays) (Selbmann et al., 2011; Pacelli et al., 2018a, 2020; Shuryak et al., 2019b; Aureli et al., 2020; Schultzhaus et al., 2020; Malo et al., 2021). These microorganisms have been investigated as possible biological means for radioprotection in contaminated environments and in manned space missions (Cordero et al., 2017; Averesch et al., 2022). Additionally, the study of radioresistant microorganisms is of astrobiological significance to unveil the survival and persistence capacity of life in highly irradiated extraterrestrial environments (Dartnell, 2011, Moissl-Eichinger et al., 2016; Horne et al., 2022).

Despite these advances, a vast bulk of questions still remain unanswered. In particular, there are three major sources of uncertainties that have precluded scientists to untangle how and why black fungi manage to resist ionizing radiation. First, most efforts have focused on a few strains (i.e. *Cryomyces*, *Friednmanniomyces* and *Exophiala* spp.) only, while a comprehensive study exploring the potential diverse radioresistance abilities among

phylogenetically and ecologically distinct members, including those colonizing both natural and polluted anthropized niches, is still lacking. Second, most isolates come from a narrow range of environmental conditions and local regions, while a more comprehensive study on black fungi across broader spatial distribution is lacking. Finally, very little is known about how environmental stressors, including the solar radiation levels of the regions from which these taxa are isolated, explain the actual levels of radioresistance in individual taxa.

Here, we tested the resistance of 101 black fungal strains to acute exposure to gamma radiation to relate these responses to the environmental conditions. The specimens were selected from *Dothideomycetes* and *Eurotiomycetes* classes and had a worldwide spatial distribution to cover the broadest range of different ecologies, life-styles, and geography (e.g. from Antarctica to temperate regions and from anthropic impacted to polluted sites). We aimed to: i) define the radioresistance limits of the broadest selection of black fungi tested so far; ii) identify new possible model organisms for radioprotection and astrobiology studies; iii) evaluate the potential differences in radioresistance between *Dothideomycetes* and *Eurotiomycetes*. Indeed, the first are mainly isolated from extreme dry and cold natural environments, whereas the latter show a remarkable ability to colonize hot and polluted anthropized environments (Selbmann et al., 2005; Isola et al., 2021; Tesei, 2022); iv) identify the main environmental parameters driving radioresistance in these fungi. Altogether, this information will provide new insights into the ability of black fungi to cope with high doses of ionizing radiation, paving the way for further genomic and metabolic investigations and providing a fundamental contribution to defining the habitability of terrestrial environments contributing to speculations on a potential terrestrial-like life in the Solar System and beyond.

4.2 Materials and Methods

4.2.1 Strains selection

For the study, 101 strains of black meristematic fungi were selected from the Culture Collection of Fungi from Extreme Environments (CCFEE) and National Antarctic Museum Culture Collection of Fungi from Extreme Environments (MNA-CCFEE), Mycological Section of the Italian National Museum of Antarctica. The strains belong to 20 species of the order *Capnodiales* (class *Dothideomycetes*) and 7 species of the order *Chaetothyriales* (*Eurotiomycetes*) (Table S4.1, Fig. 4.1a, b). The strain selection was performed to study phylogenetically distinct members of meristematic black fungi and to cover a range of different environmental conditions (Table S4.2).

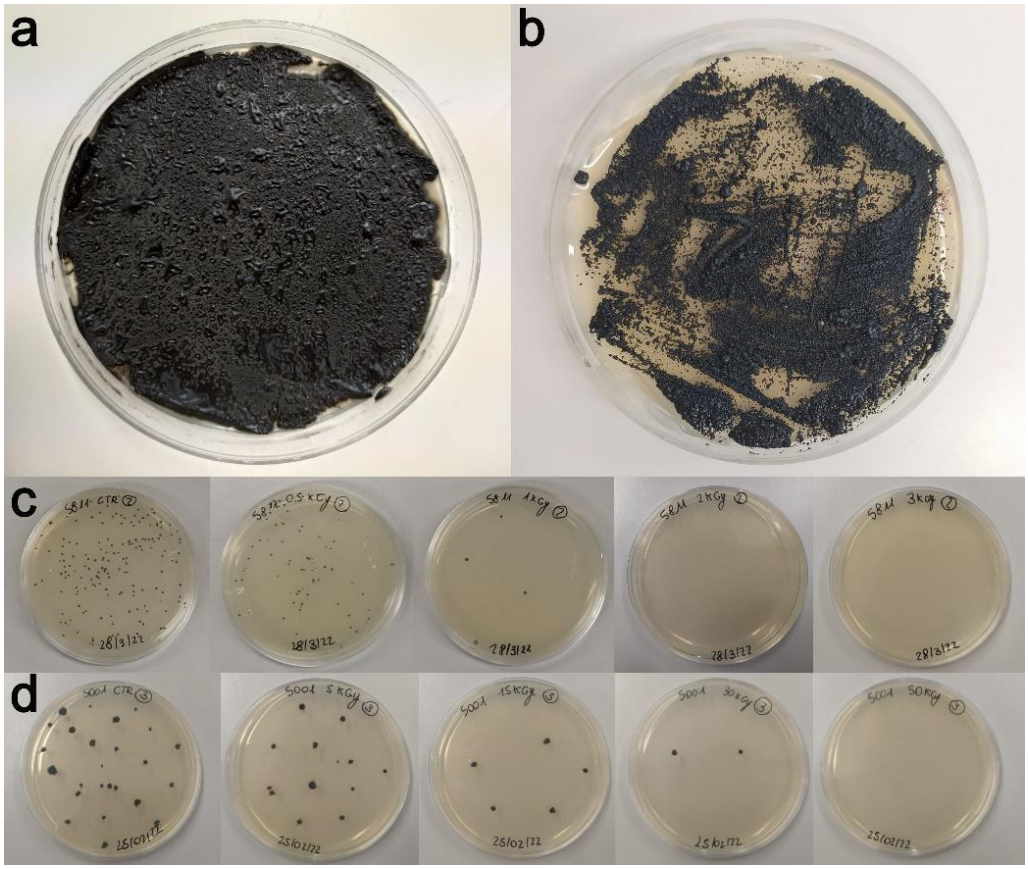

Figure 4.1. Representative strains of black fungi tested in this study. (a) Colony aspect of *E. xenobiotica* CCFEE6194 (*Eurotomycetes*); (b) colony aspect of *C. antarcticus* MNA-CCFEE515 (*Dothideomycetes*); (c) colony growth of *E. xenobiotica* CCFEE5811 after gamma irradiation at 0, 0.5, 1, 2, and 3 kGy (from left to right panel); (d) colony growth of *F. endolithicus* MNA-CCFEE5001 after gamma irradiation at 0, 5, 15, 30 and 50 kGy (from left to right panel).

4.2.2 Exposure conditions

Fungal colonies of the selected strains were incubated in triplicate on Malt Extract Agar (MEA) medium in Petri dishes according to the temperatures recorded in the localities from which the strains were isolated and the optimum growth temperature and growth rate recorded in representative strains of the tested species in previous laboratory tests: 15 °C for 3 months for *Dothideomycetes* and 25 °C for 1 week for *Eurotiomycetes* (Selbmann et al., 2005; Egidi et al., 2014). After the growth, the colonies were retrieved from each replicate and separately desiccated under laminar flow in a sterile cabinet. Dried colonies from each triplicate were exposed to gamma radiation under ambient conditions using a ^{60}Co source at the Gamma Irradiation CALLIOPE Facility (ENEA Casaccia Research Centre, Rome) (Baccaro et al., 2019). The irradiation was performed at doses of 0.1, 0.5, 1, 2, 3, 5, 15, 30, 50, and 100 kGy through different exposure times at a dose rate of 1.12 kGy(air)/h. To obtain control samples, colonies from each desiccated replicate were not exposed to gamma radiation but maintained under the same environmental conditions as the irradiated samples.

4.2.3 Survival assessment

The survival of microorganisms after exposure to each gamma radiation dose was measured using the colony-forming unit (CFU) test. Three colonies from each replicate exposed to gamma radiation were separately rehydrated in NaCl 0.9% solution for 72 h at 25 °C and 15 °C for *Eurotiomycetes* and *Dothideomycetes*, respectively. After rehydration, 0.1 mL of each cellular suspension at a concentration of 15,000 CFU/mL was plated in triplicate on MEA medium in Petri dishes (Fif. 4.1c, d. The dishes inoculated with *Eurotiomycetes* strains were incubated for 1 week at 25 °C, whereas dishes with *Dothideomycetes* strains for 3 months at 15 °C. The survival of microorganisms at each dose was expressed as the ratio between the mean of colonies scored in the exposed replicates and the mean of colonies scored in non-exposed samples. The decimal reduction dose (D_{10}) value, defined as the absorbed radiation dose required to inactivate 90% of the microbial population, was estimated for each strain from its survival curve. To calculate D10 values, the best curves describing the survival of each strain were determined by fitting the exponential function ($y = \exp^{(-bx)}$) to the observed data through the Python SciPy package V.1.9.0. The curve fits were evaluated through the χ^2 test by using the Python code.

4.2.4 Intraspecific differences in radioresistance

Among the selected species, *Exophiala xenobiotica*, *Recurvomyces mirabilis*, *Meristemomyces frigidus*, *Elasticomyces elasticus*, *Extremus antarcticus*, *Friedmanniomyces endolithicus*, and *Cryomyces antarcticus* species were represented by more than one strain. To quantify the radioresistance variability in species including more than one strain, the coefficient of variation (CV) was calculated through the Python SciPy package. The one-way ANOVA post hoc Tukey HSD test and t-test were performed through Python bioinfokit package V.2.1.0. to assess the difference in D10 values between strains of *E. elasticus*, *M. frigidus*, *R. mirabilis* and *F. endolithicus* collected from distinct localities and among the mean D10 values calculated in the resistance groups.

4.2.5 Environmental metadata acquisition

The ecological bases of the resistance to ionizing radiation was investigated by considering 27 environmental parameters obtained from the localities where the strains were isolated: Annual Mean Temperature (AMT); Mean Temperature of the Warmest Quarter (MTWAQ); Mean Temperature of the Coldest Quarter (MTCQ); Annual Precipitation (AP); Precipitation of the Wettest Month (PWEM); Precipitation of the Driest Month (PDM); Precipitation Seasonality (Coefficient of Variation) (PS); Precipitation of the Wettest Quarter (PWEQ); Precipitation of the Driest Quarter (PDQ); Precipitation of the Warmest Quarter (PWAQ); Precipitation of the Coldest Quarter (PCQ); Mean Diurnal Range (Mean of monthly (maximum temperature - minimum temperature)) (MDR); Temperature Seasonality (standard deviation ×100) (TS); Maximum Temperature of the Warmest Month (MTWAM); Minimum Temperature of Coldest Month (MTCM); Temperature Annual Range (calculated as MTWAM

- MTCM) (TAR); Mean Temperature of the Wettest Quarter (MTWEQ); Mean Temperature of the Driest Quarter (MTDQ); Isothermality (calculated as MDR/TAR) (×100) (IT); solar radiation; UV index; biome type (biome); isolation source; country of isolation (country); Köppen-Geiger climate classification subgroup (KG climate); class to which the strains belong (Class); the coordinates of the localities where the samples were collected. The environmental data were available for 86 of the 101 strains tested in the study, related to 36 different localities (Supplementary Table 4.2, Fig. 4.2).

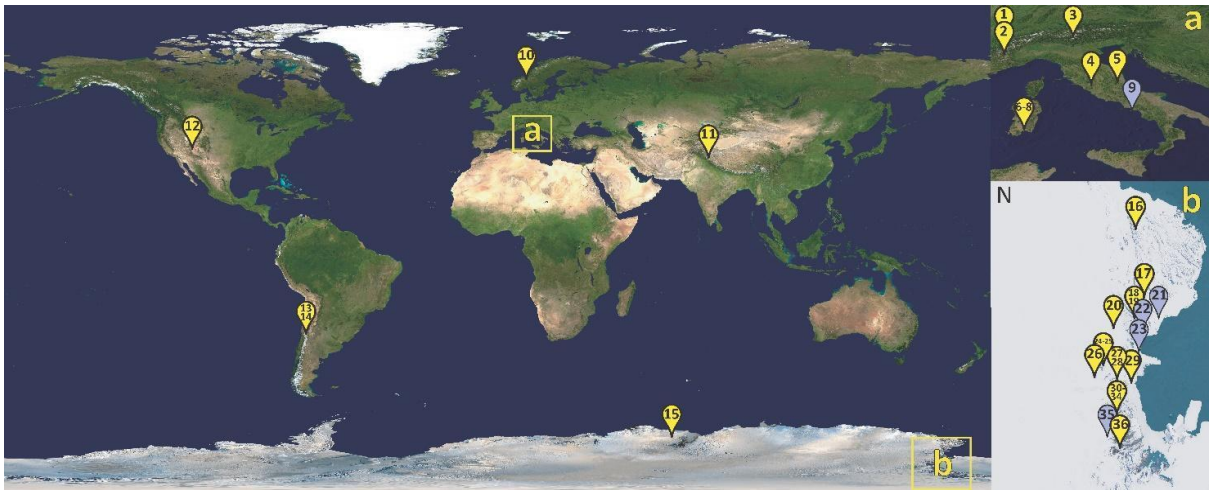

Figure 4.2. Map of the sites from which the strains were isolated. The localities with environmental data available are in yellow. Coordinates, environmental data and strains are reported in Table S4.2. Sampling sites in a) Italy, and b) Victoria Land, Antarctica are detailed in the enlarged squares on the right.

4.2.6 Identification of the most important environmental parameters and statistical analyses

To identify the environmental parameters that are linked to the radioresistance of the strains, a classification predictive model was constructed through the eXtreme Gradient Boosting (XGBoost) ensemble tree-based learning algorithm. The algorithm was implemented using the Python XGBoost package V.1.6.2. Categorical data (biome, isolation source, country, KG climate, Class) were converted through ordinal encoding pre-processing. Similarly, the D10 values were grouped into 9 categories and transformed into an ordinal variable. We then estimated the importance of each environmental parameter by evaluating the mean decrease in the model score when the values of the parameter were randomly shuffled in 1000 repeats through the permutation feature importance approach by using the Python ELI5 package V.0.13.0. The XGBoost model and the permutation were first performed considering all the strains with environmental data available. Successively, the analyses on subgroups consisting of *Dothideomycetes* and *Eurotiomycetes* were performed to identify predictors of radioresistance in strains from the two classes. Finally, the 24 strains of *F. endolithicus* were considered in relation to environmental data to identify parameters that may influence intraspecific differences in radioresistance. The *F. endolithicus* species was selected due to the availability of environmental data observed in 9 distinct localities where the strains were

collected. Along with *F. endolithicus*, *C. antarcticus*, *E. elasticus* and *E. xenobiotica* were the most represented species (8, 10 and 30 strains, respectively). However, the lack of environmental data related to part of *C. antarcticus* and *E. elasticus* strains did not allow the construction of a model, whereas most of *E. xenobiotica* strains were isolated from the same locality.

To examine the differences in mean decreases in the model score obtained for each environmental variable, we performed the one-way ANOVA post hoc Tukey HSD test through the Python bioinfokit package V.2.1.0. Spearman's rank correlation coefficient and p-value were calculated through the Python SciPy packageV.1.9.0.

4.3 Results

4.3.1 Survival of fungal strains after gamma radiation exposure

The ability to generate colonies after gamma radiation exposure revealed a non-linear effect of radiation on black fungi cell survival, which was highly dependent on taxonomy. Indeed, three distinct responses can be observed from the dose-survival curves of *Eurotiomycetes* and *Dothideomycetes* strains, despite all exhibiting a similar trend that can be described by the exponential curve $y = \exp^{(-bx)}$ (Fig. S4.1, S4.2 and S4.3). Specifically, in all *Eurotiomycetes*, a drop in cell survival was reported between 0.1 and 0.5 kGy, with the survival fraction reaching values below 50%. However, a drastic change in the slopes occurred beyond 0.5 kGy, thus determining a slower decrease in cell survival until reaching the maximum resistance doses of each strain (Fig. 4.3).

On the other hand, two different general responses to gamma radiation were shown among *Dothideomycetes* strains. The first observed response was displayed by 33 strains. Although the slopes of the curves among these strains were highly variable, they all showed a drop in cell survival from the dose of 0.5 kGy followed by a slower decrease while approaching the maximum doses of resistance. Instead, the remaining 37 strains, that included exclusively the totality of *Friedmanniomyces* and *Cryomyces* strains, showed a general drop in cell survival between 3 and 15 kGy, followed by a slight decline in survival fraction (Fig. 4.3).

The D10 values obtained from the survival curves ranged from 0.30 (*Eurotiomycetes* sp. CCFEE6388) to 23.5 kGy (*C. minteri* MNA-CCFEE5187) (Table S4.1). Although marked differences were observed in the survival among the studied strains, colonies from most samples were able to grow after exposure at doses higher than 0.1 kGy. Furthermore, except for *E. xenobiotica* CCFEE5985, all strains formed colonies at doses higher than 1 kGy, with overall higher survival fractions observed in the *Dothideomycetes* strains (Fig.4. 4).

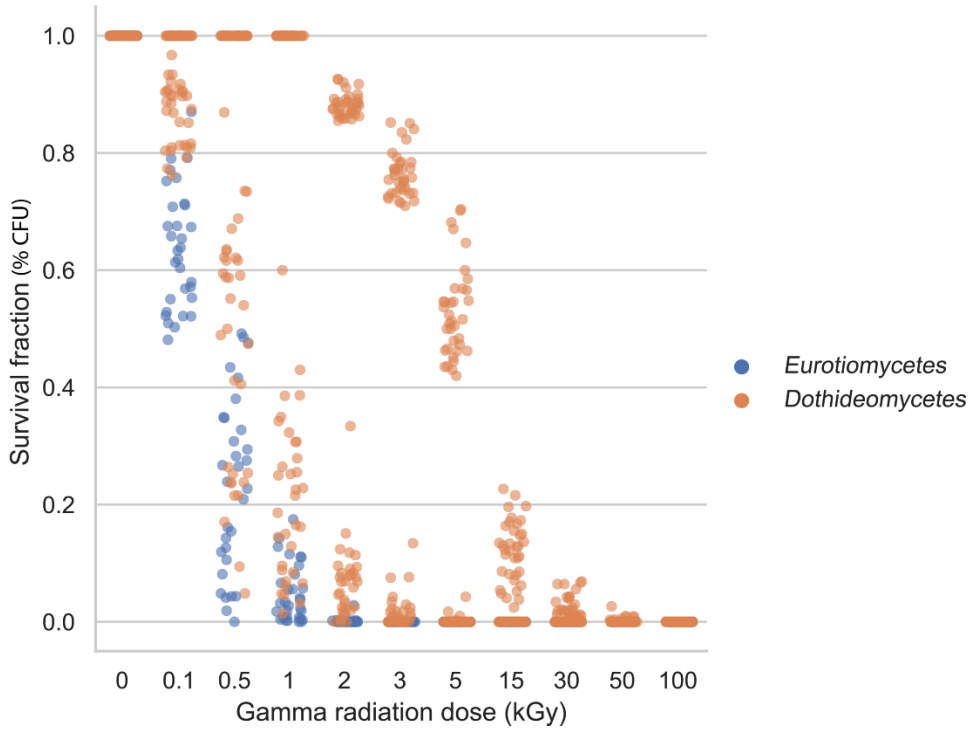

Figure 4.3. CFU expressed as a percentage (survival fraction) in the tested strains in both classes *Eurotiomycetes* and *Dothideomycetes* dose of gamma radiation.

In *Eurotiomycetes*, the mean D10 was 0.8 ± 0.3 kGy with a CV 0.45. The values of the group were distributed between 0.3 and 1.4 kGy (Fig. 4.4), shown by *Eurotiomycetes* sp. CCFEE6388, *Chaetothyriales* sp. CCFEE6169, and *E. xenobiotica* CCFEE6180, respectively (Table S4.1). Moreover, only the strains *E. xenobiotica* CCFEE5819, CCFEE6180, CCFEE6182, CCFEE6196 and CCFEE6237 showed D10 above 1 kGy. The maximum resistance dose of 3 kGy was recorded for the strain *E. xenobiotica* CCFEE5877, whereas 21 out of 31 strains showed the ability to grow at the maximum dose of 1 kGy (Table S4.1). In contrast, high variability in radioresistance was observed among *Dothideomycetes*, whose values ranged between 0.4 and 23.5 kGy, observed in *M. frigidus* CCFEE5401 and *C. minteri* MNA-CCFEE5187, respectively (Fig. 4.4). The D10 values showed a discontinuous distribution that defined two groups of radioresistance in *Dothideomycetes*. The first group was represented by strains exhibiting D10 below 4 kGy (mean D10, mean 1.5 ± SD 0.7 kGy), whose values partially overlapped the values found in *Eurotiomycetes*. However, all the strains of the group survived at doses of 2 kGy or higher, with 12 strains reaching the maximum survival dose at 5 kGy. This group consisted of all tested species of *Dothideomycetes*, with the exception of species belonging to *Cryomyces* and *Friedmanniomyces* genera. The D10 values of the second group ranged between 13.4 and 23.5 kGy, making these strains the most resistant among the tested black fungi (mean D10 17.6 ± 2.9 kGy, CV 0.15). Furthermore, all the strains of the second group formed colonies at a dose of 15 kGy or higher, with 10 strains reaching the maximum survival dose at 50 kGy (Supplementary Table S4.1).

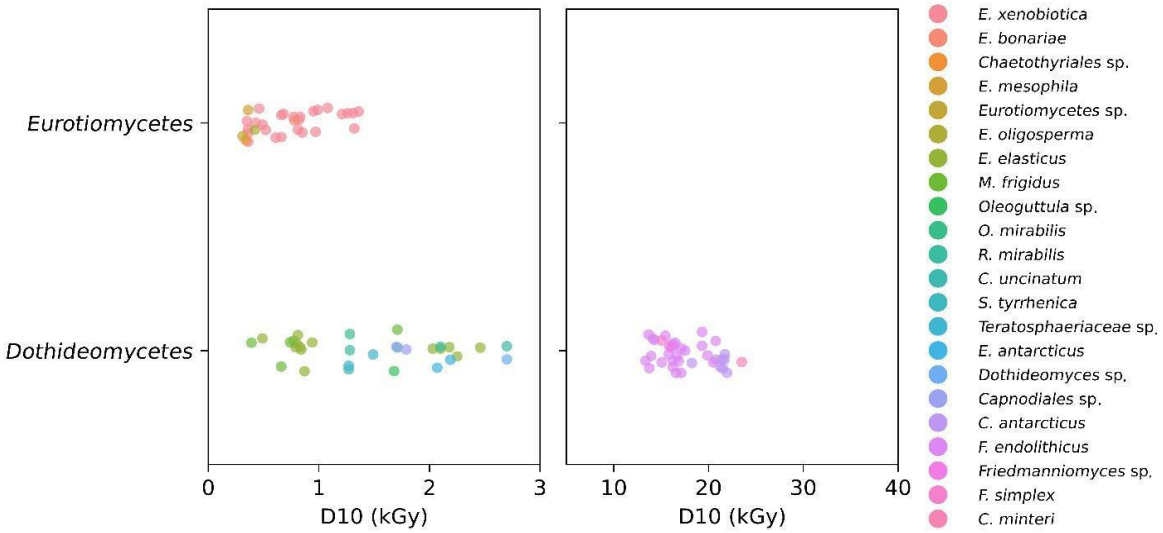

Figure 4.4. Distributions of D10 values calculated for all tested strains in the classes *Eurotiomycetes* and *Dothideomycetes*.

4.3.2 Relation between radioresistance and environmental parameters, taxonomy and geographical distribution

We further investigate the correlation between environmental and spatial conditions with the capacity of black fungi to withstand radiation. To investigate the ecological bases of the radioresistance in black fungi, we considered the importance of geography and a set of crucial environmental parameters occurring in the localities from which the strains were isolated in predicting the D10 values. The permutation feature importance scores obtained from the models indicated the spatial distribution (i.e. the longitude and the distance from the equator) of the localities as the major predictors of the radioresistance while considering the strains altogether and *Dothideomycetes* separately, although the relative importance of the two variable varies between them. Among the environmental variables, the main predictors of the radioresistance considering both the strains altogether and *Dothideomycetes* only were those related to the solar radiation exposure (i.e. UV index and solar radiation) and precipitation (i.e. precipitation in the driest month (PDQ) and precipitation seasonality (PS)) (Fig. 4.5a, b).

Unlike *Dothideomycetes*, strains of *Eurotiomycetes* were collected from both environments directly exposed to natural factors (e.g. surfaces of monuments) and anthropogenic and polluted environments (i.e. fuel tanks). When considering only strains exposed to natural environmental factors, parameters linked to temperature (the annual mean temperature (AMT) and the mean temperature of the coldest quarter (MTCQ)) and the distance from the equator were the most important variables, whereas the solar radiation exposure and precipitation levels were shown not to play a pivotal role in radioresistance prediction for this class (Fig. 4.5c).

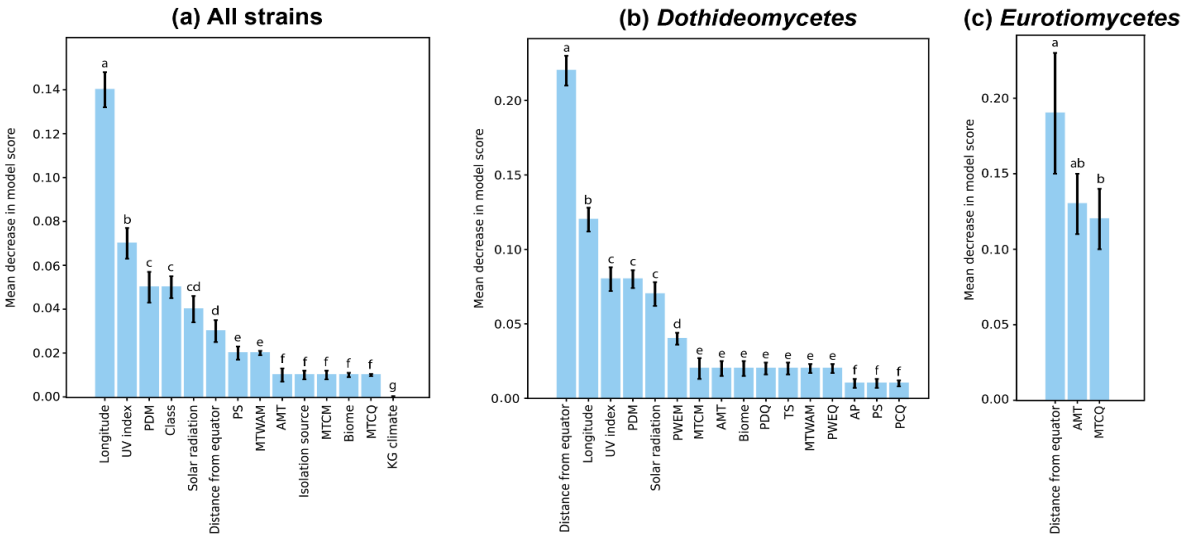

Figure 4.5. Main environmental predictors of radioresistance prediction ordered by their importance obtained for (a) all the strains; (b) *Dothideomycetes* strains; (c) *Eurotiomycetes* strains. The importance of each parameter is expressed as the mean of decreases in the XGBoost model score after the values of the parameter were shuffled 1000 times. PDM: precipitation of the driest month; PS: precipitation seasonality; MTWAM: maximum temperature of the warmest month; AMT: annual mean temperature; MTCM: minimum temperature of the coldest month; MTCQ: mean temperature of the coldest quarter; KG climate: Köppen-Geiger climate classification subgroup; PWEM: precipitation of the wettest month; PDQ: precipitation of the driest quarter; TS: temperature seasonality; PWEQ: precipitation of the wettest quarter; AP: annual precipitation; PCQ: precipitation of the driest quarter; MDR: mean diurnal range. Letters indicate statistically significant differences in one-way ANOVA post hoc Tukey HSD test ($P < 0.05$).

4.3.3 Intraspecific differences in radioresistance and their correlation to environmental factors

In our study, 7 fungal species are represented by more than one strain (Table S4.1). Among them, the highest intraspecies variation in the survival data was observed in the *E. elasticus* and *M. frigidus* strains (CV 0.5 and 0.6, respectively), whereas *F. endolithicus* strains had a relatively lower CV (i.e. 0.1). In *E. elasticus*, we observed significantly higher radioresistance (D10 above 2 kGy) in strains isolated from Antarctica compared to those isolated from temperate regions (D10 below 1 kGy) (Fig. 4.6a). Similar responses were observed among the strains of *M. frigidus*, whose strains from Argentinian Andes were observed to be significantly more resistant than the strains from Italy, with a difference in D10 of about 1 kGy among the two groups (Fig. 4.6b). These data indicated that geography and the local environmental conditions may influence the level of radioresistance in these fungi.

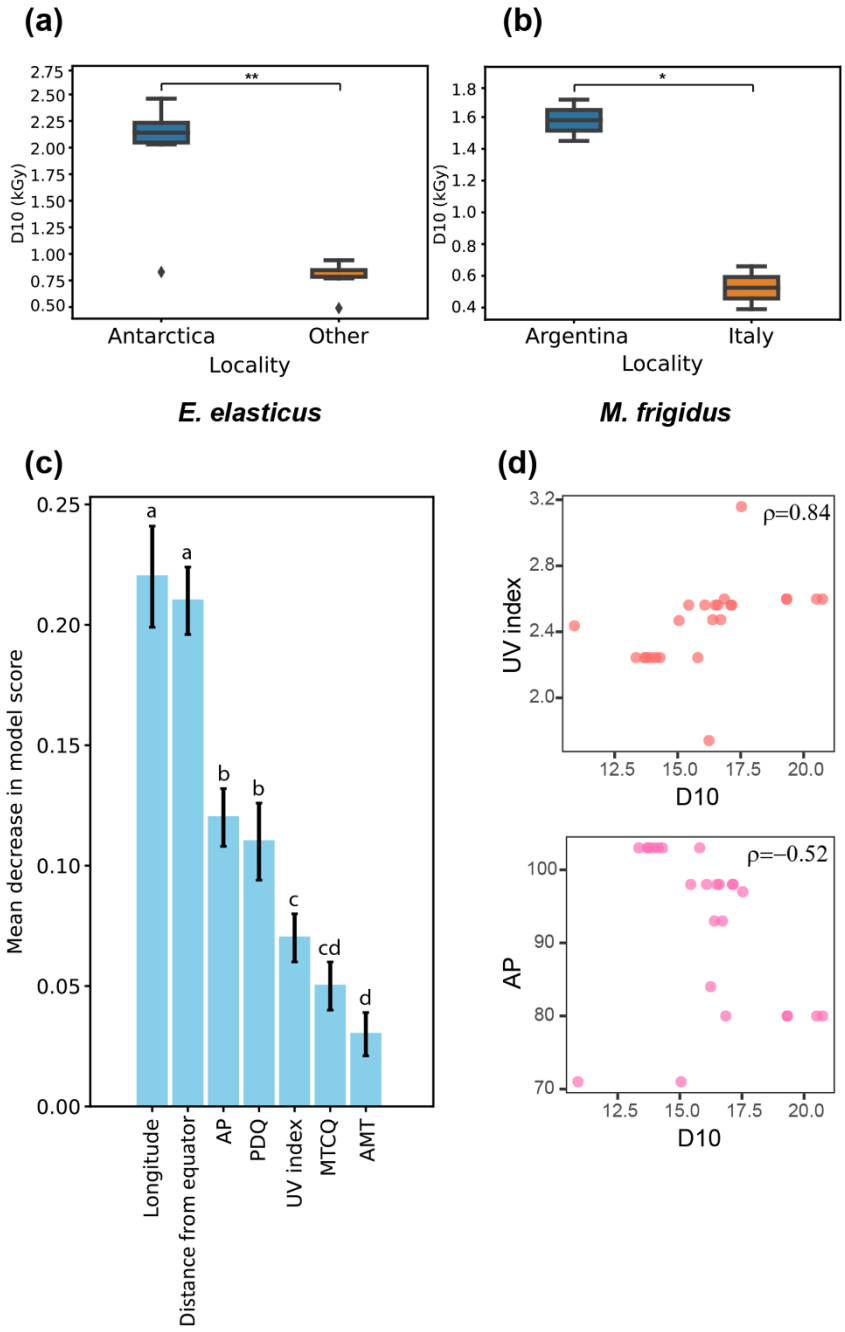

Figure 4.6. Differences in radioresistance among strains isolated from distinct localities. (a) Difference between strains of *E. elasticus* isolated in Antarctica and other localities (India and Italy); (b) differences in radioresistance between strains of *M. frigidus* isolated in Argentina and Italy. Statistical significance was calculated by using the t-test (*P ≤ 0.001. **P < 0.05); (c) importance of the main environmental parameters related to radioresistance in *F. endolithicus* strains, expressed as the mean of decreases in the XGBoost model score; (d) Spearman's rank correlation between representative environmental factors identified in (c) and D10 values (P<0.05). Parameter abbreviations are reported in the main text. AP: annual precipitation; PDQ: precipitation of the driest quarter; MTCQ: mean temperature of the coldest quarter; AMT: annual mean temperature. Letters indicate statistically significant differences in one-way ANOVA post hoc Tukey HSD test (P<0.05).

F. endolithicus species was represented by 27 strains isolated from 11 different localities in Antarctica (Fig. 4.1, Table S4.1). The analysis showed the geography, the precipitation parameters (AP and PDQ), the UV index, the temperature (AMT and MTCQ) as the major predictors of the radioresistance in *F. endoliticus* strains (Fig. 4.6c). The relationship between AP, PDQ and UV index and the radioresistance was confirmed by the Spearman's correlation (Fig. 4.6d).

4.4 Discussion

Major unknowns persist about how and why different black fungi taxonomies withstand radiation across large environmental gradients worldwide. Here, the ability of 101 *Dothideomycetes* and *Eurotiomycetes* black fungi to form colonies after acute exposure to gamma radiation was assessed to define the radioresistance limits of the broadest range of these extreme-tolerant guilds tested so far. Moreover, we correlated this radioresistance with environmental and spatial conditions supporting black fungi across global environmental gradients. We showed that taxonomy is a critical component when explaining the capacity of black fungi to resist radiation. Moreover, environmental conditions were critical in explaining the variation in black fungi radioresistance with UV light being an important predictor. These results suggest that black fungi radioresistance levels are consistent with the environment surrounding these organisms.

The amplitude of radioresistance capacity varied considerably among black fungi in our wide selection; many of them were able to form colonies after gamma radiation exposure doses from 0.5 to 5 kGy. Yet, some others were still viable when exposed at the extraordinary value of 50 kGy. D10 also varied considerably among strains tested, ranging from 0 kGy up to above 23 kGy, and the species falling into two distinct categories. In this study, we found a general higher aptitude to cope with ionizing radiation in dothideomycetous black fungi; in fact, the capacity to grow after lethal dose exposition over 5 kGy was an exclusive prerogative of few *Dothideomycetes*, indicating a class-tendency throughout this ability. In addition, the highest radioresistance observed (up to 50 kGy) was displayed specifically by black fungal *Dothideomycetes*, which have been isolated in the driest and coldest desert on Earth only: the ice-free areas in continental Antarctica, including the Martian analogue McMurdo Dry Valleys. Based on this evidence, we investigated in deeper detail the origin of this difference studying the effect of various environmental factors in shaping radioresistance tendency in black fungi, taking into consideration that dothideomycetous do prefer highly stressing cold-dry natural environments, while eurotiomycetous spread preferentially in hot or anthropic impacted or polluted environments.

Our study showed that biogeography, sun exposure, and the levels of precipitation were the major predictors of D10 in strains exposed to natural parameters, indicating that the ability to cope with ionizing radiation may be related to the adaptation to other environmental stressors (Shuryak et al., 2019a). Indeed, factors encountered in extreme environments such as UV exposure, drought, and low and high temperatures can also cause oxidative stress, requiring the activation of cellular mechanisms similar to those that mediate the responses to ionizing

radiation (Leprince et al., 2010; Lushchak, 2011; Kostadinova et al., 2012; Braga et al., 2015; Mejía-Barajas et al., 2017; Gostinčar et al., 2018). The burden of skills for success in such environments, therefore, may represent a pre-adaptation for radioresistance in these fungi (Etemadifar et al., 2016; Sharma et al., 2017; Lim et al., 2019; Coleine et al., 2022). In fact, although exhibiting overall high radioresistance, none of the strains tested in our study was isolated from radioactive environments; either, the environmental background radiation should not have represented an evolutionary driver for this ability.

In our study, the adaptation of black fungi to a broad range of different habitats may explain the large diversity that we observed in their radioresistance. In addition to interspecific fluctuation in radioresistance, the distinct localities may have driven the intraspecific variability in different species by inducing the local adaptation to various environmental factors (Ellison et al., 2011; Gladieux et al., 2014; Branco, 2019). Consistently with this hypothesis, the highest intraspecific variability observed was exhibited by strains of *E. elasticus* and *M. frigidus*, whose distribution spans different continents, which was highly correlated to increasing environmental pressure; indeed, the most resistant strains were found in Antarctica and Argentinian Andes, respectively.

The importance of environmental factors for radioresistance was also confirmed by our results on the Antarctic endemic species *F. endolithicus* strains, living in the driest, coldest highly solar and UV radiation impacted environment and here resulted in the far most radioresistant guild, together with *Cryomyces* strains living in the same desert (i.e. Antarctica). The relation occurring between the radioresistance and the adaptation to other environmental stressors may be mediated by both morphological and physiological properties of the fungal cells. Previous studies have indicated morphological characteristics of black fungi as possible determinants against environmental stressors (Kogej et al., 2006). Furthermore, the melanized cell wall was shown to play a key role in mediating the resistance of pigmented fungi to ionizing radiation (Dadachova et al., 2008; Shuryak et al., 2014). Recent advances showed various possible trends, represented by both linear and non-linear threshold correlations (Pacelli et al., 2018b; Schultzhaus et al., 2020). In our study, all the tested strains showed a non-linear exponential relationship between the gamma rays doses and the survival fraction, suggesting that radioresistance may be mediated by additional physiological and molecular processes differentially expressed in distinct species of black fungi (Robertson et al., 2012; Sharma et al., 2017; Romsdahl et al., 2021; Kreusch et al., 2021; Das et al., 2022; Kanekar & Kanekar, 2022). This may indicate how the response of microorganisms to ionizing radiation depends not only on the tested organisms, but also on the exposure conditions. In this perspective, future studies focusing on the genetic and molecular mechanisms mediating the radioresistance in black fungi should be performed.

Our study confirms black fungi as excellent models for the study of the mechanisms used by eukaryotic cells to cope with ionizing radiation (Selbmann et al., 2018). We observed general stunning radioresistance of most of the black fungi if compared to other microorganisms and some of them exceed the survival limits of the most radioresistant prokaryotic and eukaryotic forms of life (e.g. Cox et al., 2005; Daly, 2009; Sukhi et al., 2009; Singh et al., 2013; Krisko, 2013). However, it should be highlighted that the response to

ionizing radiation in microorganisms can vary markedly with the cellular state and exposure conditions (Hafer et al., 2010; Schultzhaus et al., 2020; Couceiro et al., 2021). Considering the dose rates recorded in the most radioactive environments on Earth, our results show how part of black fungi may hypothetically survive there even after thousands of years of exposure to ionizing radiation in a silent desiccated state (Kashparov et al., 2018; Matsuo et al., 2019). Similarly, the radiation levels recorded in interplanetary space and on the surface of celestial bodies that could host forms of life, such as Mars, are remarkably lower than those tested in our experiment (Zeitlin et al., 2013; Hassler et al., 2014; Inozemtsev et al., 2015).

Taken together, by simultaneously testing a broad set of ecologically and phylogenetically distinct fungal strains, the present study supplies the first characterization of the radioresistance in black fungi. Along with ecological information on the strains, these results allowed us to display how the radioresistance in black fungi may be the result of their adaptation to various environmental variables. From an evolutionary perspective, our findings demonstrate how the pressure exerted by a few stressors may induce mechanisms that enable the microorganisms to cope with a broader range of possible damaging factors. In overall, this work may give new insights into the prediction of evolutionary responses to extreme environments and into the ability of life to adapt and persist in harsh terrestrial and extraterrestrial environments (e.g. Mars). This information represents the baseline for untangling the genomic and metabolomic traits underlying the radioresistance of black fungi, which may pave the way to untangle the limits of life in extreme radioactive environments.

References

Aureli, L., Pacelli, C., Cassaro, A., Fujimori, A., Moeller, R., and Onofri, S. (2020) Iron ion particle radiation resistance of dried colonies of *Cryomyces antarcticus* embedded in Martian regolith analogues. *Life* 10,306.

Averesch, N.J., Shunk, G.K., and Kern, C. (2022) Cultivation of the Dematiaceous Fungus *Cladosporium sphaerospermum* Aboard the International Space Station and Effects of Ionizing Radiation. *Frontiers in microbiology* 13.

Azzam, E.I., Jay-Gerin, J.-P., and Pain, D. (2012) Ionizing radiation-induced metabolic oxidative stress and prolonged cell injury. *Cancer letters* 327,48–60.

Braga, G.U., Rangel, D.E., Fernandes, E.K., Flint, S.D., and Roberts, D.W. (2015) Molecular and physiological effects of environmental UV radiation on fungal conidia. *Current genetics* 61,405–425.

Branco, S. (2019) Fungal diversity from communities to genes. *Fungal Biology Reviews* 33, 225–237.

Coleine, C. and Delgado-Baquerizo, M. (2022) Unearthing terrestrial extreme microbiomes for searching terrestrial-like life in the Solar System. *Trends in Microbiology*.

Coleine, C., Stajich, J.E., and Selbmann, L. (2022) Fungi are key players in extreme ecosystems. *Trends in Ecology & Evolution*.

Cordero, R.J., Vij, R., and Casadevall, A. (2017) Microbial melanins for radioprotection and bioremediation. *Microbial Biotechnology* 10,1186.

Couceiro, J. da C., Fatoretto, M.B., Demétrio, C.G.B., Meyling, N.V., and Delalibera Jr, Í. (2021) UV-B Radiation Tolerance and Temperature-Dependent Activity Within the Entomopathogenic Fungal Genus *Metarhizium* in Brazil. *Frontiers in Fungal Biology* 2,645737.

Cox, M.M. and Battista, J.R. (2005) *Deinococcus radiodurans*—the consummate survivor. *Nature Reviews Microbiology* 3,882–892.

Dadachova, E., Bryan, R.A., Howell, R.C., Schweitzer, A.D., Aisen, P., Nosanchuk, J.D., and Casadevall, A. (2008) The radioprotective properties of fungal melanin are a function of its chemical composition, stable radical presence and spatial arrangement. *Pigment cell & melanoma research* 21,192–199.

Daly, M.J. (2009) A new perspective on radiation resistance based on *Deinococcus radiodurans*. *Nature Reviews Microbiology* 7,237–245.

Dartnell, L.R. (2011) Ionizing radiation and life. *Astrobiology* 11,551–582.

Dartnell, L.R., Desorgher, L., Ward, J.M., and Coates, A. (2007) Martian sub-surface ionising radiation: biosignatures and geology. *Biogeosciences* 4,545–558.

Das, T., Al-Tawaha, A.R., Pandey, D.K., Nongdam, P., Shekhawat, M.S., Dey, A., et al. (2022) Halophilic, Acidophilic, Alkaliphilic, Metallophilic, and Radioresistant Fungi: Habitats and Their Living Strategies. In Extremophilic Fungi. Springer, pp. 171–193.

Egidi, E., De Hoog, G., Isola, D., Onofri, S., Quaedvlieg, W., De Vries, M., et al. (2014) Phylogeny and taxonomy of meristematic rock-inhabiting black fungi in the Dothideomycetes based on multi-locus phylogenies. *Fungal Diversity* 65,127–165.

Eisenman, H.C. and Casadevall, A. (2012) Synthesis and assembly of fungal melanin. *Applied microbiology and biotechnology* 93,931–940.

Ellison, C.E., Hall, C., Kowbel, D., Welch, J., Brem, R.B., Glass, N., and Taylor, J.W. (2011) Population genomics and local adaptation in wild isolates of a model microbial eukaryote. *Proceedings of the National Academy of Sciences* 108: 2831–2836.

Etemadifar, Z., Gholami, M., and Derikvand, P. (2016) UV-resistant bacteria with multiple-stress tolerance isolated from desert areas in Iran. *Geomicrobiology journal* 33,1–7.

Evans, L.G., Boynton, W.V., Reedy, R.C., Starr, R.D., and Trombka, J.I. (2003) Background lines in the Mars Odyssey 2001 gamma-ray detector. SPIE, pp. 31–44.

Ferrara, G., Di Sarcina, I., Cemmi, A., and Baccaro, S. (2019) Gamma irradiation Calliope facility at ENEA-Casaccia Research Centre (Rome, Italy).

Gabani, P. and Singh, O.V. (2013) Radiation-resistant extremophiles and their potential in biotechnology and therapeutics. *Applied microbiology and biotechnology* 97,993–1004.

Gladieux, P., Ropars, J., Badouin, H., Branca, A., Aguileta, G., De Vienne, D.M., et al. (2014) Fungal evolutionary genomics provides insight into the mechanisms of adaptive divergence in eukaryotes. *Molecular ecology* 23,753–773.

Gostinčar, C. and Gunde-Cimerman, N. (2018) Overview of oxidative stress response genes in selected halophilic fungi. *Genes* 9,143.

Hafer, K., Rivina, L., and Schiestl, R.H. (2010) Cell cycle dependence of ionizing radiation-induced DNA deletions and antioxidant radioprotection in Saccharomyces cerevisiae. *Radiation research* 173,802–808.

Hassler, D.M., Zeitlin, C., Wimmer-Schweingruber, R.F., Ehresmann, B., Rafkin, S., Eigenbrode, J.L., et al. (2014) Mars' surface radiation environment measured with the Mars Science Laboratory's Curiosity rover. *Science* 343,1244797.

Horne, W.H., Volpe, R.P., Korza, G., DePratti, S., Conze, I.H., Shuryak, I., et al. (2022) Effects of Desiccation and Freezing on Microbial Ionizing Radiation Survivability: Considerations for Mars Sample Return. *Astrobiology* 22,1337–1350.

Hu, Q.-H., Weng, J.-Q., and Wang, J.-S. (2010) Sources of anthropogenic radionuclides in the environment: a review. *Journal of environmental radioactivity* 101,426–437.

Ichimiya, T., Narita, T., and Kitao, K. (1998) Natural background gamma-ray spectrum. List of gamma-rays ordered in energy from natural radionuclides.

Inozemtsev, K., Kushin, V., Tolochek, R., and Shurshakov, V. (2015) Measurement of space radiation doses and linear energy transfer spectra inside biological satellite BION-M1. Aviakosmicheskaia i Ekologicheskaia Meditsina= *Aerospace and Environmental Medicine* 49,16–22.

Isola, D., Scano, A., Orrù, G., Prenafeta-Boldú, F.X., and Zucconi, L. (2021) Hydrocarbon-contaminated sites: Is there something more than *Exophiala xenobiotica*? New insights into black fungal diversity using the long cold incubation method. *Journal of Fungi* 7,817.

Jung, K.-W., Lim, S., and Bahn, Y.-S. (2017) Microbial radiation-resistance mechanisms. *Journal of Microbiology* 55,499–507.

Kanekar, P.P. and Kanekar, S.P. (2022) Radiophilic, Radioresistant, and Radiotolerant Microorganisms. In Diversity and Biotechnology of Extremophilic Microorganisms from India. Springer, pp. 251–267.

Kashparov, V., Levchuk, S., Zhurba, M., Protsak, V., Khomutinin, Y., Beresford, N.A., and Chaplow, J.S. (2018) Spatial datasets of radionuclide contamination in the Ukrainian Chernobyl Exclusion Zone. *Earth System Science Data* 10,339–353.

Khan, I., Qin, Z., Xie, T., Bin, Z., Li, H., Sun, W., and Lewis, E. (2020) Evaluation of health hazards from radionuclides in soil and rocks of North Waziristan, Pakistan. *International Journal of Radiation Research* 18,243–253.

Kogej, T., Gorbushina, A.A., and Gunde-Cimerman, N. (2006) Hypersaline conditions induce changes in cell-wall melanization and colony structure in a halophilic and a xerophilic black yeast species of the genus *Trimmatostroma*. *Mycological research* 110,713–724.

Kostadinova, N., Krumova, E., Stefanova, T., Dishliyska, V., and Angelova, M. (2012) Transient cold shock induces oxidative stress events in Antarctic fungi. *Oxidative Stress Book* 1,75–99.

Kreusch, M.G. and Duarte, R.T.D. (2021) Photoprotective compounds and radioresistance in pigmented and non-pigmented yeasts. *Applied Microbiology and Biotechnology* 105,3521–3532.

Krisko, A. and Radman, M. (2013) Biology of extreme radiation resistance: the way of *Deinococcus radiodurans*. *Cold Spring Harbor perspectives in biology* 5,a012765.

Leprince, O. and Buitink, J. (2010) Desiccation tolerance: from genomics to the field. Plant *Science* 179,554–564.

Lim, S., Jung, J.-H., Blanchard, L., and de Groot, A. (2019) Conservation and diversity of radiation and oxidative stress resistance mechanisms in *Deinococcus* species. *FEMS microbiology reviews* 43,19–52.

Lushchak, V.I. (2011) Adaptive response to oxidative stress: Bacteria, fungi, plants and animals. Comparative Biochemistry and Physiology Part C: *Toxicology & Pharmacology* 153,175–190.

Malo, M.E., Schultzhaus, Z., Frank, C., Romsdahl, J., Wang, Z., and Dadachova, E. (2021) Transcriptomic and genomic changes associated with radioadaptation in *Exophiala dermatitidis*. *Computational and Structural Biotechnology Journal* 19,196–205.

Matsuo, M., Taira, Y., Orita, M., Yamada, Y., Ide, J., Yamashita, S., and Takamura, N. (2019) Evaluation of environmental contamination and estimated radiation exposure dose rates among residents immediately after returning home to Tomioka Town, Fukushima Prefecture. *International Journal of Environmental Research and Public Health* 16,1481.

Mejía-Barajas, J.A., Montoya-Pérez, R., Salgado-Garciglia, R., Aguilera-Aguirre, L., Cortés-Rojo, C., Mejía-Zepeda, R., et al. (2017) Oxidative stress and antioxidant response in a thermotolerant yeast. *Brazilian journal of microbiology* 48,326–332.

Moissl-Eichinger, C., Cockell, C., and Rettberg, P. (2016) Venturing into new realms? Microorganisms in space. *FEMS microbiology reviews* 40,722–737.

Mousseau, T.A. and Møller, A.P. (2020) Plants in the light of ionizing radiation: what have we learned from Chernobyl, Fukushima, and other "hot" places? Frontiers in Plant Science 11,552.

Pacelli, C., Bryan, R.A., Onofri, S., Selbmann, L., Zucconi, L., Shuryak, I., and Dadachova, E. (2018a) Survival and redox activity of *Friedmanniomyces endolithicus*, an Antarctic endemic black meristematic fungus, after gamma rays exposure. *Fungal biology* 122,1222–1227.

Pacelli, C., Bryan, R.A., Onofri, S., Selbmann, L., Zucconi, L., Shuryak, I., and Dadachova, E. (2018b) The effect of protracted X-ray exposure on cell survival and metabolic activity of fast and slow growing fungi capable of melanogenesis. *Environmental microbiology reports* 10: 255–263.

Pacelli, C., Cassaro, A., Aureli, L., Moeller, R., Fujimori, A., and Onofri, S. (2020) The responses of the black fungus *Cryomyces antarcticus* to high doses of accelerated helium ions radiation within martian regolith simulants and their relevance for Mars. *Life* 10,130.

Robertson, K.L., Mostaghim, A., Cuomo, C.A., Soto, C.M., Lebedev, N., Bailey, R.F., and Wang, Z. (2012) Adaptation of the black yeast *Wangiella dermatitidis* to ionizing radiation: molecular and cellular mechanisms. *PloS one* 7,e48674.

Romsdahl, J., Schultzhaus, Z., Chen, A., Liu, J., Ewing, A., Hervey, J., and Wang, Z. (2021) Adaptive evolution of a melanized fungus reveals robust augmentation of radiation resistance by abrogating non-homologous end-joining. *Environmental Microbiology* 23,3627–3645.

Roth, M.A., Krumholz, M.R., Crocker, R.M., and Celli, S. (2021) The diffuse γ-ray background is dominated by star-forming galaxies. *Nature* 597,341–344.

Schultzhaus, Z., Romsdahl, J., Chen, A., Tschirhart, T., Kim, S., Leary, D., and Wang, Z. (2020a) The response of the melanized yeast *Exophiala dermatitidis* to gamma radiation exposure. *Environmental microbiology* 22,1310–1326.

Selbmann, L., Benkő, Z., Coleine, C., De Hoog, S., Donati, C., Druzhinina, I., et al. (2020) Shed light in the dark lineages of the fungal tree of life—stres. *Life* 10,362.

Selbmann, L., De Hoog, G., Mazzaglia, A., Friedmann, E., and Onofri, S. (2005) Fungi at the edge of life: cryptoendolithic black fungi from Antarctic desert. *Stud Mycol* 51,1–32.

Selbmann, L., Isola, D., Zucconi, L., and Onofri, S. (2011) Resistance to UV-B induced DNA damage in extreme-tolerant cryptoendolithic Antarctic fungi: detection by PCR assays. *Fungal Biology* 115,937–944.

Share, G.H. and Murphy, R.J. (2001) Atmospheric gamma rays from solar energetic particles and cosmic rays penetrating the magnetosphere. Journal of Geophysical Research: *Space Physics* 106,77–92.

Sharma, A., Gaidamakova, E.K., Grichenko, O., Matrosova, V.Y., Hoeke, V., Klimenkova, P., et al. (2017) Across the tree of life, radiation resistance is governed by antioxidant Mn^{2+}, gauged by paramagnetic resonance. *Proceedings of the National Academy of Sciences* 114,E9253–E9260.

Shuryak, I. (2019a) Review of microbial resistance to chronic ionizing radiation exposure under environmental conditions. *Journal of environmental radioactivity* 196,50–63.

Shuryak, I., Bryan, R.A., Nosanchuk, J.D., and Dadachova, E. (2014) Mathematical modeling predicts enhanced growth of X-ray irradiated pigmented fungi. *PloS one* 9,e85561.

Shuryak, I., Tkavc, R., Matrosova, V.Y., Volpe, R.P., Grichenko, O., Klimenkova, P., et al. (2019b) Chronic gamma radiation resistance in fungi correlates with resistance to chromium and elevated temperatures, but not with resistance to acute irradiation. *Scientific reports* 9,1–11.

Singh, H., Kim, H., Song, H., Joe, M., Kim, D., Bahn, Y.-S., et al. (2013) A novel radiation-resistant strain of *Filobasidium* sp. isolated from the West Sea of Korea. *Journal of microbiology and biotechnology* 23,1493–1499.

Sukhi, S.S., Shashidhar, R., Kumar, S.A., and Bandekar, J.R. (2009) Radiation resistance of *Deinococcus radiodurans* R1 with respect to growth phase. *FEMS microbiology letters* 297,49–53.

Tesei, D. (2022) Black fungi research: Out-of-this-world implications. *Encyclopedia* 2,212–229.

Walencik-Łata, A., Szkliniarz, K., Kisiel, J., Polaczek-Grelik, K., Jędrzejczak, K., Kasztelan, M., et al. (2022) Characteristics of Natural Background Radiation in the GIG Experimental Mine 'Barbara', Poland. *Energies* 15,685.

Wissmann, F., Dangendorf, V., and Schrewe, U. (2005) Radiation exposure at ground level by secondary cosmic radiation. *Radiation measurements* 39,95–104.

Yamamoto, M., Tomita, J., Sakaguchi, A., Imanaka, T., Fukutani, S., Endo, S., et al. (2008) Spatial distribution of soil contamination by ^{137}Cs and ^{239,240}Pu in the village of Dolon near the Semipalatinsk Nuclear Test Site: new information on traces of the radioactive plume from the 29 August 1949 nuclear test. *Health physics* 94,328–337.

Zeitlin, C., Hassler, D., Cucinotta, F., Ehresmann, B., Wimmer-Schweingruber, R., Brinza, D., et al. (2013) Measurements of energetic particle radiation in transit to Mars on the Mars Science Laboratory. *Science* 340,1080–1084.

Supplementary material

Table S4.1. Fungal strains tested in the study and their response to radiation exposure in terms of D10 and the maximum survival dose.

Class	Species	Strain	D10 (kGy)	Max dose (kGy)
Eurotiomycetes	*Eurotiomycetes sp*	CCFEE6388	0.3	0.1
Eurotiomycetes	*Chaetothyriales sp*	CCFEE6169	0.3	1
Eurotiomycetes	*Exophiala xenobiotica*	CCFEE6043	0.4	1
Eurotiomycetes	*Exophiala xenobiotica*	CCFEE5985	0.4	0.5
Eurotiomycetes	*Exophiala xenobiotica*	CCFEE5816	0.4	2
Eurotiomycetes	*Exophiala mesophila*	CCFEE6314	0.4	1
Eurotiomycetes	*Exophiala xenobiotica*	CCFEE5877	0.4	3
Dothideomycetes	*Meristemomyces frigidus*	CCFEE5401	0.4	1
Eurotiomycetes	*Exophiala oligosperma*	CCFEE6327	0.4	1
Eurotiomycetes	*Exophiala xenobiotica*	CCFEE6357	0.4	1
Eurotiomycetes	*Exophiala xenobiotica*	CCFEE6059	0.5	1
Dothideomycetes	*Elasticomyces elasticus*	CCFEE5806	0.5	2
Eurotiomycetes	*Exophiala xenobiotica*	CCFEE5823	0.5	2
Eurotiomycetes	*Exophiala xenobiotica*	CCFEE6068	0.5	1
Eurotiomycetes	*Exophiala xenobiotica*	CCFEE6221	0.6	1
Eurotiomycetes	*Exophiala xenobiotica*	CCFEE6233	0.7	1
Eurotiomycetes	*Exophiala xenobiotica*	CCFEE5882	0.7	2
Dothideomycetes	*Meristemomyces frigidus*	CCFEE5457	0.7	1
Eurotiomycetes	*Exophiala xenobiotica*	CCFEE5874	0.7	1
Dothideomycetes	*Meristemomyces frigidus*	CCFEE5508	0.7	2
Dothideomycetes	*Elasticomyces elasticus*	CCFEE5537	0.8	2
Eurotiomycetes	*Exophiala xenobiotica*	CCFEE6036	0.8	2
Eurotiomycetes	*Exophiala bonariae*	CCFEE5792	0.8	1
Dothideomycetes	*Elasticomyces elasticus*	CCFEE5543	0.8	2
Dothideomycetes	*Elasticomyces elasticus*	CCFEE5544	0.8	3
Eurotiomycetes	*Exophiala xenobiotica*	CCFEE5784	0.8	1
Dothideomycetes	*Elasticomyces elasticus*	CCFEE5506	0.8	3
Eurotiomycetes	*Exophiala xenobiotica*	CCFEE5811	0.8	1
Eurotiomycetes	*Exophiala xenobiotica*	CCFEE6060	0.8	1
Dothideomycetes	*Elasticomyces elasticus*	CCFEE5320	0.8	3
Dothideomycetes	*Elasticomyces elasticus*	CCFEE5547	0.8	3
Eurotiomycetes	*Exophiala xenobiotica*	CCFEE5801	0.9	1
Dothideomycetes	*Elasticomyces elasticus*	CCFEE5810	0.9	3
Dothideomycetes	*Elasticomyces elasticus*	CCFEE5966	0.9	2
Eurotiomycetes	*Exophiala xenobiotica*	CCFEE6336	1	1
Eurotiomycetes	*Exophiala xenobiotica*	CCFEE6142	1	2
Eurotiomycetes	*Exophiala xenobiotica*	CCFEE6194	1	1
Eurotiomycetes	*Exophiala xenobiotica*	CCFEE5819	1.1	1
Eurotiomycetes	*Exophiala xenobiotica*	CCFEE6182	1.2	1
Dothideomycetes	*Teratosphaeriaceae sp*	MNA-CCFEE6256	1.3	2
Dothideomycetes	*Saxophila tyrrhenica*	CCFEE5935	1.3	2
Dothideomycetes	*Recurvomyces mirabilis*	MNA-CCFEE6590	1.3	3
Dothideomycetes	*Oleoguttula mirabilis*	MNA-CCFEE5522	1.3	3
Eurotiomycetes	*Exophiala xenobiotica*	CCFEE6237	1.3	2
Eurotiomycetes	*Exophiala xenobiotica*	CCFEE6196	1.3	1
Eurotiomycetes	*Exophiala xenobiotica*	CCFEE6180	1.4	2
Dothideomycetes	*Teratosphaeriaceae sp*	MNA-CCFEE6253	1.5	3

Dothideomycetes	*Oleoguttula sp*	MNA-CCFEE6097	1.7	2
Dothideomycetes	*Capnodiales sp*	MNA-CCFEE6595	1.7	5
Dothideomycetes	*Meristemomyces frigidus*	CCFEE5501	1.7	5
Dothideomycetes	*Recurvomyces mirabilis*	CCFEE5536	1.7	2
Dothideomycetes	*Capnodiales sp*	MNA-CCFEE6512	1.8	5
Dothideomycetes	*Elasticomyces elasticus*	MNA-CCFEE5313	2.0	3
Dothideomycetes	*Extremus antarcticus*	MNA-CCFEE451	2.1	3
Dothideomycetes	*Elasticomyces elasticus*	MNA-CCFEE5474	2.1	2
Dothideomycetes	*Recurvomyces mirabilis*	MNA-CCFEE5485	2.1	5
Dothideomycetes	*Elasticomyces elasticus*	MNA-CCFEE5319	2.2	3
Dothideomycetes	*Extremus antarcticus*	MNA-CCFEE5312	2.2	2
Dothideomycetes	*Elasticomyces elasticus*	MNA-CCFEE6086	2.3	3
Dothideomycetes	*Elasticomyces elasticus*	MNA-CCFEE5316	2.5	5
Dothideomycetes	*Dothideomyces sp*	CCFEE6323	2.7	5
Dothideomycetes	*Recurvomyces mirabilis*	MNA-CCFEE5264	2.7	3
Dothideomycetes	*Coniosporium uncinatum*	CCFEE5737	3.9	3
Dothideomycetes	*Friedmanniomyces endolithicus*	CCFEE5486	13.4	15
Dothideomycetes	*Friedmanniomyces endolithicus*	MNA-CCFEE5307	13.7	15
Dothideomycetes	*Friedmanniomyces endolithicus*	MNA-CCFEE5283	13.8	30
Dothideomycetes	*Friedmanniomyces endolithicus*	MNA-CCFEE5277	13.9	30
Dothideomycetes	*Friedmanniomyces endolithicus*	MNA-CCFEE5311	14.1	15
Dothideomycetes	*Friedmanniomyces endolithicus*	MNA-CCFEE5281	14.3	15
Dothideomycetes	*Friedmanniomyces simplex*	MNA-CCFEE5184	15.1	15
Dothideomycetes	*Friedmanniomyces endolithicus*	MNA-CCFEE670	15.1	30
Dothideomycetes	*Friedmanniomyces endolithicus*	MNA-CCFEE5195	15.4	15
Dothideomycetes	*Friedmanniomyces endolithicus*	MNA-CCFEE5275	15.8	15
Dothideomycetes	*Friedmanniomyces sp.*	MNA-CCFEE5328	15.9	30
Dothideomycetes	*Friedmanniomyces endolithicus*	MNA-CCFEE5001	16.1	30
Dothideomycetes	*Friedmanniomyces endolithicus*	MNA-CCFEE6096	16.2	30
Dothideomycetes	*Friedmanniomyces endolithicus*	MNA-CCFEE524	16.2	30
Dothideomycetes	*Friedmanniomyces endolithicus*	MNA-CCFEE6081	16.2	15
Dothideomycetes	*Friedmanniomyces endolithicus*	MNA-CCFEE6078	16.4	15
Dothideomycetes	*Friedmanniomyces endolithicus*	MNA-CCFEE5273	16.5	30
Dothideomycetes	*Friedmanniomyces endolithicus*	MNA-CCFEE6249	16.6	30
Dothideomycetes	*Friedmanniomyces endolithicus*	MNA-CCFEE6464	16.7	30
Dothideomycetes	*Friedmanniomyces endolithicus*	MNA-CCFEE5208	16.9	30
Dothideomycetes	*Friedmanniomyces endolithicus*	MNA-CCFEE5269	17.1	30
Dothideomycetes	*Friedmanniomyces endolithicus*	MNA-CCFEE5193	17.2	30
Dothideomycetes	*Friedmanniomyces endolithicus*	MNA-CCFEE6074	17.5	30
Dothideomycetes	*Cryomyces antarcticus*	MNA-CCFEE6465	18.2	30
Dothideomycetes	*Friedmanniomyces endolithicus*	MNA-CCFEE5200	19.3	50
Dothideomycetes	*Friedmanniomyces endolithicus*	MNA-CCFEE5199	19.3	50
Dothideomycetes	*Friedmanniomyces endolithicus*	MNA-CCFEE6082	19.9	30
Dothideomycetes	*Friedmanniomyces endolithicus*	MNA-CCFEE6250	20.5	50
Dothideomycetes	*Friedmanniomyces endolithicus*	MNA-CCFEE6296	20.8	50
Dothideomycetes	*Cryomyces antarcticus*	MNA-CCFEE6461	20.8	30
Dothideomycetes	*Cryomyces antarcticus*	MNA-CCFEE515	21.3	50
Dothideomycetes	*Cryomyces antarcticus*	MNA-CCFEE534	21.4	50
Dothideomycetes	*Cryomyces antarcticus*	MNA-CCFEE690	21.5	50
Dothideomycetes	*Cryomyces antarcticus*	MNA-CCFEE535	21.7	50
Dothideomycetes	*Cryomyces antarcticus*	MNA-CCFEE6416	21.7	30
Dothideomycetes	*Cryomyces antarcticus*	MNA-CCFEE6414	22.0	50
Dothideomycetes	*Cryomyces minteri*	MNA-CCFEE5187	23.5	50

Table S4.2. Fungal strains and the localities from where they were collected and the related environmental metadata. AMT: Annual Mean Temperature; MTWAQ: Mean Temperature of the Warmest Quarter; MTCQ: Mean Temperature of the Coldest Quarter; AP: Annual Precipitation; PWEM: Precipitation of the Wettest Month; PDM: Precipitation of the Driest Month; PS: Precipitation Seasonality (Coefficient of Variation); PWEQ: Precipitation of the Wettest Quarter; PDQ: Precipitation of the Driest Quarter; PWAQ: Precipitation of the Warmest Quarter; PCQ: Precipitation of the Coldest Quarter; MDR: Mean Diurnal Range (Mean of monthly (maximum temperature - minimum temperature)); TS: Temperature Seasonality (standard deviation ×100); MTWAM: Maximum Temperature of the Warmest Month; MTCM: Minimum Temperature of Coldest Month; TAR: Temperature Annual Range (calculated as MTWAM - MTCM); MTWEQ: Mean Temperature of the Wettest Quarter; MTDQ: Mean Temperature of the Driest Quarter; IT: Isothermality (calculated as MDR/TAR) (×100); biome: biome type; country: country of isolation; KG climate: Köppen-Geiger climate classification subgroup.

Map references	Strain number	Species	Class	Latitude	Longitude	Biome	Isolation source	Country	AMT (°C)	MTWAQ (°C)	MTCQ (°C)	AP (mm)	PWEM (mm)	PDM (mm)	PS	PWEQ (mm)	PDQ (mm)	PWAQ (mm)	PCQ (mm)	MDR (°C)	IT	TS	MTWAM (°C)	MTCM (°C)	TAR (°C)	MTWEQ (°C)	MTDQ (°C)	Solar radiation (W/m²)	KG climate	UV Index
1	CCFEE5401	*Meristemomyces frigidus*	*Dothideomycetes*	46	7,866	montane biome	rock	Italy	-4,9	2,2	-10,8	348	34	24	10,8	95	79	95	93	4,8	24,9	537,6	5,5	-13,7	19,2	2,2	-6,2	15431,25	ET Polar, tundra	5,71
1	CCFEE5457	*Meristemomyces frigidus*	*Dothideomycetes*	46	7,866	montane biome	rock	Italy	-4,9	2,2	-10,8	348	34	24	10,8	95	79	95	93	4,8	24,9	537,6	5,5	-13,7	19,2	2,2	-6,2	15431,25	ET Polar, tundra	5,71
2	CCFEE5547	*Elasticomyces elasticus*	*Dothideomycetes*	44,713	6,18	montane biome	rock	Italy	1,6	9,7	-5,1	1408	159	66	22,4	441	247	256	393	7,3	30,2	618,4	15,6	-8,6	24,2	-0,8	9,4	14800,42	Dfc Cold, no dry season, cold summer	6,24
3	CCFEE5966	*Elasticomyces elasticus*	*Dothideomycetes*	46,417	10,183	montane biome	rock	Italy	-0,7	7,1	-8,0	658	77	31	28,0	227	113	227	114	8,3	32,4	629,8	12,8	-12,7	25,5	7,1	-7,5	13363,17	ET Polar, tundra	6,29
4	CCFEE5784	*Exophiala xenobiotica*	*Eurotiomycetes*	42,383	12,264	polluted environment	motor vehicle	Italy	13,2	21,4	5,8	276	34	11	27,4	94	46	46	69	8,4	32,5	642,9	27,8	2	25,8	14,1	21,4	14465,17	Csa Temperate, dry summer, hot summer	5,73
4	CCFEE5801	*Exophiala xenobiotica*	*Eurotiomycetes*	42,383	12,264	polluted environment	motor vehicle	Italy	13,2	21,4	5,8	276	34	11	27,4	94	46	46	69	8,4	32,5	642,9	27,8	2	25,8	14,1	21,4	14465,17	Csa Temperate, dry summer, hot summer	5,73
4	CCFEE5811	*Exophiala xenobiotica*	*Eurotiomycetes*	42,383	12,264	polluted environment	motor vehicle	Italy	13,2	21,4	5,8	276	34	11	27,4	94	46	46	69	8,4	32,5	642,9	27,8	2	25,8	14,1	21,4	14465,17	Csa Temperate, dry summer, hot summer	5,73
4	CCFEE5816	*Exophiala xenobiotica*	*Eurotiomycetes*	42,383	12,264	polluted environment	motor vehicle	Italy	13,2	21,4	5,8	276	34	11	27,4	94	46	46	69	8,4	32,5	642,9	27,8	2	25,8	14,1	21,4	14465,17	Csa Temperate, dry summer, hot summer	5,73
4	CCFEE5819	*Exophiala xenobiotica*	*Eurotiomycetes*	42,383	12,264	polluted environment	motor vehicle	Italy	13,2	21,4	5,8	276	34	11	27,4	94	46	46	69	8,4	32,5	642,9	27,8	2	25,8	14,1	21,4	14465,17	Csa Temperate, dry summer, hot summer	5,73
4	CCFEE5823	*Exophiala xenobiotica*	*Eurotiomycetes*	42,383	12,264	polluted environment	motor vehicle	Italy	13,2	21,4	5,8	276	34	11	27,4	94	46	46	69	8,4	32,5	642,9	27,8	2	25,8	14,1	21,4	14465,17	Csa Temperate, dry summer, hot summer	5,73
4	CCFEE5874	*Exophiala xenobiotica*	*Eurotiomycetes*	42,383	12,264	polluted environment	motor vehicle	Italy	13,2	21,4	5,8	276	34	11	27,4	94	46	46	69	8,4	32,5	642,9	27,8	2	25,8	14,1	21,4	14465,17	Csa Temperate, dry summer, hot summer	5,73
4	CCFEE5877	*Exophiala xenobiotica*	*Eurotiomycetes*	42,383	12,264	polluted environment	motor vehicle	Italy	13,2	21,4	5,8	276	34	11	27,4	94	46	46	69	8,4	32,5	642,9	27,8	2	25,8	14,1	21,4	14465,17	Csa Temperate, dry summer, hot summer	5,73
4	CCFEE5882	*Exophiala xenobiotica*	*Eurotiomycetes*	42,383	12,264	polluted environment	motor vehicle	Italy	13,2	21,4	5,8	276	34	11	27,4	94	46	46	69	8,4	32,5	642,9	27,8	2	25,8	14,1	21,4	14465,17	Csa Temperate, dry summer, hot summer	5,73
4	CCFEE5985	*Exophiala xenobiotica*	*Eurotiomycetes*	42,383	12,264	polluted environment	motor vehicle	Italy	13,2	21,4	5,8	276	34	11	27,4	94	46	46	69	8,4	32,5	642,9	27,8	2	25,8	14,1	21,4	14465,17	Csa Temperate, dry summer, hot summer	5,73
4	CCFEE6036	*Exophiala xenobiotica*	*Eurotiomycetes*	42,383	12,264	polluted environment	motor vehicle	Italy	13,2	21,4	5,8	276	34	11	27,4	94	46	46	69	8,4	32,5	642,9	27,8	2	25,8	14,1	21,4	14465,17	Csa Temperate, dry summer, hot summer	5,73
4	CCFEE6043	*Exophiala xenobiotica*	*Eurotiomycetes*	42,383	12,264	polluted environment	motor vehicle	Italy	13,2	21,4	5,8	276	34	11	27,4	94	46	46	69	8,4	32,5	642,9	27,8	2	25,8	14,1	21,4	14465,17	Csa Temperate, dry summer, hot summer	5,73
4	CCFEE6059	*Exophiala xenobiotica*	*Eurotiomycetes*	42,383	12,264	polluted environment	motor vehicle	Italy	13,2	21,4	5,8	276	34	11	27,4	94	46	46	69	8,4	32,5	642,9	27,8	2	25,8	14,1	21,4	14465,17	Csa Temperate, dry summer, hot summer	5,73
4	CCFEE6060	*Exophiala xenobiotica*	*Eurotiomycetes*	42,383	12,264	polluted environment	motor vehicle	Italy	13,2	21,4	5,8	276	34	11	27,4	94	46	46	69	8,4	32,5	642,9	27,8	2	25,8	14,1	21,4	14465,17	Csa Temperate, dry summer, hot summer	5,73
4	CCFEE6068	*Exophiala xenobiotica*	*Eurotiomycetes*	42,383	12,264	polluted environment	motor vehicle	Italy	13,2	21,4	5,8	276	34	11	27,4	94	46	46	69	8,4	32,5	642,9	27,8	2	25,8	14,1	21,4	14465,17	Csa Temperate, dry summer, hot summer	5,73
4	CCFEE6142	*Exophiala xenobiotica*	*Eurotiomycetes*	42,383	12,264	polluted environment	motor vehicle	Italy	13,2	21,4	5,8	276	34	11	27,4	94	46	46	69	8,4	32,5	642,9	27,8	2	25,8	14,1	21,4	14465,17	Csa Temperate, dry summer, hot summer	5,73
4	CCFEE6180	*Exophiala xenobiotica*	*Eurotiomycetes*	42,383	12,264	polluted environment	motor vehicle	Italy	13,2	21,4	5,8	276	34	11	27,4	94	46	46	69	8,4	32,5	642,9	27,8	2	25,8	14,1	21,4	14465,17	Csa Temperate, dry summer, hot summer	5,73

4	CCFEE6182	*Exophiala xenobiotica*	*Eurotiomycetes*	42,383	12,264	polluted environment	motor vehicle	Italy	13,2	21,4	5,8	276	34	11	27,4	94	46	46	69	8,4	32,5	642,9	27,8	2	25,8	14,1	21,4	14465,17	Csa Temperate, dry summer, hot summer	5,73
4	CCFEE6194	*Exophiala xenobiotica*	*Eurotiomycetes*	42,383	12,264	polluted environment	motor vehicle	Italy	13,2	21,4	5,8	276	34	11	27,4	94	46	46	69	8,4	32,5	642,9	27,8	2	25,8	14,1	21,4	14465,17	Csa Temperate, dry summer, hot summer	5,73
4	CCFEE6196	*Exophiala xenobiotica*	*Eurotiomycetes*	42,383	12,264	polluted environment	motor vehicle	Italy	13,2	21,4	5,8	276	34	11	27,4	94	46	46	69	8,4	32,5	642,9	27,8	2	25,8	14,1	21,4	14465,17	Csa Temperate, dry summer, hot summer	5,73
4	CCFEE6221	*Exophiala xenobiotica*	*Eurotiomycetes*	42,383	12,264	polluted environment	motor vehicle	Italy	13,2	21,4	5,8	276	34	11	27,4	94	46	46	69	8,4	32,5	642,9	27,8	2	25,8	14,1	21,4	14465,17	Csa Temperate, dry summer, hot summer	5,73
4	CCFEE6233	*Exophiala xenobiotica*	*Eurotiomycetes*	42,383	12,264	polluted environment	motor vehicle	Italy	13,2	21,4	5,8	276	34	11	27,4	94	46	46	69	8,4	32,5	642,9	27,8	2	25,8	14,1	21,4	14465,17	Csa Temperate, dry summer, hot summer	5,73
4	CCFEE6237	*Exophiala xenobiotica*	*Eurotiomycetes*	42,383	12,264	polluted environment	motor vehicle	Italy	13,2	21,4	5,8	276	34	11	27,4	94	46	46	69	8,4	32,5	642,9	27,8	2	25,8	14,1	21,4	14465,17	Csa Temperate, dry summer, hot summer	5,73
4	CCFEE6336	*Exophiala xenobiotica*	*Eurotiomycetes*	42,383	12,264	polluted environment	motor vehicle	Italy	13,2	21,4	5,8	276	34	11	27,4	94	46	46	69	8,4	32,5	642,9	27,8	2	25,8	14,1	21,4	14465,17	Csa Temperate, dry summer, hot summer	5,73
4	CCFEE6357	*Exophiala xenobiotica*	*Eurotiomycetes*	42,383	12,264	polluted environment	motor vehicle	Italy	13,2	21,4	5,8	276	34	11	27,4	94	46	46	69	8,4	32,5	642,9	27,8	2	25,8	14,1	21,4	14465,17	Csa Temperate, dry summer, hot summer	5,73
4	CCFEE6388	*Eurotiomycetes sp*	*Eurotiomycetes*	42,383	12,264	polluted environment	motor vehicle	Italy	13,2	21,4	5,8	276	34	11	27,4	94	46	46	69	8,4	32,5	642,9	27,8	2	25,8	14,1	21,4	14465,17	Csa Temperate, dry summer, hot summer	5,73
5	CCFEE5806	*Elasticomyces elasticus*	*Dothideomycetes*	42,471	13,563	montane biome	rock	Italy	1,0	8,7	-5,6	1001	113	62	19,5	313	203	226	203	3,5	17,1	601,1	12,3	-7,9	20,2	2,3	-5,6	14114,75	ET Polar, tundra	5,42
5	CCFEE5810	*Elasticomyces elasticus*	*Dothideomycetes*	42,471	13,563	montane biome	rock	Italy	1,0	8,7	-5,6	1001	113	62	19,5	313	203	226	203	3,5	17,1	601,1	12,3	-7,9	20,2	2,3	-5,6	14114,75	ET Polar, tundra	5,42
6	CCFEE5737	*Coniosporium uncinatum*	*Dothideomycetes*	39,211	9,124	monument	rock	Italy	16,8	24,1	10,5	407	54	4	51,1	154	24	45	140	9,5	38,1	568,5	30,7	5,8	24,9	14,5	23,9	15850,58	Csa Temperate, dry summer, hot summer	5,94
6	CCFEE5792	*Exophiala bonariae*	*Eurotiomycetes*	39,211	9,123	monument	rock	Italy	16,8	24,1	10,5	407	54	4	51,1	154	24	45	140	9,5	38,1	568,5	30,7	5,8	24,9	14,5	23,9	15850,58	Csa Temperate, dry summer, hot summer	5,94
6	CCFEE5714	*Vermiconia calcicola*	*Dothideomycetes*	39,211	9,124	monument	rock	Italy	16,8	24,1	10,5	407	54	4	51,1	154	24	45	140	9,5	38,1	568,5	30,7	5,8	24,9	14,5	23,9	15850,58	Csa Temperate, dry summer, hot summer	5,94
7	CCFEE5935	*Saxophila tyrrhenica*	*Dothideomycetes*	39,223	9,121	monument	rock	Italy	16,7	24,1	10,4	420	54	4	49,8	155	25	47	144	9,4	38,0	571,5	30,6	5,8	24,8	14,4	23,9	15744,42	Csa Temperate, dry summer, hot summer	5,94
8	CCFEE6327	*Exophiala oligosperma*	*Eurotiomycetes*	39,225	9,122	monument	rock	Italy	16,7	24,1	10,4	420	54	4	49,8	155	25	47	144	9,4	38,0	571,5	30,6	5,8	24,8	14,4	23,9	15744,42	Csa Temperate, dry summer, hot summer	5,94
9	CCFEE6238	*Exophiala xenobiotica*	*Eurotiomycetes*	40,625	14,38	polluted environment	motor vehicle	Italy	15,8	22,7	9,9	972	152	21	51,4	397	78	139	319	7,7	34,9	540,9	28	5,9	22,1	13,6	22,6	15035,75	Csa Temperate, dry summer, hot summer	5,76
10	CCFEE5536	*Recurvomyces mirabilis*	*Dothideomycetes*	62,777	11,121	montane biome	rock	Norway	0,2	9,8	-8,3	737	94	39	28,3	255	126	250	160	7,8	27,5	738,1	15,8	-12,5	28,3	8,8	-5,1	8545,42	Dfc Cold, no dry season, cold summer	2,82
11	CCFEE5537	*Elasticomyces elasticus*	*Dothideomycetes*	32,893	77,194	montane biome	rock	India	-6,3	4,4	-17,5	295	53	7	55,1	134	34	134	60	10,2	29,0	899,2	10,7	-24,3	35	4,4	-10,0	15395,75	ET Polar, tundra	12,52
11	CCFEE5543	*Elasticomyces elasticus*	*Dothideomycetes*	32,893	77,194	montane biome	rock	India	-6,3	4,4	-17,5	295	53	7	55,1	134	34	134	60	10,2	29,0	899,2	10,7	-24,3	35	4,4	-10,0	15395,75	ET Polar, tundra	12,52
11	CCFEE5544	*Elasticomyces elasticus*	*Dothideomycetes*	32,893	77,194	montane biome	rock	India	-6,3	4,4	-17,5	295	53	7	55,1	134	34	134	60	10,2	29,0	899,2	10,7	-24,3	35	4,4	-10,0	15395,75	ET Polar, tundra	12,52
12	CCFEE6169	*Chaetothyriales sp*	*Eurotiomycetes*	36,865	-111,588	montane biome	rock	USA	17,0	29,4	5,0	157	23	3	40,9	59	22	47	31	14,9	36,3	987,2	39,3	-1,8	41,1	28,3	22,0	18577,92	BWk Arid, desert, cold	8,47
13	CCFEE5501	*Meristemomyces frigidus*	*Dothideomycetes*	-32,669	-69,955	montane biome	rock	Argentina	-7,2	-2,5	-12,0	415	81	10	68,8	201	35	35	198	9,3	47,3	394,0	3,2	-16,5	19,7	-10,9	-2,5	16406,00	EF Polar, frost	10,74
13	CCFEE5508	*Meristemomyces frigidus*	*Dothideomycetes*	-32,669	-69,955	montane biome	rock	Argentina	-7,2	-2,5	-12,0	415	81	10	68,8	201	35	35	198	9,3	47,3	394,0	3,2	-16,5	19,7	-10,9	-2,5	16406,00	EF Polar, frost	10,74
14	CCFEE5506	*Elasticomyces elasticus*	*Dothideomycetes*	-32,607	-69,957	montane biome	rock	Argentina	-6,5	-1,9	-11,3	374	71	10	65,9	175	33	33	170	9,6	48,2	390,6	3,9	-16,1	20	-10,2	-1,9	16845,75	ET Polar, tundra	10,74
15	MNA-CCFEE5522	*Oleoguttula mirabilis*	*Dothideomycetes*	-69,5	65	endolithic environment	rock	Antarctica	-27,3	-16,4	-34,2	241	84	0	113,0	157	5	12	140	7,5	27,7	771,1	-11,1	-38,1	27	-33,9	-16,8	11927,17	EF Polar, frost	3,28
16	MNA-CCFEE6314	*Exophiala mesophila*	*Eurotiomycetes*	-71,25	163	endolithic environment	rock	Antarctica	-19,5	-10,4	-25,5	144	25	3	54,6	54	14	19	45	5,5	24,3	644,1	-6,5	-29,1	22,6	-17,7	-11,2	12421,50	EF Polar, frost	2,64
17	MNA-CCFEE6074	*Friedmanniomyces endolithicus*	*Dothideomycetes*	-73,49	163,912	polar desert biome	rock	Antarctica	-28,1	-20,0	-32,9	97	24	0	81,4	38	9	19	38	7,1	31,6	566,1	-14,8	-37,1	22,3	-32,9	-28,4	12696,83	EF Polar, frost	3,16
18	MNA-CCFEE5001	*Friedmanniomyces endolithicus*	*Dothideomycetes*	-74,169	162,427	endolithic environment	rock	Antarctica	-30,3	-22,0	-35,3	98	22	1	76,3	33	11	26	33	7,0	30,5	579,6	-16,7	-39,5	22,8	-29,8	-30,8	12123,83	EF Polar, frost	2,56
18	MNA-CCFEE5193	*Friedmanniomyces endolithicus*	*Dothideomycetes*	-74,169	162,427	endolithic environment	rock	Antarctica	-30,3	-22,0	-35,3	98	22	1	76,3	33	11	26	33	7,0	30,5	579,6	-16,7	-39,5	22,8	-29,8	-30,8	12123,83	EF Polar, frost	2,56
18	MNA-CCFEE5195	*Friedmanniomyces endolithicus*	*Dothideomycetes*	-74,169	162,427	endolithic environment	rock	Antarctica	-30,3	-22,0	-35,3	98	22	1	76,3	33	11	26	33	7,0	30,5	579,6	-16,7	-39,5	22,8	-29,8	-30,8	12123,83	EF Polar, frost	2,56

18	MNA-CCFEE5269	*Friedmanniomyces endolithicus*	*Dothideomycetes*	-74,169	162,427	endolithic environment	rock	Antarctica	-30,3	-22,0	-35,3	98	22	1	76,3	33	11	26	33	7,0	30,5	579,6	-16,7	-39,5	22,8	-29,8	-30,8	12123,83	EF Polar, frost	2,56
18	MNA-CCFEE5273	*Friedmanniomyces endolithicus*	*Dothideomycetes*	-74,169	162,427	endolithic environment	rock	Antarctica	-30,3	-22,0	-35,3	98	22	1	76,3	33	11	26	33	7,0	30,5	579,6	-16,7	-39,5	22,8	-29,8	-30,8	12123,83	EF Polar, frost	2,56
19	MNA-CCFEE6249	*Friedmanniomyces endolithicus*	*Dothideomycetes*	-74,17	162,425	polar desert biome	rock	Antarctica	-30,3	-22,0	-35,3	98	22	1	76,3	33	11	26	33	7,0	30,5	579,6	-16,7	-39,5	22,8	-29,8	-30,8	12123,83	EF Polar, frost	2,56
20	MNA-CCFEE6078	*Friedmanniomyces endolithicus*	*Dothideomycetes*	-74,178	162,514	polar desert biome	rock	Antarctica	-27,7	-19,4	-32,8	93	22	0	73,8	34	12	17	34	6,5	29,0	586,4	-14,6	-36,9	22,3	-32,7	-28,2	12478,92	EF Polar, frost	2,47
20	MNA-CCFEE6414	*Friedmanniomyces endolithicus*	*Dothideomycetes*	-74,178	162,514	endolithic environment	rock	Antarctica	-27,7	-19,4	-32,8	93	22	0	73,8	34	12	17	34	6,5	29,0	586,4	-14,6	-36,9	22,3	-32,7	-28,2	12478,92	EF Polar, frost	2,47
20	MNA-CCFEE6464	*Friedmanniomyces endolithicus*	*Dothideomycetes*	-74,178	162,514	polar desert biome	rock	Antarctica	-27,7	-19,4	-32,8	93	22	0	73,8	34	12	17	34	6,5	29,0	586,4	-14,6	-36,9	22,3	-32,7	-28,2	12478,92	EF Polar, frost	2,47
21	MNA-CCFEE6086	*Elasticomyces elasticus*	*Dothideomycetes*	-74,066	165,3	polar desert biome	rock	Antarctica	NA	NA	NA	NA	NA	NA	NA	NA	NA	NA	NA	NA	NA	NA	NA	NA	NA	NA	NA	NA	NA	NA	1,74
22	MNA-CCFEE5316	*Elasticomyces elasticus*	*Dothideomycetes*	-74,883	163,716	polar desert biome	Fungi	Antarctica	NA	NA	NA	NA	NA	NA	NA	NA	NA	NA	NA	NA	NA	NA	NA	NA	NA	NA	NA	NA	NA	NA	1,81
22	MNA-CCFEE5319	*Elasticomyces elasticus*	*Dothideomycetes*	-74,883	163,716	polar desert biome	Fungi	Antarctica	NA	NA	NA	NA	NA	NA	NA	NA	NA	NA	NA	NA	NA	NA	NA	NA	NA	NA	NA	NA	NA	NA	1,81
22	MNA-CCFEE5320	*Elasticomyces elasticus*	*Dothideomycetes*	-74,883	163,716	polar desert biome	Fungi	Antarctica	NA	NA	NA	NA	NA	NA	NA	NA	NA	NA	NA	NA	NA	NA	NA	NA	NA	NA	NA	NA	NA	NA	1,81
22	MNA-CCFEE6096	*Friedmanniomyces endolithicus*	*Dothideomycetes*	-74,883	163,733	polar desert biome	rock	Antarctica	NA	NA	NA	NA	NA	NA	NA	NA	NA	NA	NA	NA	NA	NA	NA	NA	NA	NA	NA	NA	NA	NA	1,81
22	MNA-CCFEE6097	*Oleoguttula sp*	*Dothideomycetes*	-74,883	163,733	polar desert biome	rock	Antarctica	NA	NA	NA	NA	NA	NA	NA	NA	NA	NA	NA	NA	NA	NA	NA	NA	NA	NA	NA	NA	NA	NA	1,81
23	MNA-CCFEE515	*Cryomyces antarcticus*	*Dothideomycetes*	-75,214	164,003	endolithic environment	rock	Antarctica	NA	NA	NA	NA	NA	NA	NA	NA	NA	NA	NA	NA	NA	NA	NA	NA	NA	NA	NA	NA	NA	NA	1,45
23	MNA-CCFEE524	*Friedmanniomyces endolithicus*	*Dothideomycetes*	-75,214	164,003	endolithic environment	rock	Antarctica	NA	NA	NA	NA	NA	NA	NA	NA	NA	NA	NA	NA	NA	NA	NA	NA	NA	NA	NA	NA	NA	NA	1,45
23	MNA-CCFEE534	*Cryomyces antarcticus*	*Dothideomycetes*	-75,214	164,003	endolithic environment	rock	Antarctica	NA	NA	NA	NA	NA	NA	NA	NA	NA	NA	NA	NA	NA	NA	NA	NA	NA	NA	NA	NA	NA	NA	1,45
23	MNA-CCFEE535	*Cryomyces antarcticus*	*Dothideomycetes*	-75,214	164,003	endolithic environment	rock	Antarctica	NA	NA	NA	NA	NA	NA	NA	NA	NA	NA	NA	NA	NA	NA	NA	NA	NA	NA	NA	NA	NA	NA	1,45
23	MNA-CCFEE670	*Friedmanniomyces endolithicus*	*Dothideomycetes*	-75,214	164,003	endolithic environment	rock	Antarctica	NA	NA	NA	NA	NA	NA	NA	NA	NA	NA	NA	NA	NA	NA	NA	NA	NA	NA	NA	NA	NA	NA	1,45
23	MNA-CCFEE690	*Friedmanniomyces endolithicus*	*Dothideomycetes*	-75,214	164,003	endolithic environment	rock	Antarctica	NA	NA	NA	NA	NA	NA	NA	NA	NA	NA	NA	NA	NA	NA	NA	NA	NA	NA	NA	NA	NA	NA	1,45
24	MNA-CCFEE5199	*Friedmanniomyces endolithicus*	*Dothideomycetes*	-75,482	159,591	endolithic environment	rock	Antarctica	-23,6	-13,4	-30,0	80	17	0	61,5	34	5	7	26	5,3	21,6	720,5	-9,1	-33,7	24,6	-26,9	-13,7	13035,50	EF Polar, frost	2,60
24	MNA-CCFEE5200	*Friedmanniomyces endolithicus*	*Dothideomycetes*	-75,482	159,591	endolithic environment	rock	Antarctica	-23,6	-13,4	-30,0	80	17	0	61,5	34	5	7	26	5,3	21,6	720,5	-9,1	-33,7	24,6	-26,9	-13,7	13035,50	EF Polar, frost	2,60
24	MNA-CCFEE5208	*Friedmanniomyces endolithicus*	*Dothideomycetes*	-75,482	159,591	endolithic environment	rock	Antarctica	-23,6	-13,4	-30,0	80	17	0	61,5	34	5	7	26	5,3	21,6	720,5	-9,1	-33,7	24,6	-26,9	-13,7	13035,50	EF Polar, frost	2,60
25	MNA-CCFEE6250	*Friedmanniomyces endolithicus*	*Dothideomycetes*	-75,483	159,589	polar desert biome	rock	Antarctica	-23,6	-13,4	-30,0	80	17	0	61,5	34	5	7	26	5,3	21,6	720,5	-9,1	-33,7	24,6	-26,9	-13,7	13035,50	EF Polar, frost	2,60
25	MNA-CCFEE6253	*Teratosphaeriaceae sp*	*Dothideomycetes*	-75,483	159,589	polar desert biome	rock	Antarctica	-23,6	-13,4	-30,0	80	17	0	61,5	34	5	7	26	5,3	21,6	720,5	-9,1	-33,7	24,6	-26,9	-13,7	13035,50	EF Polar, frost	2,60
25	MNA-CCFEE6256	*Teratosphaeriaceae sp*	*Dothideomycetes*	-75,483	159,589	polar desert biome	rock	Antarctica	-23,6	-13,4	-30,0	80	17	0	61,5	34	5	7	26	5,3	21,6	720,5	-9,1	-33,7	24,6	-26,9	-13,7	13035,50	EF Polar, frost	2,60
25	MNA-CCFEE6296	*Friedmanniomyces sp*	*Dothideomycetes*	-75,483	159,589	polar desert biome	rock	Antarctica	-23,6	-13,4	-30,0	80	17	0	61,5	34	5	7	26	5,3	21,6	720,5	-9,1	-33,7	24,6	-26,9	-13,7	13035,50	EF Polar, frost	2,60
26	MNA-CCFEE6590	*Recurvomyces mirabilis*	*Dothideomycetes*	-75,704	159,227	endolithic environment	rock	Antarctica	-24,2	-14,0	-30,6	85	16	1	51,5	31	13	15	24	5,2	21,2	719,9	-10,1	-34,4	24,3	-27,5	-18,0	12246,67	EF Polar, frost	2,55
27	MNA-CCFEE6082	*Friedmanniomyces endolithicus*	*Dothideomycetes*	-75,858	159,973	polar desert biome	rock	Antarctica	-25,0	-14,8	-31,3	71	16	0	62,7	30	5	7	23	5,5	22,4	719,9	-10,4	-35,1	24,7	-28,4	-15,0	13138,42	EF Polar, frost	2,44
28	MNA-CCFEE6416	*Cryomyces sp.*	*Dothideomycetes*	-75,859	159,974	polar desert biome	rock	Antarctica	-25,0	-14,9	-31,4	72	16	0	59,7	30	5	8	22	5,5	22,4	720,6	-10,5	-35,2	24,7	-28,5	-15,1	13040,75	EF Polar, frost	2,44
28	MNA-CCFEE6461	*Cryomyces antarcticus*	*Dothideomycetes*	-75,859	159,974	endolithic environment	rock	Antarctica	-25,0	-14,9	-31,4	72	16	0	59,7	30	5	8	22	5,5	22,4	720,6	-10,5	-35,2	24,7	-28,5	-15,1	13040,75	EF Polar, frost	2,44
28	MNA-CCFEE6465	*Cryomyces antarcticus*	*Dothideomycetes*	-75,859	159,974	endolithic environment	rock	Antarctica	-25,0	-14,9	-31,4	72	16	0	59,7	30	5	8	22	5,5	22,4	720,6	-10,5	-35,2	24,7	-28,5	-15,1	13040,75	EF Polar, frost	2,44
29	MNA-CCFEE6081	*Friedmanniomyces endolithicus*	*Dothideomycetes*	-75,756	161,062	polar desert biome	rock	Antarctica	-25,2	-15,2	-31,4	84	15	0	48,6	31	10	15	24	5,9	23,7	708,2	-10,5	-35,3	24,8	-24,6	-15,4	12377,67	EF Polar, frost	1,74

30	MNA-CCFEE5264	*Recurvomyces mirabilis*	*Dothideomycetes*	-76,91	160,934	endolithic environment	rock	Antarctica	-24,2	-13,8	-30,8	103	15	2	39,7	35	18	24	24	5,4	21,4	743,2	-9,6	-34,8	25,2	-23,6	-13,9	11279,50	EF Polar, frost	2,24
30	MNA-CCFEE5275	*Friedmanniomyces endolithicus*	*Dothideomycetes*	-76,91	160,934	endolithic environment	rock	Antarctica	-24,2	-13,8	-30,8	103	15	2	39,7	35	18	24	24	5,4	21,4	743,2	-9,6	-34,8	25,2	-23,6	-13,9	11279,50	EF Polar, frost	2,24
30	MNA-CCFEE5277	*Friedmanniomyces endolithicus*	*Dothideomycetes*	-76,91	160,934	endolithic environment	rock	Antarctica	-24,2	-13,8	-30,8	103	15	2	39,7	35	18	24	24	5,4	21,4	743,2	-9,6	-34,8	25,2	-23,6	-13,9	11279,50	EF Polar, frost	2,24
30	MNA-CCFEE5281	*Friedmanniomyces endolithicus*	*Dothideomycetes*	-76,91	160,934	endolithic environment	rock	Antarctica	-24,2	-13,8	-30,8	103	15	2	39,7	35	18	24	24	5,4	21,4	743,2	-9,6	-34,8	25,2	-23,6	-13,9	11279,50	EF Polar, frost	2,24
30	MNA-CCFEE5283	*Friedmanniomyces endolithicus*	*Dothideomycetes*	-76,91	160,934	endolithic environment	rock	Antarctica	-24,2	-13,8	-30,8	103	15	2	39,7	35	18	24	24	5,4	21,4	743,2	-9,6	-34,8	25,2	-23,6	-13,9	11279,50	EF Polar, frost	2,24
30	MNA-CCFEE5307	*Friedmanniomyces endolithicus*	*Dothideomycetes*	-76,91	160,934	endolithic environment	rock	Antarctica	-24,2	-13,8	-30,8	103	15	2	39,7	35	18	24	24	5,4	21,4	743,2	-9,6	-34,8	25,2	-23,6	-13,9	11279,50	EF Polar, frost	2,24
30	MNA-CCFEE5311	*Friedmanniomyces endolithicus*	*Dothideomycetes*	-76,91	160,934	endolithic environment	rock	Antarctica	-24,2	-13,8	-30,8	103	15	2	39,7	35	18	24	24	5,4	21,4	743,2	-9,6	-34,8	25,2	-23,6	-13,9	11279,50	EF Polar, frost	2,24
30	MNA-CCFEE5312	*Extremus antarcticus*	*Dothideomycetes*	-76,91	160,934	endolithic environment	rock	Antarctica	-24,2	-13,8	-30,8	103	15	2	39,7	35	18	24	24	5,4	21,4	743,2	-9,6	-34,8	25,2	-23,6	-13,9	11279,50	EF Polar, frost	2,24
30	MNA-CCFEE5313	*Elasticomyces elasticus*	*Dothideomycetes*	-76,91	160,934	polar desert biome	Fungi	Antarctica	-24,2	-13,8	-30,8	103	15	2	39,7	35	18	24	24	5,4	21,4	743,2	-9,6	-34,8	25,2	-23,6	-13,9	11279,50	EF Polar, frost	2,24
31	MNA-CCFEE5328	*Oleoguttula sp.*	*Dothideomycetes*	-76,901	160,91	endolithic environment	rock	Antarctica	-24,1	-13,6	-30,7	105	15	1	41,3	37	17	25	24	5,4	21,3	745,1	-9,4	-34,6	25,2	-23,5	-13,7	11305,17	EF Polar, frost	2,24
32	MNA-CCFEE5474	*Elasticomyces elasticus*	*Dothideomycetes*	-76,941	161,078	endolithic environment	rock	Antarctica	-25,7	-15,2	-32,2	73	14	0	54,7	26	10	13	22	6,0	23,0	744,6	-10,3	-36,2	25,9	-29,5	-25,9	12572,75	EF Polar, frost	1,93
33	MNA-CCFEE5485	*Recurvomyces mirabilis*	*Dothideomycetes*	-76,911	160,909	endolithic environment	rock	Antarctica	-24,7	-14,3	-31,2	94	14	1	41,2	32	15	20	23	5,4	21,5	741,3	-10	-35,2	25,2	-24,1	-14,4	11493,42	EF Polar, frost	2,24
33	MNA-CCFEE5486	*Friedmanniomyces endolithicus*	*Dothideomycetes*	-76,911	160,909	endolithic environment	rock	Antarctica	-24,7	-14,3	-31,2	94	14	1	41,2	32	15	20	23	5,4	21,5	741,3	-10	-35,2	25,2	-24,1	-14,4	11493,42	EF Polar, frost	2,24
34	MNA-CCFEE5184	*Friedmanniomyces simplex*	*Dothideomycetes*	-77	160,9	endolithic environment	rock	Antarctica	-25,0	-14,5	-31,6	71	14	0	60,9	27	6	9	24	5,6	21,8	748,4	-10,1	-35,6	25,5	-28,8	-14,6	12994,25	EF Polar, frost	2,47
34	MNA-CCFEE5187	*Cryomyces minteri*	*Dothideomycetes*	-77	160,9	endolithic environment	rock	Antarctica	-25,0	-14,5	-31,6	71	14	0	60,9	27	6	9	24	5,6	21,8	748,4	-10,1	-35,6	25,5	-28,8	-14,6	12994,25	EF Polar, frost	2,47
35	MNA-CCFEE6595	*Capnodiales sp*	*Dothideomycetes*	-77,75	160,745	endolithic environment	rock	Antarctica	-25,8	-14,9	-32,6	64	13	0	58,4	25	7	8	20	5,8	21,7	776,1	-10,1	-36,7	26,6	-31,3	-19,4	12771,00	EF Polar, frost	2,62
35	MNA-CCFEE451	*Extremus antarcticus*	*Dothideomycetes*	-77,6	161,083	endolithic environment	rock	Antarctica	NA	NA	NA	NA	NA	NA	NA	NA	NA	NA	NA	NA	NA	NA	NA	NA	NA	NA	NA	NA	NA	2,44
36	MNA-CCFEE6512	*Capnodiales sp*	*Dothideomycetes*	-77,75	160,745	endolithic environment	rock	Antarctica	-25,8	-14,9	-32,6	64	13	0	58,4	25	7	8	20	5,8	21,7	776,1	-10,1	-36,7	26,6	-31,3	-19,4	12771,00	EF Polar, frost	2,62

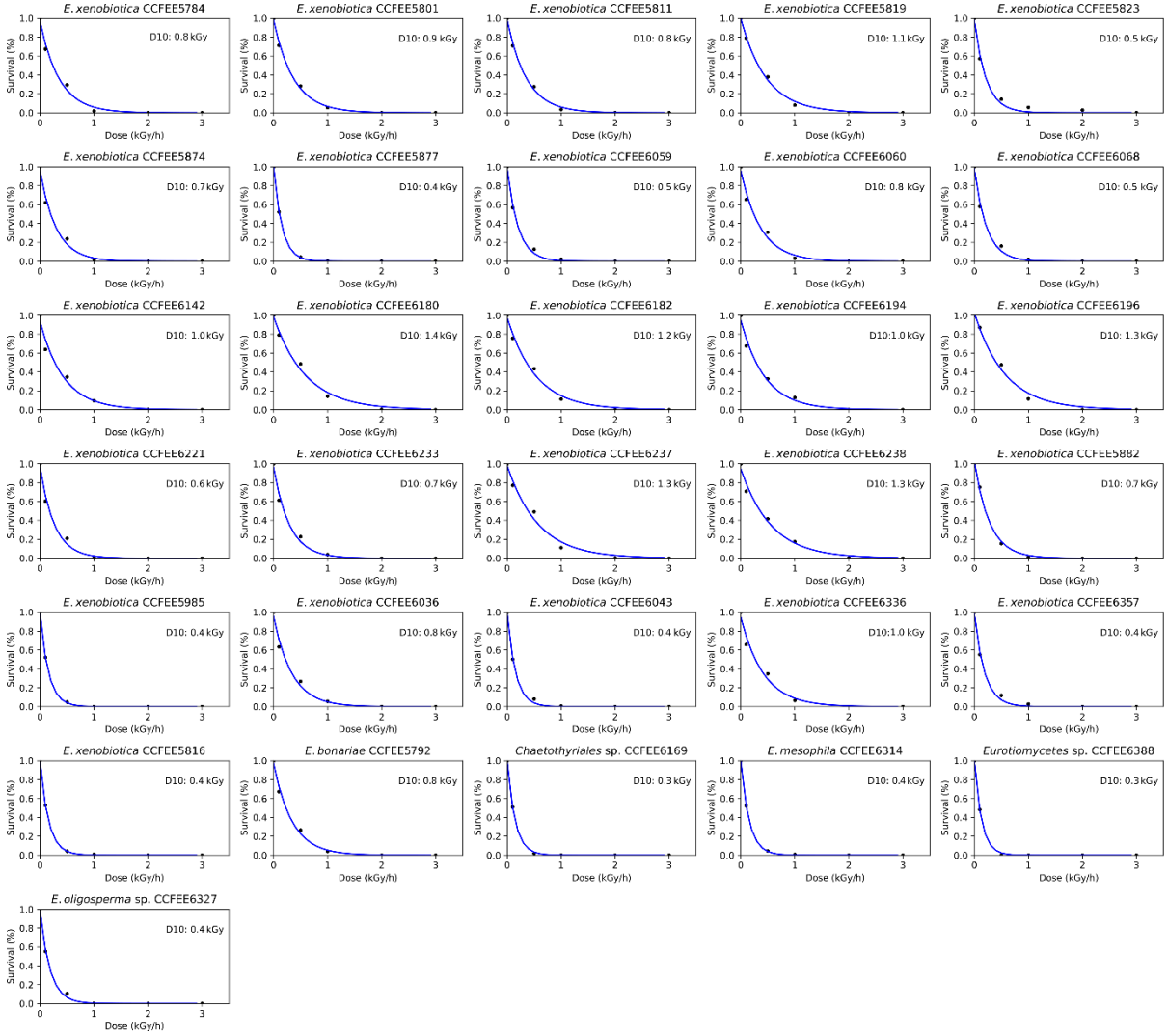

Figure S4.1. Survival curves and calculated D10 values in strains of *Eurotomycetes*.

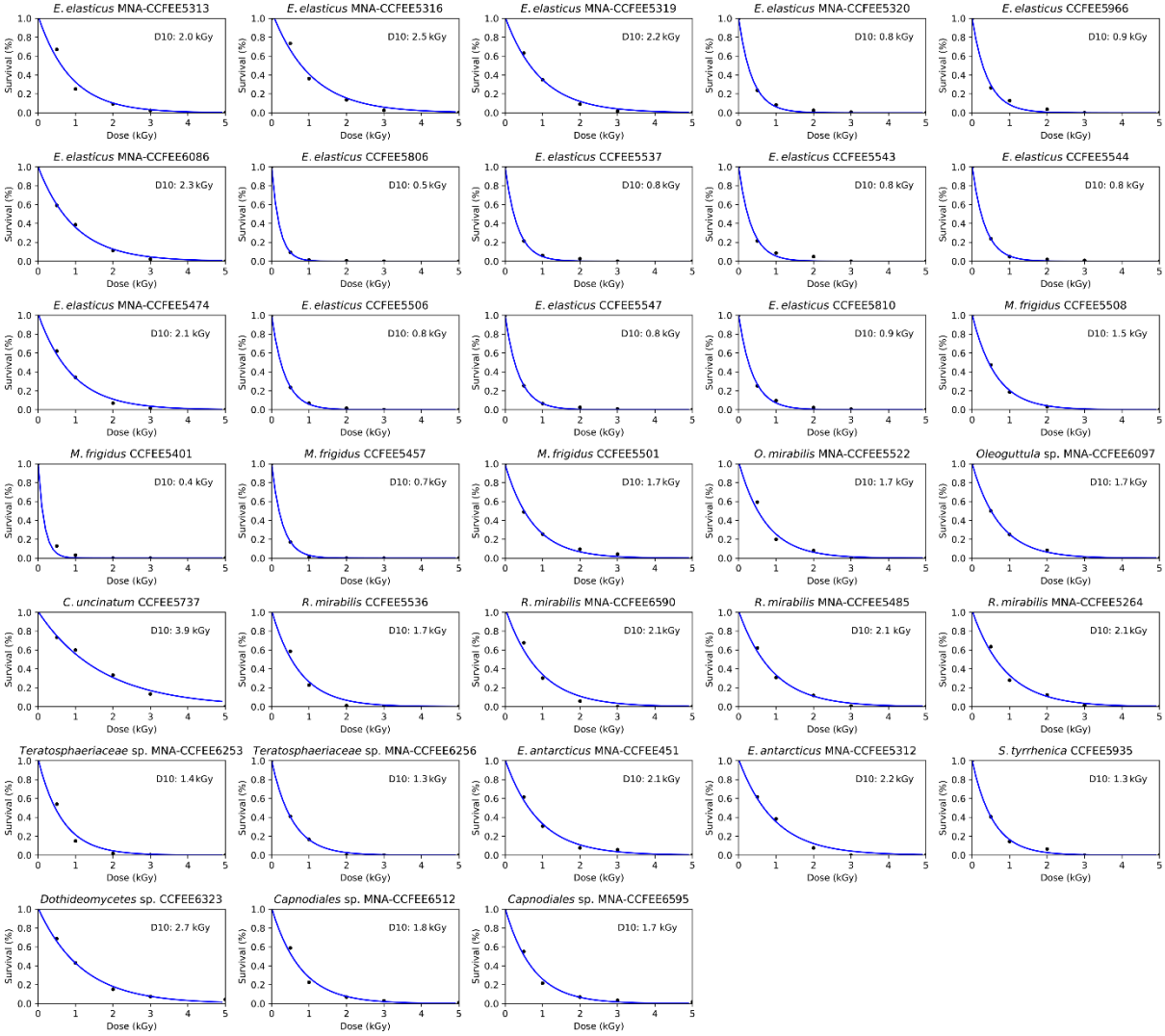

Figure S4.2. Survival curves and calculated D10 values in strains of lowly resistant *Dothideomycetes*.

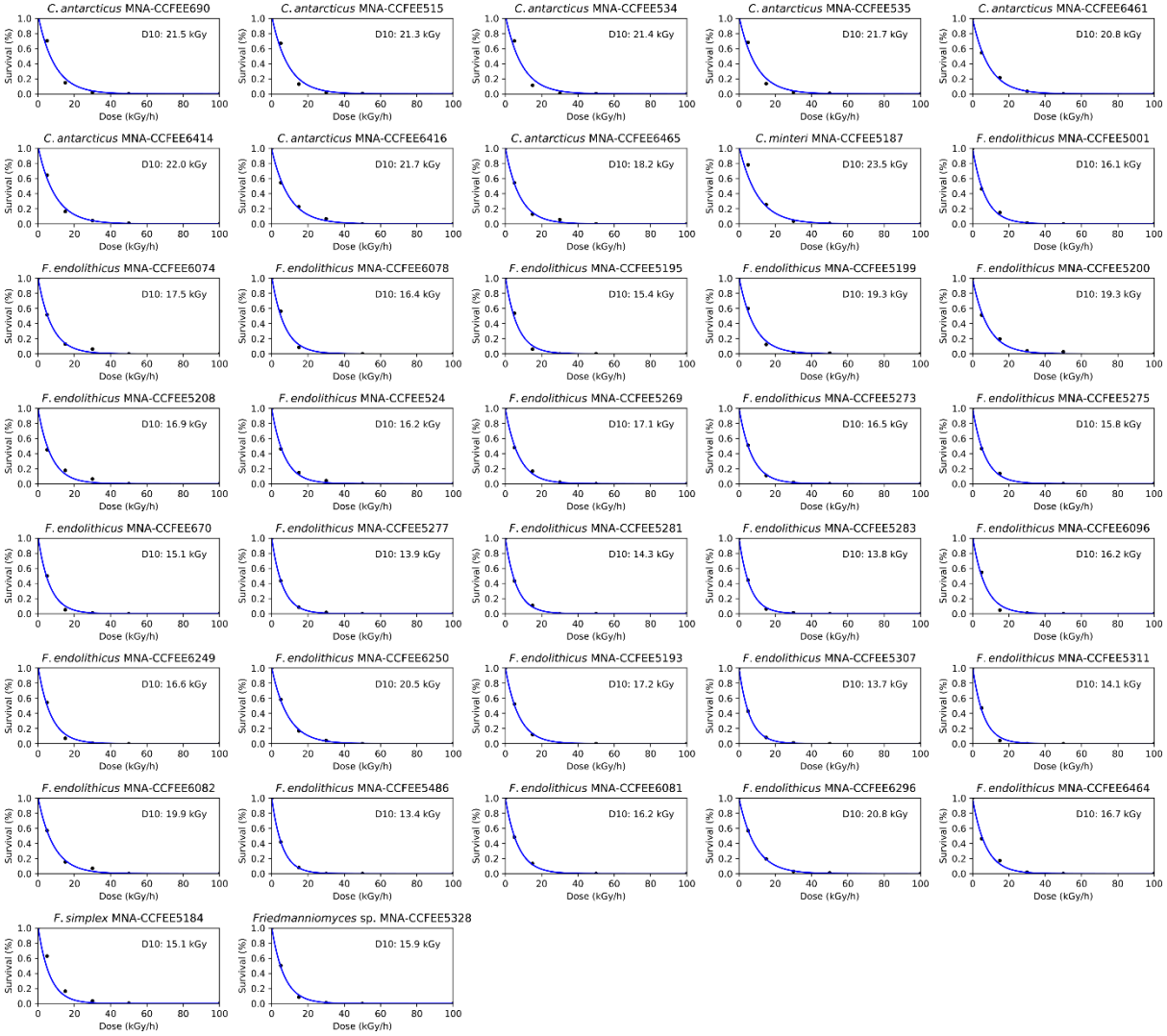

Figure S4.3. Survival curves and calculated D10 values in strains of highly resistant *Dothideomycetes*.

Chapter 5

Multiple genomic factors underlie the radioresistance of black fungi and its connection to other phenotypic traits

Lorenzo Aureli[1,2], Dag Ahren[2,3,*], Claudia Coleine[1], Silvano Onofri[1], Laura Selbmann[1,4]

[1]Department of Ecological and Biological Sciences, University of Tuscia, Viterbo, Italy

[2]Department of Biology, Lund University, Lund, Sweden

[3]National Bioinformatics Infrastructure Sweden (NBIS), Department of Biology, Lund University, Lund, Sweden

[4]Italian Antarctic National Museum (MNA), Mycological Section, Genoa, Italy.

In preparation

Abstract

The extraordinary radioresistance of black fungi makes them excellent models for the study of the genomic factors responsible for cellular defence against ionizing radiation. However, only a limited number of studies have focused on exploring the specific cellular mechanisms underlying these peculiar characteristics. Moreover, all previous research solely focused on single strains, without considering the potential taxonomic and ecological variations among the members of this diversified group, which could contribute to differences in radioresistance. In this perspective, our study represents the first comparative genomic investigation on factors that could drive the response to ionizing radiation on a vast range of different strains of black fungi, covering diverse levels of radioresistance and ecologies. Our results suggest that the radioresistance of black fungi depends on a complex network of different processes, including mechanisms involved in DNA repair and metabolic pathways linked with the defense against reactive oxygen species. Additionally, we highlighted that the genomic features responsible for the radioresistance in black fungi may be intricately associated with other factors, such as their taxonomy and their adaptation to the challenging environments in which they thrive.

Keywords: Ionizing radiation, black fungi, extremophiles, genomic traits, genomic adaptations

5.1 Introduction

The widespread presence of ionizing radiation (IR) in both space and certain areas on Earth has made the study of its consequences on organisms a critical issue in the fields of astrobiology and bioremediation (Dartnell, 2011; Shukla et al., 2017). This has prompted extensive research into the cellular mechanisms that mediate the response to radiation-induced damage (Gudkov et al., 2019; Mavragani et al., 2019). In this context, due to their simplicity and ease of handling, microorganisms represent valuable models for understanding the effects of IR on cells, as well as the genetic and molecular factors that determine the cellular ability to withstand radiation-induced damage (Confalonieri & Sommer, 2011; Moeller et al., 2017). Moreover, there are numerous eukaryotic and prokaryotic microorganisms that exhibit remarkable resistance to IR and hold the potential to provide insights into the cellular ability to cope with IR exposure (Shuryak, 2019; Lopez-Fernandez et al., 2021).

Exposure to ionizing radiation triggers the production of reactive oxygen species (ROS) in the cell, which results in oxidative damage to biomolecules such as DNA, proteins, and lipids (Reisz et al., 2014). Microorganisms exhibit various defense mechanisms to deal with the dramatic consequences of ROS on cellular functions and integrity (Jin et al., 2019). Indeed, previous studies have revealed a wide range of genes and gene sets that play a role in the microbial response to IR, indicating that radioresistance may arise from a combination of various cellular processes (Dadachova and Casadevall, 2008). Additionally, while most of these mechanisms may be ubiquitous in the majority of prokaryotic and eukaryotic cells, a few other mechanisms have been only found in a restricted number of taxa that have the propensity to tolerate IR, suggesting as they may specifically mediate the radioresistance of some microorganisms (Aridhi et al., 2016; Ryabova et al., 2020).

Among the most common mechanisms of microbial radioresistance, those involved in the repair of DNA lesions represent the most studied in the frame of the responses to IR exposure. In radioresistant prokaryotes, DNA repair mechanisms can range from the correction of mutations by excision repair to the restoration of breaks in the DNA structure by homologous recombination (HR) and non-homologous end-joining (NHEJ) in some bacteria (Cheng et al., 2020; Sharda et al., 2020; Blanchard & de Groot, 2021). Similar responses are observed in all eukaryotic microorganisms, whose response to IR exposure involves the regulation of HR and NHEJ processes and other processes of DNA repair, such as ribonucleotide excision repair (RER) (Kwang-Woo Jung et al., 2016; Romsdahl et al., 2021; Bennett et al., 2001; Servant et al., 2007; Aguileta et al., 2016; Kellner and Luke, 2020).

Similarly, prokaryotic and eukaryotic microorganisms display various systems of response to oxidative damage to proteins (Fasnacht, et al., 2021). In prokaryotic cells, the repair and degradation of misfolding and aggregation of oxidatively damaged proteins are mainly mediated by oxidoreductase activity and the activation of specific proteolytic systems, respectively (Ezraty et al., 2017). In eukaryotic microorganisms, Chaperone-mediated refolding and oxidoreductase activity is the main described mechanisms of protein refolding and repair, whereas ubiquitin-proteasome systems and chaperone-mediated autophagy

pathways are the main system for protein degradation (Chaurasia et al., 2016; Young et al., 2004; Yang et al., 2019).

In addition to these general mechanisms of response to stress, that operate in the defense against IR, previous studies have identified several compounds and complexes that play a role in mediating radioresistance in microorganisms by scavenging ROS and preventing oxidative damage. Among these, antioxidant low molecular-weight Mn^{2+} complexes, able to protect the protein damage, have been ubiquitously described both in eukaryotic and prokaryotic radioresistant microorganisms (Sharma et al., 2013; 2017). Additionally, the radioresistance observed in some microorganisms, mainly in fungi, has been demonstrated to be linked to the levels of various pigments (Avalos and Carmen Limón, 2015; Kreusch and Duarte, 2021). Among these, melanins have been supposed to provide antioxidant properties and the ability to scavenge radiation (Dadachova et al., 2008; Pacelli et al., 2017a).

Although a vast number of compounds and pathways involved in the defense against IR have been identified, several questions remain open, particularly regarding eukaryotic microorganisms such as fungi. Indeed, the complexity of eukaryotic cells and gene networks makes it difficult to unravel all the potential compounds and pathways involved in their response to IR, as well as the specific roles of genes and proteins in conferring radiation resistance. This becomes even more challenging when investigating the putative genetic factors contributing to the resistance to IR from a genomic standpoint. For instance, the adaptation of fungi to particular environmental conditions and lifestyles may depend not only on particular genes or sets of genes, but also on other genomic characteristics, such as the variation in size of the genomes, gene family contraction and expansion, and gene redundancy (Kelkar and Ochman, 2012; Naranjo-Ortiz and Gabaldón, 2020; Hage at al., 2021).

Among radioresistant microorganisms, black fungi represent a polyphyletic group of extremophilic fungi that exhibit overall radioresistance markedly higher than most of the prokaryotic and eukaryotic microorganisms (Onofri et al., 2008; Selbmann et al., 2015; Pacelli et al., 2017a; 2017b; 2018a; 2018b; 2020; 2021; Aureli et al., 2020; 2023). Interestingly, the ability of these fungi to cope with high levels of IR seems to be linked to their ability to survive and flourish in a vast range of harsh environments, spanning from polluted anthropized sites to Antarctic deserts, with differences in radioresistance dependent not only on their taxonomy but also on the adaptation to various environmental stressors (Aureli et al., 2023). Consequently, the defense against IR may depend on the same cellular mechanisms that mediate the response to other damaging factors (Shuryak et al., 2019). From a genomic perspective, these results suggest that the evolutionary pressure experienced by various fungal species may have led to the selection of specific genomic signatures that enable these microorganisms to cope with multiple damaging factors, including IR.

This possible scenario makes black fungi exciting models for investigating the genomic bases of radioresistance and its link with the extremotolerance in eukaryotic cells. However, if compared with other extremophilic microorganisms, very few studies have been conducted on their genomes aiming to untangle the drivers of their resistance to harmful environmental factors. Additionally, past research in this area has been conducted only on a limited number of strains of black fungi, also neglecting some of the most radioresistant members of the group

(Coleine et al., 2020). This paucity of studies has resulted in a limited understanding of the general and strain-specific mechanisms of radioresistance employed by these extremophilic fungi, although their knowledge has the potential to provide fundamental insights into the resistance limits of life in extreme environments.

In this optic, the aim of this study was to investigate the genomic bases of the radioresistance in black fungi and to understand if any correlation occurs with the ability of these fungi to cope with the damaging factors experienced in the habitats where they thrive. For this purpose, the gene content in the genomes of 95 strains was analyzed and compared to investigate the putative determinants of the radioresistance observed in these microorganisms. The strains were selected within different taxonomic groups (*Dothidemycetes* and *Eurotiomycetes*) to enable the most thorough comparative genomic analysis of radioresistance determinants ever performed on black fungi thus far. Indeed, this selection enabled us to investigate how the genomic drivers of radioresistance can vary among phylogenetically and ecologically distinct fungi that exhibit different levels of resistance to IR.

The results shown in this study may provide novel insights into how the selective pressure that black fungi encounter in extreme environments can shape their genomic characteristics, leading to different levels of radioresistance. Altogether, the findings we propose hold significant value not only for studying the responses and resistance of eukaryotic microorganisms to IR, but also for exploring the broader topic of life's adaptation to extreme environments.

5.2 Materials and methods

5.2.1 Strain selection and radioresistance data

For the study, 95 strains from 20 species of meristematic black fungi within the order *Capnodiales* (class *Dothideomycetes*) and the order *Chaetothyriales* (*Eurotiomycetes*) were selected. All strains belong to the Culture Collection of Fungi from Extreme Environments (CCFEE) and National Antarctic Museum Culture Collection of Fungi from Extreme Environments (MNA-CCFEE), Mycological Section of the Italian National Museum of Antarctica. The selection of strains aimed to study meristematic black fungi that were either phylogenetically related or distinct, as well as encompassing a variety of ecologies described within the group. The radioresistance data used in the analyses were from Aureli et al., 2023 (Supplementary table S5.1). The data were expressed in terms of D10 of each strain, which is defined as the dose of ionizing radiation required to inactivate 90% of a population of microorganisms. Based on D10 values, three categories of resistance to IR were established: lowly radioresistant strains (D10 < 1 kGy), moderately radioresistant strains (1 kGy < D10 < 5 kGy), and highly resistant strains (D10 > 10 kGy).

5.2.2 Genome sequencing, assembly and annotation

The dothideomycetous pure cultures, isolated mostly from cold environments, were grown on 2 % Malt Extract Agar (MEA) medium plates for 8-10 weeks at 15 °C, while

Eurotiomycetous strains, for the vast majority coming from mesophilic environments, were grown on MEA for 2-4 weeks at 20 °C. DNA was extracted from the total biomass following cetyltrimethylammonium bromide (CTAB) protocol, according to (Coleine et al. 2019b). Melanin was removed through two phenol-chloroform purification steps. Genomic DNA was sheared with Covaris S220 ultrasonic homogenizer and sequencing library constructed using the Kapa HyperPlus kit coupled with the KAPA Unique Dual Index adapters (Roche), following the instructions of the manufacturers. Sequencing libraries were prepared using the Nextera DNA Flex Library Preparation Kit (Illumina, California, USA), following the manufacturer's guidelines. Sequencing was performed on the Illumina NovaSeq 6000 platform following manufacturer's protocols.

All genomes were de novo assembled with the AAFTF pipeline (v.0.2.3)(Palmer and Stajich 2022) which performs read quality control and filtering with BBTools bbduk (v.38.86)(Bushnell 2014), followed by SPAdes (v.3.15.2)(Bankevich et al. 2012) assembly using default parameters, followed by screening to remove short contigs < 200 bp and contamination using NCBI's VecScreen. The BUSCO ascomycota_odb10 database (Manni et al. 2021) was used to determine completeness. Genes in each near-complete genome assembly with Funannotate (v1.8.1)(Palmer and Stajich 2020). A masked genome was created by generating a library of sequence repeats with the RepeatModeler pipeline(Bankevich et al. 2012). These species-specific predicted repeats were combined with fungal repeats in the RepBase (Bao, Kojima, and Kohany 2015) to identify and mask repetitive regions in the genome assembly with RepeatMasker (v.4-1-1)(SMIT A. F. A 2004). To predict genes, *ab initio* gene predictors SNAP (v.2013_11_29) (Korf 2004) and AUGUSTUS (v.3.3.3)(Stanke et al. 2006) were used along with additional gene models by GeneMark.HMM-ES (v.4.62_lic)(Brůna, Lomsadze, and Borodovsky 2020), and GlimmerHMM (v.3.0.4)(Majoros, Pertea, and Salzberg 2004) utilize a self-training procedure to optimize *ab initio* predictions. Additional exon evidence to provide hints to gene predictors was generated by DIAMOND BLASTX alignment of SwissprotDB proteins and polished by Exonerate (v.2.4.0)(Slater and Birney 2005). Finally, EvidenceModeler (v.1.1.1)(Haas et al. 2008) generated consensus gene models in Funannotate that were constructed using default evidence weights. Non-protein-coding tRNA genes were predicted by tRNAscan-SE (v.2.0.9)(Lowe and Chan 2016). Putative protein functions were assigned to genes based on sequence similarity to the Interpro database. Using InterProScan5 software(v.5.51-85.0) (Jones et al. 2014)like TIGRFAM, PANTHER, CDD, Prosite, and many others (InterProScan documentation at https://interproscan-docs.readthedocs.io/en/latest/). In this case, InterProScan was used with default parameters scanning the sequences to all databases available in November 2021. Complementary to InterProScan, EggNOG software (v.5) (Huerta-Cepas et al. 2017, 2019) was used to obtain and KEGG functional orthologs (Kanehisa et al. 2014). Both were executed as stand alone software on a High Performance Computing cluster.

5.2.3 Comparative Analysis of KEGG pathways

For functional analyses in KEGG pathways, the relative occurrences of pathways in each genome were counted and standardized. The Principal Component Analysis (PCA) was

performed considering all KEGG pathways, and those with the highest contribution to the first two PCA components were identified for further analysis. Standardization and PCA were performed through the python scikit-learn package version 1.2.0. One-sample t-test on the loadings from the two principal components of PCA was performed through the python SciPy package version 1.10.0. To identify the most critical predictors of D10 values, a Multi-Layer Perceptron (MLP) neural network classification model was implemented through the python Keras and TensorFlow packages version 2.11.0. The relative importance of KEGG pathways in the model was measured by SHapley Additive exPlanations (SHAP) through python shap package version 0.41.0. The MLP model can be found at https://github.com/lorenzoaureli?tab=repositories. The pathways that showed the higher SHAP score values were then selected for further analyses on gene ontology annotations.

5.2.4 Comparative Analysis of Gene Ontology (GO) pathways

The gene ontology (GO) analysis was performed by considering separately the Cellular Component, Biological Process and Molecular Function GO domains. The relative copy number of GO terms at each level within the three domains was counted for every genome. Counts were standardized and the PCA was carried out. The PCA was performed separately for each domain at every term level, and one-sample t-test was performed on the principal components through the python SciPy package version 1.10.0. Standardization and PCA were performed through the python scikit-learn package version 1.2.0. The GO terms with the highest contribution to the first three PCA components were identified for deeper analyses of GO hierarchy. Similarly, GO terms related to the most important KEGG pathways identified by SHAP analysis were considered in the study. For selected GO terms, all child terms were retrieved, and Spearman's correlation analysis was used to determine the correlation between the relative number of each child term in the genomes and the radioresistance categories. Bonferroni correction was performed to adjust Spearman's correlation p-value threshold. GO analysis and Spearman's correlation were performed through the python GOATOOLS package version 1.2.4 and python SciPy package version 1.10.0, respectively. GO-directed acyclic graphs (DAGs) were constructed through the python NetworkX package version 2.6.3. The script is available at https://github.com/lorenzoaureli?tab=repositories.

5.2.5 Comparison among EggNOGG Cluster of orthologous groups (COGs)

Differences in the abundances of Cluster of orthologous groups (COG) functional categories identified in the genomes were assessed to detect their possible relationships with the radioresistance of the strains. For each genome, the absolute and relative number of genes within each of the 23 COGs were calculated.

5.3 Results

5.3.1 Variance in KEGG pathways and main predictors of radioresistance

PCA analysis was carried out on KEGG pathways observed in the genomes to investigate if possible differences in pathway abundances may be related to strain radioresistance. In the obtained PCA, Principal component 1 (PC1) and Principal component 2 (PC2) explained 38.6 and 13.3% of variance, respectively (Fig. 5.1a). The variance observed in the first principal component (PC1) was primarily influenced by strong differences in KEGG

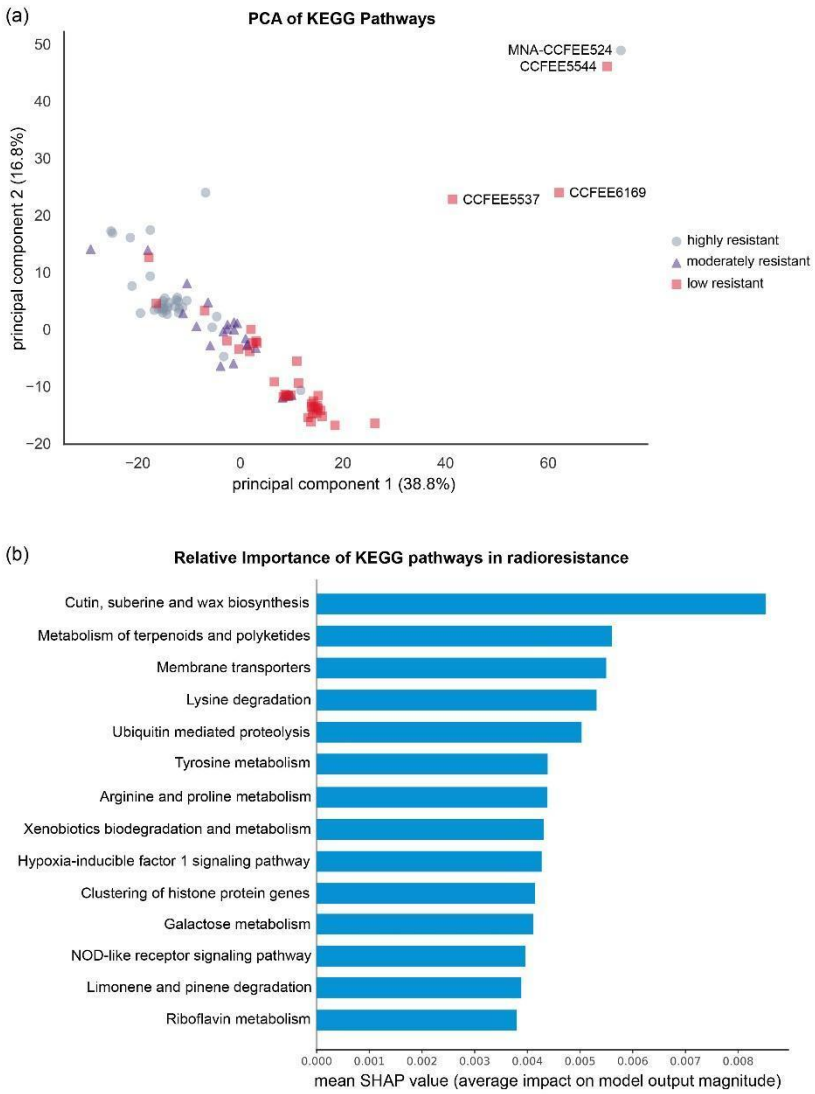

Figure 5.1. KEGG pathway variability and key radioresistance predictors. **(a)** Principal component analysis (PCA) plot visualizing principal components for KEGG pathways in studied strains. The name of the four strains that contribute the most to the two principal components is reported. **(b)** Measure of the average impact of the major KEGG pathways predictors on the model output. The pathways are ranked in descending order based on their average absolute SHAP values across all the samples.

pathways between the majority of the strains and four specific strains, namely *Elasticomyces elasticus* CCFEE5544, *Elasticomyces elasticus* CCFEE5537, *Friedmanniomyces endolithicus* MNA-CCFEE524 (*Dothideomycetes*) and *Chaetothyriales* sp. CCFEE6169 (*Eurotiomycetes*). Although they partially overlapped with moderately radioresistant strains, a separation was present between lowly and highly radioresistant categories along both PC1 and PC2 axes. However, the most significant outliers along both axes are *Friedmanniomyces endolithicus* MNA-CCFEE6078, which is classified as a highly resistant strain, and the lowly resistant strain *E. elasticus* CCFEE5547, which appear clustered with lowly and highly resistant strains, respectively. Additionally, the analysis of the variables contributing to PC1 and PC2 reveals as they depend on differences across multiple KEGG pathways instead of being driven by a few major factors (loadings below 0.1). Among these pathways, the main drivers of PC1 were identified as the spliceosome pathway (map03040; loading: 0.053), PI3K-Akt signalling pathway (map04151; loading: 0.052) and, interestingly, a few viruses related pathways (e.g. map05203, map05169, map05160; loadings: 0.052) (Supplementary Fig. S5.1). Instead, the main contributors of PC2 are pathways related to nucleobase metabolism (map00240 and map00230; loadings: 0.08), DNA repair (map03430; loading: 0.073) and protein synthesis (map00970; loading: 0.073).

To identify the KEGG pathways that are the most significant predictors of radioresistance, a SHAP analysis was conducted on an MLP classification model. The model achieved an accuracy of 98.96%. Figure 5.1b illustrates a ranking of the relative contribution of the major KEGG pathway predictors. Among these, the variable that exhibits distinctly the highest impact on the model output is represented by the cutin, suberine and wax biosynthesis pathway (normalized importance score of 0.0085). The most important variable is then followed in the ranking by a group of four major KEGG pathways, that are the metabolism of terpenoids and polyketides (0.0057), membrane transporters (0.0055), lysine degradation (0.0052), and ubiquitin-mediated proteolysis (0.0050).

5.3.2 Variance in Gene Ontology terms

PCA analyses were performed on GO terms to evaluate differences in functional traits among lowly, moderately, and highly radioresistant black fungi. The observation of a radioresistance pattern in the distribution of the strains can only be detected when examining terms within level 3 of GO. PCA plots with PC1 and PC2 for GO terms of level 3 within the Biological process (BP), Molecular function (MF) and Cellular component (CC) domains are displayed in Fig. 5.2. PC1s for terms in BP and MF, which explain 28.2 and 16.9% of the variance, appear to be mainly driven by the high diversity in GO terms exhibited by the strains *E. elasticus* CCFEE5544, *E. elasticus* CCFEE5537, *F. endolithicus* MNA-CCFEE524, *Vermiconia calcicola* CCFEE5714 (*Dothideomycetes*) and *Chaetothyriales* sp. CCFEE6169 (*Eurotiomycetes*) (Fig. 5.2a and 5.2b). However, the separation of these strains from all the others does not depend on their differences in radioresistance. Instead, a rough separation of the three radioresistance categories can be observed along the PC2 axis in MF terms (14% of variance), with the moderately radioresistant group slightly overlapping with the extremes of the other two groups. Additionally, a taxonomic-dependent overlap between moderately and

highly radioresistant fungi is displayed along PC2 in BP terms (11.1% of variance), resulting in most strains being divided into two groups, corresponding to *Dothideomycetes* and *Eurotiomycetes*.

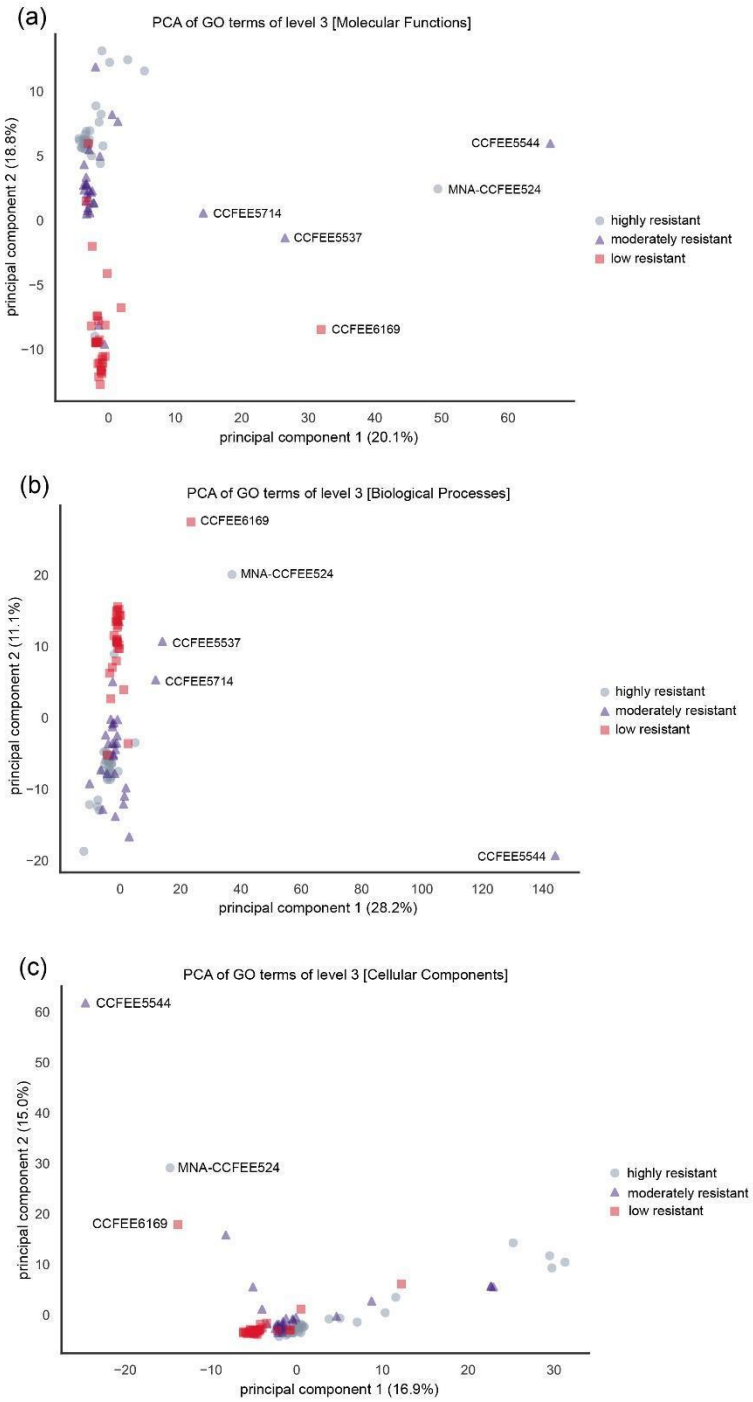

Figure 5.2. Principal component analysis (PCA) of GO terms of the level 3 within (a) molecular function domain; (b) biological process domain; (c) cellular component domain. The names of the strains representing the main outliers along the PC1 (a and b) and PC2 axes are reported.

Similarly, the distribution of strains along the PC1 axis in CC terms shows an overlap between moderately and highly radioresistant strains, whereas the PC2 primarily dependent on terms in *E.elasticus* CCFEE5544, *F. endolithicus* MNA-CCFEE524, and *Chaetothyriales* sp. CCFEE6169 strains (Fig. 5.2c). In all PCA analyses, PCs are driven by a range of GO terms showing loadings below 1%, despite being significantly different from 0 (p-value: 0.004) (Supplementary Fig. S5.2, S5.3 and S5.4). The main GO terms that contribute to PC2 of MF, which reflects a partial split among the three radioresistance categories, are linked to the oxidoreductase activity (GO:0016614 and GO:0016684), transmembrane transporter activity (GO:0015318), and DNA-binding transcription factor activity (GO:0003700).

5.3.3 Correlation of GO terms with radioresistance

A set of GO terms were selected from the previous analyses to investigate their possible relationship with radioresistance. For each term, Spearman's correlation analysis was performed to evaluate the correlation between the relative abundances of its child terms and the radioresistance of the strains. The hierarchical representations of the selected terms whose child terms exhibit the highest obtained Spearman's correlation ranks are shown in Figure 5.3.

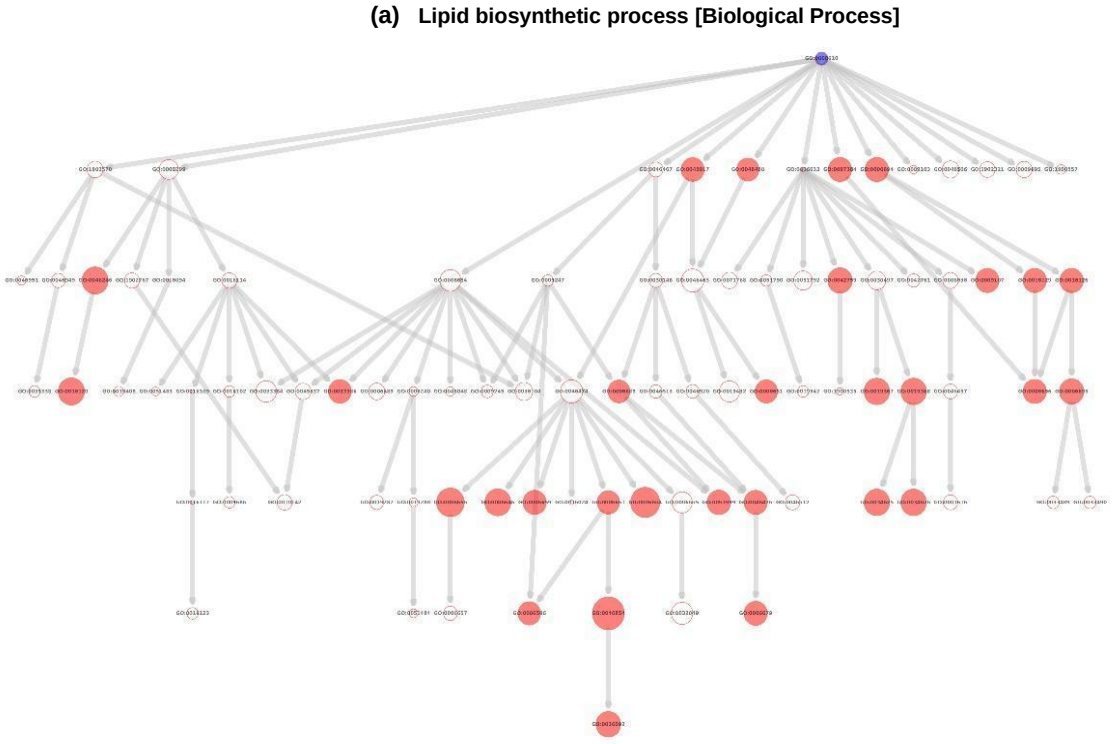

Figure 5.3. Continue in the next page.

(b) Regulation of cell cycle [Biological Process]

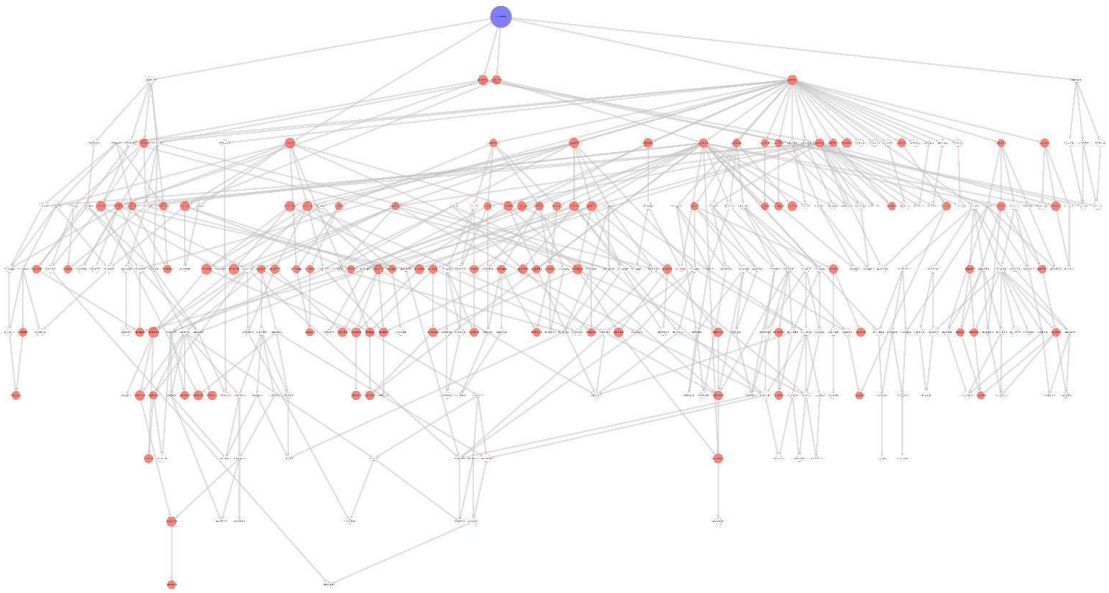

(c) DNA repair [Biological Process]

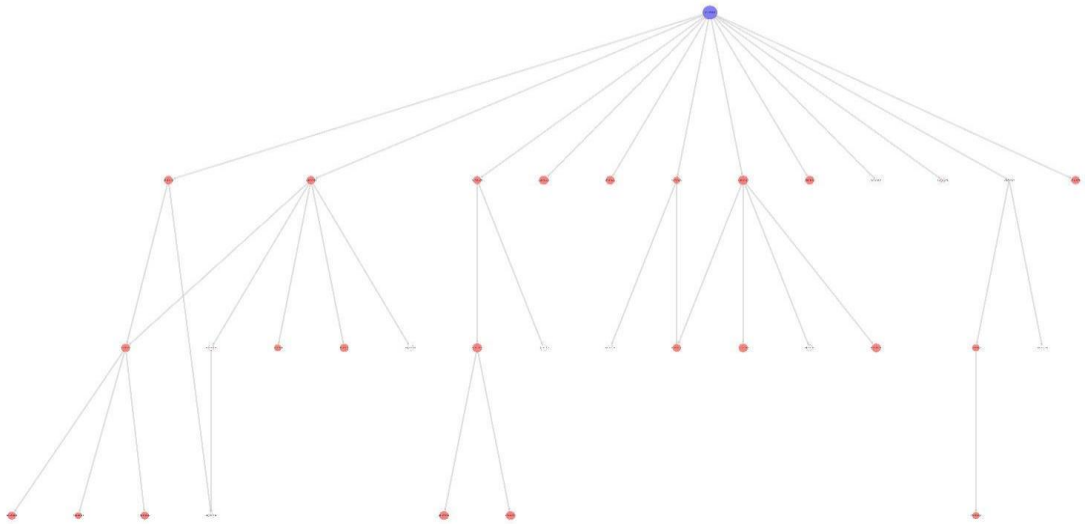

Figure 5.3. Continue in the next page.

(d) Oxidoreductase activity acting on CH-OH group of donodrs [Biological Process]

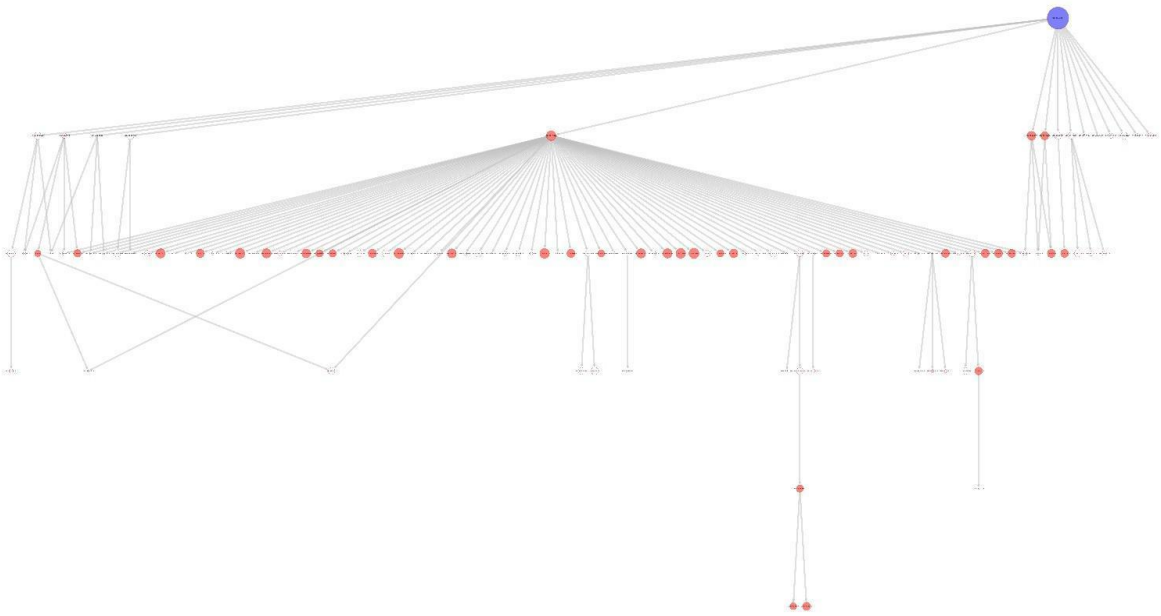

(e) Inorganic molecular entity transmembrane transporter activity [Molecular Function]

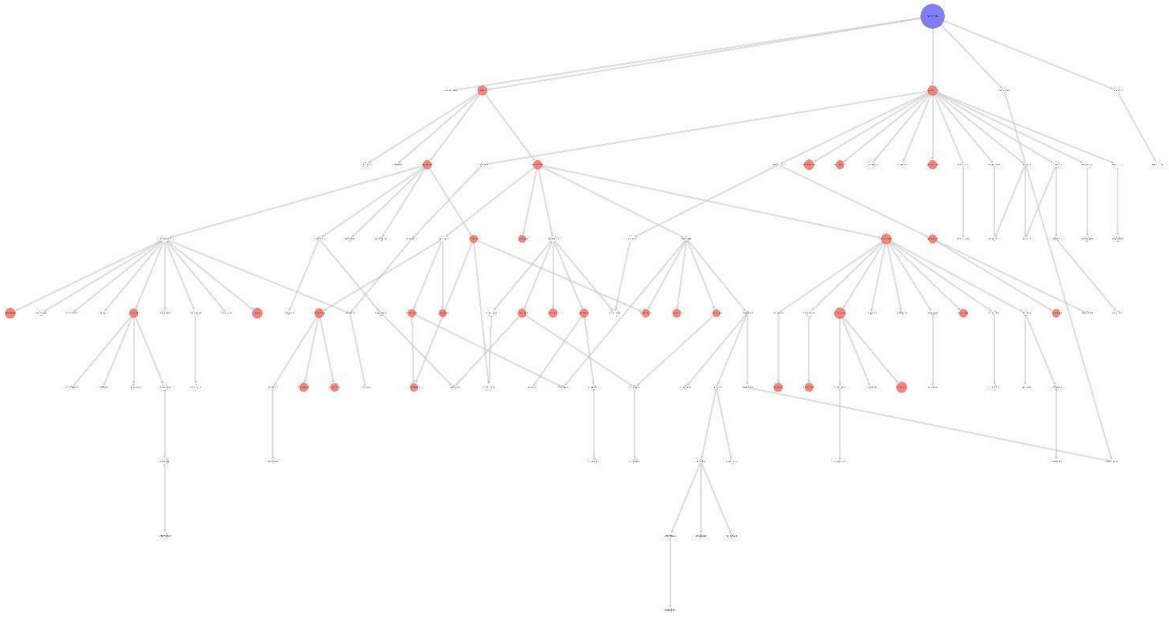

Figure 5.3. GO hierarchies of a selection of GO terms correlated with radioresistance involved in (a) lipid biosynthetic process; (b) regulation of cell cycle; (c) DNA repair; (d) oxidoreductase activity; (e) transmembrane transport activity. Red nodes indicate Spearman's correlation p-value < 0.05, whereas the size of the nodes is proportional to the absolute value of Spearman's correlation rank. Higher resolution images are available in Supplementary materials (Fig. S5.5, S5.6, S5.7, S5.8, S5.9)

The KEGG cutin, suberine and wax biosynthesis pathway, which were found to be the main predictor of the radioresistance in the studied strains, is linked to the lipid biosynthetic process GO term (GO:0008610). Among its child terms in the GO hierarchy, the term GO:0046854 (phosphatidylinositol phosphate biosynthetic process; level:7, depth:9) exhibits the highest positive correlation with radioresistance (Spearman's correlation rank: 0.71) (Fig. 5.3a). On the other hand, with a Spearman's correlation rank of -0.59, the highest negative correlation is displayed by the term GO:0006654 (phosphatidic acid biosynthetic process; level:6; depth:8).

The KEGG PI3K-Akt signaling pathway, one of the main contributors of PC1 in KEGG pathway PCA, is linked to the term GO:0051726 (regulation of cell cycle). In turn, several terms related to this term appear correlated with the fungal radioresistance with a Spearman's correlation rank higher than 0.5, suggesting as various functions underlying the regulation of the cell cycle may mediate the response to IR. Among them, the GO:2000134 term (negative regulation of G1/S transition of mitotic cell cycle; level:8, depth:9) exhibits the highest positive correlation (Spearman's correlation rank: 0.71), whereas its parent term GO:2000045 (regulation of G1/S transition of mitotic cell cycle; level:7, depth:8) shows a value of 0.69 (Fig. 5.3b). Similarly, DNA repair pathways appear among the main drivers of PC2 in KEGG pathway PCA. However, the GO terms correlated to the DNA repair function (GO:0006281) display a slight correlation with the radioresistance, with a few terms giving Spearman's correlation ranks between 0.5 and 0.6 (Fig. 5.3c).

PCA analysis on MF GO terms if level 3 shows a partial separation among the strains in the three radioresistance categories along the PC2. Among the main contributors of PC2, the GO terms associated to oxidoreductase activity (GO:0016614) show a general negative correlation with radioresistance. Among them, the terms GO: 0030266 (quinate 3-dehydrogenase (NAD+) activity) and GO:0047837 (D-xylose 1-dehydrogenase (NADP+) activity) display the highest Spearman's correlation ranks (-0.61 and -0.65, respectively) (Fig. 5.3d). Likewise, there is a general strong negative correlation between terms associated with the transmembrane transporter activity function (GO:0015318) and radioresistance, with a large number of terms exhibiting Spearman's correlation ranks higher than -0.6 (Fig. 5.3e).

5.3.4 Differences in the EggNOG Cluster of Orthologous Groups (COGs) and their relationship with radioresistance

The distribution of the genes in EggNOG COGs is reported in Fig. 5.4. This clustering is composed of a small number of highly generic classes of orthologous groups, which provide low resolution for distinguishing the various genetic functions that are present. This does not allow highlighting strong differences among the strains with different radioresistance. The most notable finding is that a significant proportion of genes are classified as belonging to the "S" class (Function Unknown). Therefore, due to the unique characteristics of these strains, this may obscure potential variations in the functions that they may express in response to environmental stressors. However, slight differences related to radioresistance are visible in the abundances of genes within the "L" class (Replication and repair) within the highly resistant strains group.

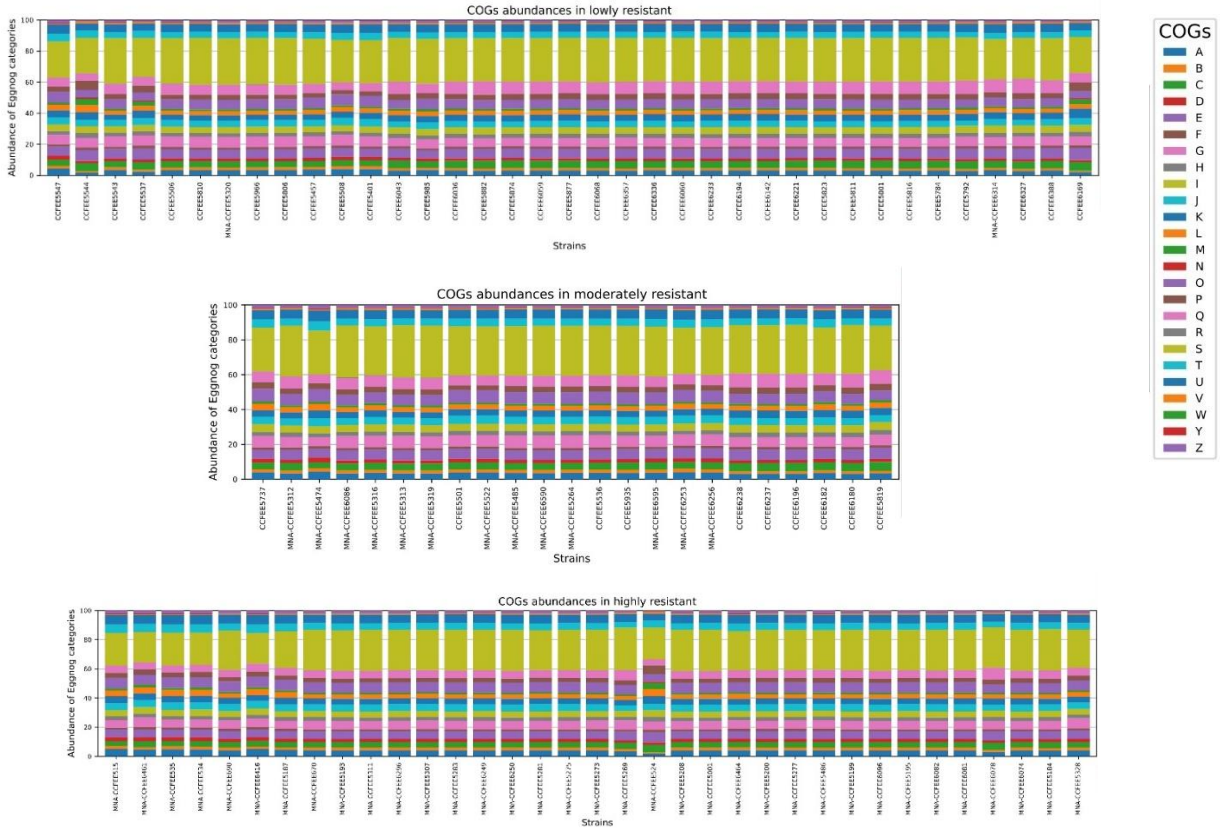

Figure 5.4. Relative abundance of genes within EggNOG Cluster of orthologous groups (COGs) in lowly (top panel), moderately (mid panel) and highly (bottom panel) radioresistant strains.

5.4 Discussion

This study identified the genomic functional traits underlying the resistance of black fungi spanning different taxonomic groups to IR. In order to achieve this objective, we evaluated the gene content of 95 strains with different levels of resistance to ionizing radiation (IR) and correlated the identified variations with their respective radioresistance levels. The functional traits of the genomes were retrieved through KEGG, EggNOG and gene ontology databases. The three types of systems offer a complementary approach to the functional annotation of genomes, providing valuable insights into the potential roles of genes and proteins in cellular physiology and helping to unravel the genetic basis of complex traits. In this context, the functional study of genome architecture can provide insights into the ability of microorganisms to respond to environmental factors through the functional diversity of genes. Indeed, previous studies indicated gene duplications, gene deletions and gene insertions as the major drivers of the changes in a metabolic capacity that enable microorganisms to adapt to different ecological niches or stressors (Fisher et al., 2018; Gorkovskiy and Verstrepen, 2021).

In our study, PCA analyses performed on the abundances of both level 3 GO terms of the three domains (MF, BP and CC) and KEGG pathways retrieved from the genomes revealed the existence of similar patterns of distribution of the strains along the principal components. In both cases, the clear separation of a few strains from the others, which does not appear to be related to taxonomical differences, reveal the extraordinary intraspecific genetic variability occurring in fungi. This variability may underlie the adaptation of the various strains to particular environmental settings that characterize the habitats where they naturally live. Additionally, the differences in genomic functional traits occurring among the strains could depend on their taxonomy, lifestyle, ecology and evolutionary history (Gueidan et al., 2011; Teixeira et al., 2017; Muggia et al., 2020). Hence, when considering the overall variance in functional traits across the genomes through PCA analyses, the distribution of the strains is expected to mirror the combination of dissimilarities occurring among the strains in these diverse parameters (Elhaik, 2022). In turn, this may mask the existence of the genomic variation in traits specific to a given phenotype, such as radioresistance. However, a distribution of the strains that reflected their differences in radioresistance was detected along PC2 axis for Molecular Function terms PCA. The variation in GO term abundances observed among the three radioresistance groups may reflect wider functional differences among the strains within these groups. Additionally, due to the absence of significant differences in IR levels among their natural environments, adaptation to IR cannot be considered a primary source of genomic variability in the selected fungi. Consequently, from an adaptive perspective, differences in radioresistance among these microorganisms may represent the consequence of differences occurring in other variables, such as their taxonomy and the environmental factors to which they are adapted (Shuryak et al., 2019; Aureli et al., 2023). From this perspective, the existence of a distribution pattern of the strains that coincides with their tolerance to IR when considering all the gene annotations linked to the cellular MF may confirm the radioresistance as a by-product of a range of other factors. Besides, the presence of a wide number of variables (KEGG pathways and GO terms) that contribute to the variation observed in all PCs is a clear confirmation of the complex nature of the taxonomic and ecological diversification of the strains. From a radioresistance perspective, this evidence supports the idea that the ability of microorganisms to withstand IR is likely mediated by a complex combination of various cellular functions rather than a restricted number of pathways and molecular factors (Jung et al., 2017; Lim et al., 2019).

Although our analysis may confirm the radioresistance as a polygenic trait, the SHAP analysis on an MLP deep learning model performed on KEGG pathways identified the pathway for cutin, suberine, and wax biosynthesis as the main predictor for the variation among the three classes of radioresistance. It is interesting to note that the synthesis of these polymers has been described in plants as a defense mechanism against different stressors including UV radiation (Nawrath, 2006; Xue et al., 2017; Lewandowska et al., 2020). Some enzymes composing this pathway, as the peroxygenase [EC:1.11.2.3] and alcohol-forming fatty acyl-CoA reductase [EC:1.2.1.84], have been identified in many *Ascomycota* species belonging to *Eurotiomycetes* (*Eurotiales*) and *Dothideomycetes* (*Pleosporales*) (Hane et al., 2007; Juhász et al., 2008; Van Den Berg et al., 2008; Ohm et al., 2012; Zeiner et al., 2016). Peroxygenase

[EC:1.11.2.3] catalyses oxidoreductase reactions of H_2O_2 with preferential substrate and co-substrate unsaturated fatty acids and fatty acid hydroperoxides, respectively (Blee et al., 1993). Instead, the alcohol-forming fatty acyl-CoA reductase is also involved in the peroxisome pathway. Given that, it is reasonable to suppose that enzymes identified in this pathway are involved in oxidoreductase activities and in the scavenging of ROS, in particular regarding lipids modifications, thus being possible strong mediators of the radioresistance on the species analysed. Moreover, within lipids metabolism, the term GO:0046854 (phosphatidylinositol phosphate biosynthetic process) exhibiting the highest positive correlation with radioresistance is of particular interest. Indeed, Phosphatidylinositol-4-phosphate is a minor constituent of both filamentous and yeast fungal cell membranes essential for polarized growth, membrane traffic, and cytoskeleton organization (Santiago-Tirado and Bretscher, 2011). Other phosphatidylinositol-phosphates have been identified in all Eukaryotes and specifically in fungi as main actors in signaling pathways activated by different environmental stressors, including oxidative stress, and can trigger different responses including DNA repair (Strahl and Thorner, 2007; Poli et al., 2019).

Another important aspect in the defense against different toxic compounds or factors that can induce DNA damage is the control of the progression of the cell cycle. Consistently, different GO terms involved in this mechanism showed strong significance when related to black fungi radioresistance (Dörter and Momany, 2016). In particular, the checkpoint for the G1/S transition is triggered by double-strand breaks (DSBs) or replication fork stalls (Frigerio et al., 2023). In *S. cerevisiae* the sensor for the presence of DSBs and replication fork stalls is the activation of the phosphatidylinositol-3-OH-like kinase, which form specific phosphatidylinositol phosphate, just described as sensors of stress (Trovesi et al., 2013). Finally, our study pointed out the correlation between fungal radioresistance and the abundance of some oxidoreductase functions. Among these, the quinate 3-dehydrogenase activity is responsible for the catabolism of quinic acid, a precursor of the shikimate pathway, in turn, involved in the biosynthesis of aromatic amino acids and other metabolites in fungi (Hawkins et al., 1982). In some fungal species, the shikimate pathway also contributes to the biosynthesis of melanin, with the activity of providing necessary aromatic amino acids for the synthesis of melanin precursors, such as L-DOPA (Gessler et al., 2014). Instead, the D-xylose 1-dehydrogenase ($NADP^+$) activity is necessary for the production of NADPH and the biosynthesis of nucleotides, amino acids, and fatty acids for cellular repair (Berghäll et al., 2007). NADPH is also important for the detoxification of ROS.

Overall, our study represents the first characterization of the genomic determinants of the radioresistance in black fungi. Our findings suggest that the radioresistance of black fungi is underpinned by a complex combination of various cellular functions, which could be related to taxonomic and ecological factors. Despite this, a few cellular processes can be observed to display a major contribution to the possible response of these microorganisms to IR. Therefore, these results may represent the first step for the further investigation of the proteomic, lipidic and metabolic factors that are expressed by black fungi as defense against the molecular and structural damage induced by IR. In turn, this research may give important insights into the understanding of the cellular mechanisms mediating the ability of eukaryotic cells to withstand

IR. Altogether, these findings provide critical clues not only to the adaptation of life to IR but also to polyextreme environments, shedding light on the potential for life to survive and evolve in hostile habitats, including some terrestrial places and other celestial bodies.

References

Aguileta, G., Badouin, H., Hood, M. E., Møller, A. P., Le Prieur, S., Snirc, A., ... & Giraud, T. (2016). Lower prevalence but similar fitness in a parasitic fungus at higher radiation levels near Chernobyl. Molecular Ecology, 25(14), 3370-3383.

Aridhi, S., Sghaier, H., Zoghlami, M., Maddouri, M., & Nguifo, E. M. (2016). Prediction of ionizing radiation resistance in bacteria using a multiple instance learning model. Journal of Computational Biology, 23(1), 10-20.

Aureli, L., Coleine, C., Delgado Baquerizo, M., Ahren, D., Cemmi, A., Di Sarcina, I., ... & Selbmann, L. (2023). Geography and environmental pressure are predictive of class-specific 1 radioresistance in black fungi. bioRxiv, 2023-02.

Aureli, L., Pacelli, C., Cassaro, A., Fujimori, A., Moeller, R., & Onofri, S. (2020). Iron ion particle radiation resistance of dried colonies of Cryomyces antarcticus embedded in Martian regolith analogues. Life, 10(12), 306.

Avalos, J., & Carmen Limón, M. (2015). Biological roles of fungal carotenoids. Current genetics, 61, 309-324.

Bennett, C. B., Lewis, L. K., Karthikeyan, G., Lobachev, K. S., Jin, Y. H., Sterling, J. F., ... & Resnick, M. A. (2001). Genes required for ionizing radiation resistance in yeast. Nature genetics, 29(4), 426-434.

Berghäll, S., Hilditch, S., Penttilä, M., & Richard, P. (2007). Identification in the mould Hypocrea jecorina of a gene encoding an NADP+: D-xylose dehydrogenase. FEMS microbiology letters, 277(2), 249-253.

Blanchard, L., & de Groot, A. (2021). Coexistence of SOS-dependent and SOS-independent regulation of DNA repair genes in radiation-resistant Deinococcus bacteria. Cells, 10(4), 924.

Chaurasia, M., Bhatt, A. N., Das, A., Dwarakanath, B. S., & Sharma, K. (2016). Radiation-induced autophagy: mechanisms and consequences. Free radical research, 50(3), 273-290.

Cheng, K., Xu, Y., Chen, X., Lu, H., He, Y., Wang, L., & Hua, Y. (2020). Participation of RecJ in the base excision repair pathway of Deinococcus radiodurans. Nucleic Acids Research, 48(17), 9859-9871.

Coleine, C., Masonjones, S., Sterflinger, K., Onofri, S., Selbmann, L., & Stajich, J. E. (2020). Peculiar genomic traits in the stress-adapted cryptoendolithic Antarctic fungus Friedmanniomyces endolithicus. Fungal biology, 124(5), 458-467.

Confalonieri, F., & Sommer, S. (2011). Bacterial and archaeal resistance to ionizing radiation. In Journal of Physics: Conference Series (Vol. 261, No. 1, p. 012005). IOP Publishing.

Dadachova, E., & Casadevall, A. (2008). Ionizing radiation: how fungi cope, adapt, and exploit with the help of melanin. Current opinion in microbiology, 11(6), 525-531.

Dadachova, E., Bryan, R. A., Howell, R. C., Schweitzer, A. D., Aisen, P., Nosanchuk, J. D., & Casadevall, A. (2008). The radioprotective properties of fungal melanin are a function of its chemical composition, stable radical presence and spatial arrangement. Pigment cell & melanoma research, 21(2), 192-199.

Dartnell, L. R. (2011). Ionizing radiation and life. Astrobiology, 11(6), 551-582.

Egas, C., Barroso, C., Froufe, H. J. C., Pacheco, J., Albuquerque, L., & da Costa, M. S. (2014). Complete genome sequence of the radiation-resistant bacterium Rubrobacter radiotolerans RSPS-4. Standards in Genomic Sciences, 9(3), 1062-1075.

Elhaik, E. (2022). Principal component analyses (PCA)-based findings in population genetic studies are highly biased and must be reevaluated. Scientific Reports, 12(1), 14683.

Ezraty, B., Gennaris, A., Barras, F., & Collet, J. F. (2017). Oxidative stress, protein damage and repair in bacteria. Nature Reviews Microbiology, 15(7), 385-396.

Fasnacht, M., & Polacek, N. (2021). Oxidative stress in bacteria and the central dogma of molecular biology. Frontiers in Molecular Biosciences, 8, 671037.

Fisher, K. J., Buskirk, S. W., Vignogna, R. C., Marad, D. A., & Lang, G. I. (2018). Adaptive genome duplication affects patterns of molecular evolution in Saccharomyces cerevisiae. PLoS genetics, 14(5), e1007396.

Gessler, N. N., Egorova, A. S., & Belozerskaya, T. A. (2014). Melanin pigments of fungi under extreme environmental conditions. Applied Biochemistry and Microbiology, 50, 105-113.

Gorkovskiy, A., & Verstrepen, K. J. (2021). The role of structural variation in adaptation and evolution of yeast and other fungi. Genes, 12(5), 699.

Gudkov, S. V., Grinberg, M. A., Sukhov, V., & Vodeneev, V. (2019). Effect of ionizing radiation on physiological and molecular processes in plants. Journal of Environmental Radioactivity, 202, 8-24.

Gueidan, C., Ruibal, C., De Hoog, G. S., & Schneider, H. (2011). Rock-inhabiting fungi originated during periods of dry climate in the late Devonian and middle Triassic. Fungal biology, 115(10), 987-996.

Hage, H., Miyauchi, S., Virágh, M., Drula, E., Min, B., Chaduli, D., ... & Rosso, M. N. (2021). Gene family expansions and transcriptome signatures uncover fungal adaptations to wood decay. Environmental microbiology, 23(10), 5716-5732.

Hawkins, A. R., Giles, N. H., & Kinghorn, J. R. (1982). Genetical and biochemical aspects of quinate breakdown in the filamentous fungus Aspergillus nidulans. Biochemical Genetics, 20, 271-286.

Jin, M., Xiao, A., Zhu, L., Zhang, Z., Huang, H., & Jiang, L. (2019). The diversity and commonalities of the radiation-resistance mechanisms of Deinococcus and its up-to-date applications. AMB Express, 9(1), 1-12.

Jung, K. W., Lim, S., & Bahn, Y. S. (2017). Microbial radiation-resistance mechanisms. Journal of Microbiology, 55, 499-507.

Jung, K. W., Yang, D. H., Kim, M. K., Seo, H. S., Lim, S., & Bahn, Y. S. (2016). Unraveling fungal radiation resistance regulatory networks through the genome-wide transcriptome and genetic analyses of Cryptococcus neoformans. MBio, 7(6), e01483-16.

Kelkar, Y. D., & Ochman, H. (2012). Causes and consequences of genome expansion in fungi. Genome Biology and Evolution, 4(1), 13-23.

Kellner, V., & Luke, B. (2020). Molecular and physiological consequences of faulty eukaryotic ribonucleotide excision repair. The EMBO journal, 39(3), e102309.

Kreusch, M. G., & Duarte, R. T. D. (2021). Photoprotective compounds and radioresistance in pigmented and non-pigmented yeasts. Applied Microbiology and Biotechnology, 105(9), 3521-3532.

Lim, S., Jung, J. H., Blanchard, L., & de Groot, A. (2019). Conservation and diversity of radiation and oxidative stress resistance mechanisms in Deinococcus species. FEMS Microbiology Reviews, 43(1), 19-52.

Liu, Y., Cui, X., Yang, R., Zhang, Y., Xu, Y., Liu, G., ... & Zhang, G. (2022). Genomic Insights into the Radiation-Resistant Capability of Sphingomonas qomolangmaensis S5-59T and Sphingomonas glaciei S8-45T, Two Novel Bacteria from the North Slope of Mount Everest. Microorganisms, 10(10), 2037.

Lopez-Fernandez, M., Jroundi, F., Ruiz-Fresneda, M. A., & Merroun, M. L. (2021). Microbial interaction with and tolerance of radionuclides: underlying mechanisms and biotechnological applications. Microbial Biotechnology, 14(3), 810-828.

Makarova, K. S., Aravind, L., Wolf, Y. I., Tatusov, R. L., Minton, K. W., Koonin, E. V., & Daly, M. J. (2001). Genome of the extremely radiation-resistant bacterium Deinococcus radiodurans viewed from the perspective of comparative genomics. Microbiology and molecular biology reviews, 65(1), 44-79.

Mavragani, I. V., Nikitaki, Z., Kalospyros, S. A., & Georgakilas, A. G. (2019). Ionizing radiation and complex DNA damage: from prediction to detection challenges and biological significance. Cancers, 11(11), 1789.

Moeller, R., Raguse, M., Leuko, S., Berger, T., Hellweg, C. E., Fujimori, A., ... & STARLIFE Research Group. (2017). STARLIFE—An international campaign to study the role of galactic cosmic radiation in astrobiological model systems. Astrobiology, 17(2), 101-109.

Muggia, L., Ametrano, C. G., Sterflinger, K., & Tesei, D. (2020). An overview of genomics, phylogenomics and proteomics approaches in Ascomycota. Life, 10(12), 356.

Naranjo-Ortiz, M. A., & Gabaldón, T. (2020). Fungal evolution: cellular, genomic and metabolic complexity. Biological Reviews, 95(5), 1198-1232.

Onofri, S., Barreca, D., Selbmann, L., Isola, D., Rabbow, E., Horneck, G., ... & Zucconi, L. (2008). Resistance of Antarctic black fungi and cryptoendolithic communities to simulated space and Martian conditions. Studies in Mycology, 61(1), 99-109.

Pacelli, C., Bryan, R. A., Onofri, S., Selbmann, L., Shuryak, I., & Dadachova, E. (2017). Melanin is effective in protecting fast and slow growing fungi from various types of ionizing radiation. Environmental microbiology, 19(4), 1612-1624.

Pacelli, C., Bryan, R. A., Onofri, S., Selbmann, L., Zucconi, L., Shuryak, I., & Dadachova, E. (2018b). Survival and redox activity of Friedmanniomyces endolithicus, an Antarctic endemic black meristematic fungus, after gamma rays exposure. Fungal biology, 122(12), 1222-1227.

Pacelli, C., Bryan, R. A., Onofri, S., Selbmann, L., Zucconi, L., Shuryak, I., & Dadachova, E. (2018a). The effect of protracted X-ray exposure on cell survival and metabolic activity of fast and slow growing fungi capable of melanogenesis. Environmental microbiology reports, 10(3), 255-263.

Pacelli, C., Cassaro, A., Aureli, L., Moeller, R., Fujimori, A., & Onofri, S. (2020). The responses of the black fungus Cryomyces antarcticus to high doses of accelerated helium ions radiation within martian regolith simulants and their relevance for Mars. Life, 10(8), 130.

Pacelli, C., Cassaro, A., Siong, L. M., Aureli, L., Moeller, R., Fujimori, A., ... & Onofri, S. (2021). Insights into the survival capabilities of Cryomyces antarcticus hydrated colonies after exposure to Fe particle radiation. Journal of Fungi, 7(7), 495.

Pacelli, C., Selbmann, L., Moeller, R., Zucconi, L., Fujimori, A., & Onofri, S. (2017b). Cryptoendolithic Antarctic black fungus Cryomyces antarcticus irradiated with accelerated helium ions: survival and metabolic activity, DNA and ultrastructural damage. Frontiers in Microbiology, 8, 2002.

Pacelli, C., Selbmann, L., Zucconi, L., Raguse, M., Moeller, R., Shuryak, I., & Onofri, S. (2017a). Survival, DNA integrity, and ultrastructural damage in Antarctic cryptoendolithic eukaryotic microorganisms exposed to ionizing radiation. Astrobiology, 17(2), 126-135.

Reisz, J. A., Bansal, N., Qian, J., Zhao, W., & Furdui, C. M. (2014). Effects of ionizing radiation on biological molecules—mechanisms of damage and emerging methods of detection. Antioxidants & redox signaling, 21(2), 260-292.

Romsdahl, J., Schultzhaus, Z., Chen, A., Liu, J., Ewing, A., Hervey, J., & Wang, Z. (2021). Adaptive evolution of a melanized fungus reveals robust augmentation of radiation resistance by abrogating non-homologous end-joining. Environmental Microbiology, 23(7), 3627-3645.

Ryabova, A., Kozlova, O., Kadirov, A., Ananeva, A., Gusev, O., & Shagimardanova, E. (2020). DetR DB: A database of ionizing radiation resistance determinants. Genes, 11(12), 1477.

Selbmann, L., Zucconi, L., Isola, D., & Onofri, S. (2015). Rock black fungi: excellence in the extremes, from the Antarctic to space. Current Genetics, 61, 335-345.

Servant, P., Jolivet, E., Bentchikou, E., Mennecier, S., Bailone, A., & Sommer, S. (2007). The ClpPX protease is required for radioresistance and regulates cell division after γ-irradiation in Deinococcus radiodurans. Molecular microbiology, 66(5), 1231-1239.

Sharda, M., Badrinarayanan, A., & Seshasayee, A. S. N. (2020). Evolutionary and comparative analysis of bacterial nonhomologous end joining repair. Genome Biology and Evolution, 12(12), 2450-2466.

Sharma, A., Gaidamakova, E. K., Grichenko, O., Matrosova, V. Y., Hoeke, V., Klimenkova, P., ... & Daly, M. J. (2017). Across the tree of life, radiation resistance is governed by antioxidant Mn2+, gauged by paramagnetic resonance. Proceedings of the National Academy of Sciences, 114(44), E9253-E9260.

Sharma, A., Gaidamakova, E. K., Matrosova, V. Y., Bennett, B., Daly, M. J., & Hoffman, B. M. (2013). Responses of Mn2+ speciation in Deinococcus radiodurans and Escherichia coli to γ-radiation by advanced paramagnetic resonance methods. Proceedings of the National Academy of Sciences, 110(15), 5945-5950.

Shukla, A., Parmar, P., & Saraf, M. (2017). Radiation, radionuclides and bacteria: An in-perspective review. Journal of environmental radioactivity, 180, 27-35.

Shuryak, I. (2019). Review of microbial resistance to chronic ionizing radiation exposure under environmental conditions. Journal of environmental radioactivity, 196, 50-63.

Shuryak, I., Tkavc, R., Matrosova, V. Y., Volpe, R. P., Grichenko, O., Klimenkova, P., ... & Daly, M. J. (2019). Chronic gamma radiation resistance in fungi correlates with resistance to chromium and elevated temperatures, but not with resistance to acute irradiation. Scientific reports, 9(1), 11361.

Shuryak, I., Tkavc, R., Matrosova, V. Y., Volpe, R. P., Grichenko, O., Klimenkova, P., ... & Daly, M. J. (2019). Chronic gamma radiation resistance in fungi correlates with resistance to

chromium and elevated temperatures, but not with resistance to acute irradiation. Scientific reports, 9(1), 11361.

Teixeira, M. D. M., Moreno, L. F., Stielow, B. J., Muszewska, A., Hainaut, M., Gonzaga, L., ... & de Hoog, G. S. (2017). Exploring the genomic diversity of black yeasts and relatives (Chaetothyriales, Ascomycota). Studies in mycology, 86(1), 1-28.

Yang, Q., Wang, R., & Zhu, L. (2019). Chaperone-mediated autophagy. Autophagy: Biology and Diseases: Basic Science, 435-452.

Young, J. C., Agashe, V. R., Siegers, K., & Hartl, F. U. (2004). Pathways of chaperone-mediated protein folding in the cytosol. Nature reviews Molecular cell biology, 5(10), 781-791.

Supplementary material

Table S5.1. List of the strains assessed in the study. The geographical coordinates (Latitude and Longitude) and the country where the strains were collected are reported. The D10 values are from Aureli et al., 2023.

Strain number	Species	Class	Latitude	Longitude	Country	D10 (kGy)	Radioresistance category
CCFEE6388	*Eurotiomycetes sp*	*Eurotiomycetes*	42,383	12,264	Italy	0,3	lowly radioresistant
CCFEE5792	*Exophiala bonariae*	*Eurotiomycetes*	39,211	9,123	Italy	0,3	lowly radioresistant
CCFEE6169	*Chaetothyriales sp*	*Eurotiomycetes*	36,865	-111,588	USA	0,3	lowly radioresistant
CCFEE6327	*Exophiala oligosperma*	*Eurotiomycetes*	39,225	9,122	Italy	0,4	lowly radioresistant
CCFEE5401	*Meristemomyces frigidus*	*Dothideomycetes*	46	7,866	Italy	0,4	lowly radioresistant
CCFEE5816	*Exophiala xenobiotica*	*Eurotiomycetes*	42,383	12,264	Italy	0,4	lowly radioresistant
CCFEE5877	*Exophiala xenobiotica*	*Eurotiomycetes*	42,383	12,264	Italy	0,4	lowly radioresistant
CCFEE5985	*Exophiala xenobiotica*	*Eurotiomycetes*	42,383	12,264	Italy	0,4	lowly radioresistant
CCFEE6043	*Exophiala xenobiotica*	*Eurotiomycetes*	42,383	12,264	Italy	0,4	lowly radioresistant
CCFEE6357	*Exophiala xenobiotica*	*Eurotiomycetes*	42,383	12,264	Italy	0,4	lowly radioresistant
MNA-CCFEE6314	*Exophiala mesophila*	*Eurotiomycetes*	-71,25	163	Antarctica	0,4	lowly radioresistant
CCFEE5823	*Exophiala xenobiotica*	*Eurotiomycetes*	42,383	12,264	Italy	0,5	lowly radioresistant
CCFEE6059	*Exophiala xenobiotica*	*Eurotiomycetes*	42,383	12,264	Italy	0,5	lowly radioresistant
CCFEE6068	*Exophiala xenobiotica*	*Eurotiomycetes*	42,383	12,264	Italy	0,5	lowly radioresistant
CCFEE5806	*Elasticomyces elasticus*	*Dothideomycetes*	42,471	13,563	Italy	0,5	lowly radioresistant
CCFEE6221	*Exophiala xenobiotica*	*Eurotiomycetes*	42,383	12,264	Italy	0,6	lowly radioresistant
CCFEE5457	*Meristemomyces frigidus*	*Dothideomycetes*	46	7,866	Italy	0,7	lowly radioresistant
CCFEE5874	*Exophiala xenobiotica*	*Eurotiomycetes*	42,383	12,264	Italy	0,7	lowly radioresistant
CCFEE5882	*Exophiala xenobiotica*	*Eurotiomycetes*	42,383	12,264	Italy	0,7	lowly radioresistant
CCFEE6233	*Exophiala xenobiotica*	*Eurotiomycetes*	42,383	12,264	Italy	0,7	lowly radioresistant
CCFEE5508	*Meristemomyces frigidus*	*Dothideomycetes*	-32,669	-69,955	Argentina	0,7	lowly radioresistant
CCFEE5547	*Elasticomyces elasticus*	*Dothideomycetes*	44,713	6,18	Italy	0,8	lowly radioresistant
CCFEE5784	*Exophiala xenobiotica*	*Eurotiomycetes*	42,383	12,264	Italy	0,8	lowly radioresistant
CCFEE5811	*Exophiala xenobiotica*	*Eurotiomycetes*	42,383	12,264	Italy	0,8	lowly radioresistant
CCFEE6036	*Exophiala xenobiotica*	*Eurotiomycetes*	42,383	12,264	Italy	0,8	lowly radioresistant
CCFEE6060	*Exophiala xenobiotica*	*Eurotiomycetes*	42,383	12,264	Italy	0,8	lowly radioresistant
CCFEE5537	*Elasticomyces elasticus*	*Dothideomycetes*	32,893	77,194	India	0,8	lowly radioresistant
CCFEE5543	*Elasticomyces elasticus*	*Dothideomycetes*	32,893	77,194	India	0,8	lowly radioresistant
CCFEE5544	*Elasticomyces elasticus*	*Dothideomycetes*	32,893	77,194	India	0,8	lowly radioresistant
CCFEE5506	*Elasticomyces elasticus*	*Dothideomycetes*	-32,607	-69,957	Argentina	0,8	lowly radioresistant
MNA-CCFEE5320	*Elasticomyces elasticus*	*Dothideomycetes*	-74,883	163,716	Antarctica	0,8	lowly radioresistant
CCFEE5966	*Elasticomyces elasticus*	*Dothideomycetes*	46,417	10,183	Italy	0,9	lowly radioresistant
CCFEE5801	*Exophiala xenobiotica*	*Eurotiomycetes*	42,383	12,264	Italy	0,9	lowly radioresistant
CCFEE5810	*Elasticomyces elasticus*	*Dothideomycetes*	42,471	13,563	Italy	0,9	lowly radioresistant
CCFEE6142	*Exophiala xenobiotica*	*Eurotiomycetes*	42,383	12,264	Italy	1	moderately radioresistant
CCFEE6194	*Exophiala xenobiotica*	*Eurotiomycetes*	42,383	12,264	Italy	1	moderately radioresistant
CCFEE6336	*Exophiala xenobiotica*	*Eurotiomycetes*	42,383	12,264	Italy	1	moderately radioresistant
CCFEE5819	*Exophiala xenobiotica*	*Eurotiomycetes*	42,383	12,264	Italy	1,1	moderately radioresistant
CCFEE6182	*Exophiala xenobiotica*	*Eurotiomycetes*	42,383	12,264	Italy	1,2	moderately radioresistant
CCFEE6196	*Exophiala xenobiotica*	*Eurotiomycetes*	42,383	12,264	Italy	1,3	moderately radioresistant
CCFEE6237	*Exophiala xenobiotica*	*Eurotiomycetes*	42,383	12,264	Italy	1,3	moderately radioresistant
CCFEE5935	*Saxophila tyrrhenica*	*Dothideomycetes*	39,223	9,121	Italy	1,3	moderately radioresistant
CCFEE6238	*Exophiala xenobiotica*	*Eurotiomycetes*	40,625	14,38	Italy	1,3	moderately radioresistant
MNA-CCFEE5522	*Oleoguttula mirabilis*	*Dothideomycetes*	-69,5	65	Antarctica	1,3	moderately radioresistant

MNA-CCFEE6256	*Teratosphaeriaceae sp*	*Dothideomycetes*	-75,483	159,589	Antarctica	1,3	moderately radioresistant
MNA-CCFEE6590	*Recurvomyces mirabilis*	*Dothideomycetes*	-75,704	159,227	Antarctica	1,3	moderately radioresistant
CCFEE6180	*Exophiala xenobiotica*	*Eurotiomycetes*	42,383	12,264	Italy	1,4	moderately radioresistant
MNA-CCFEE6253	*Teratosphaeriaceae sp*	*Dothideomycetes*	-75,483	159,589	Antarctica	1,5	moderately radioresistant
CCFEE5536	*Recurvomyces mirabilis*	*Dothideomycetes*	62,777	11,121	Norway	1,7	moderately radioresistant
CCFEE5501	*Meristemomyces frigidus*	*Dothideomycetes*	-32,669	-69,955	Argentina	1,7	moderately radioresistant
MNA-CCFEE6595	*Capnodiales sp*	*Dothideomycetes*	-77,75	160,745	Antarctica	1,7	moderately radioresistant
MNA-CCFEE5313	*Elasticomyces elasticus*	*Dothideomycetes*	-76,91	160,934	Antarctica	2	moderately radioresistant
MNA-CCFEE5474	*Elasticomyces elasticus*	*Dothideomycetes*	-76,941	161,078	Antarctica	2,1	moderately radioresistant
MNA-CCFEE5485	*Recurvomyces mirabilis*	*Dothideomycetes*	-76,911	160,909	Antarctica	2,1	moderately radioresistant
MNA-CCFEE5319	*Elasticomyces elasticus*	*Dothideomycetes*	-74,883	163,716	Antarctica	2,2	moderately radioresistant
MNA-CCFEE5312	*Extremus antarcticus*	*Dothideomycetes*	-76,91	160,934	Antarctica	2,2	moderately radioresistant
MNA-CCFEE6086	*Elasticomyces elasticus*	*Dothideomycetes*	-74,066	165,3	Antarctica	2,3	moderately radioresistant
MNA-CCFEE5316	*Elasticomyces elasticus*	*Dothideomycetes*	-74,883	163,716	Antarctica	2,5	moderately radioresistant
MNA-CCFEE5264	*Recurvomyces mirabilis*	*Dothideomycetes*	-76,91	160,934	Antarctica	2,7	moderately radioresistant
CCFEE5737	*Coniosporium uncinatum*	*Dothideomycetes*	39,211	9,124	Italy	3,9	moderately radioresistant
MNA-CCFEE5486	*Friedmanniomyces endolithicus*	*Dothideomycetes*	-76,911	160,909	Antarctica	13,4	highly radioresistant
MNA-CCFEE5307	*Friedmanniomyces endolithicus*	*Dothideomycetes*	-76,91	160,934	Antarctica	13,7	highly radioresistant
MNA-CCFEE5283	*Friedmanniomyces endolithicus*	*Dothideomycetes*	-76,91	160,934	Antarctica	13,8	highly radioresistant
MNA-CCFEE5277	*Friedmanniomyces endolithicus*	*Dothideomycetes*	-76,91	160,934	Antarctica	13,9	highly radioresistant
MNA-CCFEE5311	*Friedmanniomyces endolithicus*	*Dothideomycetes*	-76,91	160,934	Antarctica	14,1	highly radioresistant
MNA-CCFEE5281	*Friedmanniomyces endolithicus*	*Dothideomycetes*	-76,91	160,934	Antarctica	14,3	highly radioresistant
MNA-CCFEE670	*Friedmanniomyces endolithicus*	*Dothideomycetes*	-75,214	164,003	Antarctica	15,1	highly radioresistant
MNA-CCFEE5184	*Friedmanniomyces simplex*	*Dothideomycetes*	-77	160,9	Antarctica	15,1	highly radioresistant
MNA-CCFEE5195	*Friedmanniomyces endolithicus*	*Dothideomycetes*	-74,169	162,427	Antarctica	15,4	highly radioresistant
MNA-CCFEE5275	*Friedmanniomyces endolithicus*	*Dothideomycetes*	-76,91	160,934	Antarctica	15,8	highly radioresistant
MNA-CCFEE5328	*Oleoguttula sp.*	*Dothideomycetes*	-76,901	160,91	Antarctica	15,9	highly radioresistant
MNA-CCFEE5001	*Friedmanniomyces endolithicus*	*Dothideomycetes*	-74,169	162,427	Antarctica	16,1	highly radioresistant
MNA-CCFEE6096	*Friedmanniomyces endolithicus*	*Dothideomycetes*	-74,883	163,733	Antarctica	16,2	highly radioresistant
MNA-CCFEE524	*Friedmanniomyces endolithicus*	*Dothideomycetes*	-75,214	164,003	Antarctica	16,2	highly radioresistant
MNA-CCFEE6081	*Friedmanniomyces endolithicus*	*Dothideomycetes*	-75,756	161,062	Antarctica	16,2	highly radioresistant
MNA-CCFEE6078	*Friedmanniomyces endolithicus*	*Dothideomycetes*	-74,178	162,514	Antarctica	16,4	highly radioresistant
MNA-CCFEE5273	*Friedmanniomyces endolithicus*	*Dothideomycetes*	-74,169	162,427	Antarctica	16,5	highly radioresistant
MNA-CCFEE6249	*Friedmanniomyces endolithicus*	*Dothideomycetes*	-74,17	162,425	Antarctica	16,6	highly radioresistant
MNA-CCFEE6464	*Friedmanniomyces endolithicus*	*Dothideomycetes*	-74,178	162,514	Antarctica	16,7	highly radioresistant
MNA-CCFEE5208	*Friedmanniomyces endolithicus*	*Dothideomycetes*	-75,482	159,591	Antarctica	16,9	highly radioresistant
MNA-CCFEE5269	*Friedmanniomyces endolithicus*	*Dothideomycetes*	-74,169	162,427	Antarctica	17,1	highly radioresistant
MNA-CCFEE5193	*Friedmanniomyces endolithicus*	*Dothideomycetes*	-74,169	162,427	Antarctica	17,2	highly radioresistant
MNA-CCFEE6074	*Friedmanniomyces endolithicus*	*Dothideomycetes*	-73,49	163,912	Antarctica	17,5	highly radioresistant
MNA-CCFEE5199	*Friedmanniomyces endolithicus*	*Dothideomycetes*	-75,482	159,591	Antarctica	19,3	highly radioresistant
MNA-CCFEE5200	*Friedmanniomyces endolithicus*	*Dothideomycetes*	-75,482	159,591	Antarctica	19,3	highly radioresistant
MNA-CCFEE6082	*Friedmanniomyces endolithicus*	*Dothideomycetes*	-75,858	159,973	Antarctica	19,9	highly radioresistant
MNA-CCFEE6250	*Friedmanniomyces endolithicus*	*Dothideomycetes*	-75,483	159,589	Antarctica	20,5	highly radioresistant
MNA-CCFEE6296	*Friedmanniomyces sp*	*Dothideomycetes*	-75,483	159,589	Antarctica	20,8	highly radioresistant
MNA-CCFEE6461	*Cryomyces antarcticus*	*Dothideomycetes*	-75,859	159,974	Antarctica	20,8	highly radioresistant
MNA-CCFEE515	*Cryomyces antarcticus*	*Dothideomycetes*	-75,214	164,003	Antarctica	21,3	highly radioresistant
MNA-CCFEE534	*Cryomyces antarcticus*	*Dothideomycetes*	-75,214	164,003	Antarctica	21,4	highly radioresistant
MNA-CCFEE690	*Friedmanniomyces endolithicus*	*Dothideomycetes*	-75,214	164,003	Antarctica	21,5	highly radioresistant
MNA-CCFEE535	*Cryomyces antarcticus*	*Dothideomycetes*	-75,214	164,003	Antarctica	21,7	highly radioresistant
MNA-CCFEE6416	*Cryomyces sp.*	*Dothideomycetes*	-75,859	159,974	Antarctica	21,7	highly radioresistant
MNA-CCFEE5187	*Cryomyces minteri*	*Dothideomycetes*	-77	160,9	Antarctica	23,5	highly radioresistant

Chapter 6

Conclusions

Although meristematic black fungi have been found to be interesting potential models for studying the limits of life's resistance in extreme conditions, there is still a significant gap in our understanding of their responses to various harmful factors (Selbmann et al., 2015; Coleine et al., 2022). Among these, Ionizing Radiation (IR) is one of the primary limiting environmental stressors for the survival and persistence of life in both extraterrestrial and some terrestrial environments. Previous research showed how a few members of black fungi have the capacity to cope with high levels of a limited part of the IR spectrum experienced on Earth and beyond the terrestrial atmosphere and magnetic field (Pacelli et al., 2017a; 2017b; 2018a;2018b; Selbmann et al., 2018). However, the ability of black fungi to tolerate a broader spectrum of IR is still unknown. Similarly, the general radioresistance limits of the group have not been defined yet, as well as the ecological and genetic bases of the various possible levels of radioresistance characterizing different strains and species of black fungi.

In this optic, the first part of this research aimed to test the responses of the black fungus *C. antarcticus* MNA-CCFEE515 to two of the most damaging components of the cosmic rays spectrum making the space and Martian radiation environments, i.e. accelerated iron ions and accelerated helium ions (Chapters 2 and 3). Our research showed how this fungus is able to survive exposure to accelerated iron and helium ions until a dose of 1 kGy, also maintaining the integrity of DNA and metabolic activity. These findings, in addition to confirming *C. antarcticus* MNA-CCFEE515 as one of the most known radioresistant microorganisms, have several important implications from an astrobiological standpoint. Indeed, our results show how putative extraterrestrial microorganisms may survive in the Martian radiation environment even thousands of years, changing the idea of IR as a critical limiting factor for the persistence of life beyond Earth. Additionally, these findings can have significant implications for the advancement of research in radioprotection, especially in the context of prolonged manned missions to other planets like Mars.

While resistance limits of the black fungus *C. antarcticus* MNA-CCFEE515 to various types of IR have been characterized, the radioresistance of most of the species within black fungi has remained unknown so far. In this context, the study conducted on a set of 101 strains from 20 species has allowed the first comprehensive definition of the radioresistance limits of the group (Chapter 4). In addition to suggesting these fungi as the most known radioresistant microorganisms, we highlighted remarkable variability in the resistance limits to IR even among strains within the same species. These results suggest that these microorganisms have developed a variety of mechanisms to cope with the harsh IR that may have been driven by

multiple factors. Moreover, the remarkable ability of black fungi to withstand IR levels that are significantly higher than those found in their natural habitats raises intriguing questions about the possible underlying factors that contribute to this extraordinary resistance. From an ecological point of view, the radioresistance of black fungi may represent the by-product of the adaptation to various possible environmental parameters occurring in the extreme habitats in which they often thrive (Shuryak, 2019). Indeed, our results demonstrated that the geography and a few parameters, such as UV exposure and precipitation levels, are predictive of the values of resistance to IR. In fact, IR and other environmental stressors may induce similar cellular damages; for instance, IR exposure, environmental stressors such as UV exposure and desiccation induce oxidative damage in the cells, thereby triggering the same defence and response mechanisms induced by IR (Wong et al., 2019; Gasulla et al., 2021). This may justify the correlation found in this study between the response to IR and other environmental stressors. The adaptation to these factors could have exerted an extensive positive selection on genes involved in the response to various stresses, resulting in the ability to withstand high levels of IR as well. Thus, these findings expand the investigation of the ability of black fungi to tolerate ionizing radiation (IR) to the wider domain of the ecological and genetic bases of extremotolerance. Indeed, the results strongly suggest that the exposure of microorganisms to specific environmental stressors could potentially lead to the development of a broader tolerance to a range of harmful factors. In turn, this could have significant implications for studying how life adapts to extreme environments.

From a genomic point of view, the environmental pressure that has driven the radioresistance in black fungi could have shaped the genomic characteristics of the various strains by selecting genes involved in the cellular mechanisms of response to different stresses, including IR (Kondrashov, 2012; Gorkovskiy and Verstrepen, 2021). In this context, this study showed that the response to IR of black fungi may be mediated by a complex network of different pathways and molecular processes that work together to counteract its detrimental effects (Chapter 5). Consistently with the previous observations, we found differences in genomic functional traits that are associated with the responses to other environmental stressors as main drivers of fungal radioresistance, confirming this character as a by-product of the adaptation to these other factors. Therefore, these suggested that a set of genes exist in extremophilic microorganisms which may mediate their tolerance to a variety of harmful conditions experienced in polyextreme environments. Again, these results give new insights for understanding the mechanisms that allow life to persist under challenging conditions, not only from an IR perspective.

Altogether, this thesis shed light on the resistance limits of fungi to IR and the underlying genetic and ecological factors that may have driven their ability to persist in extreme environments. In a broader context, these findings have wider implications in the adaptation of life to extreme environments. Finally, the study highlights the potential of black fungi as a model system to explore the fundamental mechanisms of radiation resistance in eukaryotes from both an astrobiological perspective and the development of new radioprotective strategies for humans and other organisms. Overall, this research represents a critical step towards a better understanding of the limits of life on Earth and its potential to survive in harsh environments.

Finally, our findings may provide crucial insights into the future investigation of the metabolomic factors utilized by black fungi to counteract the harmful effects of ionizing radiation, paving the way to a thorough understanding of the molecular bases of radioresistance.

References

Coleine, C., Stajich, J.E., and Selbmann, L. (2022) Fungi are key players in extreme ecosystems. *Trends in Ecology & Evolution*.

Gasulla, F., Del Campo, E. M., Casano, L. M., & Guéra, A. (2021). Advances in understanding of desiccation tolerance of lichens and lichen-forming algae. Plants, 10(4), 807.

Gorkovskiy, A., & Verstrepen, K. J. (2021). The role of structural variation in adaptation and evolution of yeast and other fungi. Genes, 12(5), 699.

Kondrashov, F. A. (2012). Gene duplication as a mechanism of genomic adaptation to a changing environment. Proceedings of the Royal Society B: Biological Sciences, 279(1749), 5048-5057.

Pacelli, C., Bryan, R.A., Onofri, S., Selbmann, L., Zucconi, L., Shuryak, I., and Dadachova, E. (2018a) Survival and redox activity of *Friedmanniomyces endolithicus*, an Antarctic endemic black meristematic fungus, after gamma rays exposure. *Fungal biology* 122,1222–1227.

Pacelli, C., Bryan, R.A., Onofri, S., Selbmann, L., Zucconi, L., Shuryak, I., and Dadachova, E. (2018b) The effect of protracted X-ray exposure on cell survival and metabolic activity of fast and slow growing fungi capable of melanogenesis. *Environmental microbiology reports* 10: 255–263.

Pacelli, C., Selbmann, L., Moeller, R., Zucconi, L., Fujimori, A., & Onofri, S. (2017a). Cryptoendolithic Antarctic black fungus Cryomyces antarcticus irradiated with accelerated helium ions: survival and metabolic activity, DNA and ultrastructural damage. *Frontiers in Microbiology*, *8*, 2002.

Pacelli, C., Selbmann, L., Zucconi, L., Raguse, M., Moeller, R., Shuryak, I., & Onofri, S. (2017b). Survival, DNA integrity, and ultrastructural damage in Antarctic cryptoendolithic eukaryotic microorganisms exposed to ionizing radiation. *Astrobiology*, *17*(2), 126-135.

Selbmann, L., Pacelli, C., Zucconi, L., Dadachova, E., Moeller, R., de Vera, J. P., & Onofri, S. (2018). Resistance of an Antarctic cryptoendolithic black fungus to radiation gives new insights of astrobiological relevance. Fungal biology, 122(6), 546-554.

Shuryak, I. (2019). Review of microbial resistance to chronic ionizing radiation exposure under environmental conditions. Journal of environmental radioactivity, 196, 50-63.

Wong, H. J., Mohamad-Fauzi, N., Rizman-Idid, M., Convey, P., & Alias, S. A. (2019). Protective mechanisms and responses of micro-fungi towards ultraviolet-induced cellular damage. Polar Science, 20, 19-34.